2-26-2009

Control Of Kinetics And Thermodynamics In Microwave-Assisted Synthesis Of Nanocrystals

Aaron Lynn Washington II
Florida State University

FLORIDA STATE UNIVERSITY

COLLEGE OF ARTS AND SCIENCES

CONTROL OF KINETICS AND THERMODYNAMICS IN MICROWAVE-ASSISTED SYNTHESIS OF NANOCRYSTALS

By

AARON LYNN WASHINGTON, II

A Dissertation submitted to the
Department of Chemistry
in partial fulllment of the
requirements for the degree of
Doctor of Philosophy

Degree Awarded:
Spring Semester 2009

The members of the Committee approve the Dissertation of Aaron L. Washington, II defended on February 26, 2009.

_____
Professor Geoffrey F. Strouse
Professor Directing Dissertation

_____
Professor William Landing
Outside Committee Member

_____
Professor Kenneth Goldsby
Committee Member

_____
Professor Alan Marshall
Committee Member

Approved:

_____
Professor Joseph Schlenoff, Chair, Department of Chemistry and Biochemistry

_____
Professor Joseph Travis, Dean, College of Arts and Sciences

The Graduate School has verified and approved the above named committee members.

First and foremost, thank God for allowing me to make it through.

To my loving wife Marie, you'll never know how much you mean to me. You always keep me on the path.

To my Mom, thank you for the encouragement and strength to allow me to reach my goals.

To my Dad, I wish you could see me now. To Donald, thanks for picking up where he left off and showing this young kid how to be a man.

To my grandparents, thank you for always being there, I love you always.

ACKNOWLEDGEMENTS

I would not be able to achieve such great success without the people that helped me become the person that I am today. Everyone that I have encountered in my journey throughout graduate school has influenced my growth in knowledge through their experiences and perspectives. However, there are a few people that I would like to emphasize.

I would like to first thank my professor Geoff Strouse for taking a chance on a young man without much direction and a lot of ambition. Who would have thought that the same person who spent four hours in your office the first day that we met would turn out to be the person I am today. There were some days where I couldn't see the forest for the trees but you always gave me an opportunity to prove myself through your many challenges and ideas.

I would also like to thank my committee members: Dr. Goldsby, for being a great advisor when I first arrived who encouraged me to persevere even when I got discouraged, Dr. Alan Marshall, for speaking with me and offering challenging opinions about my work, and Dr. William Landing, showing me the perfect mid range jump shot.

I would also like to thank the following people:

- My family, who always encouraged me to continue pursuing my dreams and never giving up. I also want to thank my brother Jovan and my sister Jaceta.
- My church family who continued to pray for me and encourage me to continue reaching higher heights.
- Mani, for always listening when I feel discouraged and feeding me all your great Indian food (even the experimental food…lol). You're a great friend whom I hope to always keep in touch with. I'll never forget dumblings and mojitos with the original three.
- Donny, for all your inspiration and knowledge about everything including cars, science, writing, marriage, etc. Hopefully we'll cross paths again.
- Travis, the juggling master, thanks for showing me that grad school is fun and challenging at the same time. It's nice to know that there is a balance in life and you're the definition of that.
- Jeff, for taking the time to show me how to make quantum dots and how great microwave chemistry can be.

- Lindsey, you always ran the office when you were here. Thanks for showing the strength and determination to get things done.
- Weiwei, you are now the best athlete in the group now that I'm gone.
- Chris R., you're the best wingman I never had. If we had met years before, the world wouldn't be ready. The phenom with limitless potential and a great friend.
- Corey T, you are a great friend and a fellow true gator. Thanks for helping me achieve my goals and keep the spice in life with our adventures.
- The Strouse group, thank you for the helpful conversations and debates. Though we are ever changing we still seem to remain the same.
- Dr. Dalal, Dr. Stiegman, and Dr. Singh, thank for helpful conversations and suggestions.
- There are other people that I have not included that have also helped me and encouraged me to pursue my dream. Thank you.

TABLE OF CONTENTS

LIST OF FIGURES

LIST OF ABBREVIATIONS

MW……..…Microwave
CdSA…….....Cadmium Stearate
TOP…….....Tri-n-Octyl Phosphide
TOPS……...Tri-n-Octyl Phosphine Sulfide
TOPSe…….....Tri-n-Octyl Phosphine Selenide
TOPTe…….....Tri-n-Octyl Phosphine Telluride
pXRD……..…Powder X-ray Diffraction
PLE……..Photoluminescence Excitation
PL…….……..Photoluminescence
TEM…….....Transmission Electron Microscopy
LED……..…….Light Emitting Diode
PV…….…….……...Photovoltaics
QDs……..……..Quantum Dots
K_{sp}……..……..Solubility Product
HDA……....……Hexadecylamine
FWHM……..….……..….Full Width Half Maximum
PLQY……..Photoluminescence Quantum Yield
IL……..……..Ionic Liquid
Abs…….....Absorption
MOCVD…….....Metal-Organic Chemical Vapor Deposition
A.U……..….Arbitrary Units

ABSTRACT

This dissertation describes the methodology for using microwave chemistry to control the reaction kinetics and/or thermodynamics of semiconductor nanocrystalline materials. The introduction provides a background of synthetic methods for semiconductor quantum dots evolved from using micelles to highly reactive precursors and finally to high temperature injection and microwave chemistry to produce the maximum number of nucleation events. Therefore, the control over the dispersity and size of the materials to allow semiconductor nanocrystals to be grown has led to a vast amount of research and experimentation for modeling the best reaction in the most efficient method of formation. The production of the best quality materials is driven through selectively isolating the precursors that actively contribute to the most nucleation events followed by efficient growth of the nanomaterials through the use of microwave chemistry (Chapter 2). Using microwave chemistry, the formation of CdS quantum dots of high quality and tight dispersity is achieved using TOPS as the sulfur source which has not been achieved previously (Chapter 3). The application of classical nucleation theory to microwave chemistry is further explored to determine how the Ostwald ripening phenomenon applies to the different growth mechanisms in the synthetic methodology to explore the idea of re-nucleation (Chapter 4). This synthetic method can also be utilized to explore multiple crystal structures that are produced by simple manipulation of the precursor solution and are fully characterized using absorption, emission, powder X-ray diffractometry (XRD), and transmission electron microscopy (TEM) (Chapter 5).

CHAPTER 1 INTRODUCTION

Richard Feynmann (1959) predicted in a lecture entitled "There is plenty of room at the bottom" that chemistry and physics in a confined environment may produce exciting observations.[1] L.E. Brus (1984) observed quantum confinement in CdS semiconductors and analyzed the observation in terms of a particle in a three dimensional box. The quantum confinement of materials resulted in the field of nanoscience as we know it today. According to classical thermodynamics, the "bulk" crystal is the most stable size for semiconductor materials. Through efforts by L. E. Brus and R. Feynmann, we have now begun to realize that the bulk crystal is only the beginning of the potentials for crystalline materials, especially semiconductors and metals. The humble beginnings of a physicist to restrict the growth of materials into the nano-sized regime has lead to an exponential explosion of nanomaterials research that has touched every aspect of human culture including renewable energy, biology, and memory applications. The idea of confining the wavefunction of an exciton to a smaller and smaller area effectively producing quantum confinement was initially discussed and formulated by L.E. Brus (1984).[2] Soon after, the National Science Foundation began funding numerous research projects targeted at developing and improving nanotechnology in the scientific community. This is considered the cause for the big explosion in both the industrial and academic communities for research in nanoscience. Industrially, nanomaterials present a way to make products smaller and manufacturing more cost efficient. The industrial applications for nanoscience have quickly become the cornerstone of most industrial companies with a vast majority of them implementing nanoscience into their production system. The success in the nano field provides a whole new world for industrial and academic advancement which would allow the ability to probe the realms of technology such as nanocircuits, nanomedicine, phosphors for solid state lighting,[3] lasers[4], light emitting diodes,[5] as well as the possibility for the best light energy conversion materials to date.

Over the years, the synthesis of semiconductors and metal nanoparticles has evolved dramatically due to the overwhelming initial interest in materials that have vastly different properties as their size begins to reduce. Early success in synthesizing nanoparticles was realized by researchers including Murray, Bawendi, and Alivisatos. The early work was determined that

as a semiconductor crystalline material reduced in size, the semiconductor began to exhibit size dependent optical properties. This new development began to spark immense interest in the scientific community and research efforts were investigated to controllably synthesize smaller materials.

1.1 Theory of Confinement

The best evidence for quantum confinement is the obvious shift in the optical absorption and emission spectra based on the size of the nanoparticles. The absorption event occurs when an electron is promoted from the valence band to the conduction band producing an electron carrier (e^-) leaving an electropositive hole (h^+) behind in the valence band. So in reality, the creation of an exciton produces two charges, electron and the hole. The electrostatic attraction between the electronegative electron and electropositive hole creates an exciton in effect an e^- and h^+ pair with a defined binding energy. As a particle continues to decrease in size, the conduction band continues to separate into discrete energy levels effectively increasing the amount of energy needed to promote the electron from the valence band as shown in Figure 1.1. This increase in energy is better understood using a physical approach of confining a wavefunction of the exciton to a smaller area than the bulk would allow. The confinement of the wavefunction to a smaller region causes the frequency of the wave to increase with the decreasing wavelength available thus changing the energy required to achieve the exciton. The calculated internal energy of the exciton for CdSe is calculated as[6,7]:

$$E_{ex} = \frac{h^2}{8R^2}\left(\frac{1}{m_e} + \frac{1}{m_h}\right) - \frac{1.8e^2}{4\pi\varepsilon_{CdSe}\varepsilon_0 R} + \frac{e^2}{R}\overline{\sum_{k=1}^{\infty} a_k \left(\frac{S}{R}\right)^{2k}} \qquad (1)$$

where the first term is defined as the quantum confinement term with *h* being Planck's constant, R is the radius of the nanoparticles, m_e is the mass of the electron, and m_h is the mass of the hole. The confinement term functions as $1/R^2$ which begins to rapidly increase as the particle goes from the weak confinement regime into the strong confinement regime.[8] The second term denotes the Columbic interaction between the electron and the hole left behind where e is the elementary charge of a particle, ε_{CdSe} is the dielectric constant of bulk CdSe (10.6)[9] and can range anywhere from 5-12 in inorganic semiconductors in the bulk, and ε_0 is the vacuum permittivity. The Columbic term functions as 1/R, where the decrease in size causes an increase in this term however; since the electronic interactions would effectively decrease the exciton

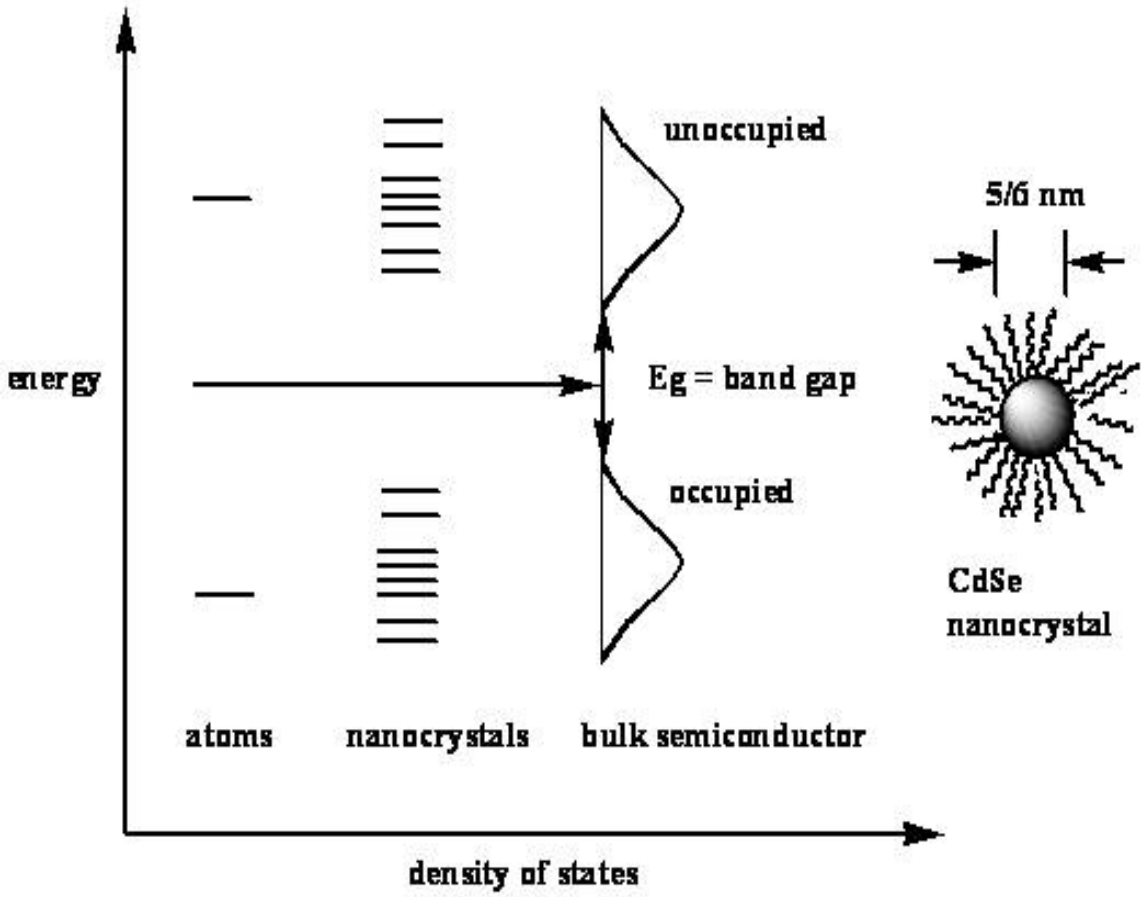

Figure 1.1. Density of States vs Energy Levels for CdSe

This image shows the density of states diagram that shows the bandgap and the splitting of electronic states for a semiconductor as a function of material size starting from atoms to bulk crystals.

energy the term is negative. The third term is defined as the polarization term where the bar denotes the average over the entire wavefunction and though most of its energy is lost by solvation, it also increases by 1/R similar to the columbic term. However, the polarization term adds energy to the exciton as the size of the particle decreases due to the increase in the solvation energy. The confinement term which rapidly increases the energy much faster than the columbic interaction decreases the energy through the electrostatic attraction of the electron and hole. The solvation term actually helps to increase the energy of the exciton as the size decreases due to the increasing amorphous nature of smaller particles.[10]

1.2 Historical Development

Classically, during the growth of a crystal from a precursor, the size dispersity is dictated by the homogeneity of the nucleation event and whether macroscopic or on the nanometer scale crystal growth is governed by Ostwald ripening. These processes, just presented in an oversimplified statement, actually require great control over the synthetic pathways and growth mechanisms. In attempting to grow these materials, problems arose from the lack of the ability to control the surface energy of the growing particle in order to produce a stable crystalline material that was smaller than the thermodynamic equilibrium size. Ostwald ripening was known to occur through the coagulation and flocculation of amorphous meso-crystalline materials leading to the formation of larger crystalline particles at the expense of smaller ones. The ability to generate smaller particles than bulk is possible by the control of the high surface energy of these materials. The high surface to volume ratio of these materials contributes to the instability of the particle due to the equilibrium of dissolution and crystallization, according to nucleation theory. Polymers such as styrene/maleic acid were used to control the aggregation of these materials by acting as a stabilizing agent to impede growth. The negative carboxylate group complexes with the cation surface ions to control particle-particle interactions. The ability to control the surface was first realized by Brus et al. where the addition of a surface passivant (or ligand) stabilized the amorphous agglomerated colloids thereby allowing their stable crystallization out of the reaction mixture, as long as the surface energy remained low. In actuality, the surfactants demonstrate the ability to slow the rate of growth by providing a stable intermediate size regime where particles can remain on the nanometer scale for extended periods of time. These new smaller but stable particles are allowed to grow at a much slower rate allowing for the isolation of much smaller sizes at low temperatures even at longer reaction times. Another advantage of

using these surfactants to restrict the growth of semiconductors is the ability to provide separation for the materials in the reaction mixture. According to the phenomenon known as Ostwald Ripening, the aggregation of amorphous colloids leads to selective precipitation of only the larger more stable materials through the dissolution of smaller materials. The sterics and sheer volume of the long alkyl chained phosphines and amines prevent aggregation of the materials. The scientists that initially tackled this problem were some of the first to use the well understood facets of metal ligand acid/base theory from inorganic chemistry to create stable interactions allowing for the reduction of the surface energy in a nanomaterial, thus controlling size. [11] The early experiments were carried out on CdS semiconductors due to their simplistic synthesis and semi toxic nature.[12,13,14]

Synthetic developments in the early 90s that didn't utilize aqueous methods for growing semiconductors were successfully developed by Bawendi[15] and Steigerwald[16] relying heavily on very reactive monomers and strong passivating ligands (good Lewis base) precursors to try and control the progress of the reaction. The use of dialkyl cadmium and zinc precursors along with tri-n-alkyl phosphine chalcogenides or bis(trimethyl)silyl chalcogenides were chosen to allow for very fast formation of materials which in effect separated nucleation and growth. Carrying out the reaction in the presence of a strongly passivating ligand allowed growth to be controlled. The resultant materials exhibited narrow size dispersity, but were prone to surface defects. Shortly afterward Guyot-Sionnest et al. produced highly luminescent materials by applying a better method to control the surface energy of the materials thus eliminating surface states. [17] The core-shell materials are prepared by layering the core nanoparticles with a different semiconductor having a higher direct bandgap with that protects the surface of the materials from oxidation and allows the exciton to expand into the shell typically causing a red shift in the optical data. Additionally, as the surface begins to reach the optimal thickness, the exciton recombination has less non-radiative relaxation allowing for a more efficient emission event effectively increasing the quantum yield of the sample.

From this point, the scientific community begins to separate into different methods of synthesis. One approach that has become very popular is the continuation of the work began by Bawendi and Murray using high temperature injection techniques to generate nearly instantaneous nucleation and growth of the materials.[18] The research led by Peng et al, has evolved from the use of highly reactive and toxic dialkyl metals (Cd and Zn) to using relatively

A)

$Li_4[Cd_{10}Se_4(SPh)_{16}]$ CdSe Quantum Dots

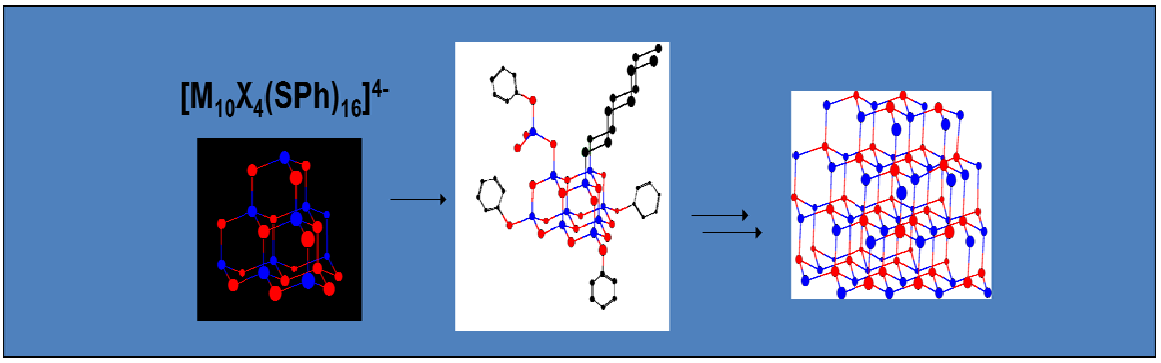

B)

$$CdSA + TOPS \xrightarrow[240^\circ C]{AlkaneSolvent} CdS$$

$$CdSA + TOPSe \xrightarrow[240^\circ C]{AlkaneSolvent} CdSe$$

$$CdSA + TOPTe \xrightarrow[240^\circ C]{AlkaneSolvent} CdTe$$

Figure 1.2. Synthesis of CdX (X=S, Se, Te)

A) Synthesis of CdSe from a single source precursor and B) from single molecular precursors can be performed using traditional round bottom synthesis or in the microwave reactor (except the CdS).

inert metal oxides as starting materials. These materials are mixed with a carboxylate to free the metal and introduced to a reactive anion (TOPX, X=S, Se, Te) at high reaction temperatures. The injection and initial reaction generates a nucleation event which is subsequently followed by growth. This method is most commonly used to produce quantum dots in literature to date despite its lack of reproducibility and multi-stepped process. The biggest limitation to this approach is the inability to safely scale up the reaction for industrial applications.

Another approach that has been followed by many in the scientific community is the use of a single source precursor for the synthesis of semiconductor nanomaterials (Figure 1.2A).[19,20,21,22] Use of a single source precursor has the advantage that the elimination of high temperature injection of two monomers is more ideal for industrial processing and these batch reactions. The initial synthesis of most single precursors stemmed from the work of Strouse where molecular clusters were used to generate nanocrystals following the lead of Herron and Wang.[23, 24, 25, 26] The growth of quantum dots from this precursor produces the most stable raw batch materials available due to the strong structured core the cluster provides. The best aspect of using single source precursors for nanomaterial growth is the slow reconstruction step that is required to form a stable critical nucleus for growth allowing for the intentional incorporation of dopant ions that alter the optical, structural, and magnetic properties of the growing material.[27,28]

A third direction for the nanomaterial field was work towards developing new materials on the nanoscale where more applications could be explored such as infrared sensors and photovoltaics. Most new materials included exploring III-V chemistry with the development of InP, InGaP, GaAs, and AlN (aluminum nitride). The materials offered the opportunity to explore a new group of semiconductors in the nano regime. In addition, oxides and heavy metal II-VI materials provide avenues to exploring both the UV and IR regions of the electromagnetic spectrum.

Lastly, in only the last 8-10 years, the development of alternative heating processes have surfaced including microfluidics and microwave heating to try and enhance the heating efficiency of the reactions. One of the best methods for heating materials is using microwave chemistry. The use of microwaves to generate and accelerate chemical reactions was initially developed for aqueous based organic synthesis back in the early 1980s.[29] Since that time, microwaves have been used as alternative instruments to provide fast efficient heating due to its selectivity polar molecules. In general, microwave heating systems have been used exclusively to

heat solvents with strong dipole in order to reach reaction temperature faster; however, only recently has the selectivity of microwave heating been fully utilized to target specific precursor materials where the reaction is designed to take full advantage to the microwave system (Figure 1.2B).[30] The application of microwave (MW) chemistry to problems in nanotechnology allows exquisite control over the reaction pathway for nanocrystal (NC) formation and growth through the control of the nucleation / precursor activation event. The production of nanomaterials involves the decomposition of molecular precursors followed by nucleation and growth of nanocrystals.

1.3 Nucleation theory

Nanocrystal growth is in essence the fundamental process of crystallization. In crystallization, two critical steps must occur: nucleation and growth. The nucleation event can best be thought of as a phase transition from a unimolecular reaction to a surface mediated reaction following formation of a nucleus of a critical size, which is the thermodynamically stable state for transition. In the multi-molecular reaction using a crystallization process, the best way to describe the nucleation event is using the solubility products (K_{sp}) showing the crystallization from aggregated particles in solution due to a supersaturation of the precursor and solubility in a given solvent. The solubility product helps to explain how the equilibrium between precursor and crystallite particle is heavily dependent on many factors including the precursor reactivity, concentration, solubility, and temperature of the reaction mixture. These factors regulate the nucleation event by controlling the progress of the reaction, which in essence controls the kinetics of the reaction. The reaction can be selectively limited or accelerated using the reactivity or concentration of the precursor solution allowing for a single homogenous nucleation event to occur controlling the dispersity of the crystalline materials formed, as well as the concentration of the nucleated product.

Classically, nucleation theory has been considered as a phase transition, which can be explored in both the homogenous and heterogeneous regimes. In terms of phase transitions, the problem has been theorized using the formation of the water droplets from a supersaturated air with the formation of a mathematical number of bubbles corresponding to the number of critical embryo bubbles needed to form a droplet of radius r* (Figure 1.3A) for a given supersaturation value. As shown in Figure 1.3A, critical crystalline size

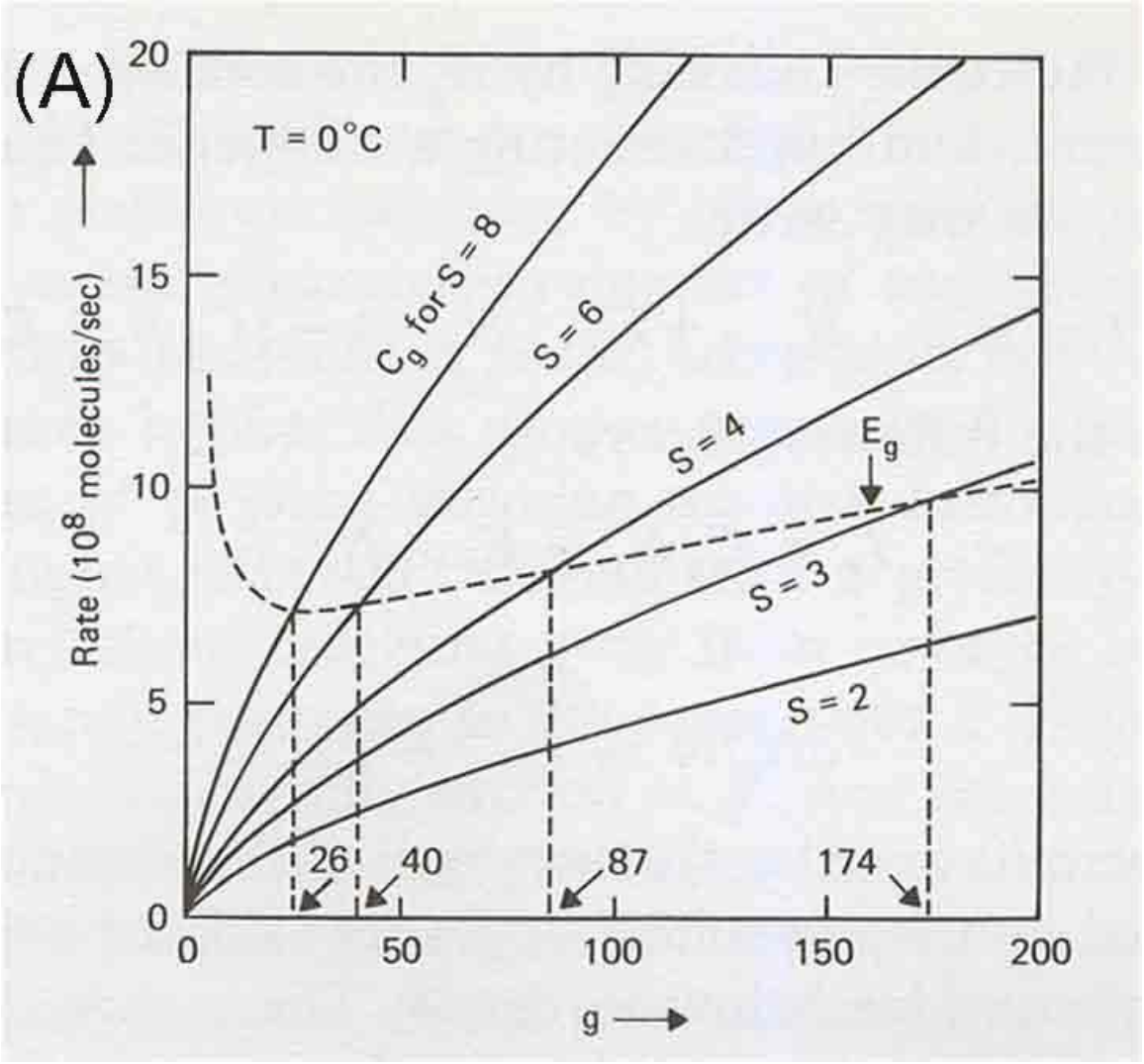

Figure 1.3A. Number of Aggregate Particles vs. Rate of Growth

Shows the change in the number of molecules that aggregate at a specific supersaturation and the rate of molecule aggregation as at different supersaturations. (Image obtained from Ref. 30)

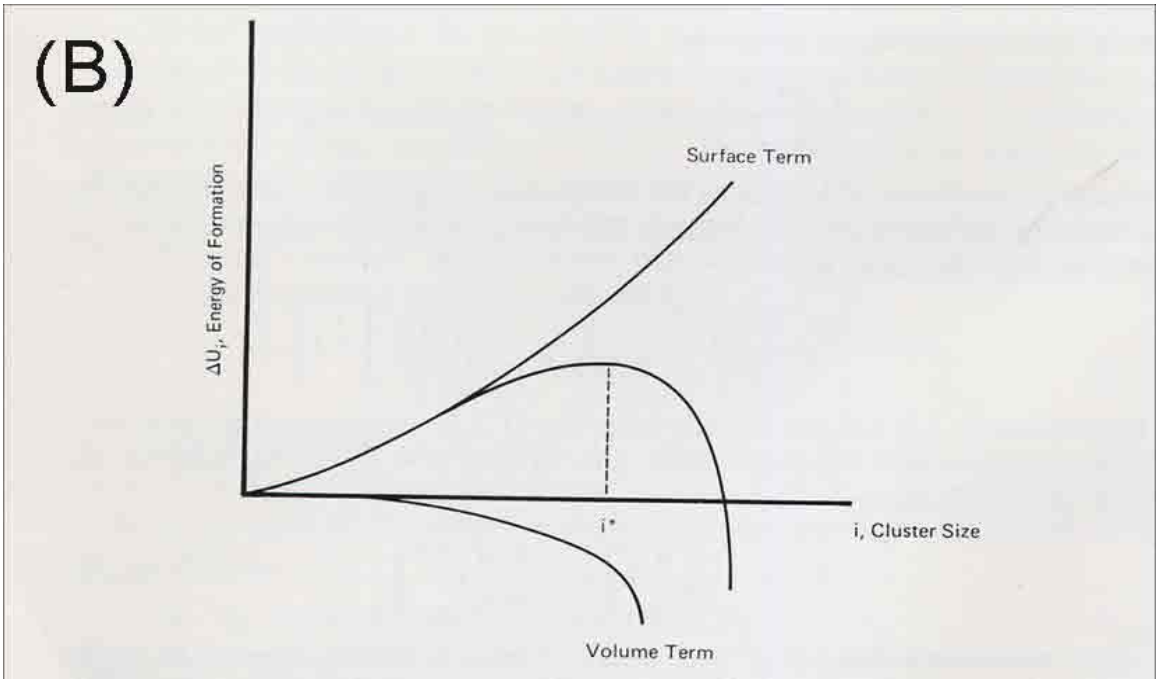

Figure 1.3B. Cluster Size vs. Energy of Formation

The energy diagram for the growth of a molecule with respect to its surface and core energy terms as well as the total energy required for formation as a function of size.
(Image obtained from Ref. 30)

(number of molecules) for nuclei formation varies inversely with the supersaturation of the solution while the rate of growth increase exponentially with supersaturation. A supersaturated reaction mixture either spontaneously or through temperature modulation initiates nucleation of colloidal materials in the form of precipitation. This precipitation produces a selective amount of amorphous aggregated colloids in the solution. These particulates began to crystallize and form small microcrystalline aggregates that are more thermodynamically stable in solution than their amorphous counterparts. The formation of crystalline materials only occurs after aggregation of the product to achieve a certain critical crystalline sized particle allowing the mixture to proceed forward spontaneously to the other side of the equilibrium. The Gibbs free energy change for the reaction is thus described by:

$$\Delta G = 4\pi R^2\gamma + 4/3\pi R^3\Delta F_v \qquad (4)$$

where the γ is the surface free energy term which destabilizes the crystal toward solvation and the ΔF_v is described as the difference in the free energies between the solvated and crystalline forms of the material contributing to the reaction coordinate in proportion to the crystal's volume driving the reaction toward crystallization. The energy of formation becomes favorable only after the critical crystalline size is achieved.[31] (Figure 1.3B) This information is very useful in assisting the scientist to understand how nanoparticles form in solution as well as what is required not only in terms of energy but also the concentration of precursor monomer to induce crystallization.

Through continued core crystalline formation in these microcrystalline materials, the formation of coarse crystals finally occurs producing the most stable products. The crystallization process is most adequately annotated via Ostwald ripening. This process has been illustrated best by the LaMer plot shown in Figure 1.4A monitoring the progression from a supersaturated solution leading to subsequent nucleation and growth of crystallite particles.[32] During the growth process Ostwald ripening takes place and is the major factor that contributes to the growth of crystallite materials under diffusion controlled conditions. The nucleation event results in the formation of amorphous microcrystalline materials with a slight distribution in size even in the best homogenous nucleation event. Dissolution of the smaller particles produces fresh precursor to allow growth of the larger particles. (Figure 1.4B) This occurs because of the higher surface energy of the smaller materials. The rate of growth will be dictated by the passivants in solution which can reduce the surface energy and thus dissolution and growth

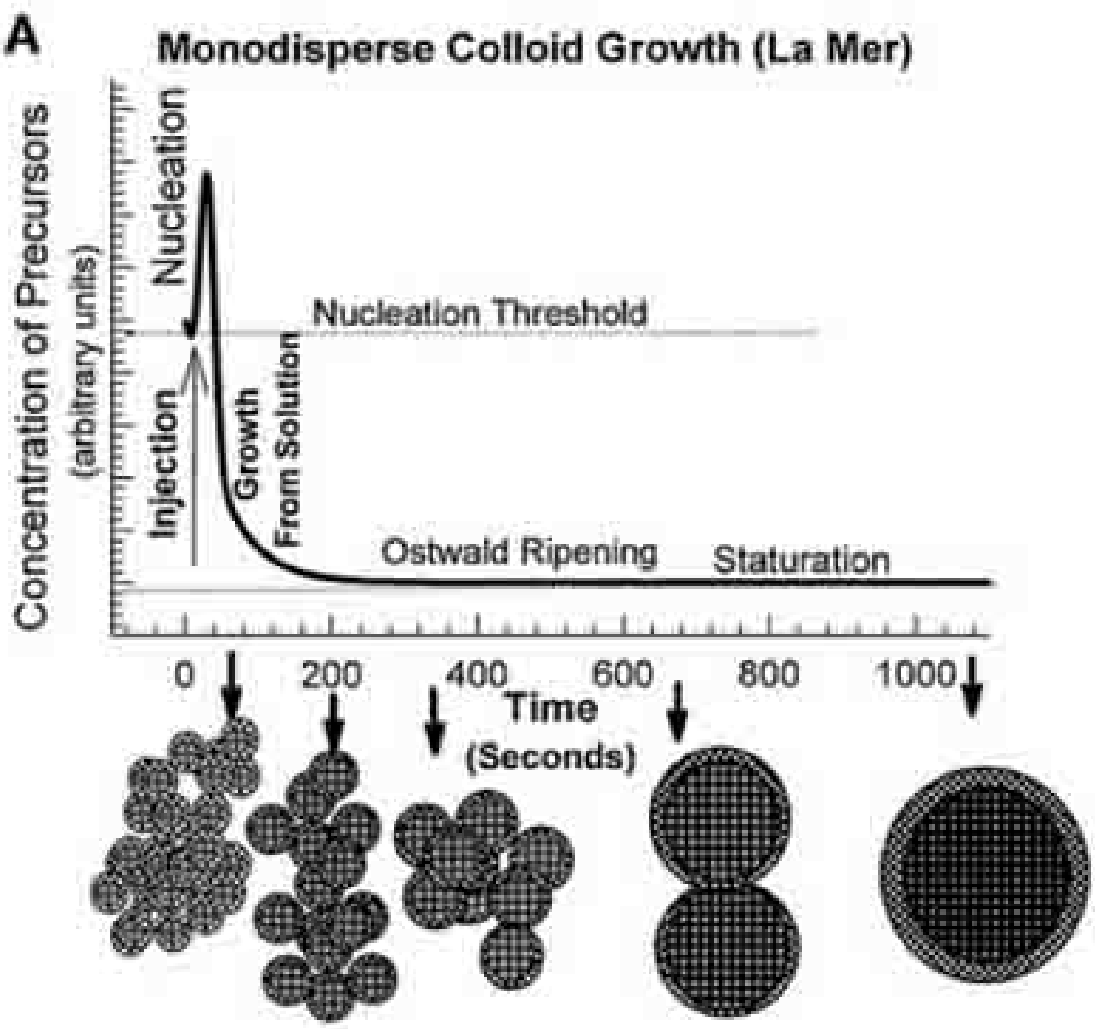

Figure 1.4A. LaMer Diagram.

The LaMer plot showing nucleation and growth on crystals as a function of precursor concentration. This plot illustrates the Ostwald ripening process as crystals grow to larger sizes.

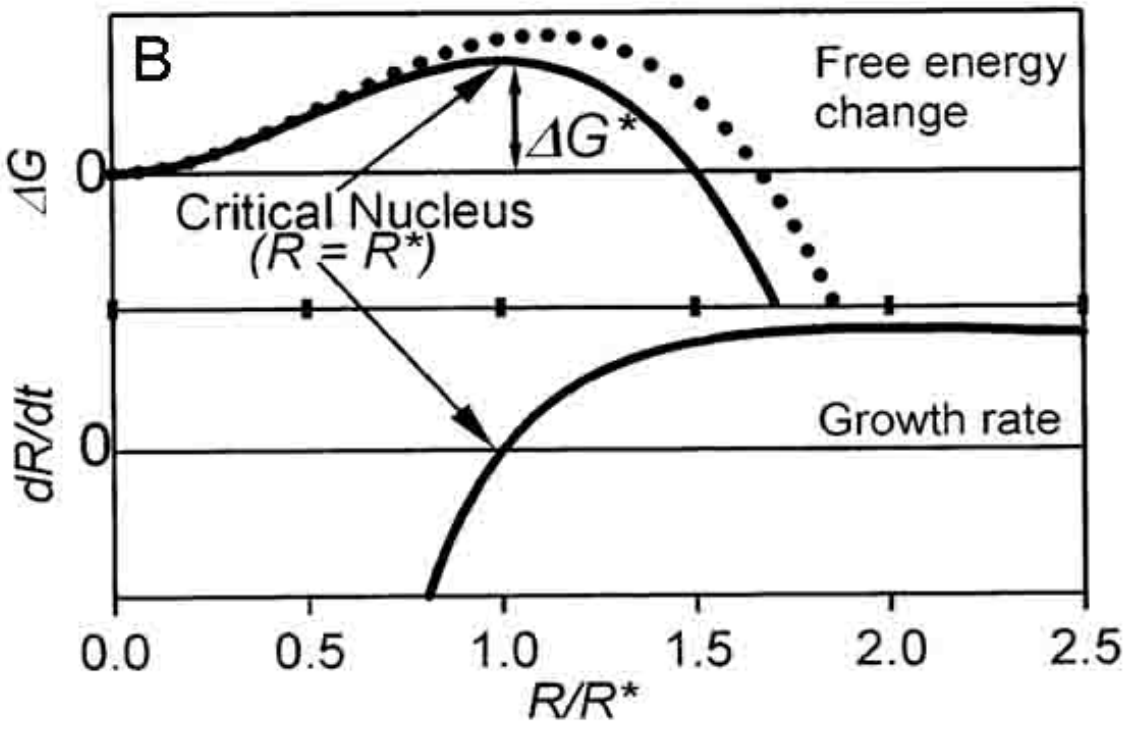

Figure 1.4B. Growth Rate and Free Energy vs. Size

A plot showing the change in free energy of a crystal as a function of growth relative to critical crystal size while the bottom plot shows how the growth rate changes.
(Images obtained from Ref. 32)

rates.[33]

Other factors used to regulate growth and control the nucleation event include the precursor monomer concentrations and reactivity, the solubility of the monomer in the given solvent, the temperature of the reaction, and the metal-ligand interactions stemming from the passivants in the reactions mixture. In addition, one of the best methods to control the formation of crystalline precipitates is to utilize the K_{sp} for crystal formation based on the concentration and reactivity of the each monomer in the reaction mixture.

1.4 Microwave Chemistry

The crystallization processes can be controlled by selectively triggering nucleation of a core by programmed precursor decomposition, which is achievable in a MW reactor. Control over the atom addition is achieved by concentration effects and more importantly the thermodynamics of the precursors, which in this case are the reactivity and mobility of the cation and anion reagents. Coupled to the control of nucleation and growth is a requirement of high temperature growth conditions to ensure control over glide plane defects and ion vacancies common to solid state materials.

In the MW, the ability to selectively energize a species in the presence of lower dipole moment reaction components allows one to systematically trigger the nucleation / growth step of a single precursor component in the reaction resulting in controlled nucleation, rapid depletion of the absorbing precursor, and growth following energizing the MW reactor. Nucleation is then controlled by the MW cross section of the precursor and not the temperature of reaction, while the dispersity of the material is controlled by the MW power and temperature due to the selective microwave effect and not the rate of injection.

Microwave chemistry is a vastly expanding field in the area of organic and organometallic synthesis of materials including polymers, semiconductor nanomaterials, and catalytic materials. The microwave offers the ability to specifically heat certain materials over others through a mechanism known as the “specific microwave effect” due to the selectivity of heating in the reaction mixture. Microwave heating possesses several characteristics that are different from conventional convective heating. First, the microwave regime has very long wavelengths ranging from 1mm (300GHz) to 1m (300MHz) including penetration radiation, controllable electric field distributions, rapid heating, selective heating of materials through

differential absorption of polarizable materials, and self-limiting reactions due to the ability to remove the heat source by a simple switch.[34]

The polarizability change as a function of changing particle size is shown to effect the particle growth especially in the microwave. According to Rosenthal, the polarization term is one of the two components comprising the potential energy part of the Hamiltonian in the case of an electron-hole pair created by an exciton of a semiconductor. This term is represented by:

$$\hat{V}_{pol}(S_e, S_h) = \frac{e^2}{2}\sum_{k=1}^{\infty} \alpha_k \frac{S_e^{2k}+S_h^{2k}}{R^{2k+1}} \qquad (2)$$

where

$$\alpha_k = \frac{(\epsilon-1)(n+1)}{[\epsilon_2(\epsilon n+n+1)]} \qquad (3)$$

and

$$\epsilon = \epsilon_2/\epsilon_1$$

where e represents the elementary charge and S_e and S_h represent the positions of the electron and the positive hole inside the sphere.(Brus,1984) The polarization (dielectric solvation) energy is controlled by 1/R which also contributes to the increase in the energy of the internal exciton. This term is especially important for microwave chemistry due to its incredible impact in the heating and therefore growth of the nanoparticles.

In the MW, the ability to selectively energize a species in the presence of a smaller transition dipole reaction component allows one to systematically trigger the nucleation / growth step of a single precursor component in the reaction resulting in controlled nanocrystal nucleation, rapid depletion of the absorbing precursor, and growth following energizing the MW reactor. Nucleation is then controlled by the MW cross section of the precursor and not the temperature of reaction, while the dispersity of the material is controlled by the MW power and temperature due to the selective microwave effect and not the rate of injection.

MW reactions have several unique advantages over convective heating, 1) selective activation of the target precursor to initiate nucleation and subsequent growth, 2) reproducibility from batch to batch, 3) the convenience of a non-injection reaction, and 4) a stopped flow near-continuous synthesis protocol. The demonstration of the selective triggering of material nucleation and growth for cadmium and zinc chalcogenides by choosing a molecular chalcogenide that is MW absorptive has validated the “specific microwave effect” for

Figure 1.5. Stop-Flow Microwave Reaction

Shows the Discover microwave system by CEM with the Voyager Stop-Flow attachment. Freshly synthesized CdSe nanoparticles are being actively pumped out of the microwave chamber at 70°C and are illuminated by a UV hand lamp to show their luminescent properties.

nanocrystal preparation.[35]

1.4.1 Theory

In the field of microwave (MW) chemistry, much effort has focused on the tailoring of the reactants dipole and volume to produce a desired product via the specific microwave effect.[36,37,38] The largest dipole moment will selectively absorb MW energy in the presence of poorly absorbing reaction components and solvents. The absorption of MW energy selectively by a reactant provides the energy to overcome potential activation barriers associated with the transition state or reactive intermediates. While the specific microwave effect is prolific in the literature,[39,40,41] proving the effect is very challenging. In order to take advantage of the specific microwave effect for nanocrystal synthesis, particularly for high throughput synthesis (Figure 1.5), a single reactive precursor must be a strong microwave absorber, while the solvent, other precursors and the growing material must be non-absorptive.

For a solution containing reactants in a solvent system, microwave heating can occur through three different processes depending on the relative microwave absorption of the solute and solvent molecules (Figure 1.6). The differential absorption of the two components can lead to differential heating which can affect mechanistically the outcome of the process.

In the microwave region, changes in the permittivity occur through polarizations induced in the material by the oscillating electric field of the radiation. The net polarization of a material can be broken down into several constituent polarization processes which are shown in equation 5.

$$\alpha_t = \alpha_{electrionic} + \alpha_{atomic} + \alpha_{dipolar} \qquad (5)$$

shows the net polarization where the $\alpha_{electrionic}$, the electronic polarization, arises from the realignment of the electrons in a nucleus molecule; α_{atomic}, the atomic polarization, results from the relative displacement of nuclei due to unbalance distribution of charge; and $\alpha_{dipolar}$, the dipolar polarization, results from the reorientation of the permanent dipole by the electric field. The oscillating field produced in the microwave region triggers a certain response time that are allocated to the frequency of the radiation. The time scales for the electronic and atomic polarization are much faster than the microwave frequency used and therefore have no contribution to the observed dielectric effect. However, the time scales for the dipolar

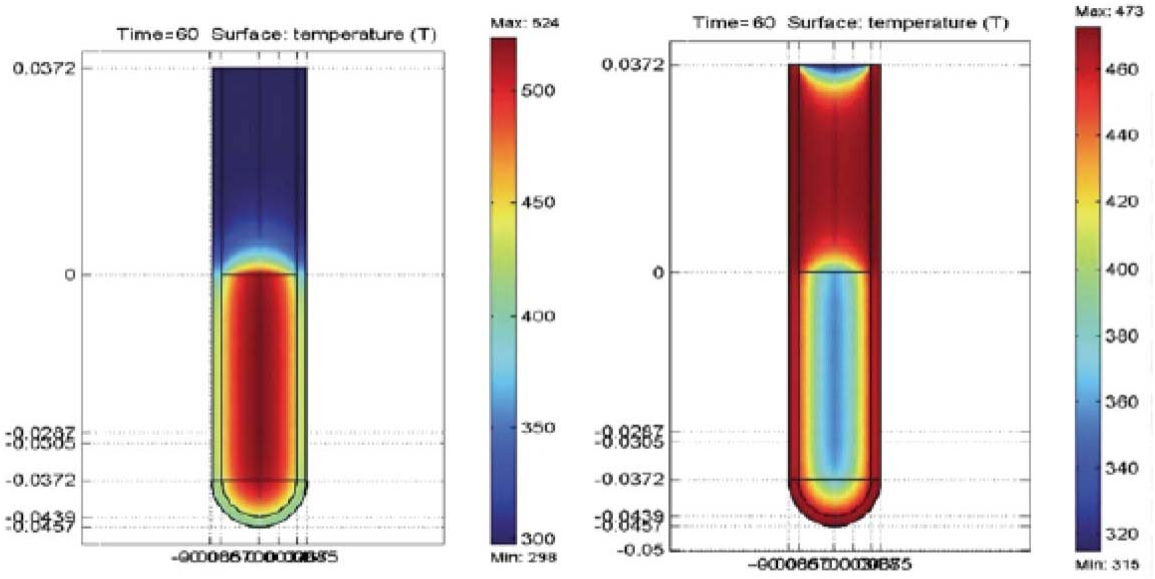

Figure 1.6. Thermal Scan of Microwave Reaction

A thermal scan of how the reaction is heated in the microwave reactor (left) and by conventional round bottom heating. (Image taken from Ref. 35)

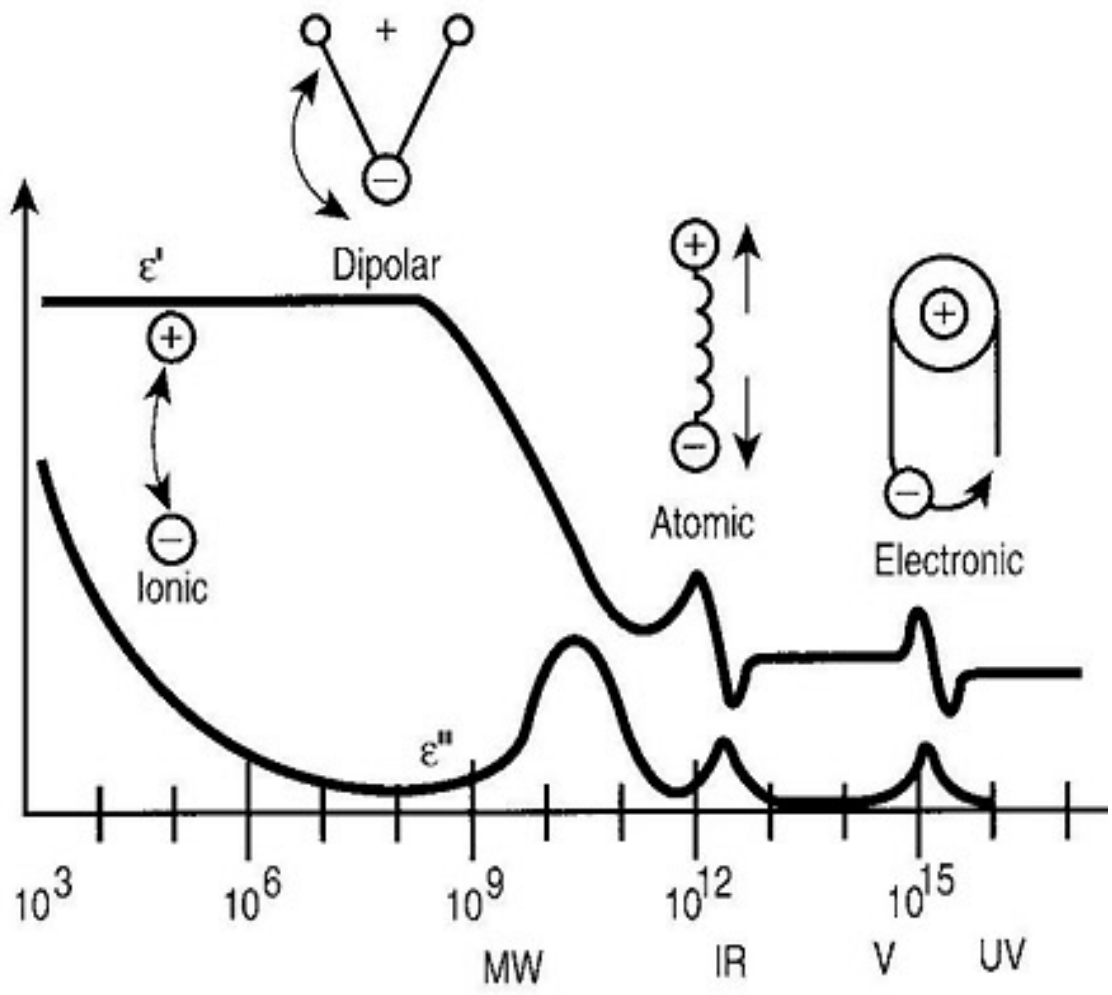

Figure 1.7. Dielectric Spectrum with Different Frequencies

Dielectric spectrum indicating the molecular and atomic processes that occurs in different frequency regions. (Image taken from Ref. 33)

polarization are very comparable to the microwave frequencies and contribute the majority of the observed dielectric effect.[42]

The dipolar polarization is due to the alignment of a static dipole with the oscillating field. The ability to polarize a dipole depends on the dipole moment of a material as well as the frequency of the applied electromagnetic field. At very low frequencies, the polarization of the static dipole keeps in constant alignment with the microwave producing some heat but not very efficient heating. In addition, at very high microwave frequencies, the electric field rotates so fast that the dipole reorientation does not have an opportunity to re-align before the field is back in alignment with the molecules dipole. In this case, there is very little to no heat observed since there is no rotation to create any interactions in the solution. In certain microwave frequencies, the dipolar molecule experience intense torque in their rotation caused by the slight lag in polarization with the microwave field. The optimization of this torques produces the maximum amount of interactions between molecules, which through friction produce intense local heating around the rotating molecules. The conversion of absorbed microwaves into heat in a dielectric (i.e. nonconductive) material is described macroscopically through the dielectric continuum model in equation 6. In the dielectric continuum model, the bulk permittivity of a material is expressed in its complex form:

$$\varepsilon = \varepsilon' - i\varepsilon'' \qquad (6)$$

where ε' is the dielectric constant and the complex component, ε", is the dielectric loss. Both the real and imaginary components of the permittivity are frequency dependent with the dielectric constant representing the transmission of the radiation through the material and the complex component representing its absorption. This component can be seen in the schematic dielectric spectrum for an insulator material shown in Figure 1.7. In the visible, UV and infrared regions of the spectrum, the peaks in the complex component represent the absorption of radiation to excite electronic and vibrational states of a molecule respectively. As such, the imaginary part of the dielectric constant is related to the extinction coefficient of the optical transitions.

1.5 Conclusion

The thesis outlines our investigation of using microwave selective absorption to control QD growth processes. We have shown the ability to selectively trigger nucleation events

(Chapter 2 and 3), controllably form multiple QD sizes (Chapter 4) and using K_{sp} generate specific crystal motifs. (Chapter 5)

CHAPTER 2 MICROWAVE SYNTHESIS OF CDSE AND CDTE NANOCRYSTALS IN NON-ABSORBING ALKANES

Controlling nanomaterial growth via the "specific microwave effect" can be achieved by selective heating of the chalcogenide precursor. The high polarizability of the precursor allows instantaneous activation and subsequent nucleation leading to the synthesis of CdSe and CdTe in non-microwave absorbing alkane solvents. Regardless of the desired size, narrow dispersity nanocrystals can be isolated in less than 3 min with high quantum efficiencies and elliptical morphologies. The reaction does not require a high temperature injection step and the alkane solvent can be easily removed. In addition, batch to batch variance in size is 4.2 ± 0.14 nm for ten repeat experimental runs. The use of a stopped-flow reactor allows near continuous automation of the process leading to potential industrial benefits.

2.1 Introduction

Over the past decade, there has been a vast amount of work to optimize the synthetic methodology for the II-VI (CdS[43], CdSe[44], CdTe[45]) nanocrystalline semiconductors, leading to commercially available materials and applications for a wide range of technologies.[46,47,48] The synthetic methods for preparation of nanocrystals have improved by optimizing the reagents, ligands, solvents, and the general approach.[49,50,51] The initial synthetic breakthrough in the control of size dispersity by Murray[52] led to the recent results demonstrating the use of non-organometallic precursors for preparation of CdSe based on CdO or Cd stearate by the research group of Peng.[53] Breakthroughs by Alivisatos[54], Hyeon[55], El-Sayed[56], and Peng[57] have shown remarkable control over shape and morphology of the nanocrystals. Cao et al.[58] and Hyeon[55] have demonstrated the ability to produce nanomaterials without the hot injection step allowing the nanocrystals to be efficiently prepared. These routes all have demonstrated the ability to produce nanocrystals of high quality as measured by emissive quantum efficiency and size dispersity with reactions that can be reproduced universally at a macroscopic level for a given material (narrow size dispersity with defined crystallinity); however, at the microscopic level the materials are not identical batch-to-batch (identical size, identical shape) and may vary as a function of heating rate, mixing rate and concentrations. In other words, the size and aspect ratio

(shape) vary with each reaction reminiscent of a polymer chemistry problem; however, one can isolate nearly the same size if the absorption is actively monitored.[59]

The reaction mechanism for nanocrystal growth implies that the growth behavior should be microscopically controllable if the reaction mechanism including contributions from precursor activation, nucleation, and growth are controlled.[60] However, variance in heating rate, cooling rate, thermal gradients in the reaction, and differences in injection rate lead to size and shape variation from batch-to-batch. We have demonstrated that the use of dielectric (microwave) versus convective heating is advantageous to controlling many of the above heating variances that impact material dispersity.[61,62] In our earlier study, we developed microwave chemistry for nanocrystals showing rate acceleration for InP, InGaP, and CdSe by addition of ionic liquids or use of ionic precursors. However, organic chemists have shown not only rate improvements, but more importantly an exquisite synthetic control over the product formation can be achieved by selectively heating a polar transition state or precursor in the microwave (MW) to allow a selected product to be isolated. The selectivity offered by MW heating demonstrates the "specific microwave effect."[63] This is defined as the ability to selectively heat molecular precursors that are highly polarizable in the presence of molecules that are less polarizable.[60a] The specific microwave effect is advantageous in controlling the batch-to batch variation in nanocrystal production, particularly if selective heating allows the nucleation event to be specifically triggered by the MW and there after allowing growth to proceed.

The use of MW irradiation has several unique advantages over convective heating: 1) selective activation of the target precursor to initiate nucleation and subsequent growth, 2) reproducibility from batch to batch, 3) the convenience of a non-injection reaction, and 4) a stopped-flow near-continuous nanocrystal synthesis. The demonstration of the selective triggering of nanocrystal nucleation and growth by choosing a molecular chalcogenide source to be the only reactant with significant MW absorption, allows the manifestation of the "specific microwave effect" for nanocrystal preparation. The chalcogenide precursor selectively absorbs the microwave energy, which appears to result in the instantaneous nucleation and growth upon microwave irradiation. The nanocrystals can be grown rapidly and controlled by a combination of reactant concentration and power, while size is dictated by the reaction temperature. Selective absorption by the chalcogenide results in the isolation of elliptical (aspect ratio 1.2) CdSe and elliptical (aspect ratio 1.7) CdTe in the size range 2.5 - 8 nm. The materials are prepared in less

than 3 min with a typical out of reactor dispersity of 6% for CdSe (12% for CdTe), but more importantly a standard deviation in size for the CdSe (CdTe) reaction of 4.2 $\pm$ 0.14 nm (4.25 ± 0.3 nm) from batch-to-batch (averaged over ten individual runs). It is important to note that the size dispersity reflects the batch composition without attempting to size select the materials via selective precipitation. Although Cao[58] has demonstrated non-injection routes for convectively grown CdSe and CdTe nanocrystals, the MW reaction can utilize a similar approach, but via the use of a pump, the reactants can be continuously delivered. This allows application of the MW to a stopped-flow synthetic technique allowing continuous preparation of the material at a rate of 650 mg/h. The reproducibility from batch to batch of the method and the ability to continuously synthesize nanocrystals is fascinating, particularly for the potential automation of synthesis of these materials.

2.2 Experimental

2.2.1 Static reactions.

Synthesis of CdSe. Nanocrystalline CdSe was prepared by adaptation of the reported method of Peng et al., with the substitution of alkane solvents (pentane, heptane, octane, decane), cadmium stearate (CdSA), and microwave based dielectric heating.[44a] Briefly, stock solutions of CdSA and TOPSe were prepared by dispersing CdSA (1.0 mmol, 679.36 mg) into 20 mL of an alkane of choice by sonication, while a 1 molar solution of TOPSe was prepared under argon using Se powder (0.01mol) dissolved in 10mL of TOP.[54] The reaction mixture was added to a 10 mL reaction vessel under ambient conditions consisting of a 1:5 molar ratio of cadmium to selenium stock solutions with HDA (hexadecylamine) added in an equimolar ratio to TOP. The reaction mixture was heated in the microwave cavity to a temperature of 240°C during a 30s ramp period at a power of 300W. The mixture was then allowed to react for 30s at 240°C and immediately cooled to room temperature (< 1min) using forced air cooling. Isolation of the nanocrystals was carried out by standard re-precipitation methods. Specifically, the materials were re-suspended in minimal amounts of toluene follow by the addition of excess amounts of methanol producing a dual phase system. Afterwards, butanol is added to the solution to precipitate the nanocrystals. The reaction yields elliptical (aspect ratio of 1.2) CdSe nanocrystals with 6% size dispersity, 35 ± 5 mg of sample per 4 mL reaction volume.

Synthesis of CdTe. CdTe is prepared analogously to the reaction above, with the exception that a 25 mM CdSA in decane stock solution is prepared. The Te stock solution (1 molar TOP:Te) is

prepared under argon by heating Tellurium powder (0.005mol) in 10mL of TOP at 100°C for 24h. The stock solutions were mixed in a 1:1 molar ratio with HDA (equimolar to the TOP). This reaction mixture is heated in the microwave to 220°C, at 300W, and allowed to react for 5s. The reaction was immediately cooled to room temperature. Isolation of the nanocrystals was carried out by standard re-precipitation methods. The CdTe reaction yields 25 ± 5 mg of elliptical (aspect ratio of 1.7) nanocrystals with 12 % size dispersity per 4 mL reaction volume.

2.2.2 Stopped-flow Synthesis

The static MW synthetic method can be adapted to a stop-flow pump system by substitution of octylamine for HDA in the Cadmium stock solution, in order to dissolve the CdSA dispersion. The TOPSe stock and CdSA stock are delivered into the reaction chamber form separate sources to fill a 50mL reaction volume, and heated to 190°C at 300W for 40min. Longer reaction times are needed due to the pathway of the solvent scattering the microwave energy and a thicker reaction vessel. The reaction mixture is pumped out to a sealed vessel under Argon. Collection of the nanocrystals is achieved by precipitation using standard methods. Continuous transfer of stock and product can be carried out in the Stopped-Flow allowing continuous production of a target nanocrystal. The yield of nanocrystals is ~ 650 mg per hour.

2.3 Results and Discussion

2.3.1 Nucleation and Growth in the Microwave

In the field of microwave (MW) chemistry, much effort has focused on the tailoring of the reactants' polarizability differences to produce a desired product via the specific microwave effect. The highest polarizable material will selectively absorb MW energy in the presence of poorly absorbing materials and solvents. The absorption of MW energy by a polarizable reactant provides the requisite energy to overcome potential activation barriers associated with the transition state or reactive intermediates. While the specific microwave effect is prolific in the literature,[60,64] proving the effect is very challenging. In order to take advantage of the specific microwave effect for nanocrystal synthesis, particularly for high throughput synthesis, the reactive precursors must be strong microwave absorbers, while the solvent must be non-absorptive. (Figure 2.1) The excess energy controlled by the solvent allows for continuous

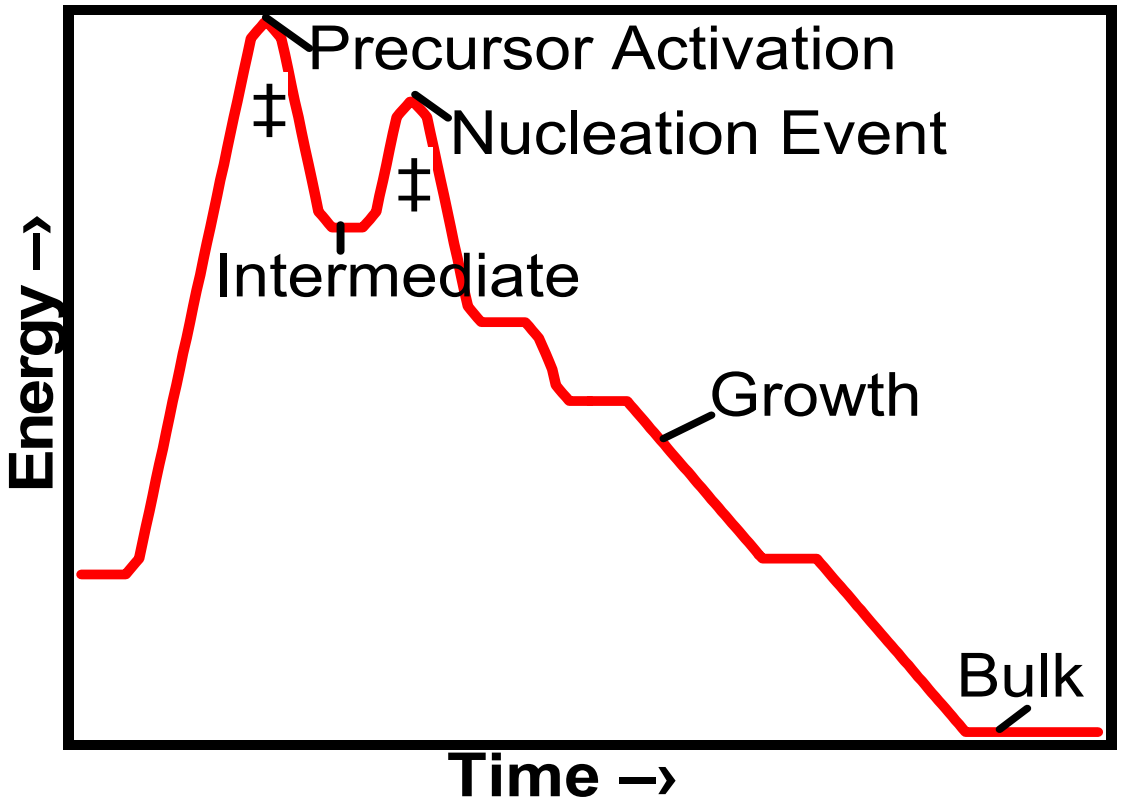

Figure 2.1. Reaction Coordinate of Nanocrystal Formation

Schematic diagram illustrating the reaction pathway for nanocrystal formation from a precursor.

growth resulting in a reverse thermal gradient and eliminates multiple nucleation events that can lead to loss of material dispersity.

The advantage of the "specific microwave effect" for nanocrystals can be understood by considering the mechanism for the formation of the nanocrystal.[60,65b] In the simplest projection of a rather complex reaction mechanism, the primary steps in a nanocrystal reaction are precursor activation, nanocrystal nucleation, and passivant controlled atom addition onto the growing nanocrystal facets (Figure 2.1). In the case of nanocrystal growth, the selective heating translates into a controlled nucleation event, thus eliminating the need for a high temperature injection step. Typically the limiting step for a nanocrystal growth is the first two events (activation and nucleation),[60,62] depending on which step requires more energy. A critical reaction size must be reached to overcome the transition state barrier for activation and/or nucleation to occur before proceeding to product. While the rate of addition of the atoms to the surface is dependent on diffusion and thermodynamics, the rate of nanocrystal growth is controlled by reaction temperature and concentration, as well as the solubility product of the reactants and the surface energy of the binary semiconductor. Pressure can also play a role by enhancing products by (small $\Delta V‡$) or inhibiting (larger $\Delta V^{‡}$) reaction rates depending on the volume at the transition state, $\Delta V^{‡}$. Nucleation theory predicts that a critical crystallite size must be achieved prior to sustained nanocrystal growth. Gamelin, et al. has demonstrated the applicability of nucleation theory to describing nanocrystal growth.[66] The nucleation event is a kinetic problem, where the rate of growth must exceed the rate of dissolution for nanocrystal nucleation to occur.[63] The nucleation transition state is influenced by the chemical activity of the precursor, as shown by Peng[63,67] and Cao[58] and can therefore be used to control the nucleation event by introducing a barrier to nucleation. For a lyothermal reaction, the energy required for nucleation is provided indirectly through convective heating of the precursors via solvent heating. To achieve controlled growth after nucleation, lyothermal methods rely on induced cooling upon injection of the precursors. For a convective reaction, the subsequent steps are dictated by precursor activity.

A higher level control can be achieved in a microwave reaction if the energy barrier is larger for the precursor activation than the nucleation event. In this regime, the specific microwave effect can be utilized to drive a reaction by selectively activating a desired precursor to initiate nucleation. Since the precursor is only activated under microwave irradiation (the

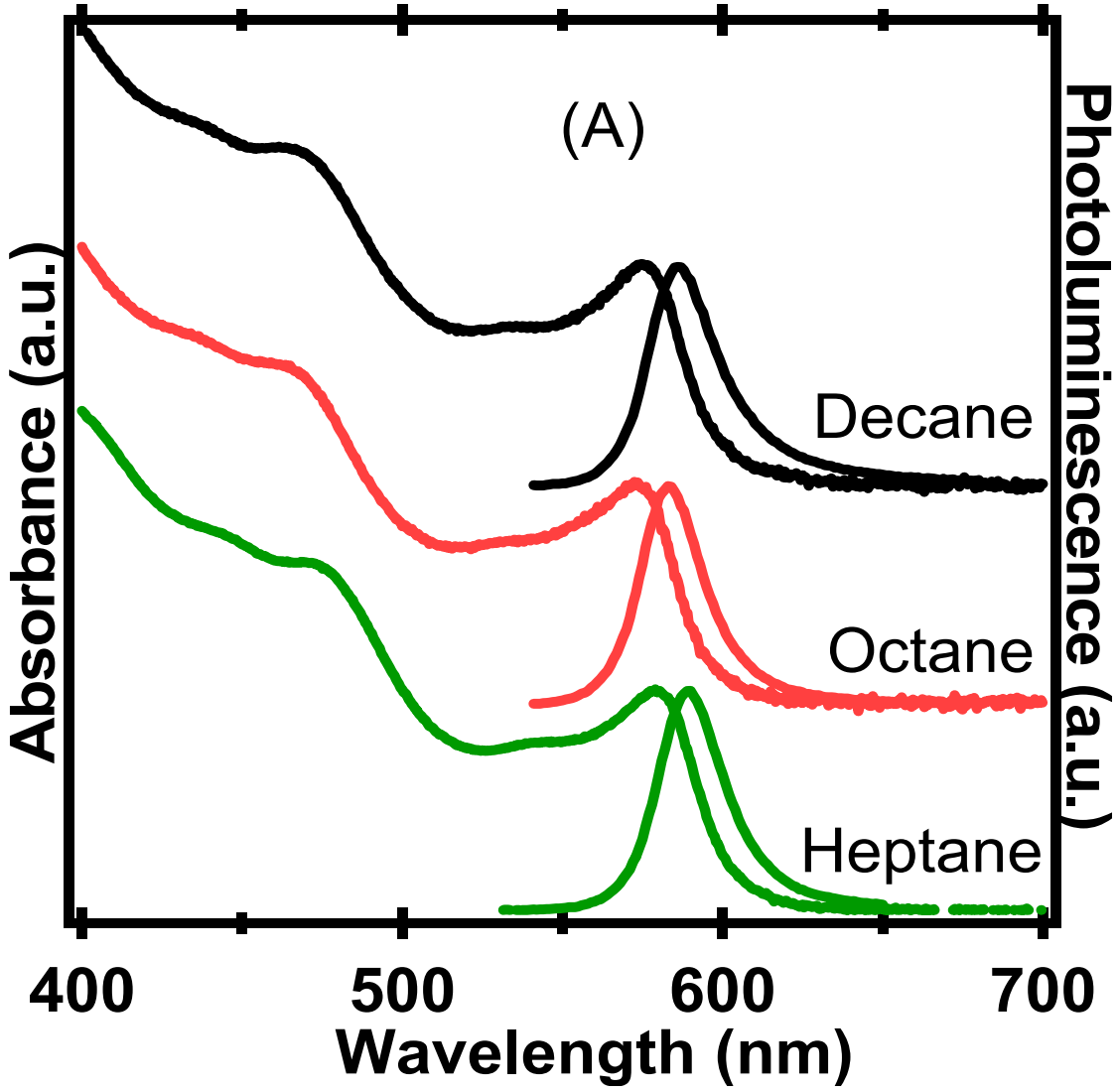

Figure 2.2A. Abs/EM CdSe in Different Solvents

Optical absorption and photoluminescence of A) CdSe using solvents of different alkyl chain lengths. CdSe was grown at 240°C for 30s with the power set to 300W.

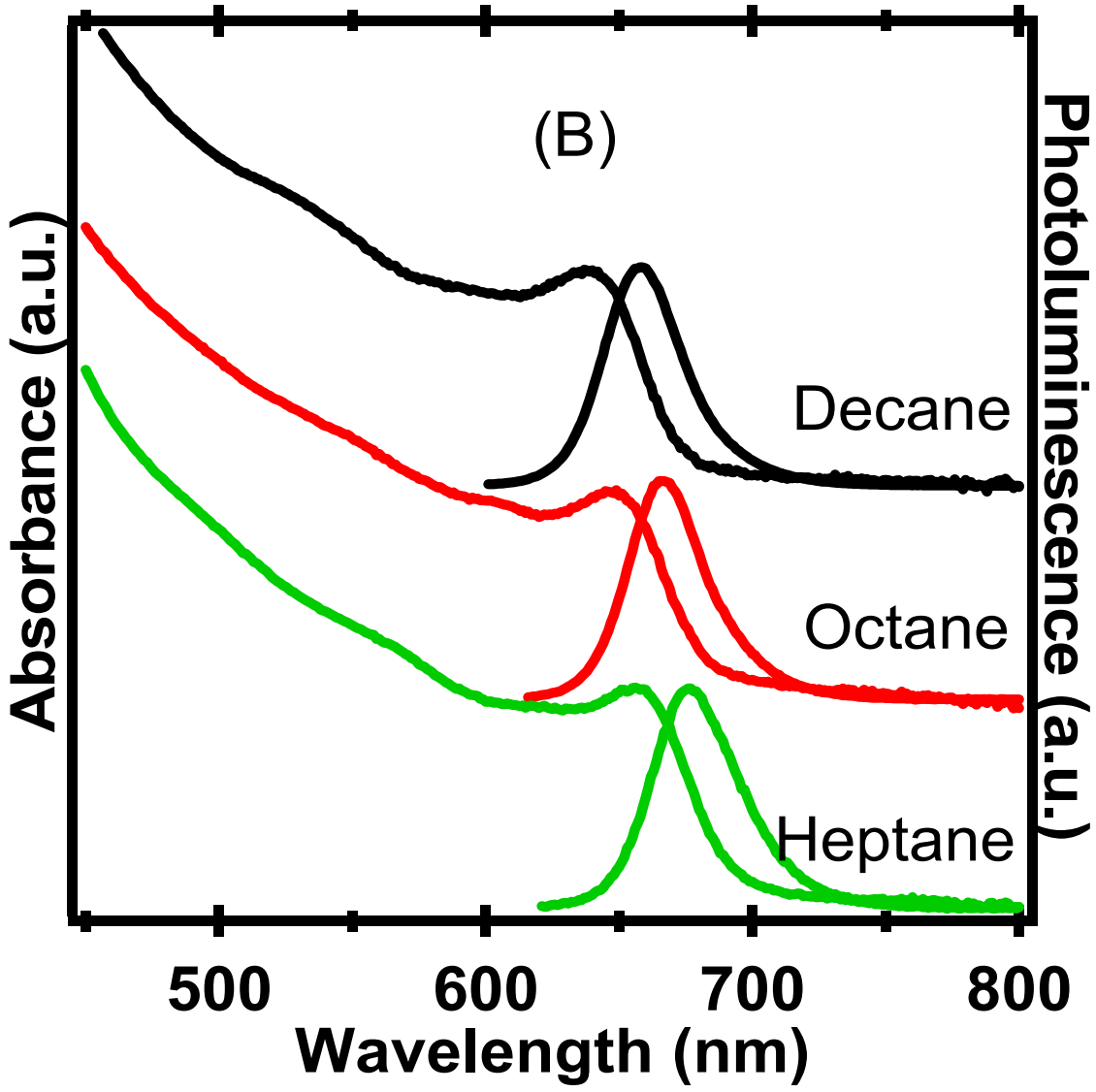

Figure 2.2B. Abs/EM CdTe in Different Solvents

Optical absorption and photoluminescence of B) CdTe using solvents of different alkyl chain lengths. CdTe was grown at 220°C for 5s with the power set to 300W.

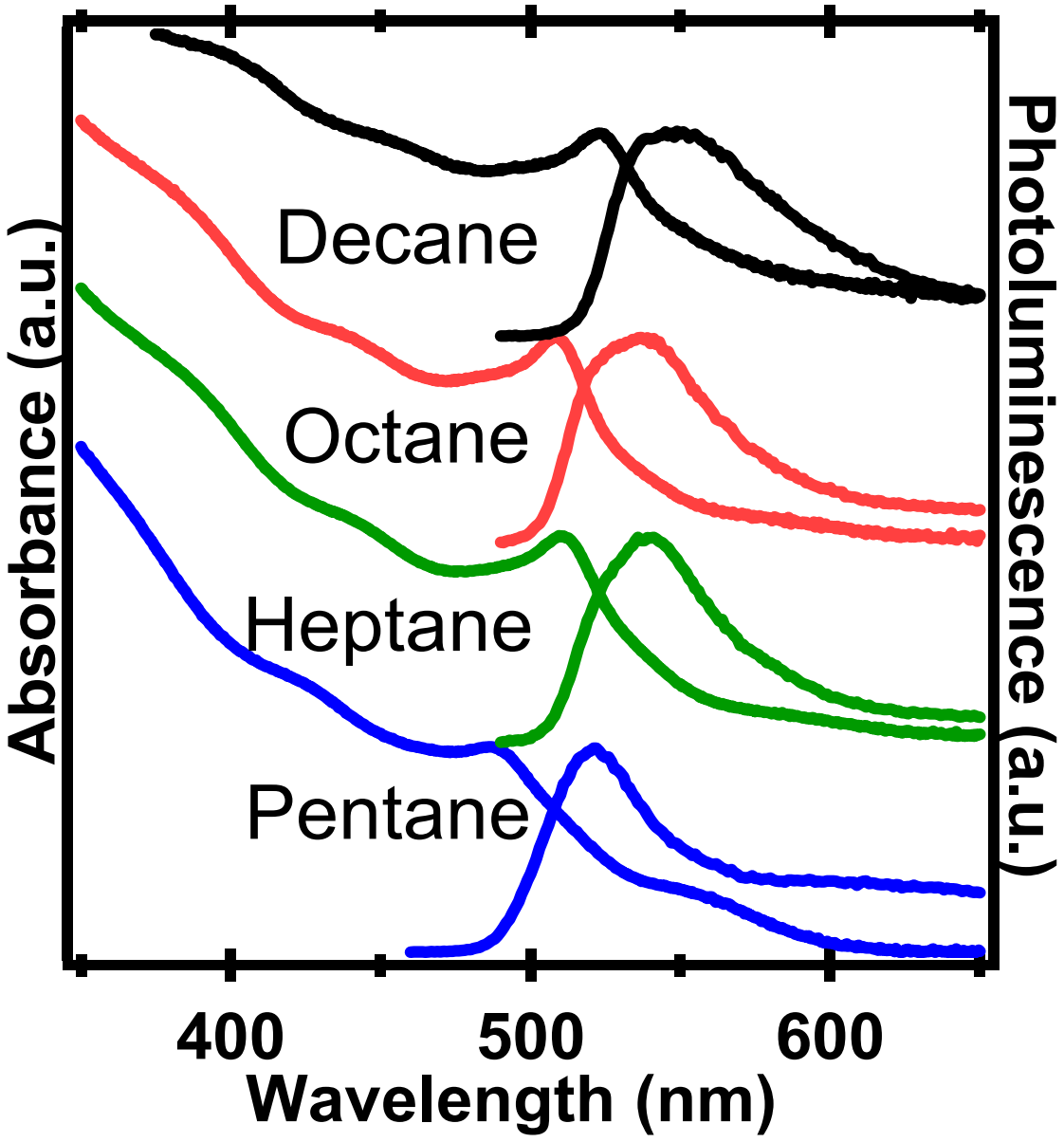

Figure 2.3. Abs/Em CdSe in Different Solvents at 180° C

Microwave synthesis of CdSe grown at 180°C in various alkane solvents. This figure shows the ability to use higher volatility solvent such as pentane in lower temperature reactions.

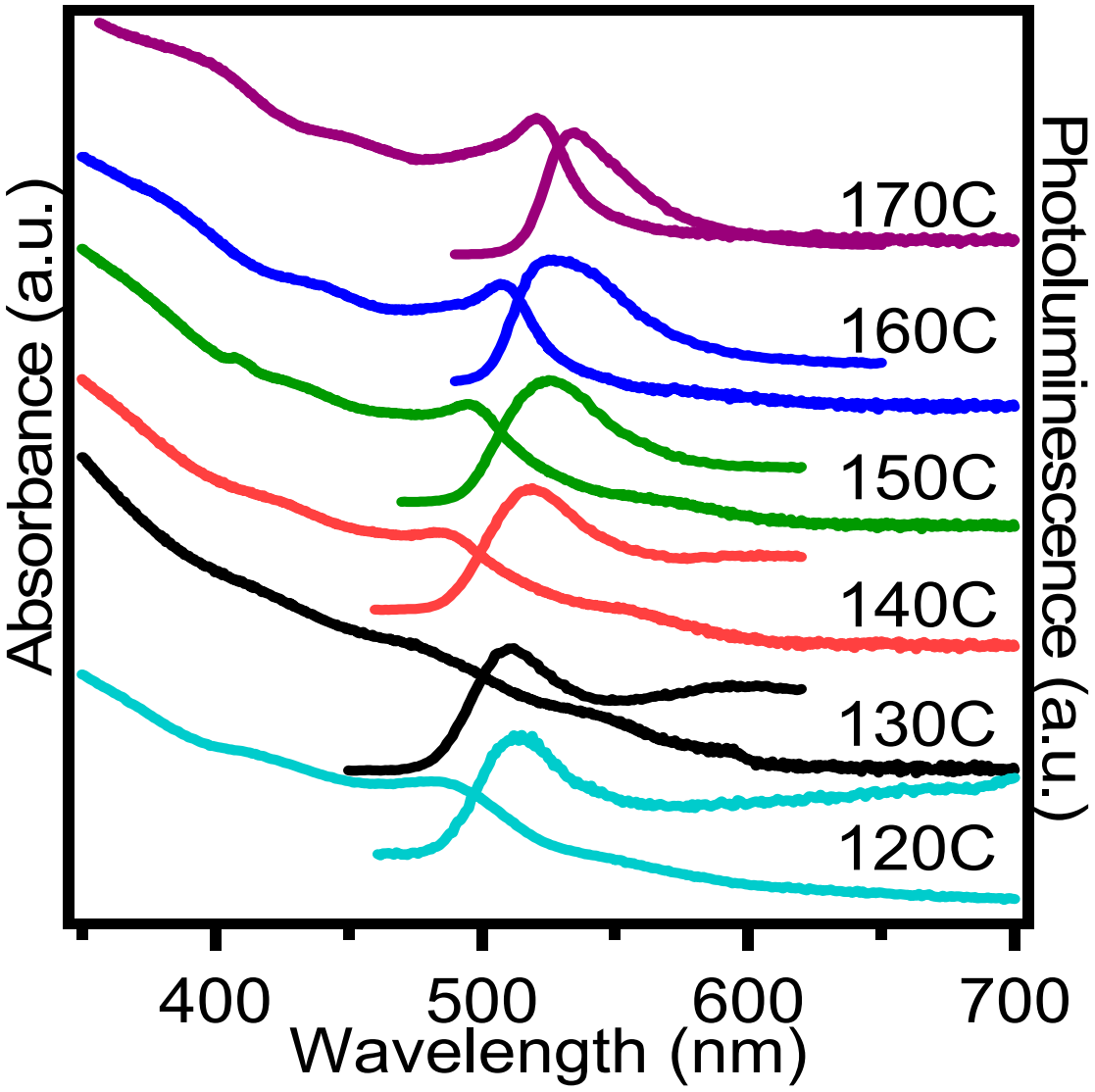

Figure 2.4. Abs/Em Low Temperature Synthesis of CdSe

CdSe synthesized at low temperature using 50mM Cd stearate and TOPSe precursor solutions with the time set at 30s.

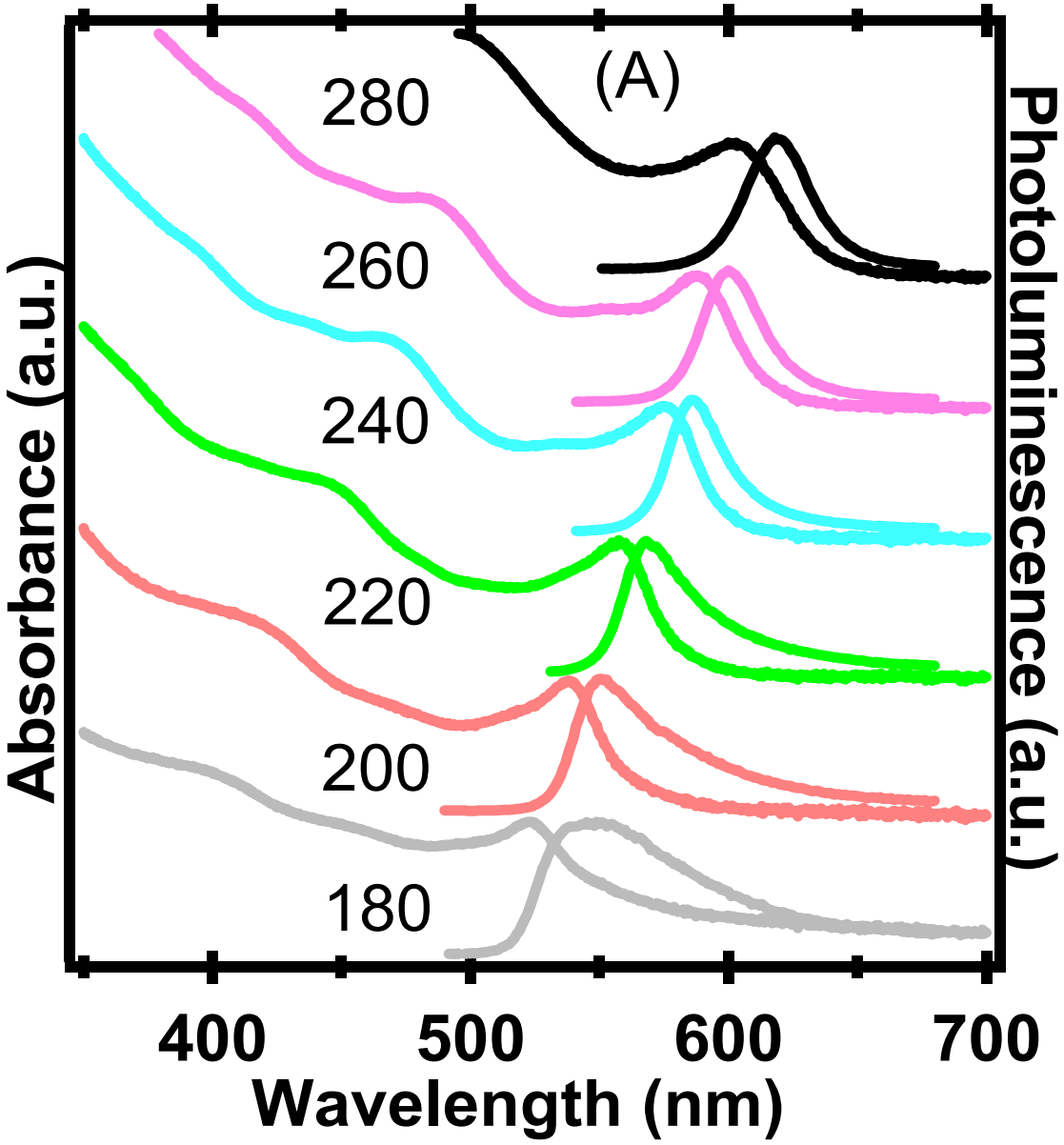

Figure 2.5A. CdSe Temperature Dependent Growth

Optical data for temperature (°C) dependent growth of CdSe. The reaction conditions fixed power at 300W and time at 30s.

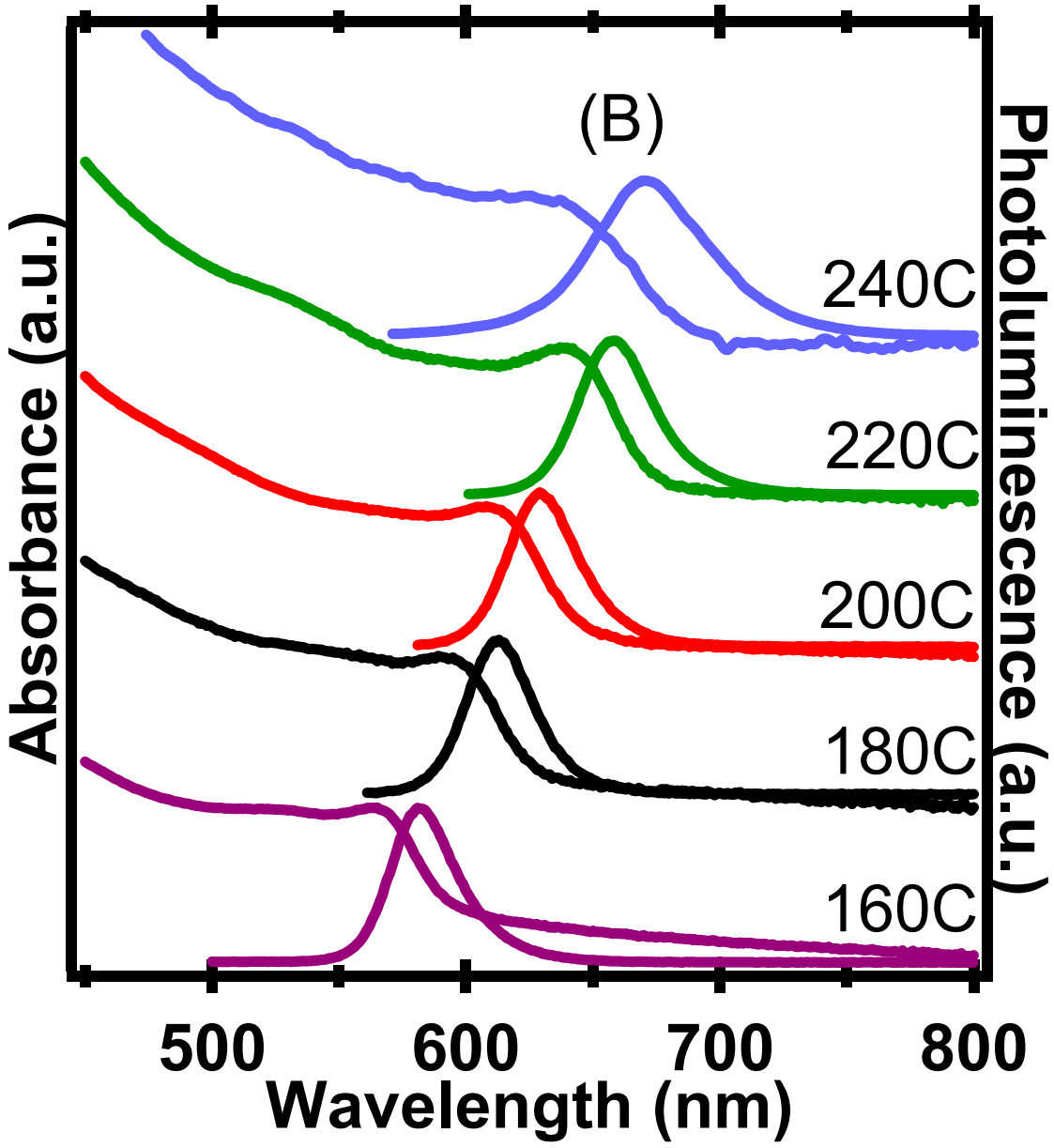

Figure 2.5B. CdTe Temperature Dependent Growth

Optical data for temperature (°C) dependent growth of CdTe. The reaction conditions fixed power at 300W and time at 5s.

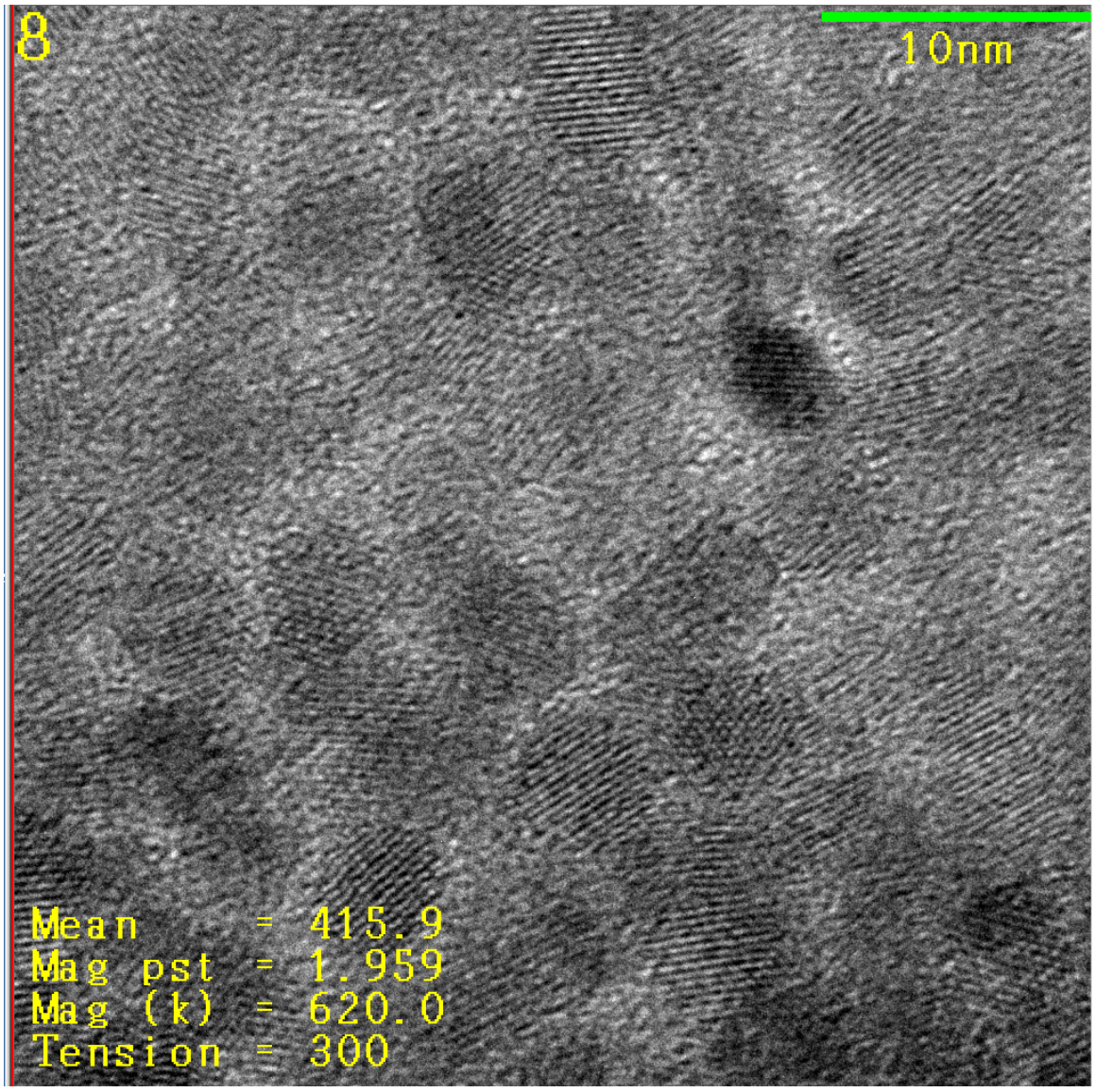

Figure 2.6A. TEM CdSe 5.8 nm

TEM image of 5.8 nm CdSe nanocrystals. The image is taken at high magnification on a high resolution (Tietz Tem-Cam F415 slow scan CCD). The TEM image was collected on 400 mesh holey-carbon on copper with formvar removed using a 300 KeV field emission gun. The microwave power was set to 300W and allowed to fluctuate in order to optimize the temperature.

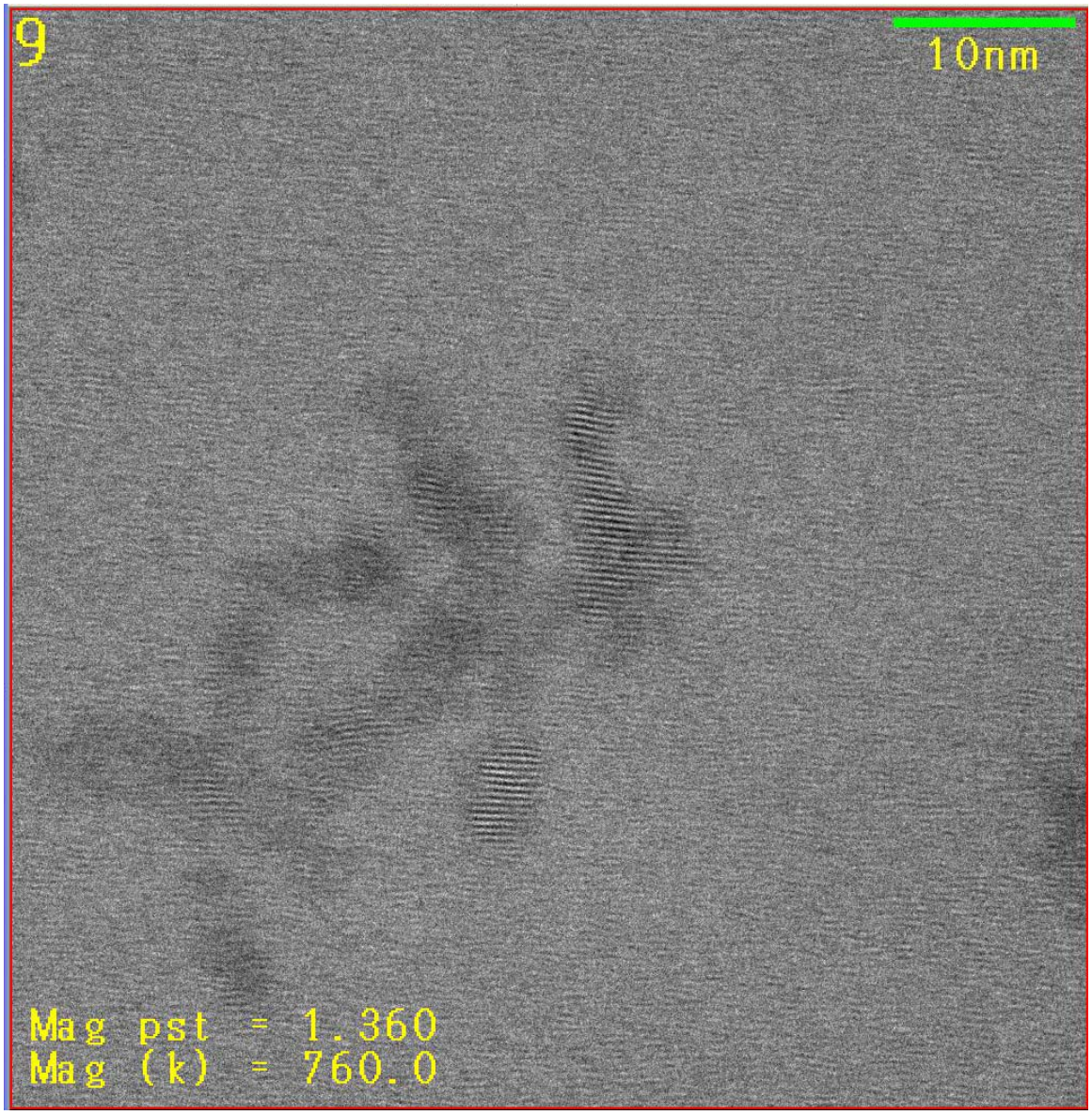

Figure 2.6B. TEM CdTe 4.3 nm

TEM image of 4.3 nm CdTe nanocrystals. The image is taken at high magnification on a high resolution (Tietz Tem-Cam F415 slow scan CCD). The TEM image was collected on 400 mesh holey-carbon on copper with formvar removed using a 300 KeV field emission gun. The microwave power was set to 300W and allowed to fluctuate in order to optimize the temperature.

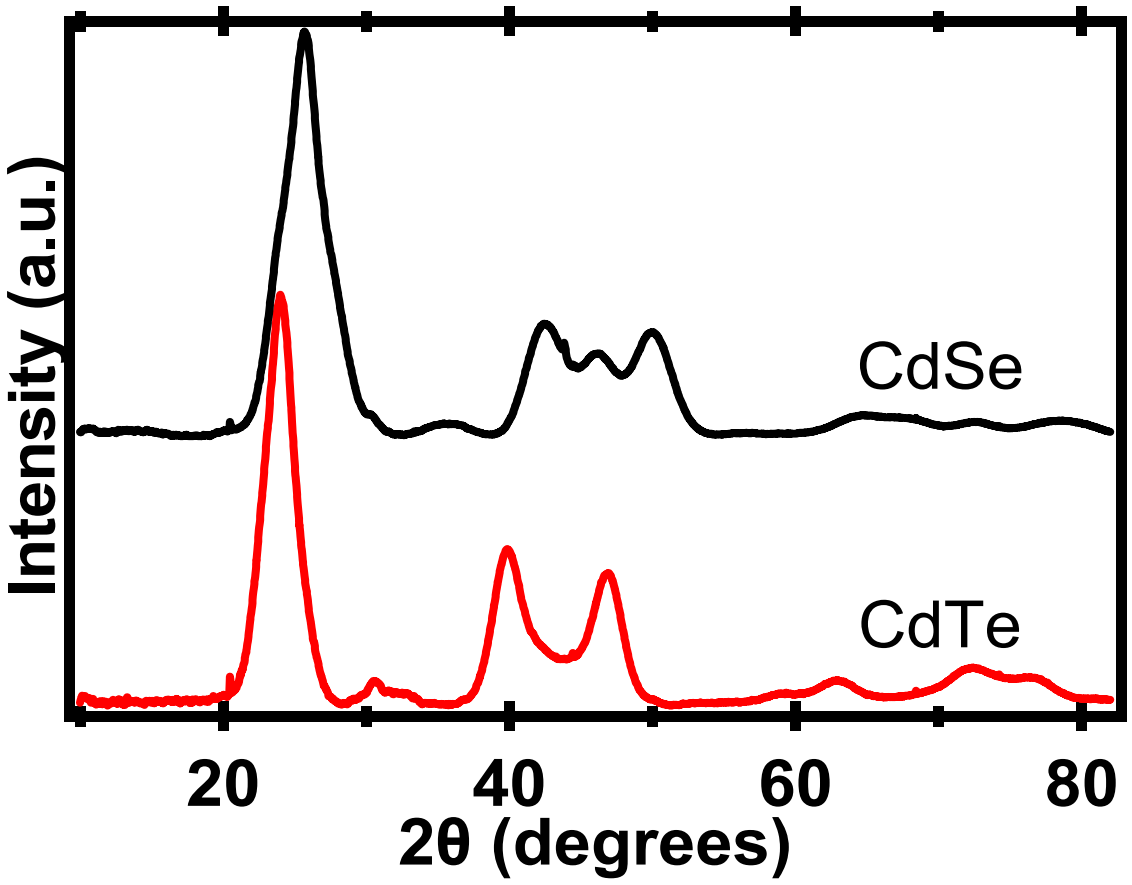

Figure 2.7. pXRD CdSe/CdTe

Powder X-ray diffraction pattern of CdSe and CdTe nanocrystals measured using Cu Kα. CdSe has hexagonal (Wurtzite) structure while CdTe displays the cubic (Zinc Blende) structure.

cleavage of the TOP-Se or TOP-Te bound),[68] the accessibility of the chalcogenide monomer to the growing nanocrystal is controlled by the MW cross-section. The MW absorption of the chalcogenide monomer results in a remarkable degree of control over the reaction path. This requires that the precursor is the dominant absorber in the reaction and the solvent acts merely as a reaction moderator to control the explosive growth. It is also important in controlling growth that the evolving nanocrystal is also a moderate MW absorber, to ensure the reaction is under thermodynamic control. In effect, the absorption of the MW energy is the on-off switch for the reaction.

2.3.2 Preparation of CdX (X = Se, Te) Nanocrystals.

In Figure 2.2, we demonstrate the ability to synthesize CdSe, and CdTe nanocrystals in non-polar, low boiling alkane solvents (decane, octane, heptane) in the microwave. CdSe and CdTe nanocrystals may also be prepared in pentane, (Figure 2.3) but lower reaction temperatures are required due to reactor pressurization limits, thus generating a smaller range of achievable nanocrystal sizes under the current microwave design (Figure 2.4). In addition, using this microwave technique, CdSe nanocrystals have been grown at temperatures as low as 120°C. (Figure 2.5) There is no observed dependence on the optical properties or growth behavior as a function of the alkane solvent (with the exception of pentane), although pressurization of the reaction in the microwave occurs when the boiling point of the solvent is exceeded.

The isolated nanocrystals are mostly elliptical (aspect ratio 1.2) and exhibit narrow size dispersities (6 % RMS in CdSe, and 12% RMS in CdTe) based on TEM analysis (Figure 2.6). The CdSe crystal motif is wurtzite, while the CdTe is zinc blende (Figure 2.7). Nanocrystal size and structure are verified by powder X-ray diffraction using the Scherer expression and verified through TEM. The materials exhibit well defined optical properties (linewidth, quantum yield) comparable to lyothermally grown materials and exhibit identical quantum efficiencies to materials grown by the traditional CdO lyothermal methods developed by Peng.[54] The absorption data in Figure 2.2 and 2.4 are for the isolated batch rather than a size-selectively precipitated reaction and the loss of the 1s-1p transition in comparison to the CdO grown materials we believe reflects a combination of the slightly larger polydispersity of the material, as well as the elliptical shape of the materials. The 1s-1p transition intensity, while a marker for monodispersity, is highly variable in the literature and as shown by Alivisatos[63b], Cao[58], and Ferreria[69] can be impacted by shape. A better measure of near monodispersity is the absorption

linewidth for the 1s-1s exciton. For the MW grown CdSe the linewidth is 27-28 nm for the batch, which compares well with the absorption FWHM for Pengs CdO grown with an absorption line width of 26-28 nm (Figure 2.8). For CdTe the absorption linewidth is broader (40 nm) consistent with the larger polydispersity of the sample.

In the microwave, the nanocrystal size is potentially influenced by reaction time, temperature and applied power. The reaction temperature is the most critical of these parameters as shown in Figure 2.3, where the PL profile is broadened at low T. The MW power (200 - 300 W, Figure 2.9) and reaction time (CdSe: 5s - 10m, CdTe 5s – 1m, Figure 2.10) do not influence material size, shape or quality. The quality of the materials is impacted if the ramp rate is altered; due to the fact nanocrystal growth occurs instantaneously in the reaction due to precursor activation and subsequent nucleation, while reaction temperature requires convective losses from the molecules to the solvent via thermal conduction and exhibits a lag in response.

Other factors that influence the final material include the rate of cooling, the absence of microwave power, and the presence of non-absorptive precursors.[60,70,71] Slow cooling from the reaction temperature to ambient conditions result in larger size dispersities. Such behavior is consistent with the domination of Ostwald ripening rather than MW precursor activation in the reaction once the MW power is removed. In the microwave, the presence of non-absorptive precursors or low microwave power also leads to large poly-dispersities and poor optical performance, presumably due to the slow heating and multiple nucleation events in the reaction.

2.3.3 Implication for Mechanism.

The enhanced reaction rates under MW irradiation may reflect either the control of the activation/nucleation step via selective heating with the excess energy leading to solvent heating or can effectively be a rapid solvent heating process leading to nucleation followed by an Ostwald ripening process. In Figure 2.11, a plot of the dependence on nanocrystal size is shown for two fixed points in the reaction parameter space, namely P = 300W, reaction time = 30s (blue) and P = 300W, T = 240°C (red).

Inspection of Figure 2.11 indicates that following nucleation the growth rate is linear with temperature, which is expected for a reaction under thermodynamic control where nanocrystal growth is determined by the diffusion of ions to the reactive nanocrystal surface. In the growth rate versus time plot a non-linear, exponential dependence is observed implying the reaction is first order. While this is unexpected for a convective reaction, where both cadmium and selenium

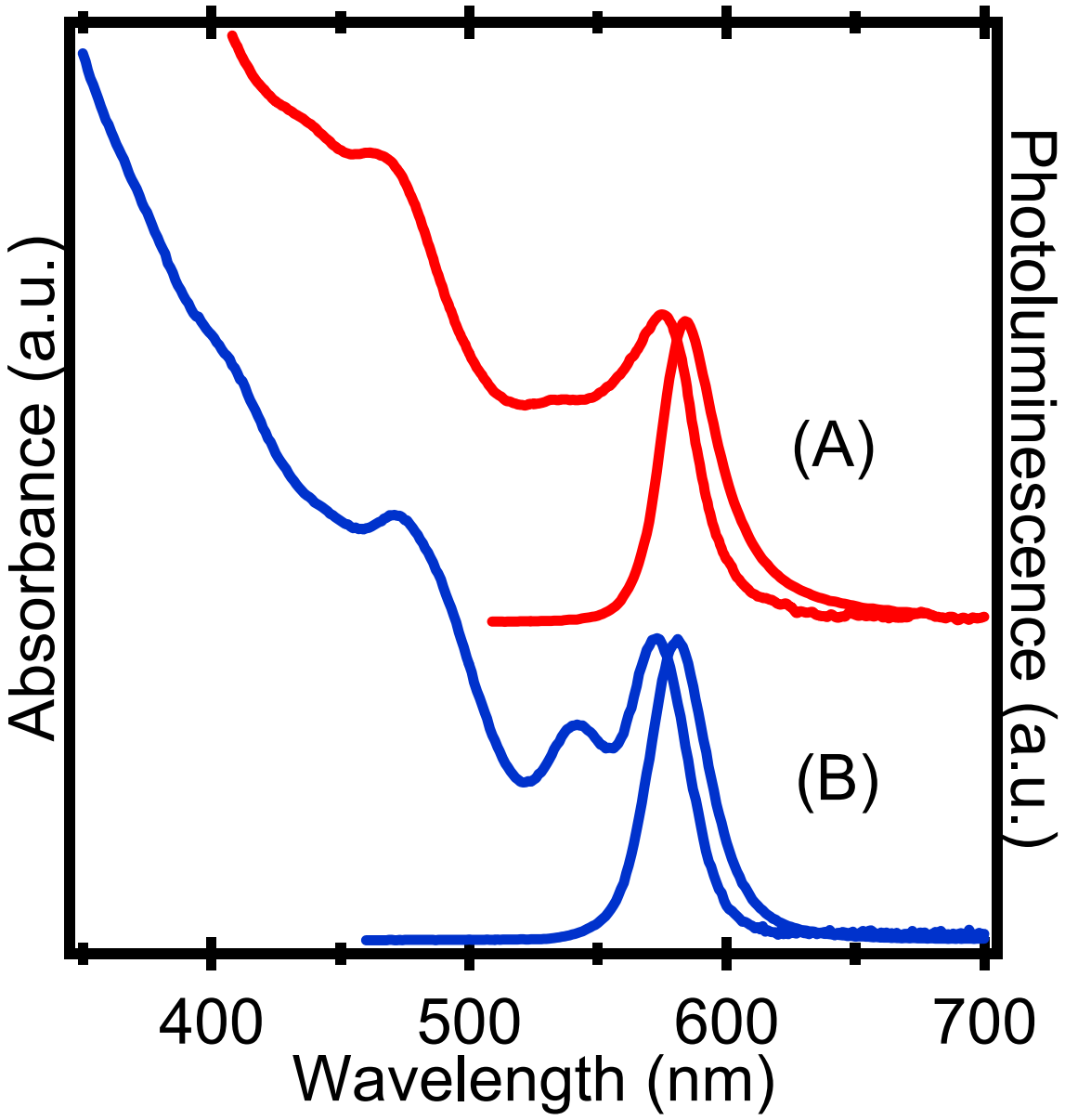

Figure 2.8 . Abs/Em Single Batch MW vs. CdO Grown Thermally

Comparison of (A) microwave grown HDA / TOP passivated CdSe from Cadmium stearate and (B) thermally grown HDA / TOP-passivated CdSe following the procedures for CdO (Peng[2a]). The comparison of the absorption spectra for identical CdSe sizes shows nearly identical FWHM for the first exciton (1s → 1s), but differences in the intensity of the 2nd exciton (1s→1p). The intensity difference may be due to dispersity or more likely the aspect ratio differences between the isolated materials.

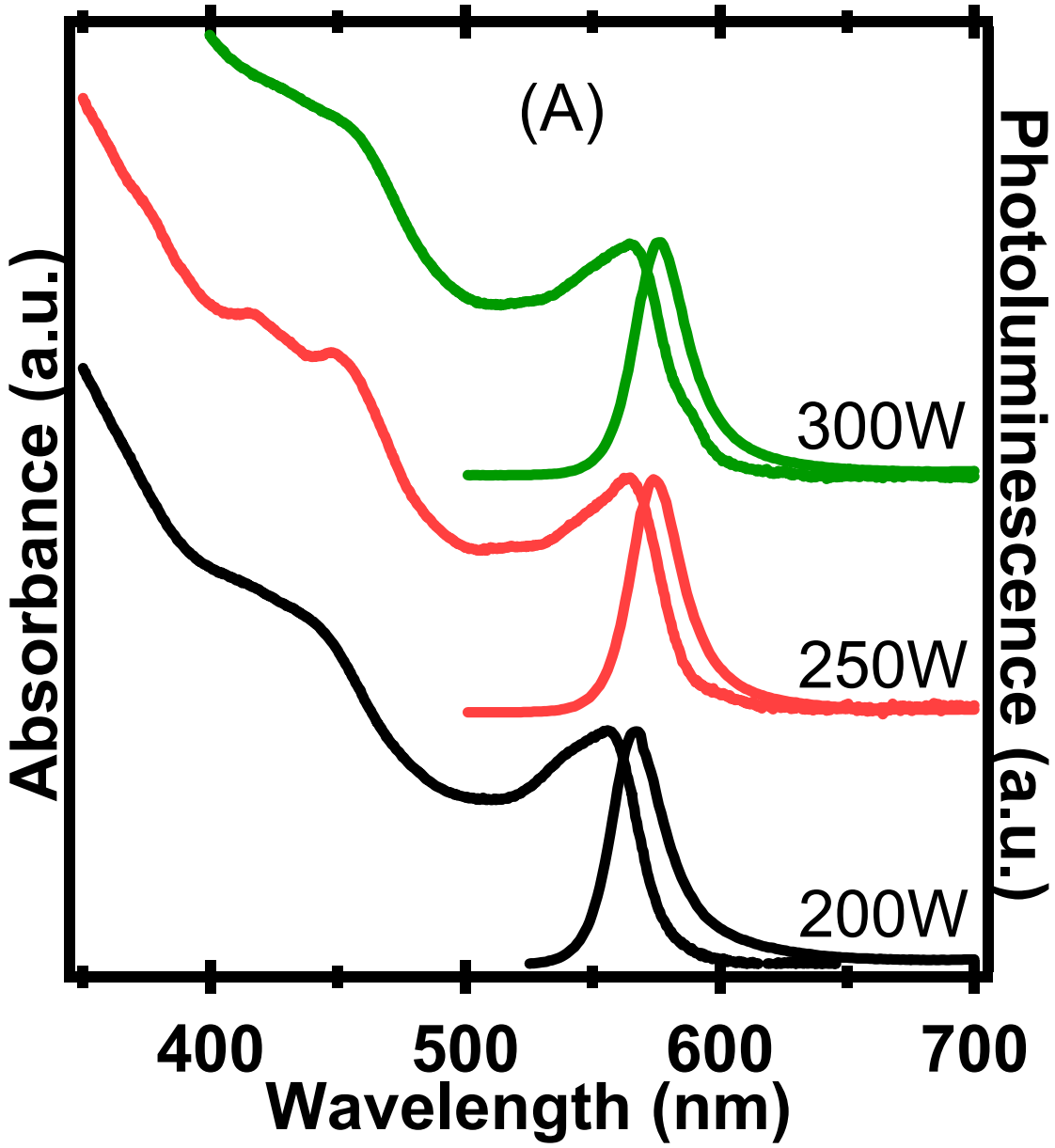

Figure 2.9A. CdSe Power Dependence

Absorption and PL spectra for CdSe carried out at different MW powers (200W, 250W, 300W) using decane as the solvent. The ramp rate was allowed to fluctuate as needed leading to larger size in the lower power reactions. The temperature was maintained at 220°C through use of active cooling. The reaction was allowed to run for 30s.

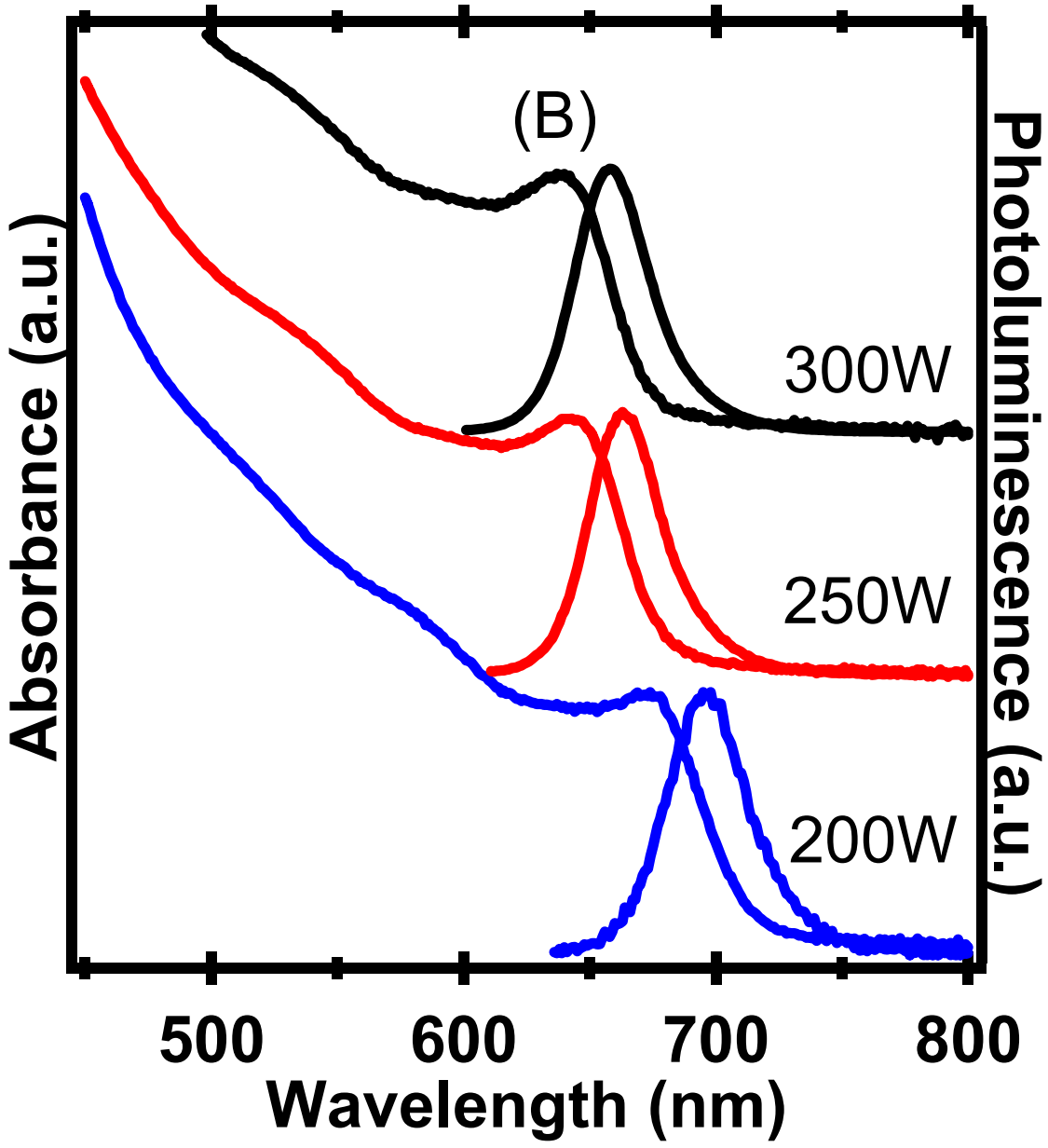

Figure 2.9B. CdTe Power Dependence

Absorption and PL spectra for CdTe carried out at different MW powers (200W, 250W, 300W) using decane as the solvent. The ramp rate was allowed to fluctuate as needed leading to larger size in the lower power reactions. The temperature was set to 220°C and because of the short reaction time and the lower polarizability of the P-Te bond. The power was maintained at a high level without active cooling being used.

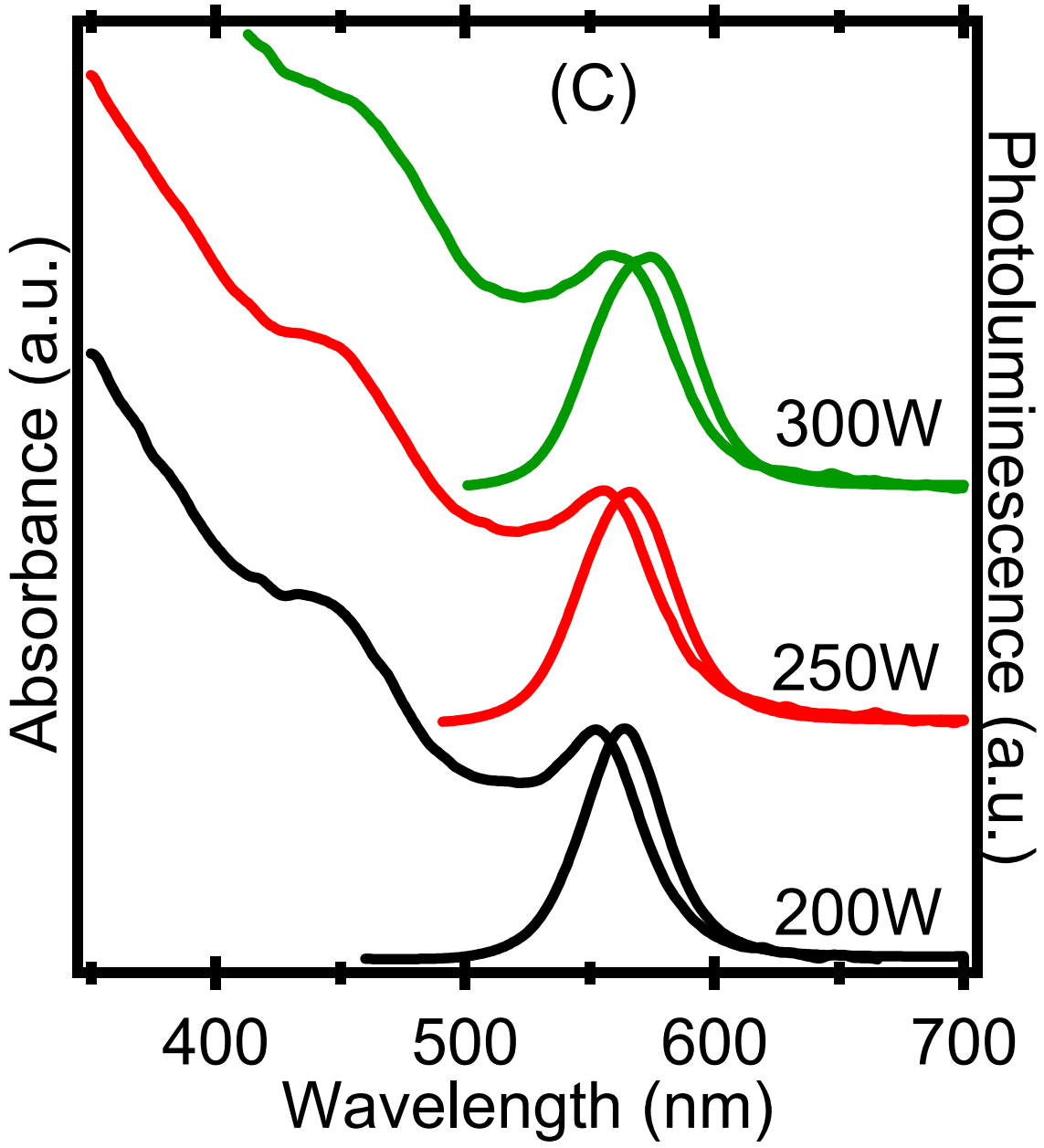

Figure 2.9C. CdSe Power Dependence w/ Fixed Heating Times

Absorption and PL spectra for CdSe carried out at different MW powers (200W, 250W, 300W) using decane as the solvent. The samples had fixed ramp times of 2 minutes and 5 minutes, respectively. The temperature was maintained at 220°C through use of active cooling. The reaction was allowed to run for 30s.

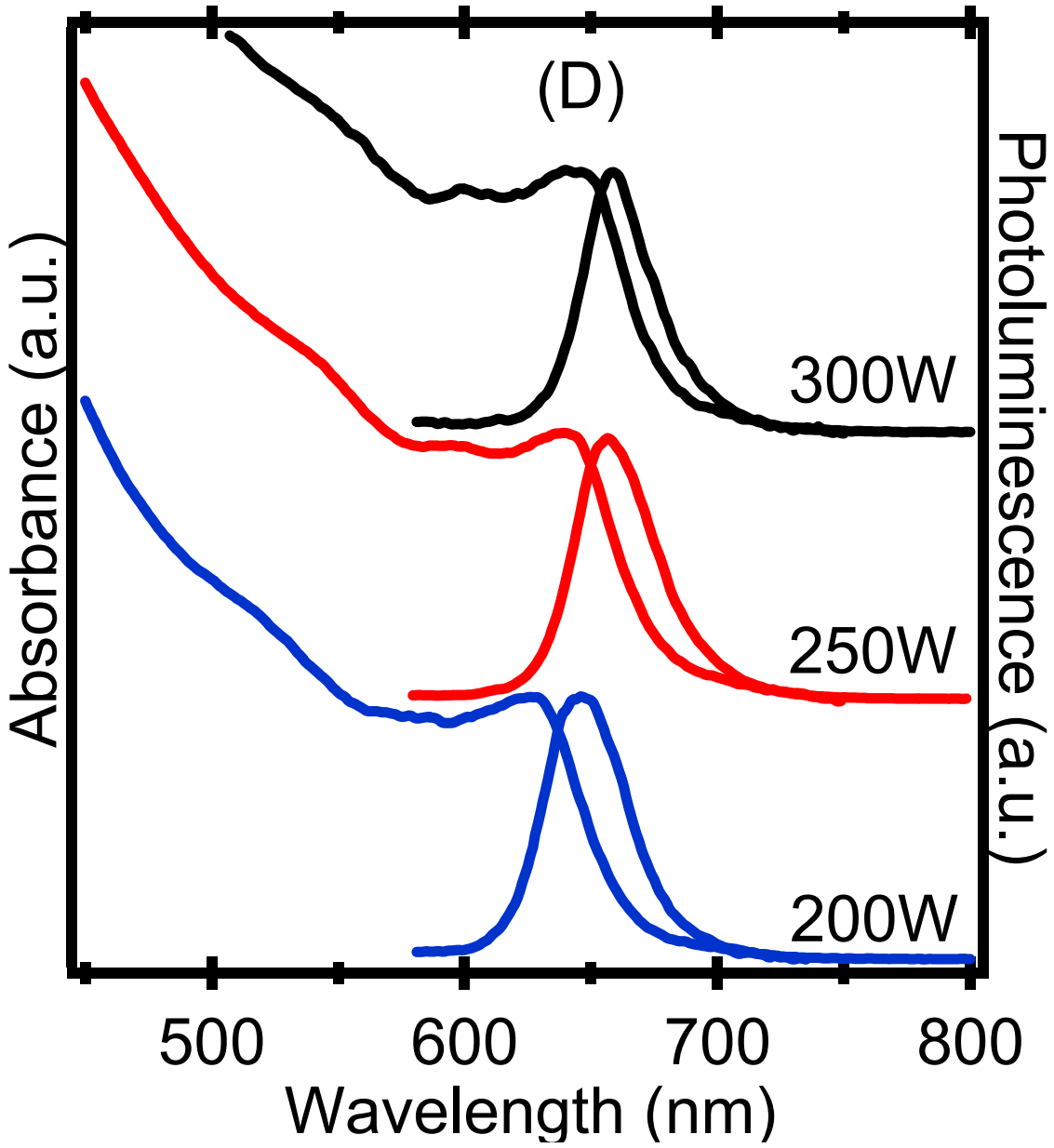

Figure 2.9D. **CdTe Power Dependence w/ Fixed Heating Times**

Absorption and PL spectra for CdTe carried out at different MW powers (200W, 250W, 300W) using decane as the solvent. The reactions had fixed ramp times of 2 minutes and 5 minutes, respectively. The temperature was set to 220°C and because of the short reaction time and the lower polarizability of the P-Te bond. The power was maintained at a high level without active cooling being used.

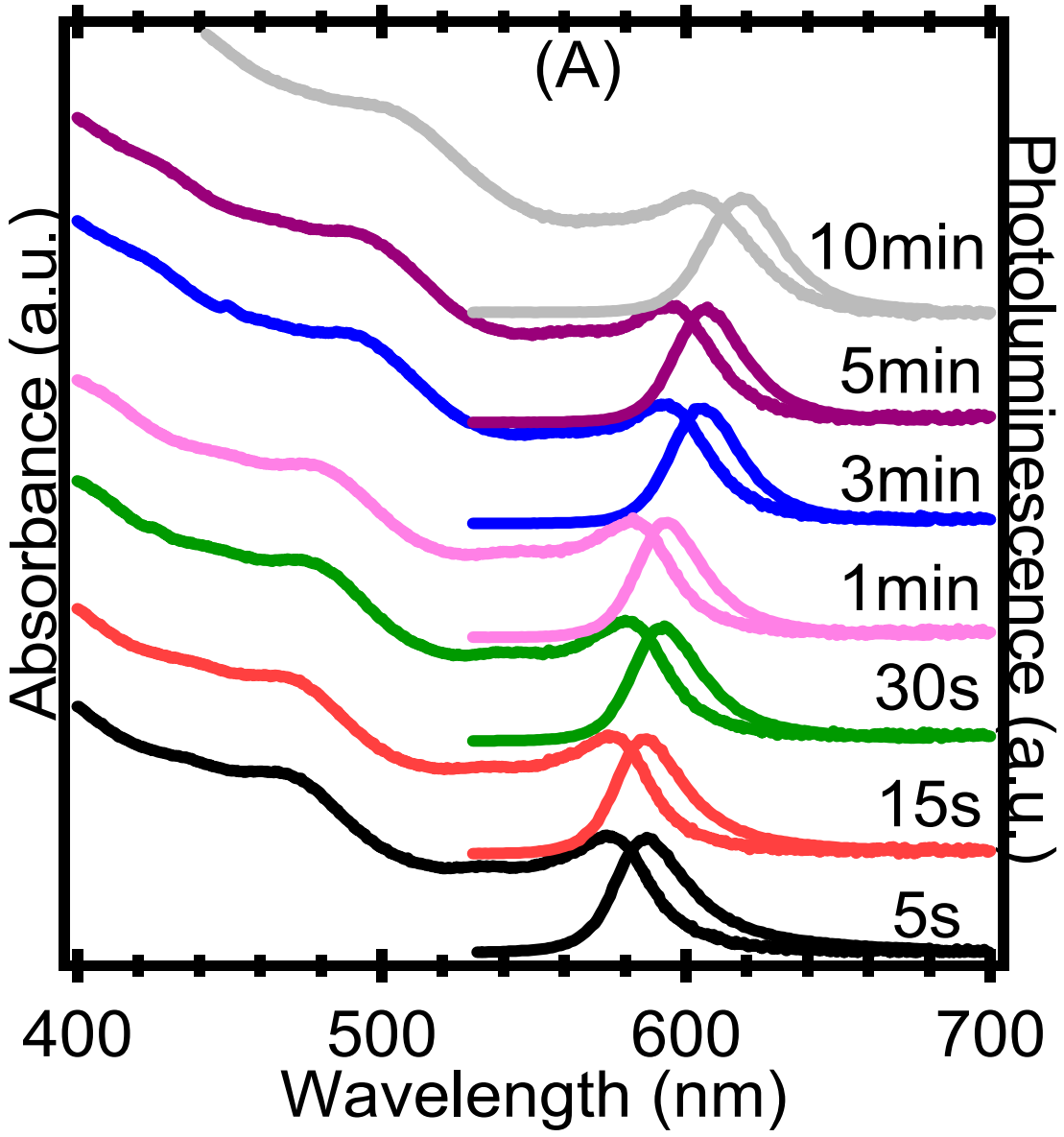

Figure 2.10A. **CdSe Time Dependent Growth**

Absorption and PL spectra for the growth of CdSe was carried out in the MW (300W) as a function of time. The temperature was held at 240°C for each synthesis. The power was set to 300W but was allowed to adjust in order to maintain the set temperature.

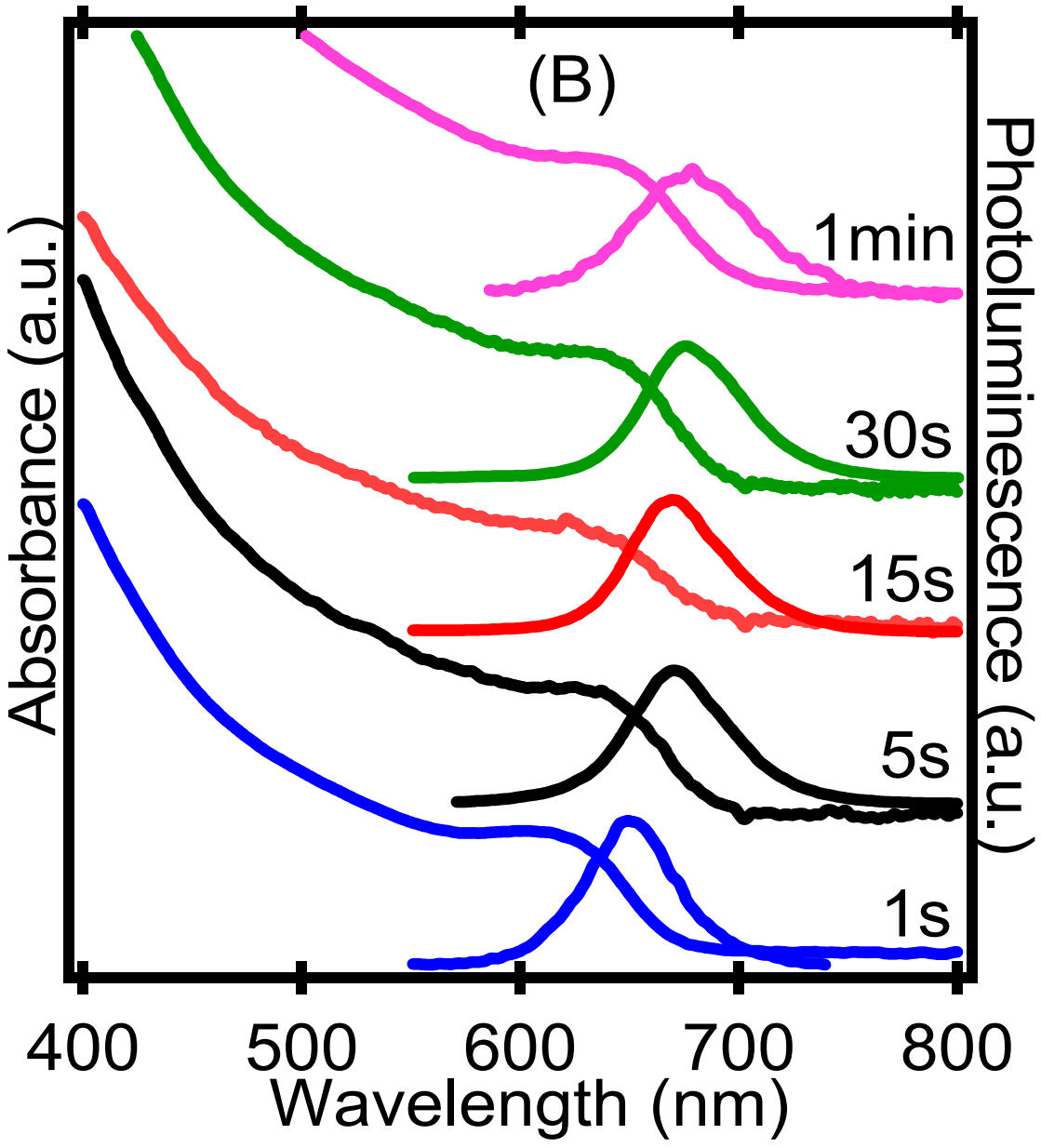

Figure 2.10B. CdTe Time Dependent Growth

Absorption and PL spectra for the growth of CdTe was carried out in the MW (300W) as a function of time. The temperature was held at 220°C for each synthesis. The power was set to 300W but was allowed to adjust in order to maintain the set temperature.

should contribute to the overall order at nucleation (overall rate order =2), it is not surprising for a microwave reaction if the rate limiting step is the precursor activation, namely the cleavage of the TOP-Se bond. This reduces the rate as the concentration of R_3P is reduced, leading to less MW energy being absorbed and thus fewer precursors to monomer production. If nucleation is dictated by the concentration and the selective absorption cross-section for the precursor, then the microwave irradiation is enhancing the initial two steps.

Distinguishing between these two possibilities (activation versus nucleation) can be accomplished by analyzing the pressure dependent growth behavior in these reactions. Using the alkane as a pressure generator, due to boiling points, we observe that at high pressures the rate of reaction is slowed implying that one of the transition states has a large $\Delta V^{\ddagger}$.[72] The slowed reaction rate is logical for the nucleation step rather than the activation step, since a larger number of atoms must assemble for nanocrystal growth to begin. The pressure may be used to manipulate the nucleation event. The result supports the assumption that nucleation is the critical reaction step for nanocrystal formation.[73]

2.3.4 Specific Microwave Effect

The absorbed microwave power (J/s) by a reagent can be related to the produced heat in time $(Q)dt = (mC\Delta T)\,dt$, where C is the specific heat, m is the mass and T is temperature. The rate of heating ((Q) dt) is proportional to the MW absorption cross section using a simple Beer-Lambert law analogy, where $A = \varepsilon bc$. The MW cross section in this equation is ε and bc represent the precursor cross section or concentration per unit volume. The ramp rate to temperature depends on the absorptive cross section of the molecules in solution and the convective losses from the molecules to the solvent via thermal conduction. Thermal transfer depends on the thermal conductivity of the precursors.

The selectivity of microwave absorption by molecules in the reaction mixture can be observed in Figure 2.12 (Table 2.1). The rates of heating for TOP-Se and TOP-Te in decane are an order magnitude larger than observed for just decane, HDA in decane, CdSA in decane, or the nanocrystals in decane indicative of selective microwave absorption for the most polarizable precursor. No experimental difference is observed for various nanocrystal sizes, or concentration suggesting the microwave cross section for the nanocrystal is small. The low heating rate for decane, CdSA, and the alkyl amines is logical due to the low-polarizability of these molecules leading to minute microwave absorption as evidenced in Figure 2.12 (Table 2.1). CdSA shows

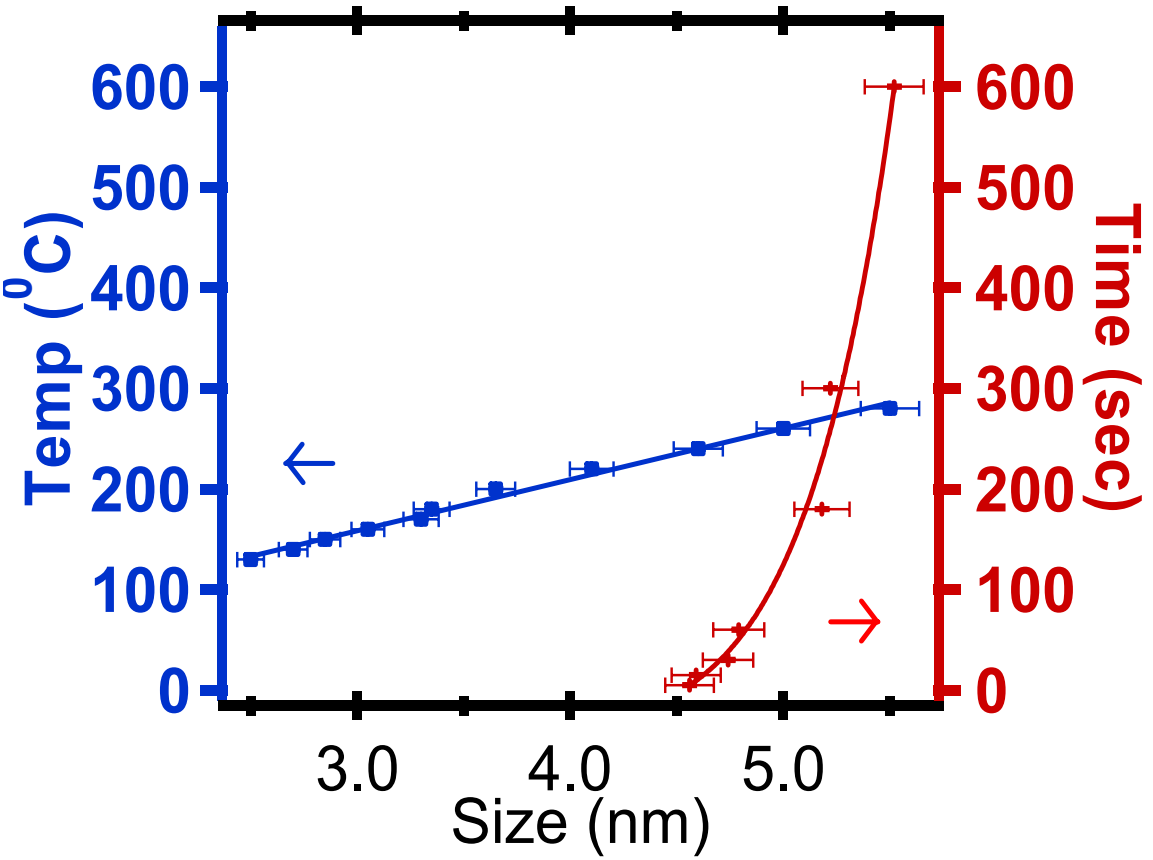

Figure 2.11. Size vs. Temperature/Time

The size of CdSe is plotted against two parameters that are controlled during the microwave reaction: time (red) at a fixed temperature of 240°C and temperature (blue) at a fixed time of 30s.

little influence on heating rate over the alkane solvent and likewise has little impact on reaction temperature or precursor activation. The concentration dependence of CdSA shows a doubling of heating rate for a five-fold increase in concentration, suggesting CdSA does absorb the MW energy, but is not a significant absorber in comparison to the phosphine chalcogenide. The rapid rate of heating for the tri-n-alkyl phosphine chalcogenide is predictable since it repents the most polarizable molecule in the reaction mixture due to the large electronegativity differences between P and the chalcogenide. In fact, based on electronegativity arguments, one can predict that the R_3P-Te is slower to heat then R_3P-Se, where the difference in rate is observed between TOP-Se and TOP-Te. This suggests that the heating of the reaction occurs only by thermal convection from the phosphine chalcogenide to the solvent.

Inspection of the cadmium source,[74] while a minor contributor to the MW absorption also shows the expected trend, where a more covalent source produces better nanocrystals (Figure 2.13). Reactants that are ionic are expected to show no reaction, while highly polarizable reactants will react rapidly. Analysis of a series of cadmium sources (CdSA, CdO, $CdNO_3$, $CdCl_2$) reveal the predicted trend. Only the polarizable starting precursors, CdSA, CdO, and $CdNO_3$ produce nanocrystals. The CdO is a poorer precursor we believe due to the high energy precursor activation step associated with CdO decomposition prior to nucleation of the II-VI materials. No reaction is observed for the ionic $CdCl_2$ under identical reaction conditions.

Alternate selenium precursors as also explored to accurately determine the importance of the phosphine chalcogenides precursor to this high quality synthesis. Selenourea was used as an attempt to synthesize CdSe nanocrystals in an identical methodology to the method presented in this work. Although there is evidence of growth of nanocrystals, the quality of the materials pales in comparison our work.

The impact of the selective microwave effect is observable in the reaction rates for formation of CdSe vs. CdTe nanocrystals. For the chalcogenides, the trend of reaction rate is the Te reacts fastest, followed by the Selenium. If one considers the reactivity and bond strengths of P-Se vs P-Te, the observation is consistent with Te having a weaker covalent bond due to the increased electron density around the atom leading to a larger size. As a result, the more reactive P-Te contributes more energy into nucleating nanocrystals rather than heating the solution. This

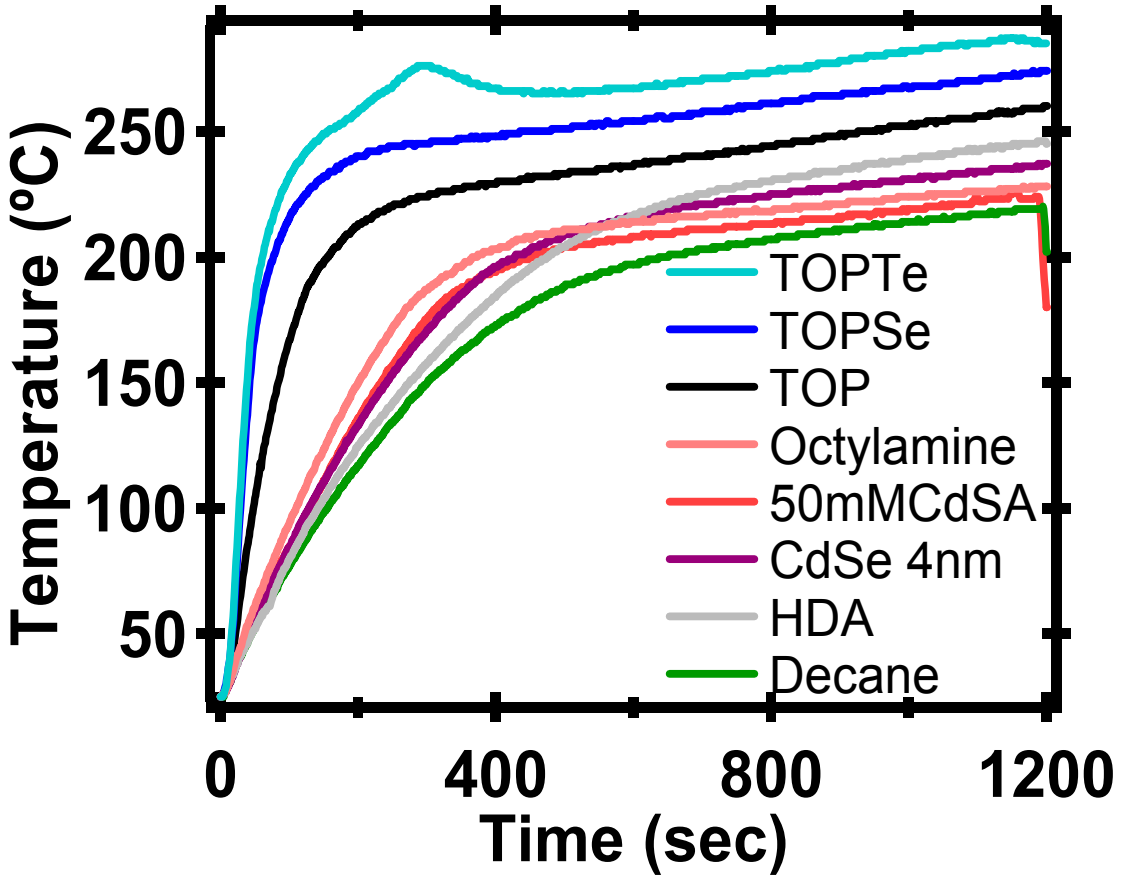

Figure 2.12. Micraowave Heating Rates Time vs. Temperature

The microwave heating rates for different precursors, solvents, ligands, and nanocrystals in decane heated at 300W.

Table 2.1. Microwave Heating Rates

Heating rates of precursors, existing quantum dots, and solvents. Rate determined based of double exponential fit. Heating Rate k_2 shows the fast component. Heating Rate k_4 shows the slow component.

Compound	Heating Rate k_2	Heating Rate k_4
TOPS	1.44E-03	2.24E-02
TOPSe	9.86E-04	2.36E-02
TOPTe	8.30E-04	2.33E-02
TBPSe	9.12E-04	2.41E-02
TBPTe	8.80E-04	2.82E-02
TOP	9.37E-04	1.21E-02
TBP	8.02E-04	1.22E-02
Hexadecylamine	3.12E-03	3.11E-03
CdSe tbpse	5.32E-03	5.24E-03
CdSe 250c30s	3.37E-03	3.37E-03
CdSe 220c30s	4.03E-03	4.14E-03
CdSe 190c30s	3.79E-03	3.65E-03
Octylamine	5.56E-03	5.45E-03
CdCl2	6.12E-03	6.08E-03
50mMCdSA	4.88E-03	4.77E-03
10mMCdSA	2.74E-03	2.72E-03
Cd(NO3)2	2.32E-03	3.30E-02
Decane	3.49E-03	3.49E-03
Heptane	8.59E-04	6.52E-03
Pentane	1.01E-03	1.19E-02

explanation is consistent with the longer ramp time but much shorter reaction time.

Surprisingly a difference is observed between TBP and TOP on the surface of the nanocrystal. While on the same order of magnitude, in both cases the reactivity of TBP is slightly higher than that of TOP. The reactivity difference implies a difference in the nature and strength of the bonding at both the Se and the nanocrystal surface for these two ligands.[75] Considering a Tolman cone-angle argument for the trialkylphosphines,[76] two plausible explanations are differences in the polarizability of R_3P-X bond due to changes in the orbital hybridization in the R_3P, or more likely a decrease in packing density due to the steric interaction for the longer chained TOP. Since one would predict the cone angle, and thus electronic properties, to be essentially the same for the two systems, the steric bulk of the TOP may result in the lower rate of heating due to fewer molecular interactions. While potentially within experimental error, the reproducibility of the results suggest further investigation is needed to evaluate this empirical observation.

2.3.5 Stopped-Flow Synthesis of II-VI Nanocrystals

The scalability of a reaction is always complicated by the presence of thermal gradients and difficulty in mixing of the reactants in larger volumes.[77] This is particularly true for nanocrystal growth, where the transition of the synthetic methodology from a small reactor size (~ 5mL) to a larger system (50 mL) suffers from thermal gradients in the reaction leading to larger poly-dispersities and poorer material performance. Microwave reactors offer an advantage over convective heat sources, due to their ability to heat without thermal gradients since selective heating is achieved by the absorption into the chalcogenide precursor triggering the nucleation event. This is accomplished in a stop-flow configuration, where the reactants are pumped into the MW cavity.

A comparison of the absorption and photoluminescence spectra for the stopped-flow dynamic and normal static reaction is shown in Figure 2.14. The advantage of the stopped-flow geometry is that a continuous stream of nanocrystals can therefore be generated from a stock precursor solution (>10 mg nanocrystal / min). In addition, the ability to synthesize nanomaterials in a variety of solvents using the stopped-flow setup implies explicit control over the reaction in either microwave setup. (Figure 2.15) A disadvantage of the stop-flow system is the volume of the reactor makes heating of the solvent more difficult. The reactions require 40 min for CdSe (20 min CdTe) due to the inability of the MW to penetrate the larger volume of

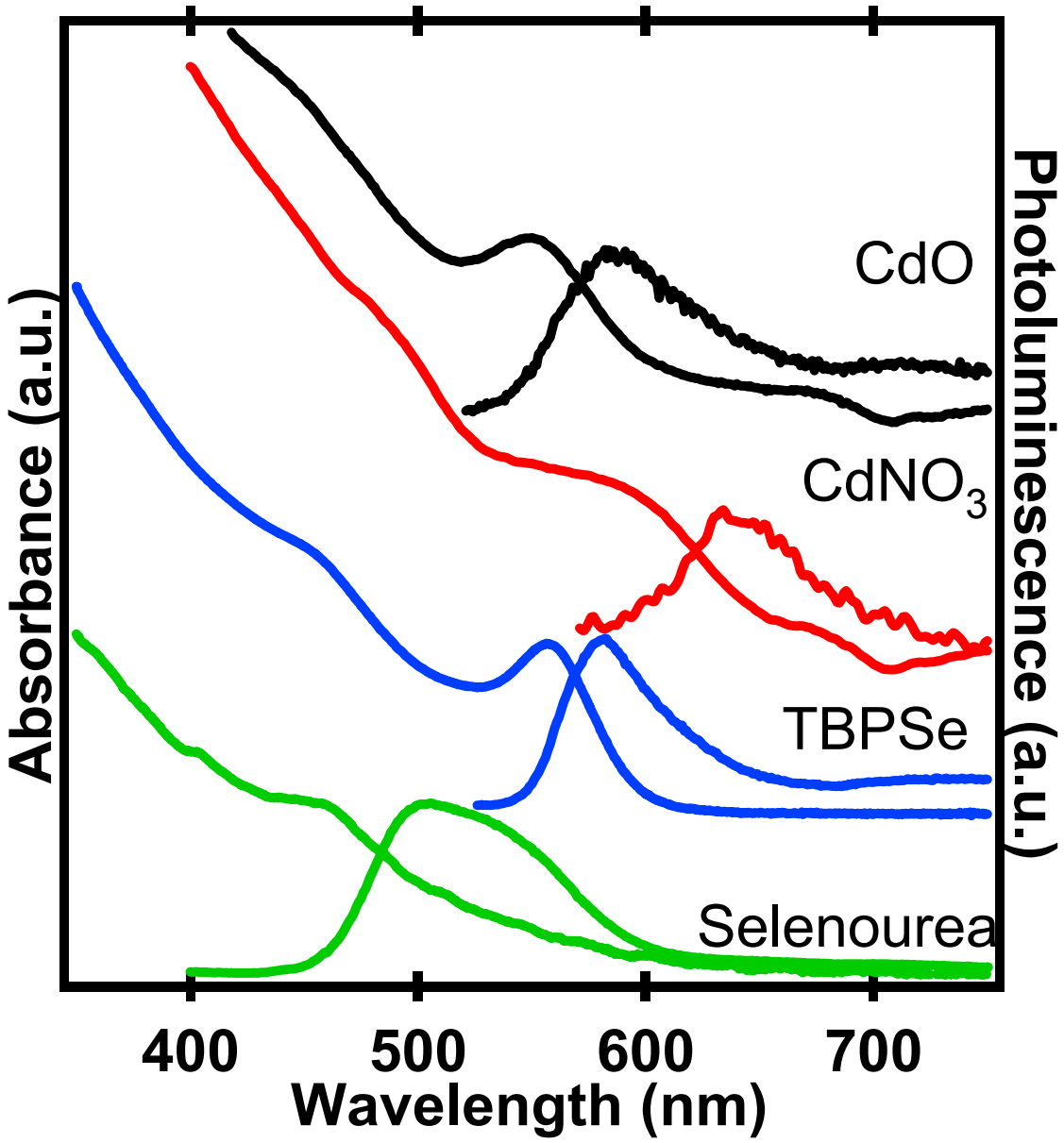

Figure 2.13. Alternate Precursors for Cd and Se

Alternate cadmium and selenium precursor sources are used to synthesize CdSe nanocrystals reacted under identical conditions of 240°C and 30s in the microwave reactor. $CdCl_2$ is not shown due to lack of nanocrystal growth. For the Cd precursors listed, TOPSe was used as the selenium source. For the Se precursors listed, cadmium stearate was used as the Cd source.

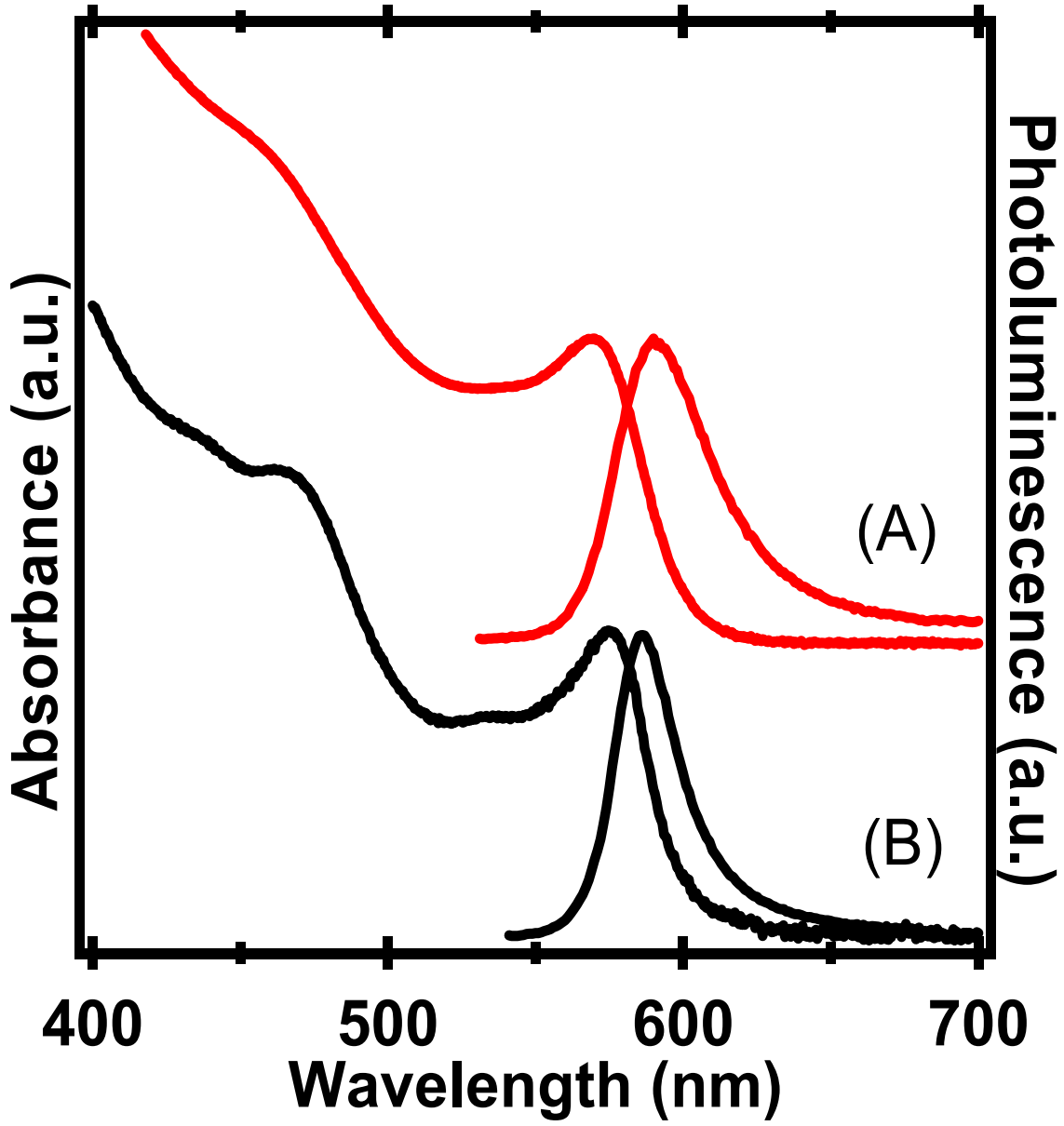

Figure 2.14. Batch Reaction vs. Stop-Flow

Absorption and photoluminescence spectra for A) stop-flowed 80mL and B) conventional 10mL reaction vessel.

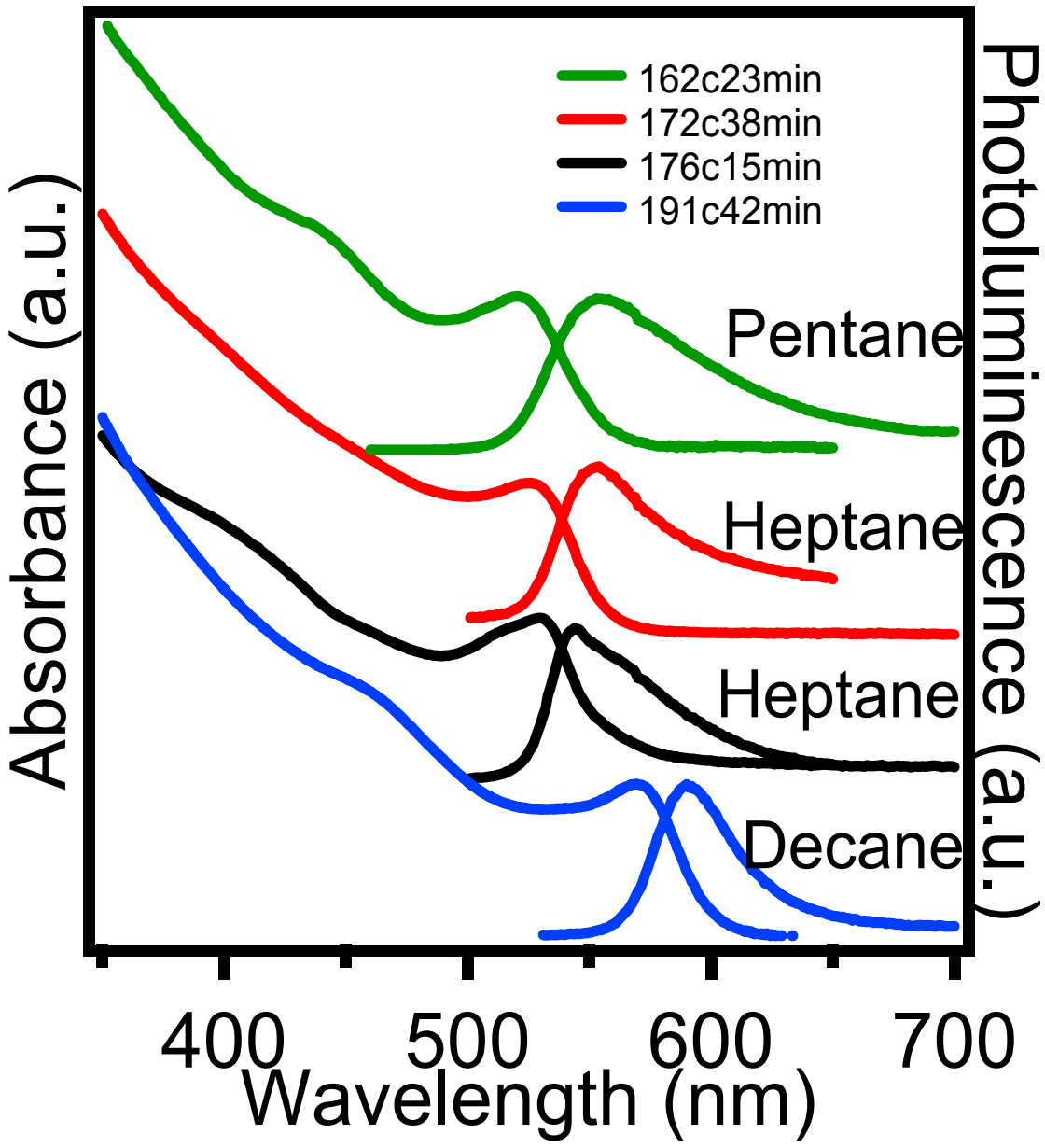

Figure 2.15. Stop-Flow Reactions w/ Different Solvents

CdSe synthesized using the CEM stop-flow reactor using various solvents to ascertain the effect of pressure in this flow system on the growth rate and quality of the materials. The different solvent produced various temperatures in the reaction at a variety of times. The temperature and time of each reaction is indication in the inset.

solvent as well as the thickness of the reactor vessel. The slow ramp rate and lower achievable temperatures are evidence of the increased problems in reaching the desired reaction temperatures in a short period. However, the fact that the materials are the same quality supports the conclusion that the precursor absorbs the energy and transfers the heat convectively. Likewise a similar size regime can be obtained at an apparent lower reaction temperature. These observations support MW absorption by the tri-n-alkyl phosphine and convective losses to the solvent, particularly in light of the fact that a larger volume reactor by definition has a larger thermal sink, thus lowering the overall reaction temperature.

In addition to conclusions made thus far, several reaction parameters of the synthesis were explored in order to determine the optimal method for the highest material quality as well as for the applicability in a wide range of technical advances.

2.4 Conclusion

While the microwave specific effect has been postulated, the observation of the selective nature of dielectric heating for nanocrystal growth is fascinating. If we assume the phosphine-chalcogenide is the predominant absorbing species in solution, the excess energy will activate the nucleation of cadmium-chalcogenide nanocrystals, while growth is achieved by the reaction temperature. The behavior of time, temperature and material quality can be traced to the chemical nature of the precursors and suggest in the reaction conditions herein, the nucleation step controls the nanocrystal formation. The observation of heating-rate dependencies supports the logic of precursor activation via selective heating triggers nucleation. This observation represents a rare demonstration of the "specific microwave effect." From a commercial perspective, the development of a stopped-flow synthetic methodology allows the researcher to produce high quality materials in a matter of minutes instead of hours, or continuously at a specific size and composition.

CHAPTER 3 MICROWAVE SYNTHETIC ROUTE FOR HIGHLY EMISSIVE TOP/TOP-S PASSIVATED CDS QUANTUM DOTS.

Through selective microwave absorption, we demonstrate the ability to activate TOPS as a sulfur donor allowing the rapid (18 m) growth of highly emissive (PLQY = 33%), Zn Blende CdS quantum dots (QDs) passivated by TOP/TOPS in the 4 - 6 nm size regime (5% size dispersity). The CdS QDs exhibit sharp absorption features and bandedge photoluminescence even for the largest CdS sample. Addition of hexadecylamine restricts the growth rate by limiting the Cd monomer activity and lowers overall PLQY, presumably due to changes in the particle facet expression. The use of MW chemistry for QD formation allows highly reproducibly synthetic protocols that are fully adaptable to industrial applications.

3. 1 Introduction

The development of II-VI semiconductor quantum dots (QDs) has expanded exponentially over the last 15 years due largely to advancements in synthetic control of the activity of reactive monomers and the QD surface under high temperature reaction conditions.[78,79,80,81,82,83,84,85,86] It has been demonstrated that the activity of the monomer in solution and on the QD surface can be systematically controlled by the addition of additives which lead to shape control.[87,88,89, 90, 91, 92, 93, 94, 95, 96] Passivants such as alkylamines or alkylphosphonic acids can lead to slowed growth rates by lowering monomer activity leading to unique crystal phases and morphologies. Recent studies have definitively correlated growth and dispersity for the QDs to the reaction operating in the diffusion controlled or reaction controlled mechanism.[90] Under conditions where slow release of the chalcogenide from the solution phase monomer is achieved, the reaction proceeds predominately through a diffusion controlled mechanism, and thus the size dispersity is controlled by monomer concentration, the equilibrium between monomer bound to the QD surface and free in solution, and at long reaction times the participation of Ostwald ripening.[97] While these efforts have clearly identified organic additives that manipulate the diffusion controlled reaction rates via controlling surface activity, little effort has focused on the activation of monomers directly through the use of selective energy absorption into the specific monomer. In a series of studies, we have explored the use of selective MW absorption into R_3P-X (X =Se, Te) leading to remarkable enhancements of

reaction rates for QD formation.[98] The realization that selective absorption can enhance the activity of the TOP-Se or TOP-Te monomer in a solvothermal reaction conducted in a MW cavity suggests that monomers with low activity might be enhanced by the absorption of MW energy.

While there is a plethora of examples of CdSe and CdTe materials generated from R_3P-X, it is surprising that there are no reports of growing CdS form R_3P-S as a precursor without the addition of alkyl phosphonic acids to enhance reaction rates, although TOP-S is a common reagent for the shelling step in a core-shell QD.[87,89,96,99,100] A more typical sulfur monomer is TMS-S due to its greater monomer activity.[81] Since nearly all the published II-VI metal chalcogenide nanocrystals are readily prepared from tri-n-alkyl phosphine chalcogenide (R_3P-X), the limited examples of CdS prepared from TOPS is surprising although it can be traced to the bond strength of P-S (444 $\pm$ 8 kJ/mol), P-Se (364 $\pm$ 10.0 kJ/mol), or P-Te (280 $\pm$ 10.0 kJ/mol).[101] The strength of the P-S interaction limits the ability for TOP-S to act as a good monomer for sulfur addition to the growing QD, thus impacting the ability to form a stable critical nuclei in solution.[79,82,89] Since the bond strength controls the monomer activity ($E_{P\text{-}S} > E_{P\text{-}Se} > E_{P\text{-}Te}$), it directly influences the growth rates for the II-VI nanocrystals (dr/dt (CdTe) > dr/dt(CdSe) > dr/dt(CdS)). Thus it is not surprising that few examples of formation of CdS from R_3P -S exist unless an activator is added to enhance the monomer activity of TOPS leading to materials that exhibit narrow size dispersity, well-defined excitonic absorption features, and strong bandedge photoluminescence at large CdS sizes.[102,103]

The low sulfur atom transfer efficiency in R_3P-S may be enhanced in this reaction if bond cleavage can be activated in this monomer through selectively energizing the monomer. In a lyothermal reaction this is impossible to achieve; however, in a microwave (MW) reaction selective absorption of MW energy can enhance reaction rates by overcoming kinetic barriers in the reaction.[104] It has been shown in both organic chemistry and nanomaterial chemistry that MW absorption is selective into the free solution monomer with the highest static dipole moment if the reactions are carried out in a solution that has a very low MW absorption cross-section.[105] In the QD reactions, whether the rate enhancement arises from local heating in the heterogeneous reaction environment or from selective activation of the monomer is still unknown. In this manuscript, we report selective absorption of microwave (MW) energy into TOPS leads to formation of 4 - 6 nm CdS quantum dots (QD) with narrow size dispersity (5% RMS based on

TEM). The CdS QDs reported herein exhibit an aspect ratio of 1.2 with a size dispersity of 5%, discrete excitonic features in the absorption spectra, band edge photoluminescence (PL), and the highest reported quantum yields (33% PLQY). Defect PL, arising from glide plane defects and/or vacancies, constitutes less than 5% of the total observed emission.

In the MW, the size of the isolated QD is dependent on reaction temperature, while the PLQY is influenced by the presence or absence of HDA (hexadecylamine) as a co-passivant to control surface energies for the growing QD. The primary function of HDA is to restrict the activity of the QD surface, thus limiting growth rates in the MW and allowing isolation of smaller QDs. The highest bandedge PLQY (PLQY = 33%) is achieved for the 4.3 nm CdS carried out in a 1:1 molar TOP : HDA. The high PLQY is remarkable when compared to earlier reports, where the PLQY is typically less than 20%.[106,107] Consistent with the bond strength argument, the formation of CdS requires much longer reaction times (18min) than observed previously for formation of CdSe (30s) or CdTe (15s) even with MW assisted activation of R_3P-S.

3.2 Experimental

Synthesis. All syntheses were performed in a single mode CEM Discover System operating at 300W, 2.45 GHz. The reactions were carried out under ambient reaction conditions in 10mL reaction vessel (4-5 mL reaction volume). The solvent temperature is monitored continuously via a remote IR sensor.

For a typical CdS QD reaction,[108] 135.2mg (0.2 mmol) of cadmium stearate is dispersed into 4 mL of decane, and 0.2 mL (0.2 mmol) of a 1M TOPS stock solution was added. For reactions carried out in the presence of hexadecylamine (HDA, 0 – 0.4 mmol) is added to the solution prior to MW heating. The reaction mixture is heated in the microwave reactor from RT to a predetermined reaction temperature at 300W and immediately cooled to RT (~ 1 min). In this manuscript, this reaction protocol will be referred to as zero hold time. The CdS QDs are isolated from the reaction mixture using standard precipitation methods via suspension in a (1:3) toluene/butanol mixture and addition of an excess of methanol to precipitate the entire QD batch.

3. 3 Results and Discussion

The formation of CdS QDs is achieved in the MW within 18 min yielding elliptical, zinc blende CdS with a 1.2:1 aspect ratio. By comparison, carrying out the identical reaction using high temperature injection of the precursors in a lyothermal approach does not yield product on

the same timescale (up to 1h). In Figure 3.1A, the optical spectra for CdS between 4.3 and 5.6 nm is shown based temperature dependent growth (. The absorption and PL reveal that over the entire size range studied in this manuscript, the CdS QDs exhibit discrete excitonic features in the absorption spectra and strong band edge PL. Well defined higher lying excitonic features in the absorption spectra are clearly observed, which are typically not observed for larger CdS QDs. The PL defect intensity accounts for < 5% of the total PL intensity in all cases. Inspection of the TEM image of a 5.3 nm CdS in Figure 3.1B indicates a dispersity of 5.4% (Supporting Figure 3.2). The CdS samples exhibit clearly resolved <001> lattice fringes (Supporting Figure 3.3). The pXRD pattern for the 5.3 nm CdS QD in Figure 3.1C indicates cubic crystal morphology. Scherrer broadening analysis of the pXRD confirms the PXRD (5.4 nm) and TEM (5.3 nm) sizes are experimentally correlated.

3.3.1 Growth

In the MW, the size of the isolated CdS QD is observed to depend on the reaction temperature, reaction time, and the presence (1:1 mole ratio HDA to TOPSe) or absence of hexadecylamine (HDA). A plot of the QD size versus reaction temperature (at zero hold time) in the presence of HDA (red) and in the absence (black) of HDA is linear but exhibits different reaction rates, as evidenced by the slopes of the lines (Figure 3.4A). For the reaction carried out with zero hold time, the presence of HDA appears to restrict CdS QD growth at a specific reaction temperature limiting the growth rate of the CdS when compared to the reaction carried out in the absence of HDA. No difference is observed for the rate to reach the reaction temperature in the presence or absence of HDA indicating MW absorption by HDA does not contribute to the reaction rate changes.

The impact on growth rates in the presence of HDA can be traced to restriction of CdS growth. Inspecting the growth of CdS as a function of time at the desired reaction temperature (240°C) exhibits an exponential growth dependence on CdS for both reaction conditions (Figure 3.4B). Unlike the temperature plot the fits for time dependent growth have the same experimental slope implying the growth rate (d_{size}/d_t) is independent of the presence or absence of HDA. Therefore, it is likely the observed size differences at the same temperature for a reaction carried out in the presence and absence of HDA may reflect a thermodynamic limitation attributable to monomer activity in the presence of HDA rather than a simplistic model where the packing of HDA on the growing QD hinders monomer accessibility as previously suggested.[90]

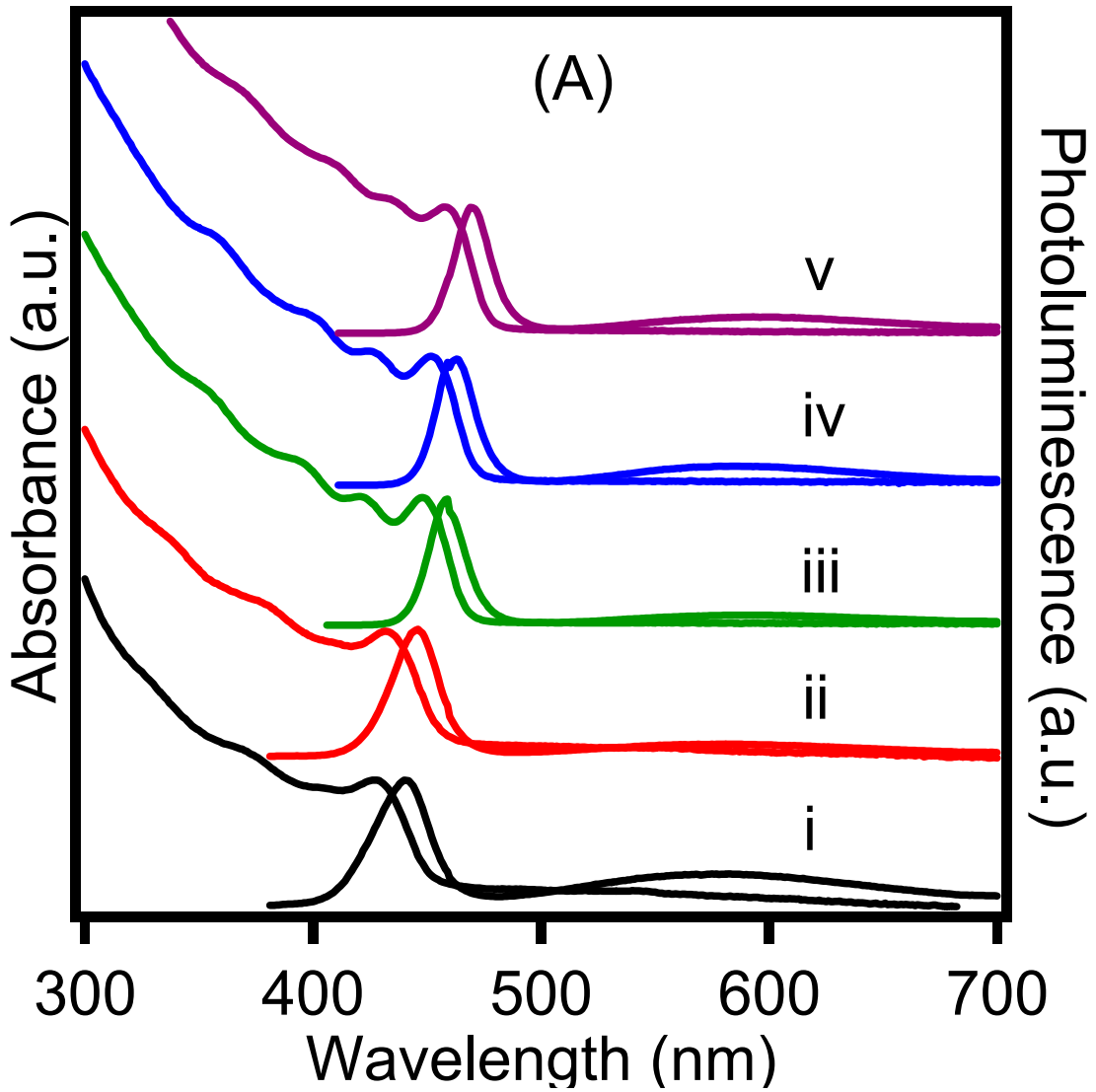

Figure 3.1A. Size vs Temperature

Optical spectra of CdS QDs i) 4.3 nm, ii) 4.5 nm, iii) 4.8 nm, iv) 5.2 nm, and v) 5.6 nm.

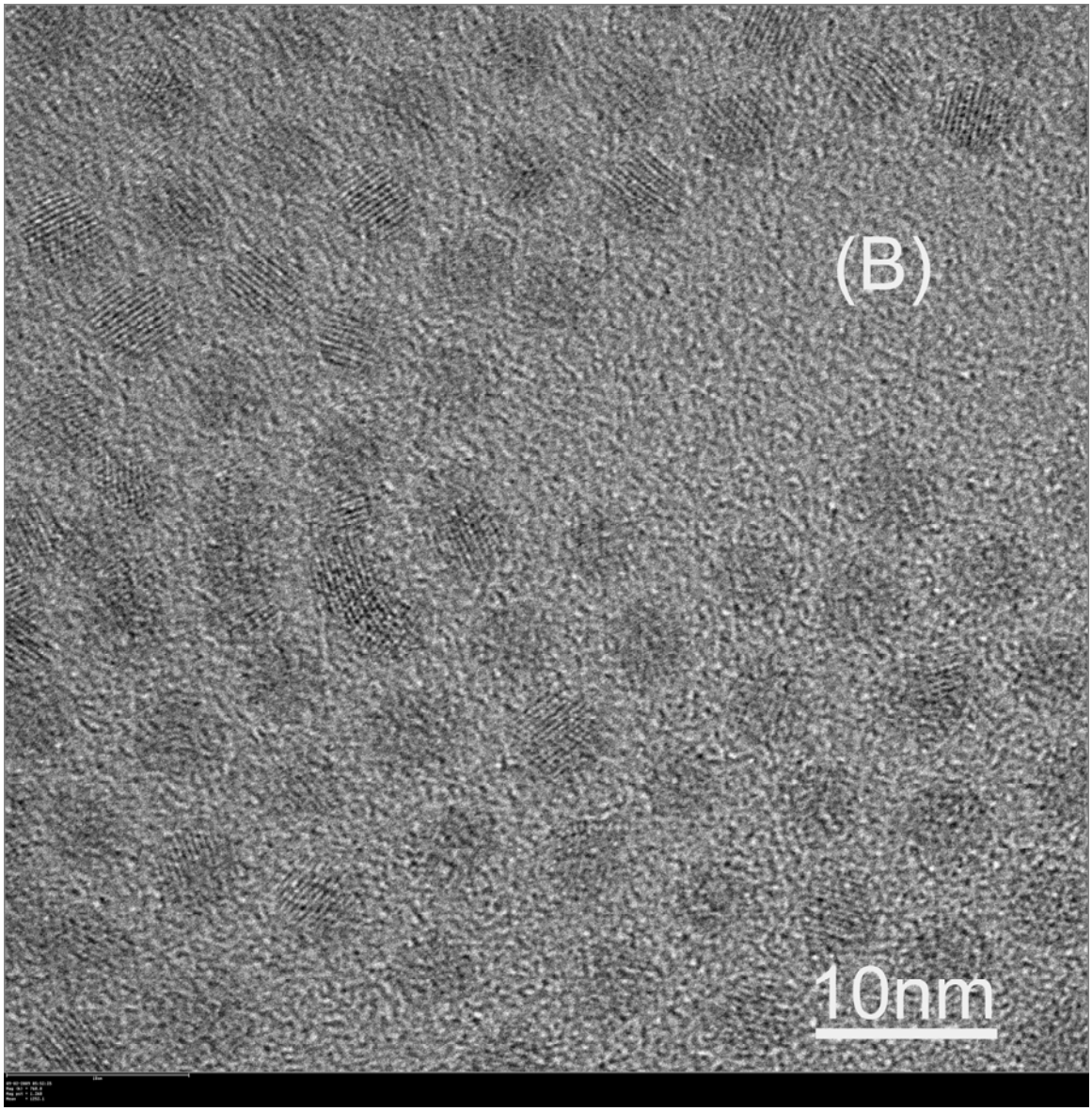

Figure 3.1B. TEM CdS 5.3 nm

TEM image of 5.3 nm QD.

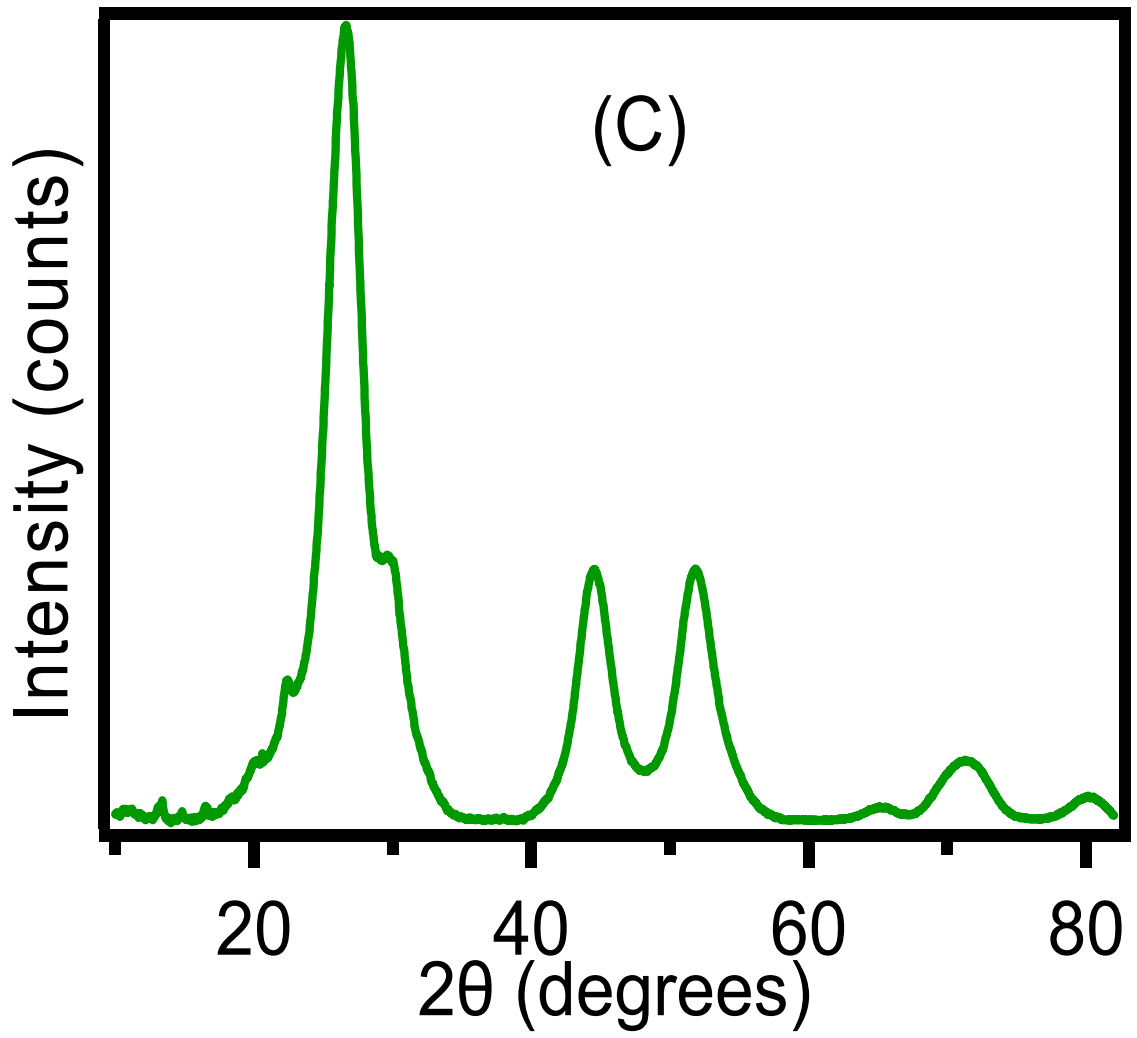

Figure 3.1C. pXRD CdS 5.3 nm

pXRD spectra of a 5.3 nm CdS QD displaying a Zinc Blende structure.

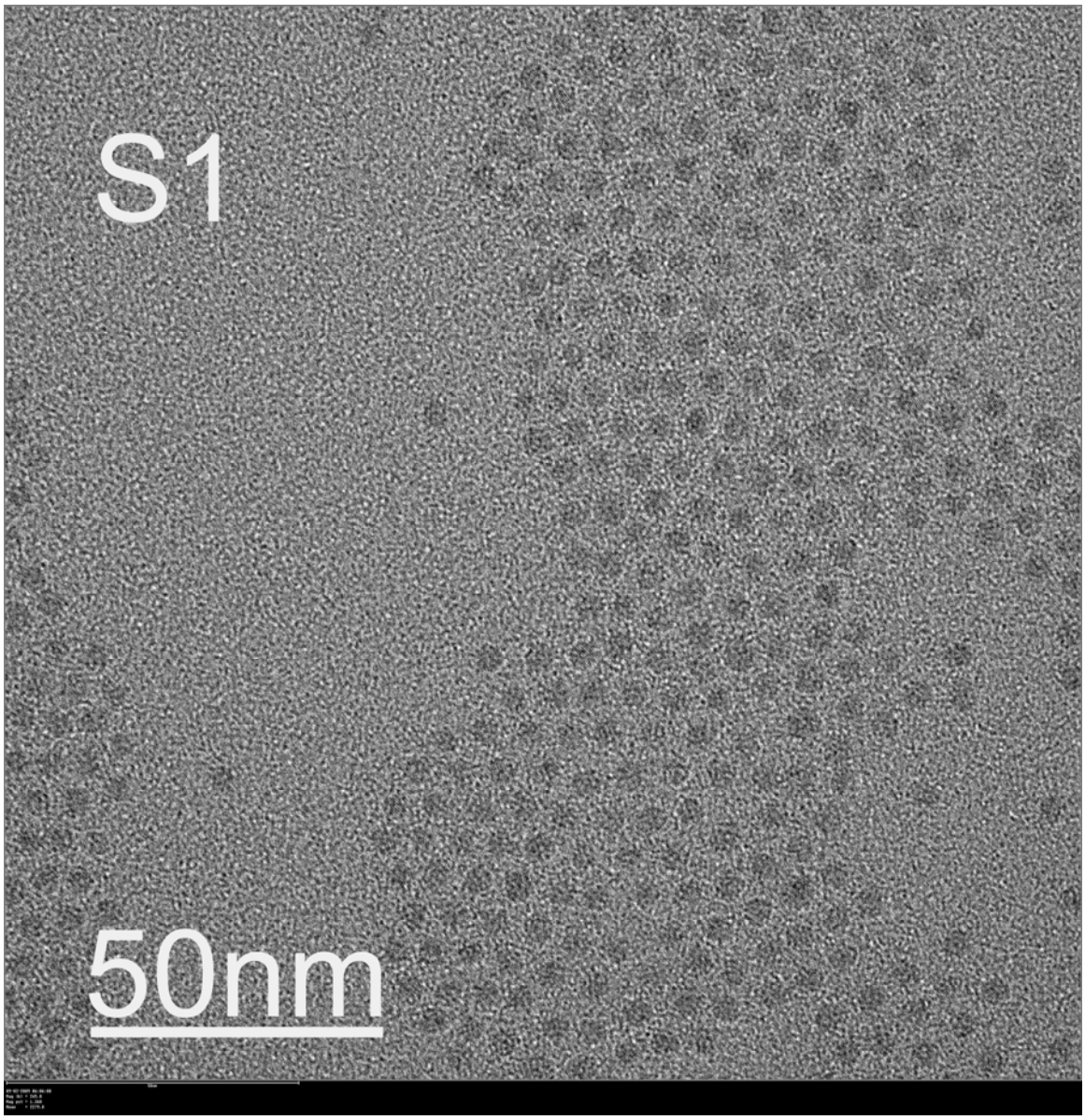

Figure 3.2. TEM of CdS showing 5.4% Dispersity

TEM image showing 5.4% dipersity of CdS quantum dots with an average size of 5.3 nm.

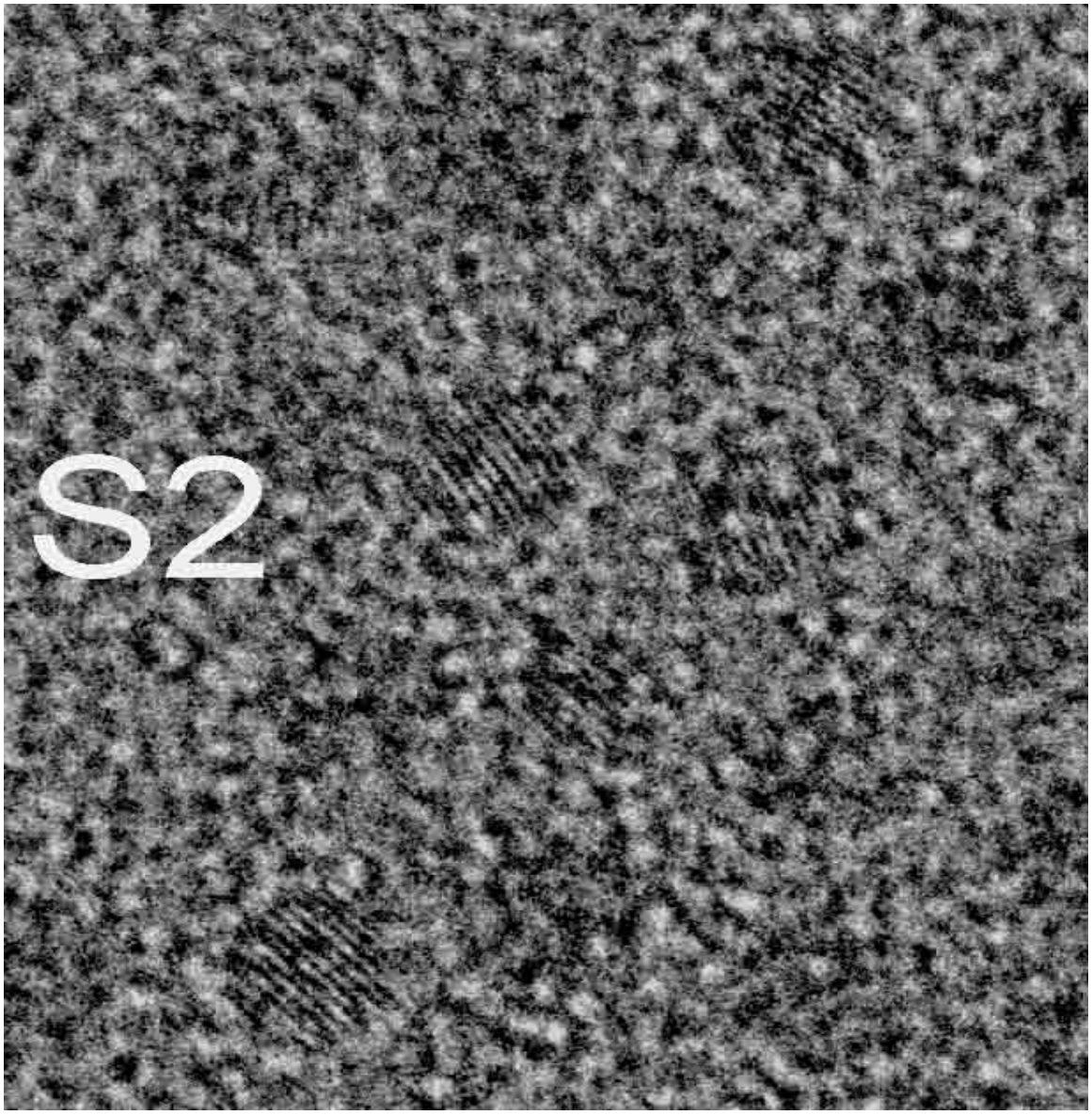

Figure 3.3. TEM of CdS w/ Clear Lattice Fringes

TEM enhanced excerpt image from Figure S1 showing clear lattice fringes with no visible glide plane defects on Zn Blende CdS QDs.

3.3.2 Absorption Properties

The linewidth of the first exciton absorption is dependent on the QD size and the presence or absence of HDA (Figure 3.5A). The linewidth is effectively invariant in the absence of HDA (24 nm), but exhibits a strong size dependence (38 → 24 nm) in the presence of HDA approaching the linewidth of non-HDA grown samples only for the largest CdS QD size. The 5.3 nm CdS grown in the absence of HDA yields the sharpest excitonic absorption features reported in the literature to date.[91,93,109]

Although the size of the CdS is strongly dependent on the presence or absence of HDA, as well as the reaction temperature and time, the dependence of the optical absorption linewidth in the presence of HDA is dependent only on the reaction time (Figure 3.5B), while in the absence of HDA no spectral sharpening is observed in time. The linewidth for the exciton absorption in the presence of HDA narrows from 34nm (18s) to 24nm (100s). The narrowing of the linewidth in the presence of HDA can be fit to an exponential function indicative of changes in either the surface of the QD via reconstruction or a size focusing of the QD due to monomer limitation. It is believed the effect of HDA is to limit the monomer activity, consistent with the smaller QD sizes observed at identical reaction temperatures. It is worth noting that the optical data for this work reflects raw batch QDs isolated by complete precipitation of the CdS QDs from solution by addition of MeOH.

3.3.3 Photoluminescence Properties

Band edge photoluminescence is observed over the entire size range for the CdS QDs with a FWHM of 18 nm (Figure 3.1A). No change in the PL linewidth or magnitude of the band edge to defect PL intensity is observed in the presence or absence of HDA as a function of reaction time. The PLQY however is size, passivant (Figure 3.6A), and time at reaction temperature (Figure 3.6B) dependent. Comparison of the PLQY for a similar sized CdS indicates the PLQY in HDA is reduced, for example the 5.2 nm CdS grown in the presence of HDA has a PLQY of 8.45%, while the CdS grown in the absence of HDA has a PLQY of 17.8%. The effect of HDA on the reaction is investigated in further detail below, but it is believed that the variability in PLQY may reflect differences in packing efficiency of the passivant on the QDs or differences arising from the reaction temperature/time to reach the larger QD sizes in the presence of HDA.[110]

The observation of passivant dependent and size dependent PLQYs for CdS are not surprising. The reported PL QY for CdS QD varies widely by the method of synthesis. A recent

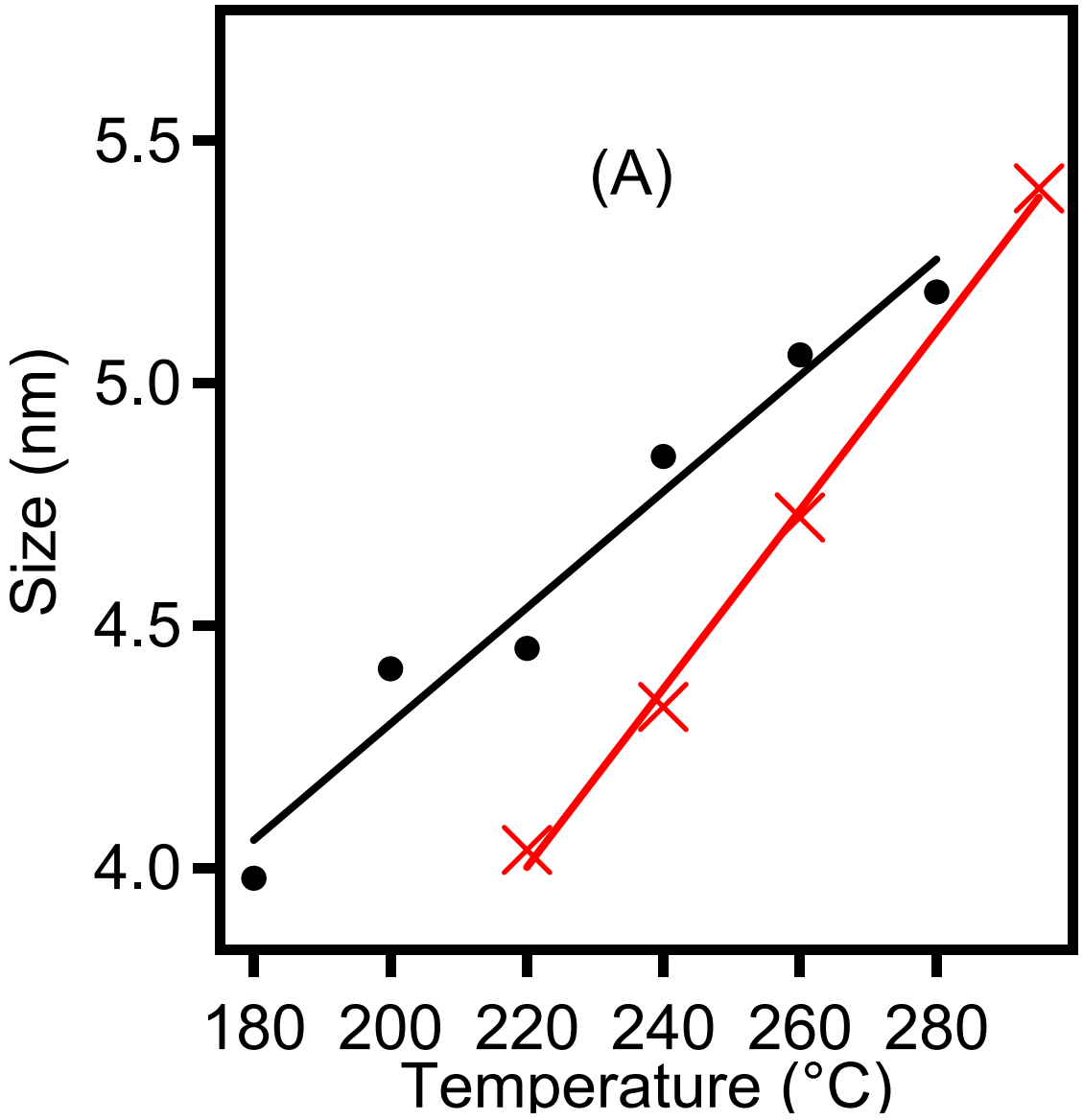

Figure 3.4A. Effect of Temperature on Size w/ and w/o HDA

The growth behavior of CdS quantum dots in the MW cavity in the presence (red) and absence (black) of HDA as a function of temperature at zero hold time.

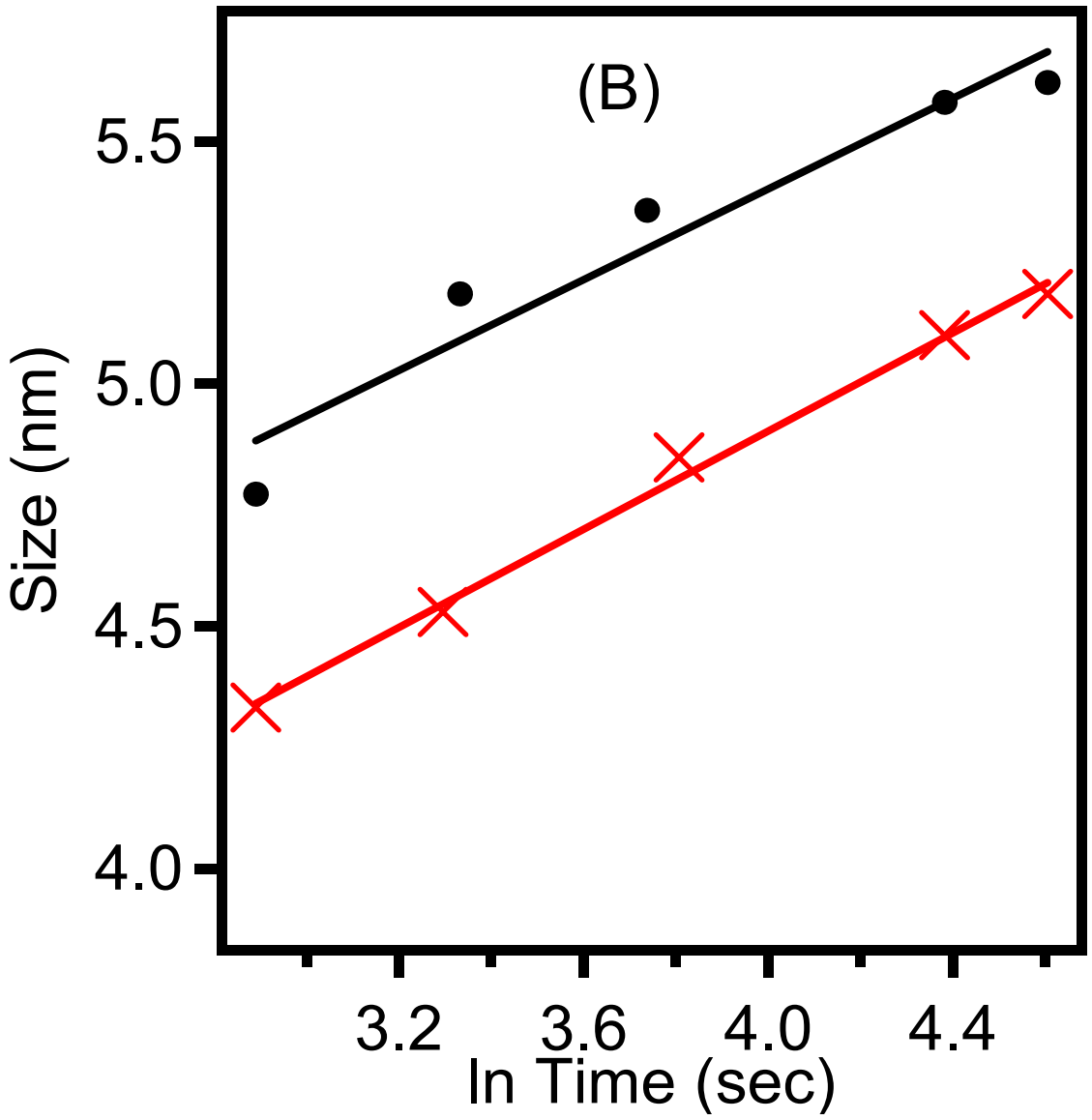

Figure 3.4B. Effect of Time on Size w/ and w/o HDA

The growth behavior of CdS quantum dots in the MW cavity in the presence (red) and absence (black) of HDA as a function of held at the reaction temperature for a specified time.

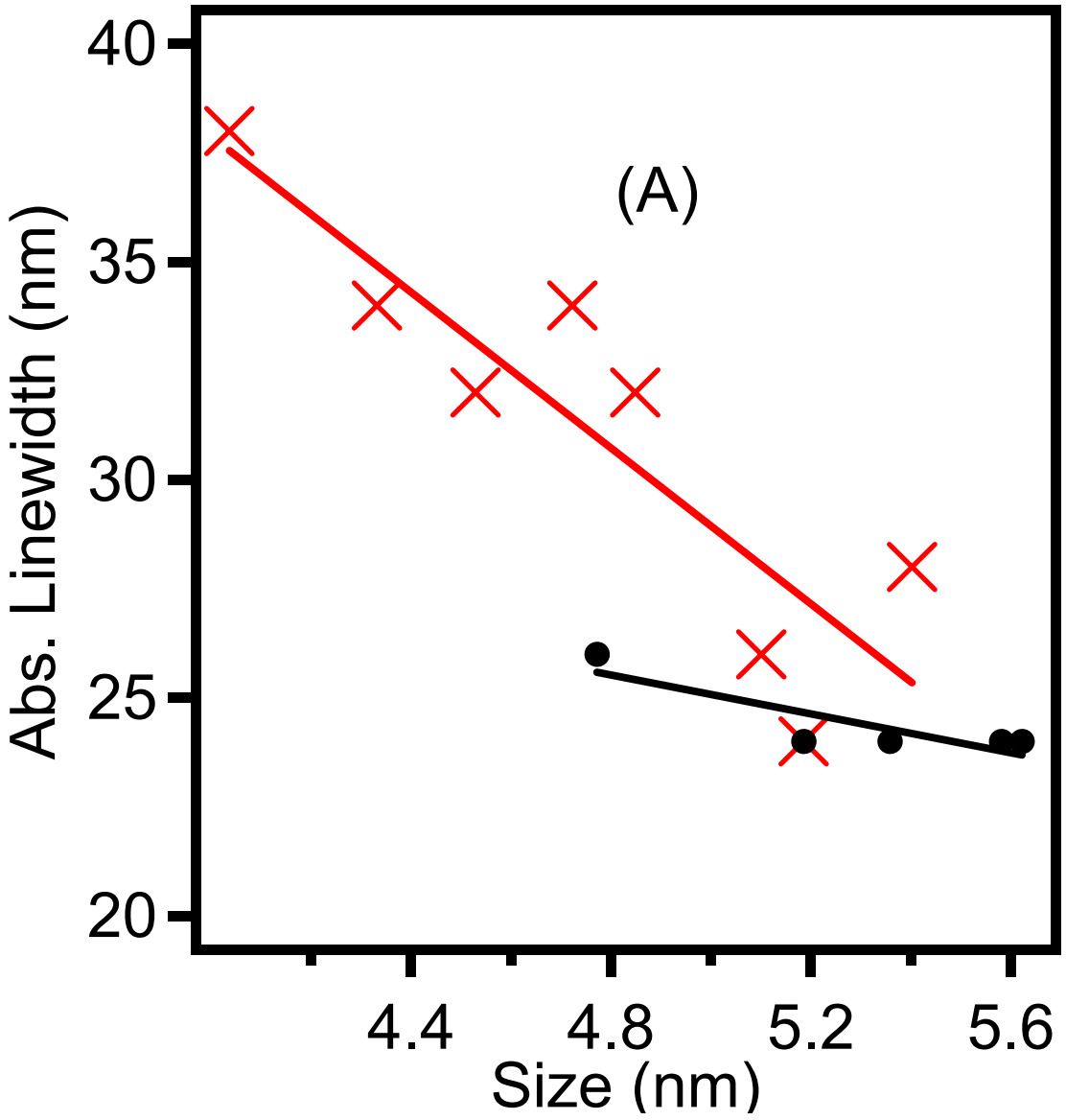

Figure 3.5A. Absorption Linewidth vs. Size

Changes in the exciton absorption linewidth for synthesis of CdS in the MW cavity in the presence (red) and absence (black) of HDA as a function of size for samples isolated at zero hold time.

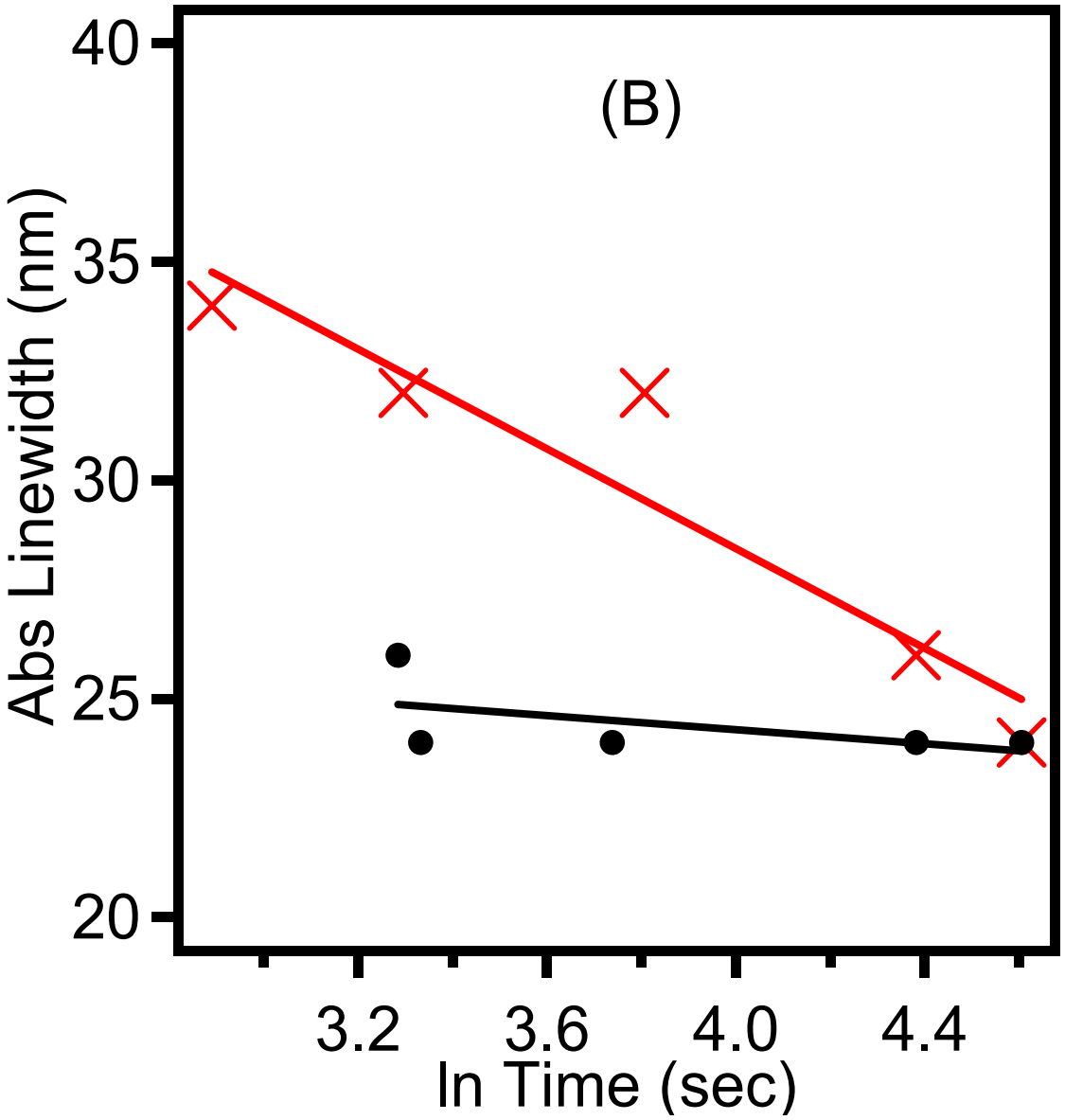

Figure 3.5B. Absorption Linewidth vs. Time

Changes in the exciton absorption linewidth for synthesis of CdS in the MW cavity in the presence (red) and absence (black) of HDA for samples held at the reaction temperature for a specified time.

report for CdS preparation within the MW cavity shows a QY of ~2% with a rapid degradation of the PL QY as the reaction times increase.[94] By comparison the lyothermal reaction of CdO, ODE, and sulfur produced a reported QY of 12%.[89]

A decrease in the PL is observed in the presence and absence of HDA for a reaction held at a specific reaction temperature. The reaction carried out at 240^0C is shown in Figure 3.6B and can be fit to an exponential function. At long time, the PLQY approaches the same value for both samples, indicating the time dependence is not due to the presence of HDA. The time dependent loss in PLQY is surprising as the linewidth of the absorption is observed to narrow over the same time domain (Figure 3.6). The time dependent evolution of the PLQY may reflect differences upon reaching the Ostwald ripening stage of the reaction surface oxidation, [90, 111, 112] or surface reconstruction influencing the facet expression in the QD and the effective surface passivation. Surface oxidation is expected to decrease the PLQY but not lead to sharpening of the absorption features; however, reconstruction of the QD surface can lead to sharpening of the absorption and loss of PLQY.[113] It is unlikely Ostwald ripening will cause this observation, as size defocusing generally occurs at longer reaction times. In the MW, the Ostwald ripening regime shows broadening of both samples at reaction times after the CdS growth stalls. This occurs approximately at 1 h at a typical reaction temperature (240^oC) and is unlikely to contribute to the observed spectral changes. (Figure 3.7A/B) Further investigation is under way to fully understand the time dependence.

3.3.4 Dependence on Reaction Composition

HDA mole ratio. The reaction to form II-VI QDs from metal and chalcogenide monomers is thermodynamically favorable and has been shown to be strongly influenced by the individual activity of the monomers in the solution relative to the monomers on the growing QD surface.[92] The observation of different behavior for formation of CdS in the presence and absence of HDA implies the presence of HDA effectively restricts monomer activity. A similar observation was suggested in the growth control of CdSe in the presence of amines.[95] In Figure 3.8A, the optical spectra as a function of the mole ratio of HDA to TOP at 240^OC is plotted at zero hold time. The linewidth of the exciton absorption is broadest (60 nm) for the 2:1 HDA:TOP mole ratio and narrows as the concentration is reduced to 0:1. The size of the QD is largely invariant with HDA concentration above a 0.5:1 mole ratio. The PLQYs are extremely sensitive to the HDA concentration exhibiting a 17.3% PLQY at 0 mmol HDA (0:1 mole ratio HDA to TOPS), 14.3 %

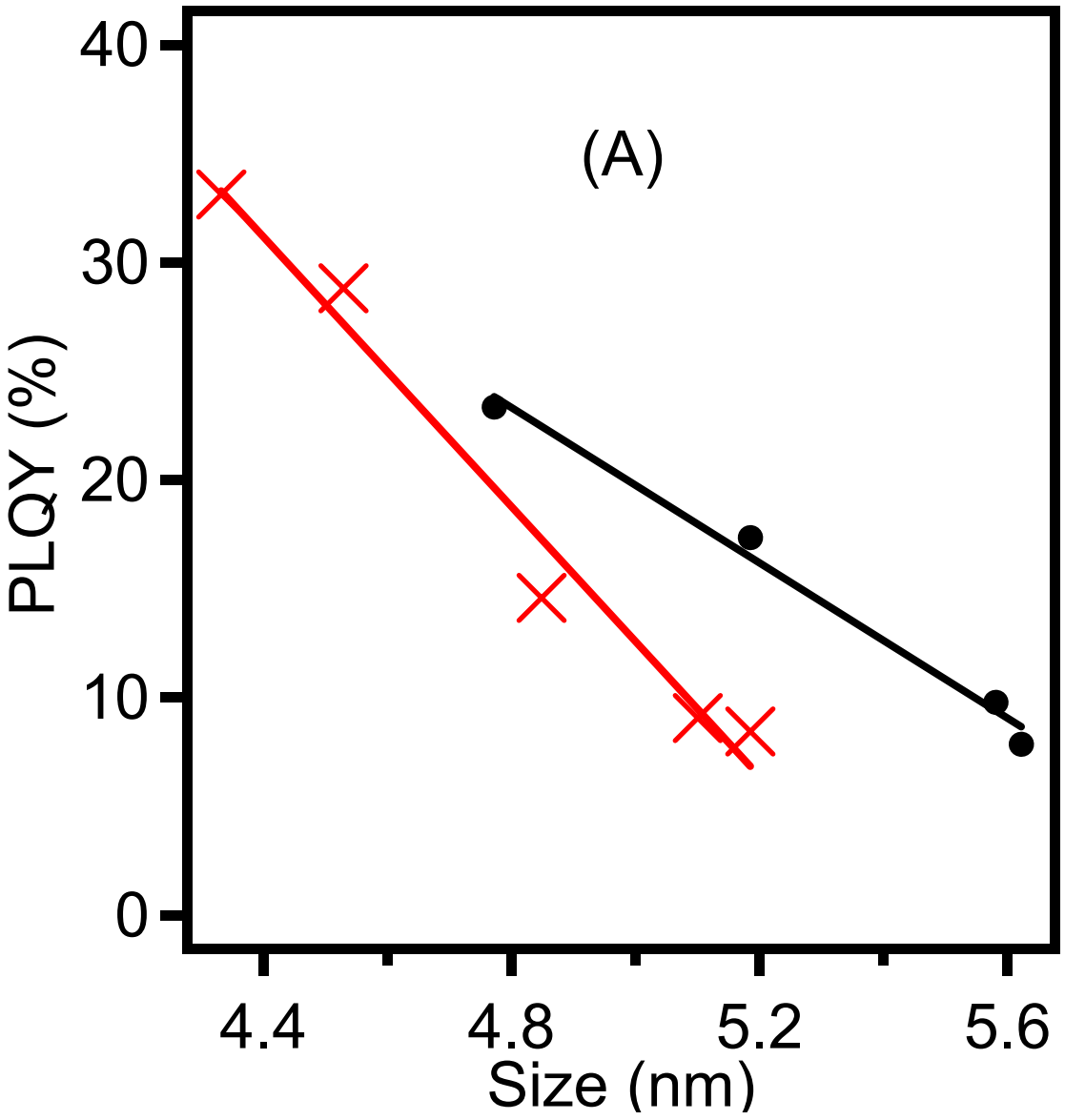

Figure 3.6A. CdS Size vs PLQY

The photoluminescence quantum yield in the presence (red) and absence (black) of HDA is plotted as a function of CdS QD size for a sample isolated at zero hold time.

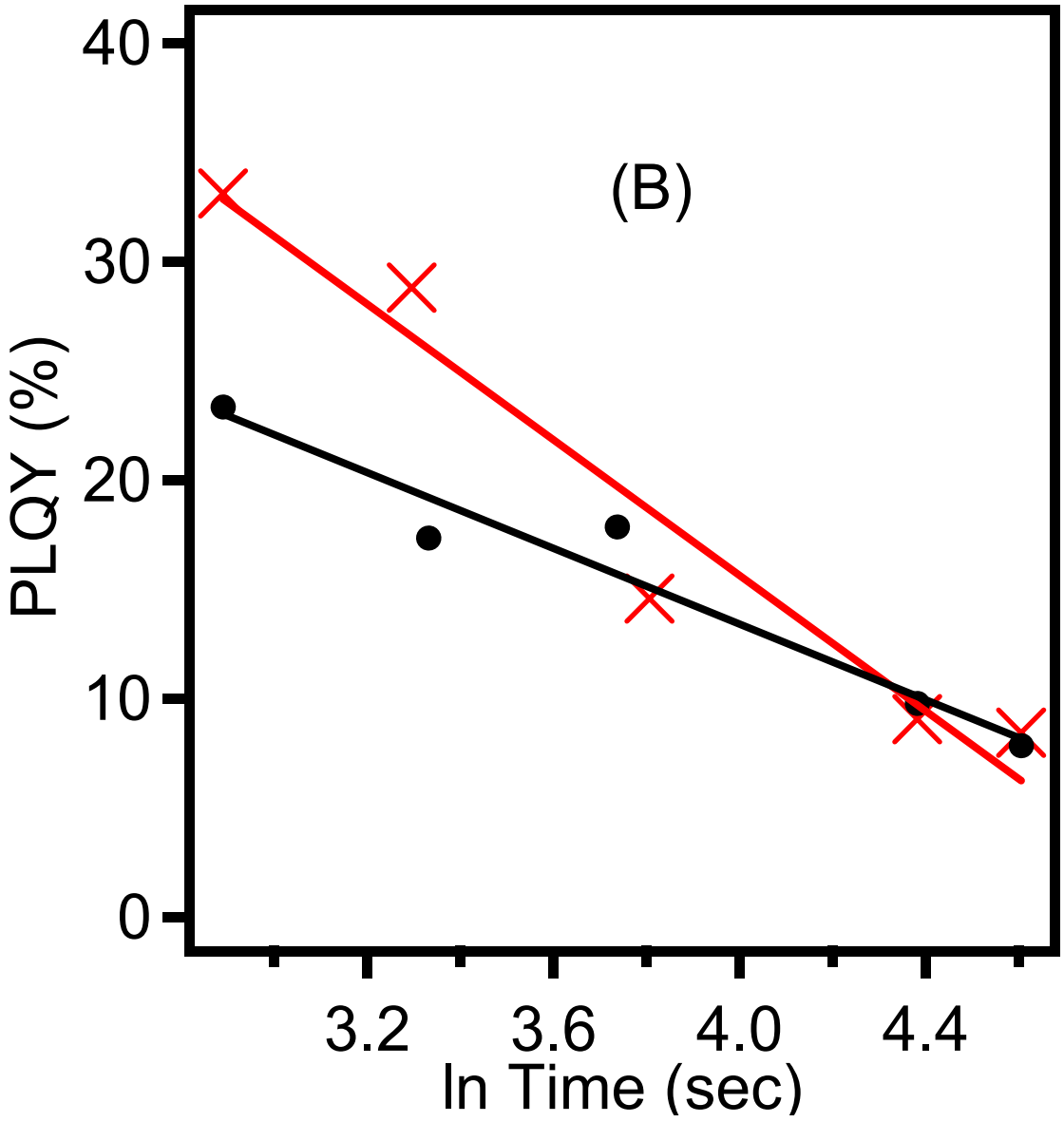

Figure 3.6B. **CdS Time vs. PLQY**

The photoluminescence quantum yield in the presence (red) and absence (black) of HDA is plotted as a function of CdS QD size for samples held at the reaction temperature for a specified time.

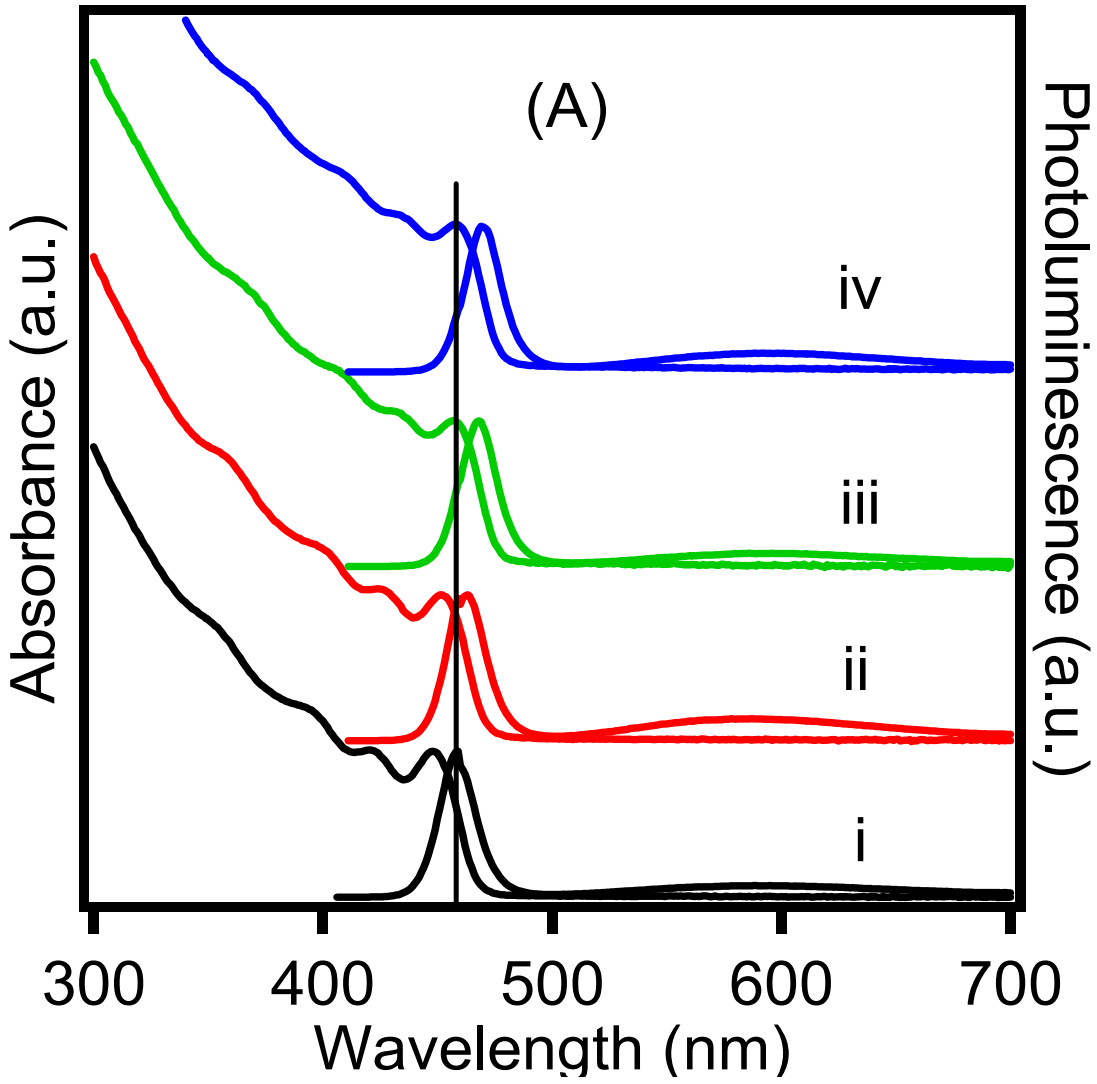

Figure 3.7A. CdS Time Dependent Growth w/o HDA

The absorption and photoluminescence of CdS QDs grown in the absence of HDA for various reaction times at the desired reaction temperature. All CdS QD samples were grown at 240°C with a ramp time of 18min with hold times at the reaction temperature of i) 0, ii) 24, iii) 62, and iv) 82 min.

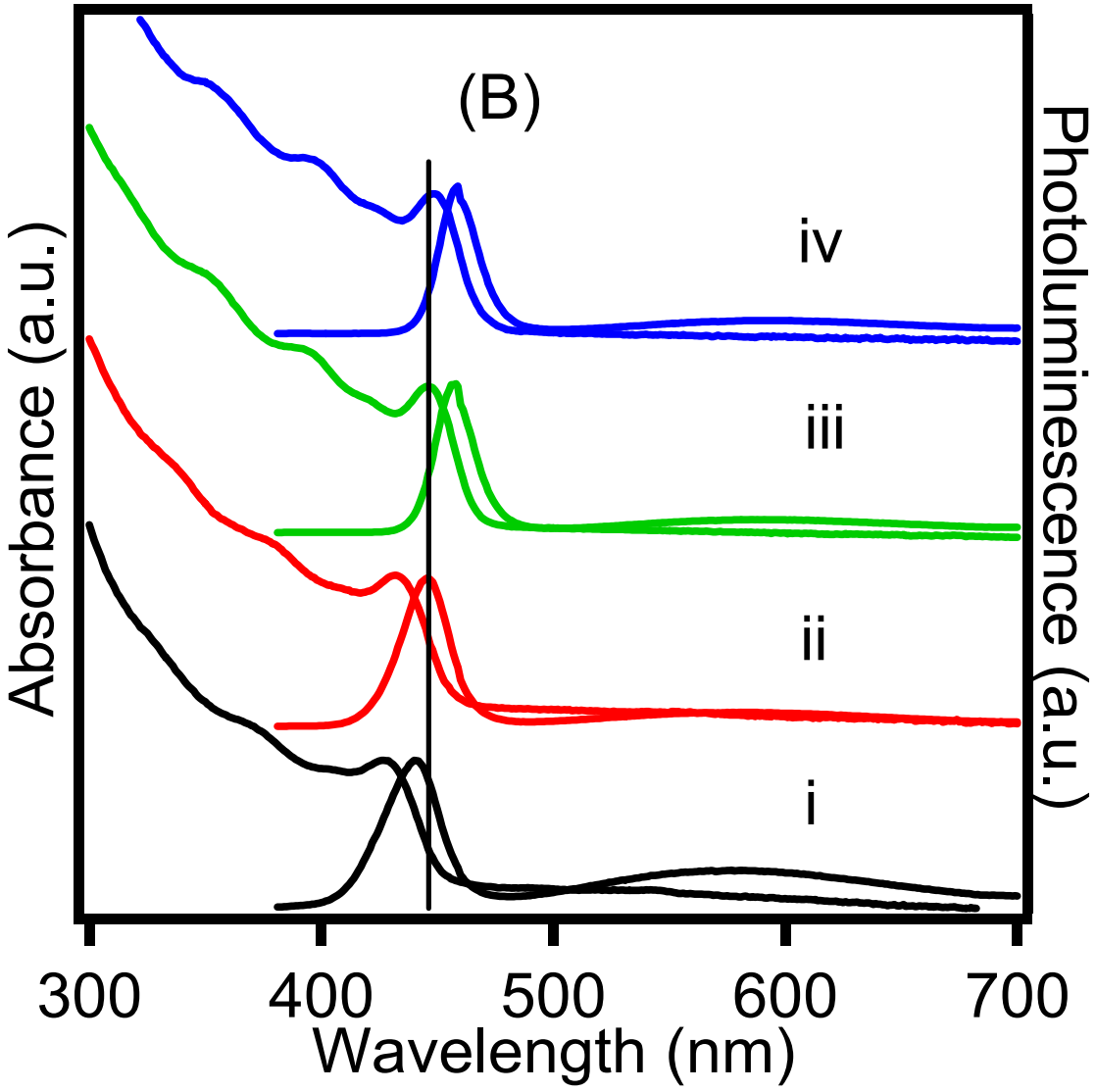

Figure 3.7B. CdS Time Dependent Growth w/ HDA

The absorption and photoluminescence of CdS QDs grown in the presence of HDA for various reaction times at the desired reaction temperature. All CdS QD samples were grown at 240°C with a ramp time of 18min with hold times at the reaction temperature of i) 0, ii) 24, iii) 62, and iv) 82 min.

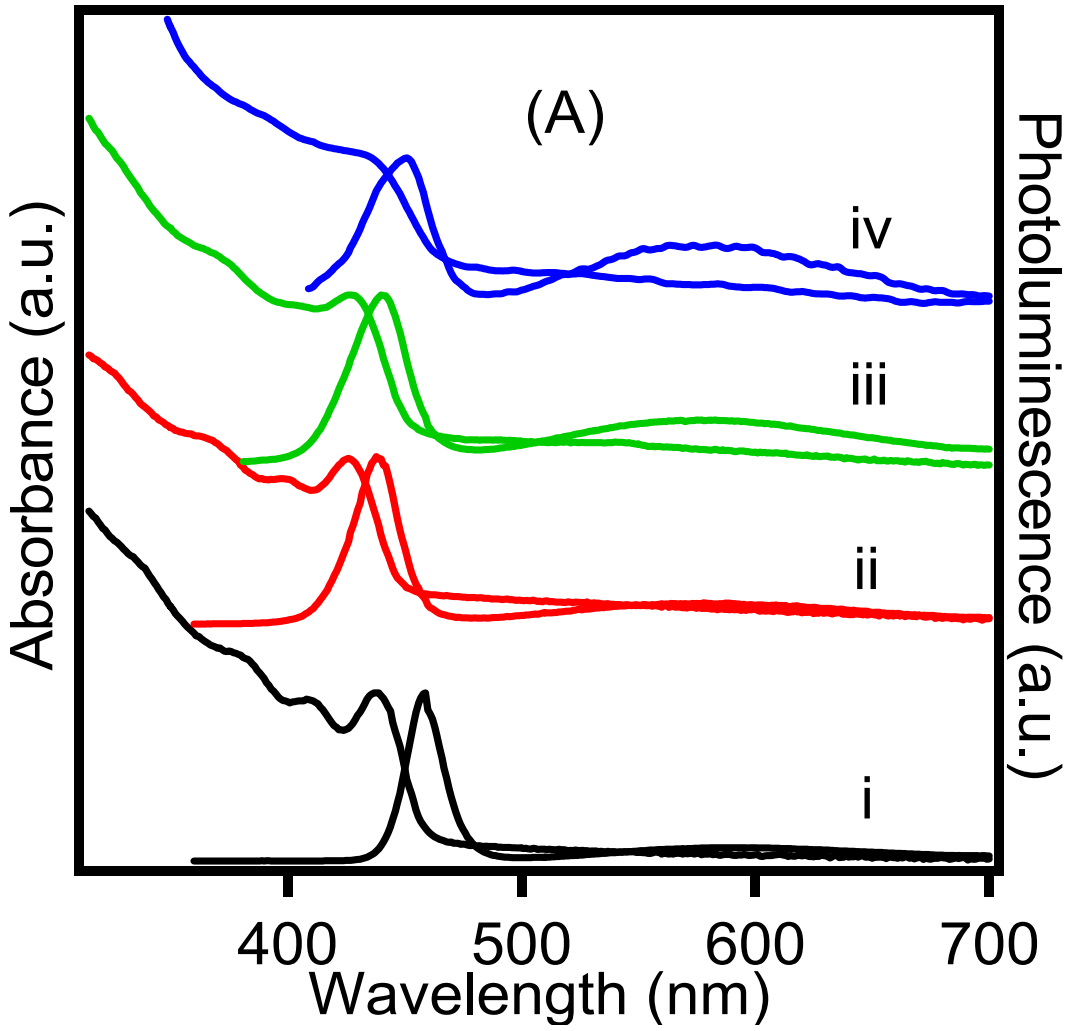

Figure 3.8A. CdS Growth w/ HDA

The absorption and PL of CdS is shown as a function of HDA concentration in the reaction mixture. The particles are grown at 240°C with a ramp time of 18 min and zero hold time time under conditions with i) no HDA added (0:1 HDA: TOPS), ii) 0.1mmol (0.5:1 HDA:TOPS), iii) 0.2mmol (1:1 HDA:TOPS), iv) 0.4mmol (2:1 HDA:TOPS).

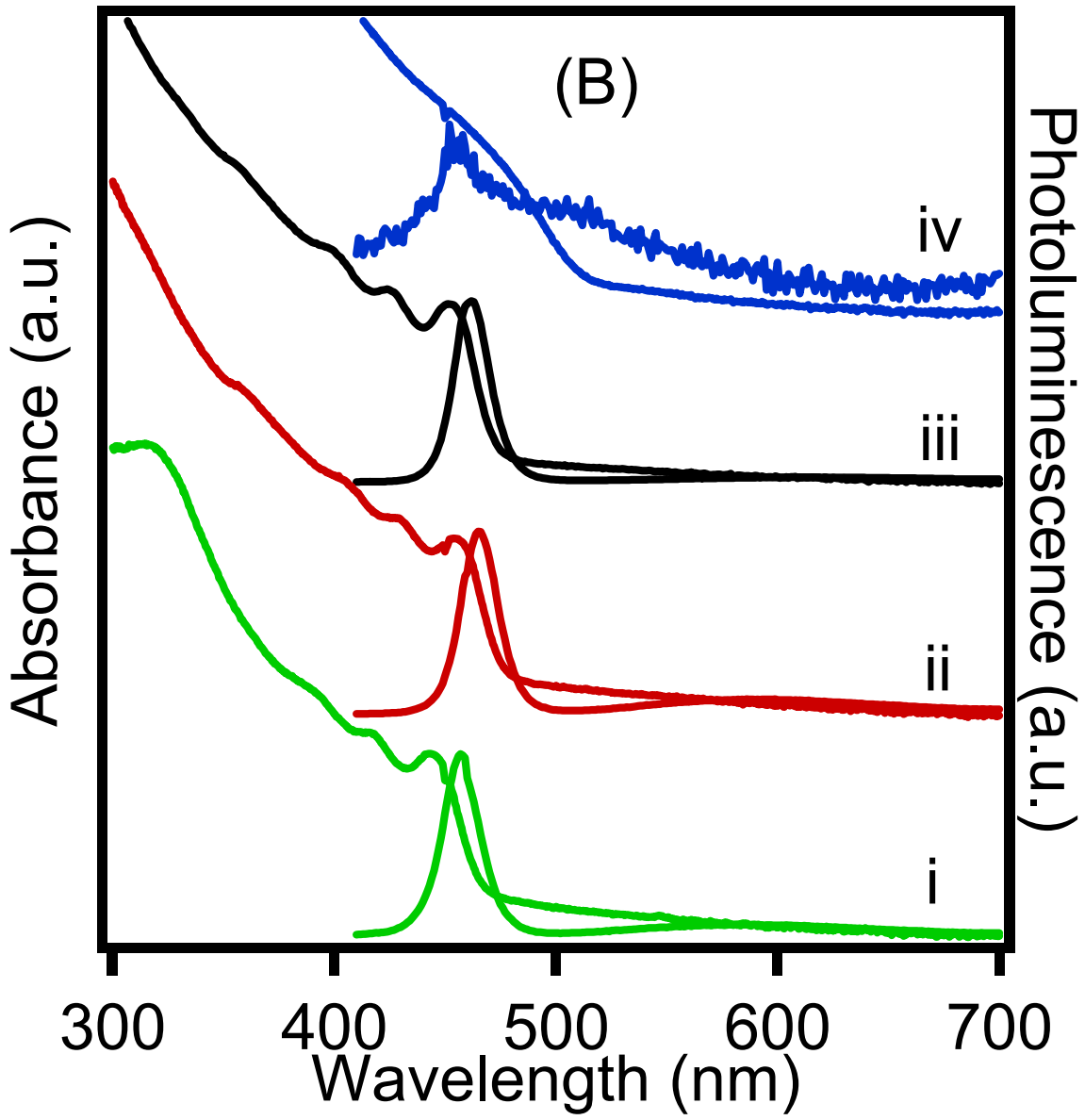

Figure 3.8B. CdS Growth at Different Sulfur Ratios

The Absorption and PL spectra for CdS grown at 220°C with Cd to S ratios ranging from i) 3:1, ii) 2:1, iii) 1:1, iv) 1:2.

PLQY at 0.1 mmol (0.5:1 HDA to TOPS), 33.1% at 0.2 mmol HDA (1:1 HDA to TOPS), and 6.4% at 0.4 mmol HDA (2:1 HDA to TOPS). The results imply the Cd monomer activity may be influenced by the presence of HDA, thus impacting the size focus of the reaction or potentially the nature of the Cd or S rich surface via changes to the facet expression if HDA enhances Cd rich over S rich face expression.

Influence of metal to chalcogenide ratio. In analogy to the observations in CdSe, the growth behavior and the resultant optical properties (exciton linewidth, PLQY) for CdS are also strongly impacted by the mole ratio of the Cd^{2+} to S^{2-} monomer in the reaction mixture.[83] In Figure 3.8B, the change in the optical properties as a function of the mole ratio of TOPS to Cd in the absence of HDA shows that the optimum conditions for growth of CdS in the MW requires a 1:1 Cd:S monomer concentration, as evidenced by the optimization of the exciton features and PLQY. For higher S monomer ratios than 1:1 relative to Cd:S, the defect intensity increases, the PLQY is reduced by a factor of 100, and the dispersity of the sample is lost. The loss of the PL features can be interpreted in terms of the reaction in a kinetic regime where excess sulfur monomer concentration leads to rapid QD formation with a net increase in vacancy and trap site formation under these experimental conditions.

3.4 Conclusion

The observed enhancement of reaction rates for CdS preparation in the MW provides further evidence that selective MW absorption into the TOP-S monomer leads to MW induced activation of the R_3P-S bond and subsequent rapid CdS nucleation and growth. The results are consistent with our earlier reports that R_3P-X, where X is the chalcogenide, completely dominates the initial MW absorption process leading to nearly instantaneous nucleation and growth.[98] In light of these results, it is instructive to consider the MW based reaction rates observed for formation of CdS (18 min), CdSe (30 s), and CdTe (15s) carried out under identical conditions. A remarkable correlation exists between the reaction time required for formation of the QD materials and the bond energy for TOP-S (444 $\pm$ 8 kJ/mol), TOP-Se (363.6 $\pm$ 10.0 kJ/mol), or TOP-Te (279.9 $\pm$ 10.0 kJ/mol).[97]

The correlation between experimental reaction times and bond strength supports the assumption that the difficulty in preparation of CdS from TOPS can be interpreted as a pure thermodynamic limitation for the activation of the chalcogenide precursor. The reaction is monomer limited by addition of HDA, which leads to a slowing of the reaction dynamics and the

observed smaller QDs at identical reaction conditions. The poorer PLQY for HDA may reflect a Cd rich surface due to the presence of HDA. The presence of amines on CdSe QDs has likewise been observed to lower PLQYs.[114] Furthermore, the results strongly support the observation that selective MW absorption can lead to monomer activation in QD reactions. The quality and ease at which CdS can be prepared from TOPS further generalizes the advantages of using selective MW absorption to control nucleation and growth in nanoscale materials.

CHAPTER 4 SELECTIVE MICROWAVE ABSORPTION BY TOPSE: DOES IT PLAY A ROLE IN PRODUCING MULTIPLE SIZED QUANTUM DOTS IN A SINGLE REACTION?

Chemical transformations carried out under MW irradiation often produce unexpected rate enhancements due to selective MW absorption by reactants in the solution. We demonstrate unprecedented control over nucleation, growth, and Ostwald ripening in the formation of CdSe quantum dots (QDs), the quintessential quantum dot. The selectivity of the process is demonstrated by the ability to generate multiple, different sized QDs in the same reaction, where each QD component exhibits 6-7% size dispersity. The number of QDs, which translates to color intensity, and the size of the QD, which translates to color index, is completely controlled by temperature and concentration in the MW reaction. The ability to repetitively generate nucleation and growth events in which a specific color index with defined color saturation is isolated from a single reaction offers potential for preparing mixed QD compositions for applications in optical bar-coding, white LEDs, and PVs.

4.1 Introduction

For the past decade organic and inorganic reactions have been shown to exhibit enhanced reaction rates for molecular conversions when carried out under microwave (MW) irradiation relative to traditional convective approaches[115,116,117]. Extrapolation of MW irradiation methods to problems in nanomaterial synthesis has also shown rate enhancement coupled to improved material properties.[118,119,120,121] The origin of the reaction rate enhancement for chemical reactions in a MW reaction is poorly understood; however, the consensus of the field implies the rate enhancement for molecular reactions can be traced to efficient dielectric heating (super heating) of the reaction components within a solvent cage.[122,123,124] This is easily understood by considering that in a MW reaction, molecules with a large static dipole are selectively heated and will rapidly thermalize to the solvent.[125] Since the rate of MW heating is described as the ratio of the real and imaginary components of the dielectric constant, the phase-lag between the applied MW field and the molecular dipole of the reaction components results in dielectric molecular

heating.[122] The rate of solvent heating will depend on solvent viscosity and molecular volume of the heated reactant in solution.

In a set of recent studies, we explored the use of MW irradiation to selectively heat the reactive monomers for quantum dot (QD) synthesis in the presence of alkanes, which are non-MW absorbing.[125] Through the use of a non-MW absorbing solvent, the reaction rate for formation of both II-VI and III-V nanocrystals was markedly accelerated[125,126,127] Interestingly in the MW, the size of the isolated QD was observed to depend on the reaction temperature and not the power while dispersity was independent of the observed temperature and power. This is counter intuitive for lyothermal reactions where size focusing and defocusing is observed in the QD reaction driven by a diffusion controlled process due to Ostwald ripening.[128,129,130,131] The difference in growth behavior for QDs in a MW and a thermal reaction can be interpreted by delineating the two independent growth regimes, namely diffusion controlled and reaction controlled.[129] A lyothermal reaction is observed to follow diffusion control resulting in the observed size focusing / defocusing behavior. In the reaction controlled limit the size of the QD will not rapidly defocus by Ostwald ripening if the activity of the monomer in solution (a_{solute}) is greater than the activity for the monomer generated by particle dissolution, which arises via an Ostwald mechanism (a_{solid}). In a reaction controlled regime, Ostwald ripening will give rise to QD growth, but the dispersity should remain focused if the QDs are not kinetically rough.[132] One way to achieve a reaction controlled QD growth regime would be the rapid depletion of the monomer in the diffusion layer around the formed nuclei. Typically this is not achievable unless the monomer can be selectively activated. Such an effect was suggested for a MW controlled reaction in our earlier study on CdSe and CdTe.[125]

In this manuscript, we interrogate the control offered by a reaction controlled growth for CdSe QDs. Although MW occurs for all the II-VI materials (CdTe, Figure 4.1), CdSe is focused on in this manuscript due to its wide usage by the broader community. The demonstration of three (and even four) independent QD sizes using the single reaction MW methodology for a decreasing reaction temperature protocol and a single larger QD if the reaction temperature is raised illustrates the control offered by a reaction controlled growth process for QDs.[129] While repeated nucleation or SILAR growth can be seen in a lyothermal reaction, the excess thermal energy results in rapid evolution to a single QD size for both experiments unless very specific reaction controls are applied.[133,134, 135] The MW QD synthetic methodology leads to highly

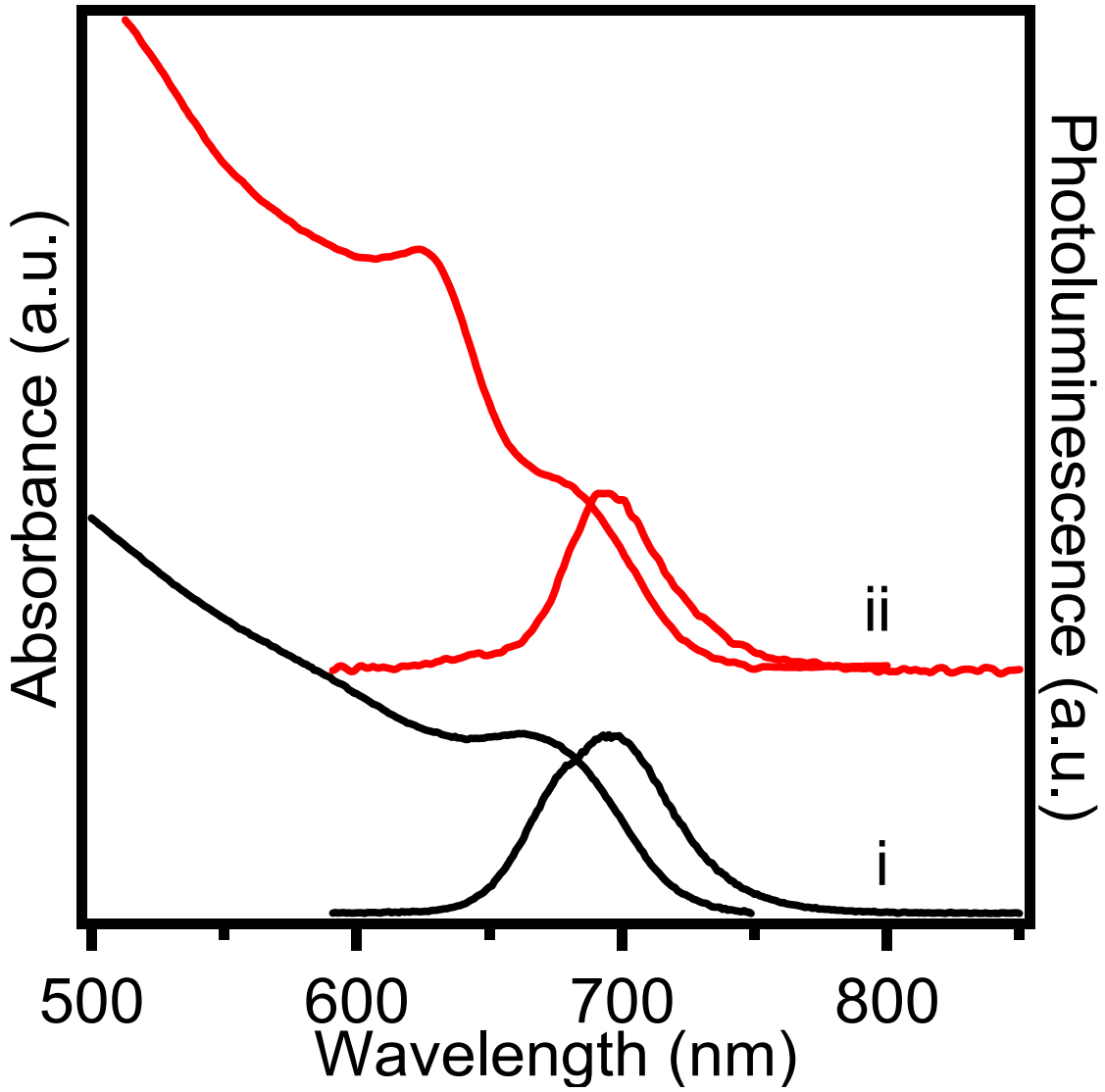

Figure 4.1. CdTe Subsequent Growth

Absorption and emission of CdTe NC grown by MW irradiation at i) 240°C for 30s and then at ii) 200°C for 30s after a second injection of precursor and a MW cycling event.

reproducible, narrow QD color codes (QD size and dispersity) and color saturation (QD concentration) controlled by the MW conditions. The MW QD synthetic methodology is compatible with industrial processing and may simplify development of applications ranging from biology to device platforms where bar-coding, controlled color or multiple QD sizes are important. [136,137,138, 139,140, 141,142,143,144]

4.2 Experimental

4.2.1 Synthesis of CdSe QDs.

The synthesis of CdSe is carried out by literature procedures[126] using tri-octyl phosphine selenide (TOPSe) as the Se^{2-} source and cadmium stearate (CdSA) as the Cd^{2+} source for the thermal and microwave reactions[125,145]. The stock cadmium solution is prepared by dispersing CdSA (1.0 mmol, 679.36 mg) into 20 mL of solvent by sonication, while a 1 molar Se stock solution is prepared under Argon using Se powder (0.01mol) dissolved in 10mL of TOP. The MW reactions are carried out in decane under ambient conditions, while the thermal reactions are carried out in Octadecene under Argon.

4.2.2 Multiple CdSe QDs.

Multiple CdS QDs were prepared in the MW in a single reaction process by sequential addition of monomers at RT followed by MW heating to successively lower reaction temperature set-points, as shown in Figure 4.2. Carrying out the same successive additions as shown in Figure 4.2, but heating the reaction to successively higher set-points yields a single QD size. In order to maintain identical total reaction times (5min) the specific times for the three MW regimes (heating, hold, cool down) are varied. The time for ramping to reaction temperature at 300W applied MW power ranges from 2 – 3 min. The hold time for the reaction at the reaction temperature ranges for 30 s – 2 min. The cool down cycle is held constant at 1 min. The same results as presented in the manuscript for CdSe growth are also obtained if the hold time is held constant. For the lyothermal reaction the identical sequence is applied, however the reaction runs for 20 min (thermal) for each monomer addition step. The microwave reactions are carried out in a single mode CEM Discover System operating at 300W, 2.45 GHz with a pressure limit of 300 psi. The thermal reactions are carried out in a standard three-neck flask with convective heating (heating rate 5° C/min) at identical temperature setpoints as the MW process.

4.2.3 Synthesis of Multiple QDs.

Synthesis of CdS/CdSe. The material from the CdS synthesis was used without any further purification or precipitation. Nanocrystal CdSe was prepared from a method by Washington et al. in which stock solutions of CdSA and TOPSe were prepared by dispersing CdSA (1.0 mmol, 679.36 mg) into 20 mL of decane by sonication, while a 1 molar solution of TOPSe was prepared under Argon using Se powder (0.01mol) dissolved in 10mL of TOP. The reaction mixture with a total volume of 2.25mL (totaling 4.3mL) was added to the same 10 mL reaction vessel under ambient conditions with the existing CdS materials using a 1:5 molar ratio of cadmium to selenium. The reaction mixture was heated in the microwave cavity to a temperature of 220°C during a 1 minute ramp period at a power of 300W. The mixture was then allowed to react for 30s at 220^{o}C and immediately cooled to room temperature using forced air cooling. In the case where nanocrystals were isolated, standard re- precipitation methods were used. They were grown in succession in the order of CdS, CdSe, and lastly CdTe without the use of any purification steps in between.

Synthesis of CdS/CdSe/CdTe. Using the materials from the previous CdS/CdSe reaction without further purification, nanocrystalline CdTe was prepared from a similar method where a 1 molar solution of TOPTe is made by dissolving elemental tellurium (10mmol, 1.276g) into 10mL of TOP. In addition, a 25mM solution of CdSA in decane is also prepared. The two solutions are mixed at a ratio of 1:1 with a volume of 2.05 mL (totaling 6.35mL) in a 10mL microwave reaction vessel.

4.3 Results and Discussion

The mechanism for growth control of QDs is well established with two critical domains, a pure diffusion controlled ($K < 0.01$) and a reaction controlled ($K > 100$) limit, where $K = a_{solute} / a_{solvent}$ (a_{solute} represents the activity of the solubilized monomer in solution, while $a_{solvent}$ represents the activity of the monomer on the solid surface).[129,132] Under the diffusion limit the monomer activity in solution approaches the monomer activity of the QD surface, thus $K \leq 1$. This condition is easily met in a lyothermal reaction. In a reaction controlled process, $K > 100$ indicating the activity of the monomer is solution is far higher than the activity of monomer generated by QD dissolution. This is an intriguing regime where the TOPSe in solution exhibits a higher activity resulting in rapid depletion of monomer within the diffusion shell. Since QD dissolution depends on surface roughness and time, the low $a_{solvent}$ implies low surface roughness

or fast reaction times must exist for the reaction to be described in the reaction control limit.[129,132]

Our earlier observation of a temperature dependent reaction with tight dispersity CdSe QDs out of the MW suggested a reaction controlled regime for QD growth exists in the MW.[125] If this is the case, one would predict that carrying out the reaction in a stepped profile with three successively lower reaction temperatures, as shown in Figure 4.2, should result in the production of three independent well-defined QD sizes with the QD dispersity identical for each step. In addition, for a reaction carried out at increasing temperatures should give rise to a single larger QD, similar to the SILAR reaction.[146]

4.3.1 Effect of Decreasing Temperature Set-points.

The optical data and TEM analysis for carrying out the CdSe QD growth using a decreasing reaction set-point profile (230^{o}C, 200^{o}C, 170^{o}C) is shown in Figure 4.3A and Figure 4.3B. In Figure 4.3A, each successive introduction of monomer at RT and heating to a lower temperature set-point yields a new lower energy PL feature and increasingly complex excitonic spectra at higher energy for the absorption spectral manifold. For the three monomer additions, based on the new spectral features it appears three individual QDs are formed in the solution. The complexity of the absorption spectral manifold arises from the overlapping higher lying excitons for the successively smaller QDs generated in the reaction. Conducting the MW reaction at four specific temperature points (240°C, 210°C, 180°C, and 150°C), yields four PL features consistent with four discrete CdSe QDs, as observed in the absorption and PL spectra (Figure 4.4).

The observable narrow PL features in Figure 4.3A can be assigned as individual PL features with discrete full width half-maxima (FWHM) at 547 nm (28 nm FWHM), 581 nm (31 nm FWHM), and 617 nm (30 nm FWHM). The PL features correlate with CdSe QDs of 3.11 nm, 3.63, and 4.92 nm, respectively. The QD sizes assigned from PL are confirmed by Scherrer analysis of the pXRD data and by inspection of the TEM of the raw sample after the third monomer addition reaction (Figure 4.3B). The narrow PL features (28-31 nm) imply tight distributions for the QD size dispersity following growth. Comparison of identical QD sizes prepared by a traditional lyothermal route yield a FWHM of 28-29 nm for 5% size dispersity sample, suggesting the stepped reaction profile does not increase the dispersity of the QD samples grown in the MWs.[147,125] Assuming no significant loss of dispersity in sequential

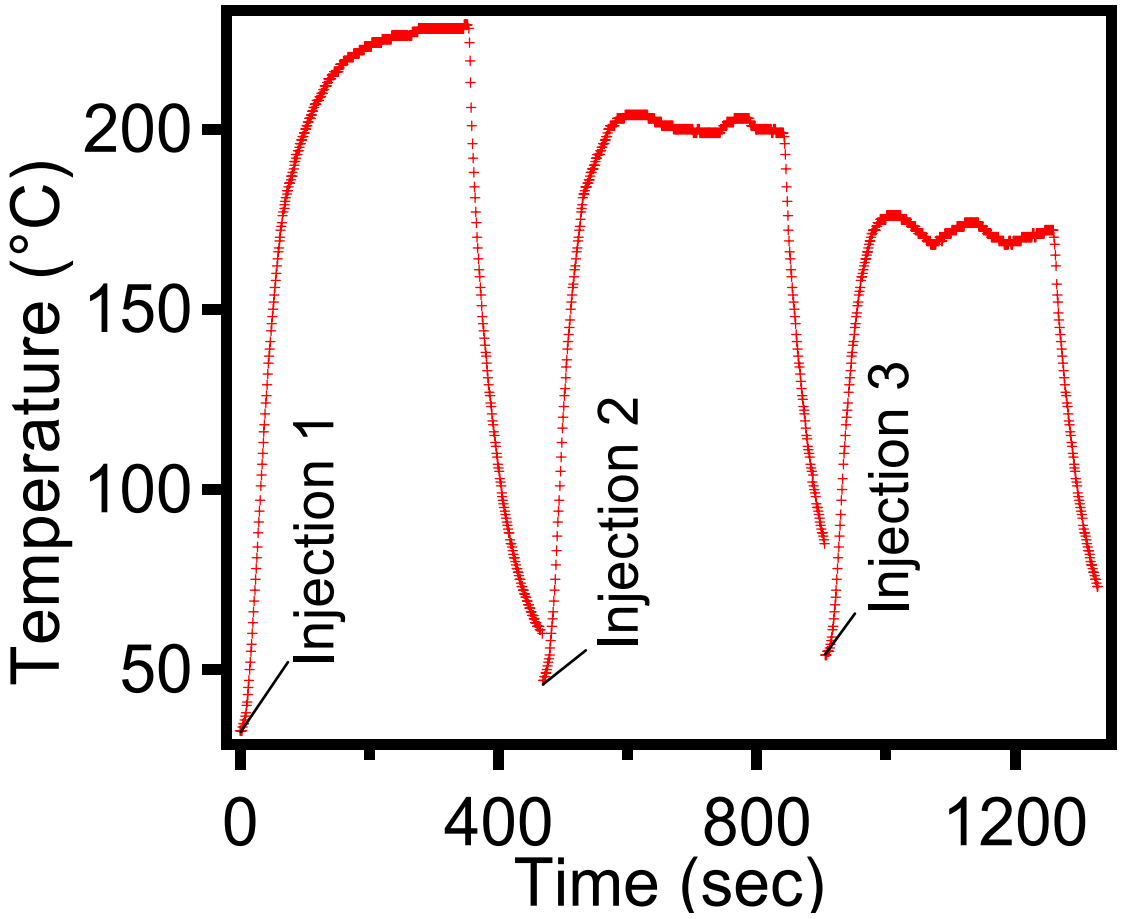

Figure 4.2. Microwave 3x Cycle Heating

MW cycling protocol used for decreasing reaction temperature sequence to produce three discrete tight dispersity QD samples in the MW cavity.

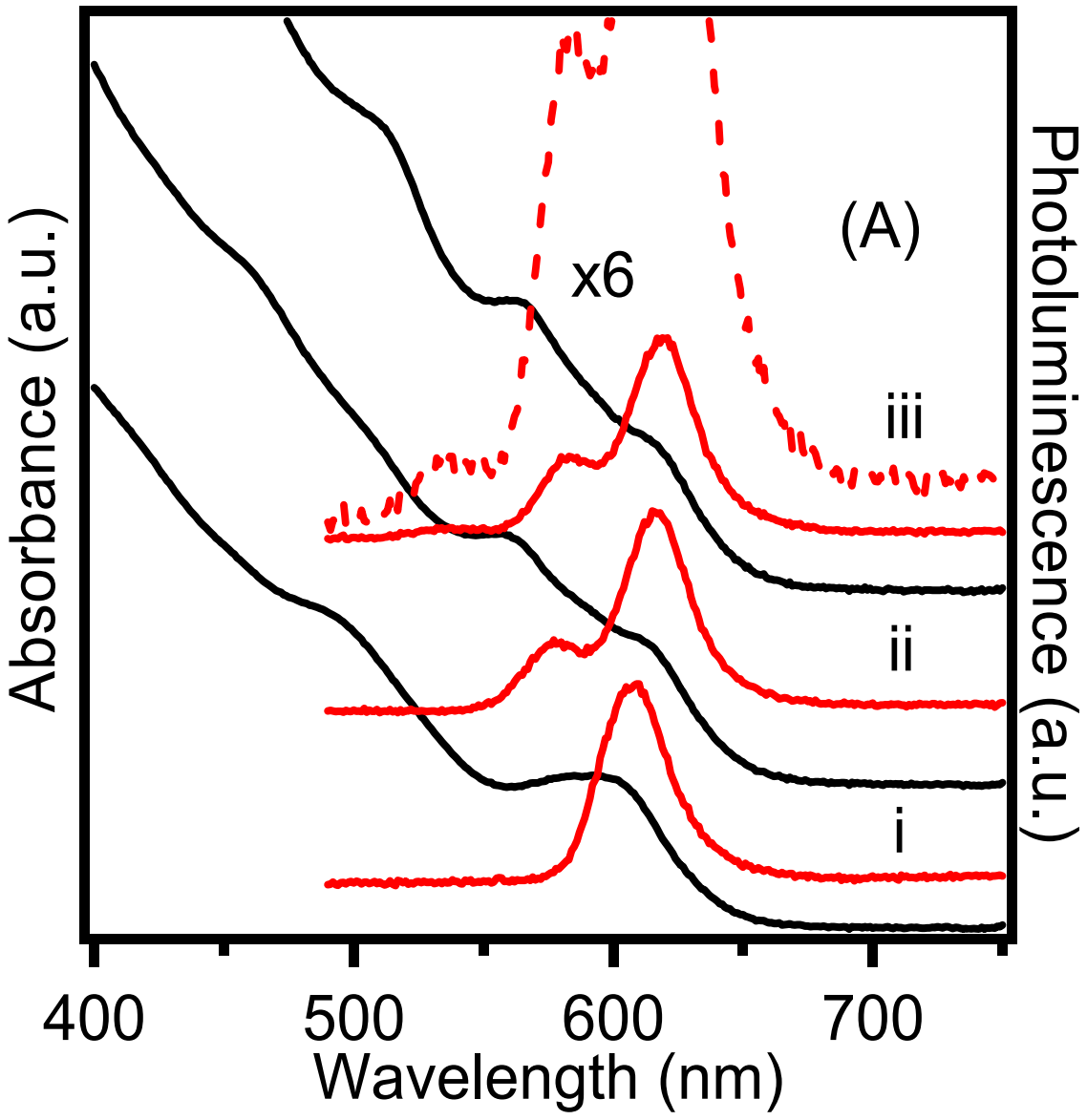

Figure 4.3A. Decreasing Temperature Setpoint on 3x Injection CdSe

Absorption and PL spectra for CdSe QDs prepared at sequentially lower reaction set-points i) 230°C, ii) 200°C, iii) 170°C.

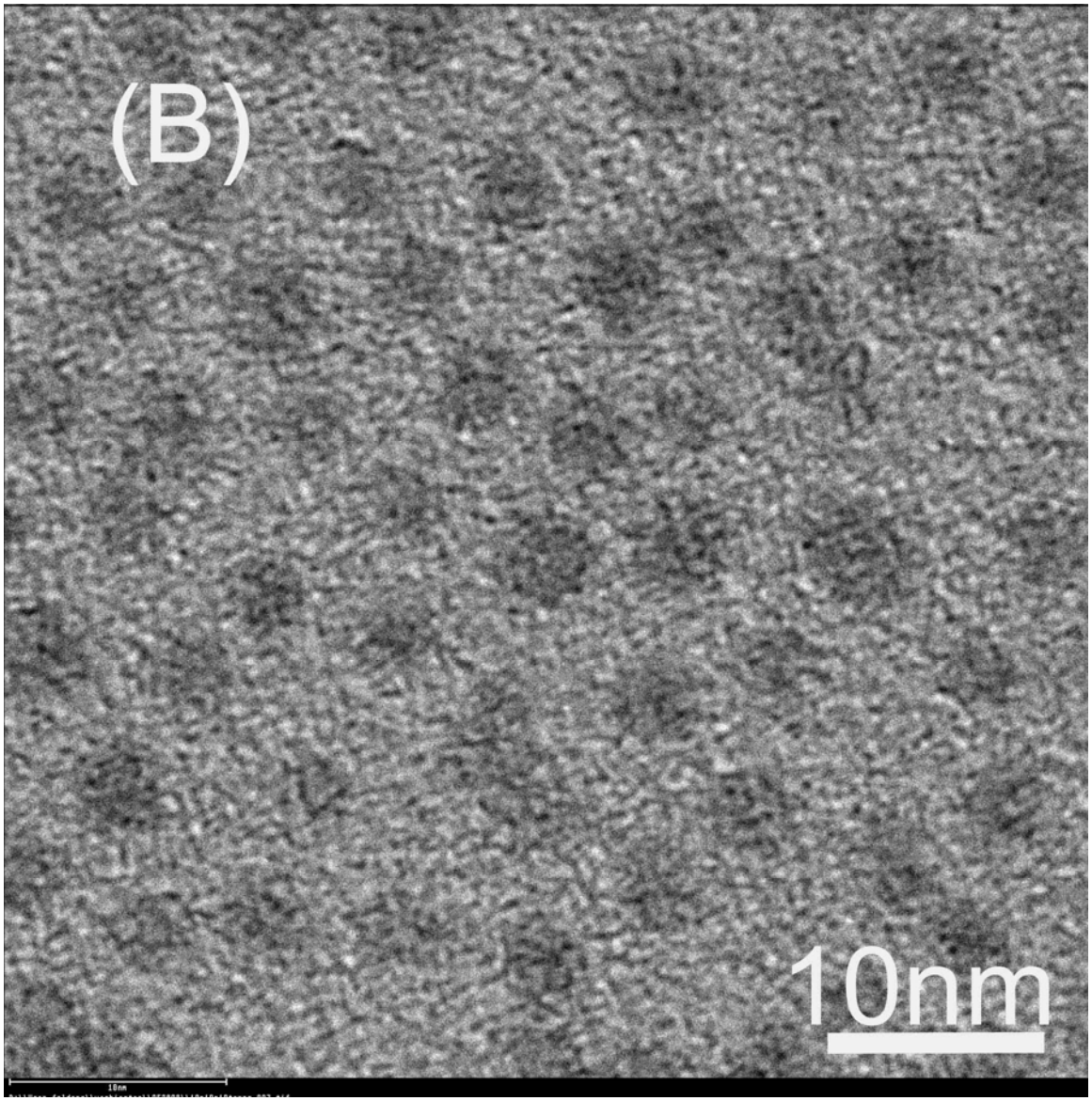

Figure 4.3B. TEM 3x Injection CdSe 3 Sizes

TEM of CdSe QDs (A iii) grown after three monomer additions at sequentially lower temperature.

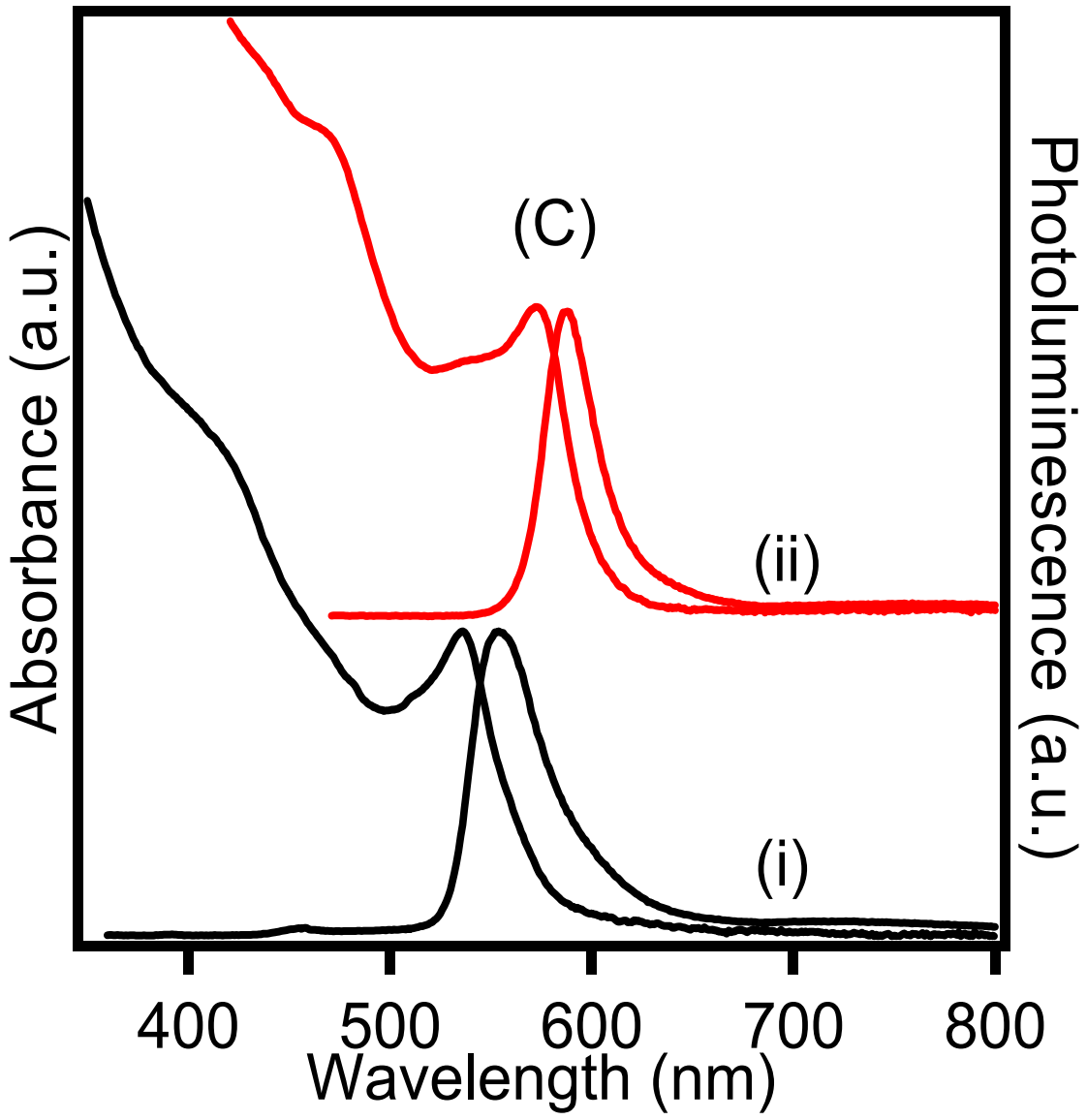

Figure 4.3C. Increasing Temperature Setpoint on 2x Injections

The absorption and PL spectra of CdSe QDs grown using an increasing temperature set-point protocol. i) 180°C and ii) at 240°C

reaction events, as suggested by the lack of change in PL FWHM for the largest QD during the reaction, this implies the initial dispersity established by the MW absorption of QD growth is maintained during the entire time of the reaction for all QDs in solution. TEM analysis for each individual step in the reaction confirms no size change occurs or changes in the size dispersity for each individual QD size generated during the MW cycling (Figure 4.5). The lack of change to the QD size dispersity or QD sizes for each subsequent reaction is surprising and implies no contribution from size defocusing during the MW reaction. The observation of no size defocusing implies Ostwald ripening is a minor contributor, which is somewhat surprising. One possible explanation is the time scale of the reaction is short or the QDs in the solution lack of kinetic roughness due to annealing of surface defects potentially by direct MW absorption by the QD following monomer depeletion.[132]

4.3.2 Effect of Increasing Temperature Set-points.

Assuming a reaction controlled growth regime in the MW, carrying out the reactor at increasing temperature set-points is expected to increase the QD size and narrow the size-dispersity, rather than produce individual QDs. In effect a size focusing reaction arising from the lower energy for a monomer to add to a pre-existing QD if the reaction to a larger QD size is thermodynamically favorable.[146] In Figure 4.3C, the absorption and PL data are shown for a two monomer additions carried out at 180°C (first monomer addition) and 240°C (second monomer addition). It is evident from the absorption profile that the initial 180°C step produces a QD of 3.6 nm in size (λabs = 536nm, λem = 554 nm). The second 220°C produces a larger CdSe QD of 4.5nm in size (λabs = 573 nm, λem = 588nm), nearly identical to the size expected for a reaction carried out at 240° C. A narrowing of the absorption excitonic features and the PL FWHM (56 nm → 32 nm) is also observed following the second monomer addition for the data in Figure 4.3C. The narrowing of the spectral features implies narrower size dispersity following the two-step MW heating at increasing temperature set-points similar to a SILAR reaction. Inspection of the absorbance intensity, which correlates to the number of QDs in solution (when corrected for ε) shows no increase in the number of QDs in the reaction mixture following the second monomer addition implying the monomer reacts with the QDs in solution and does not form a re-nucleation event. These results support that CdSe QD growth in the MW is well-described by the reaction-controlled regime (K > 100).[129,32]

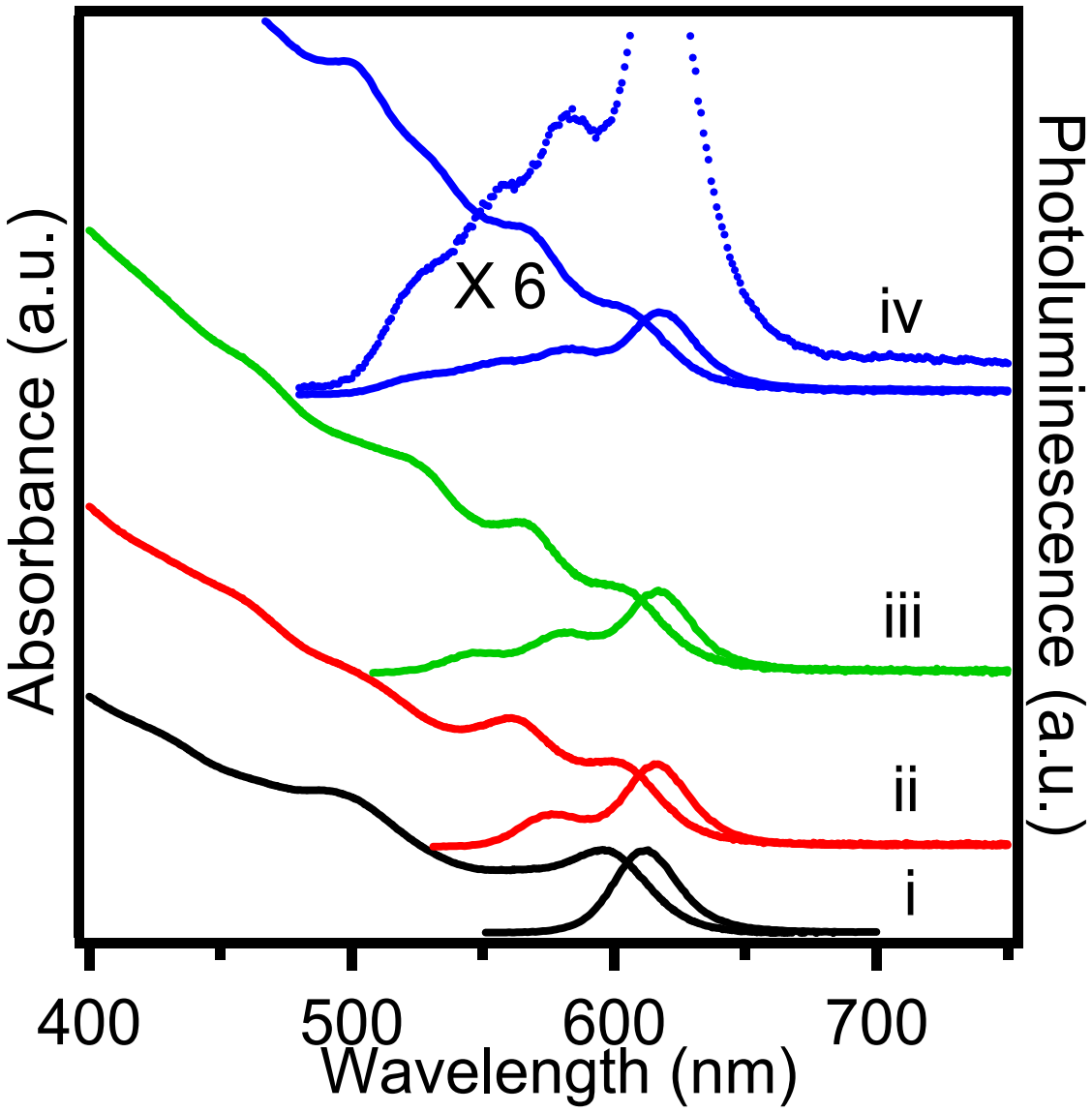

Figure 4.4. Decreasing Temperature Setpoint 4x CdSe

The absorption and emission spectra showing CdSe nucleated with successive injections (up to 4 shown here).

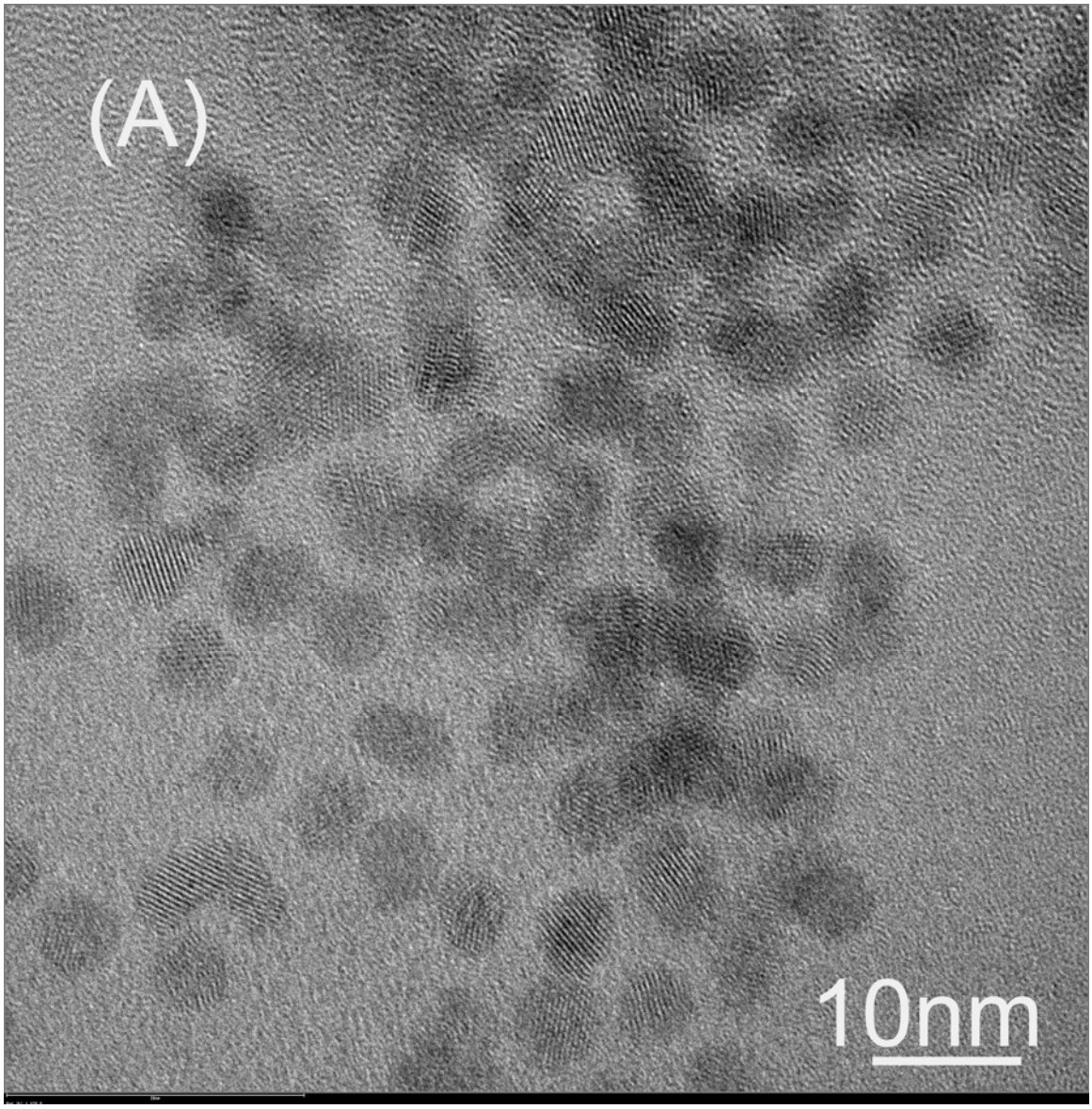

Figure 4.5A. TEM CdSe 240C 30s Microwave Reaction

TEM of CdSe grown in a single MW reaction achieved by MW cycling in the presence of added precursor for CdSe grown at 240 0C for 30s.

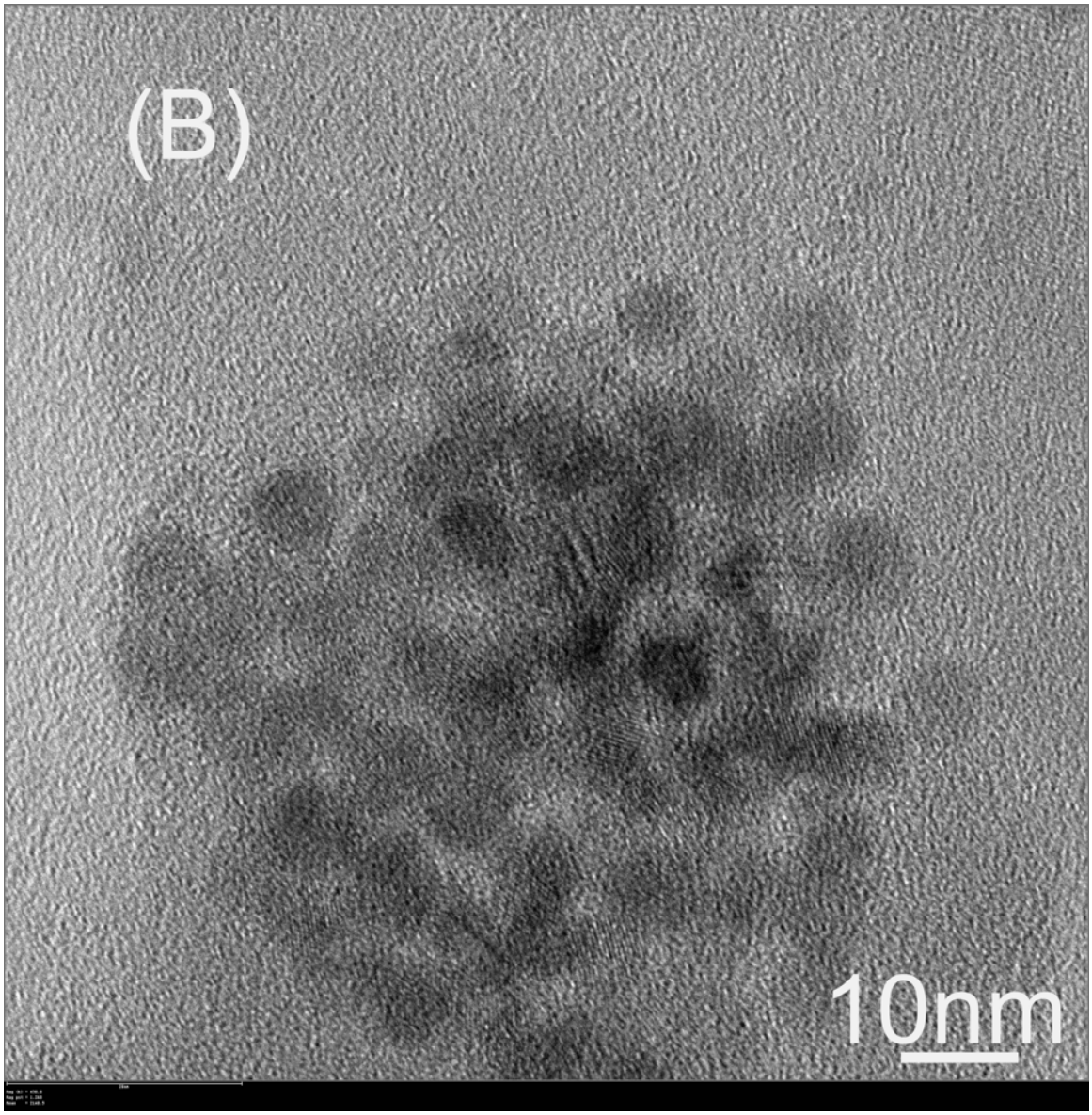

Figure 4.5B. TEM Decreasing Temperature Setpoint 2x CdSe

TEM of CdSe grown in a single MW reaction achieved by two subsequent MW cycling events in the presence of added precursor for the 2nd Precursor injection grown at 210 0C for 30s.

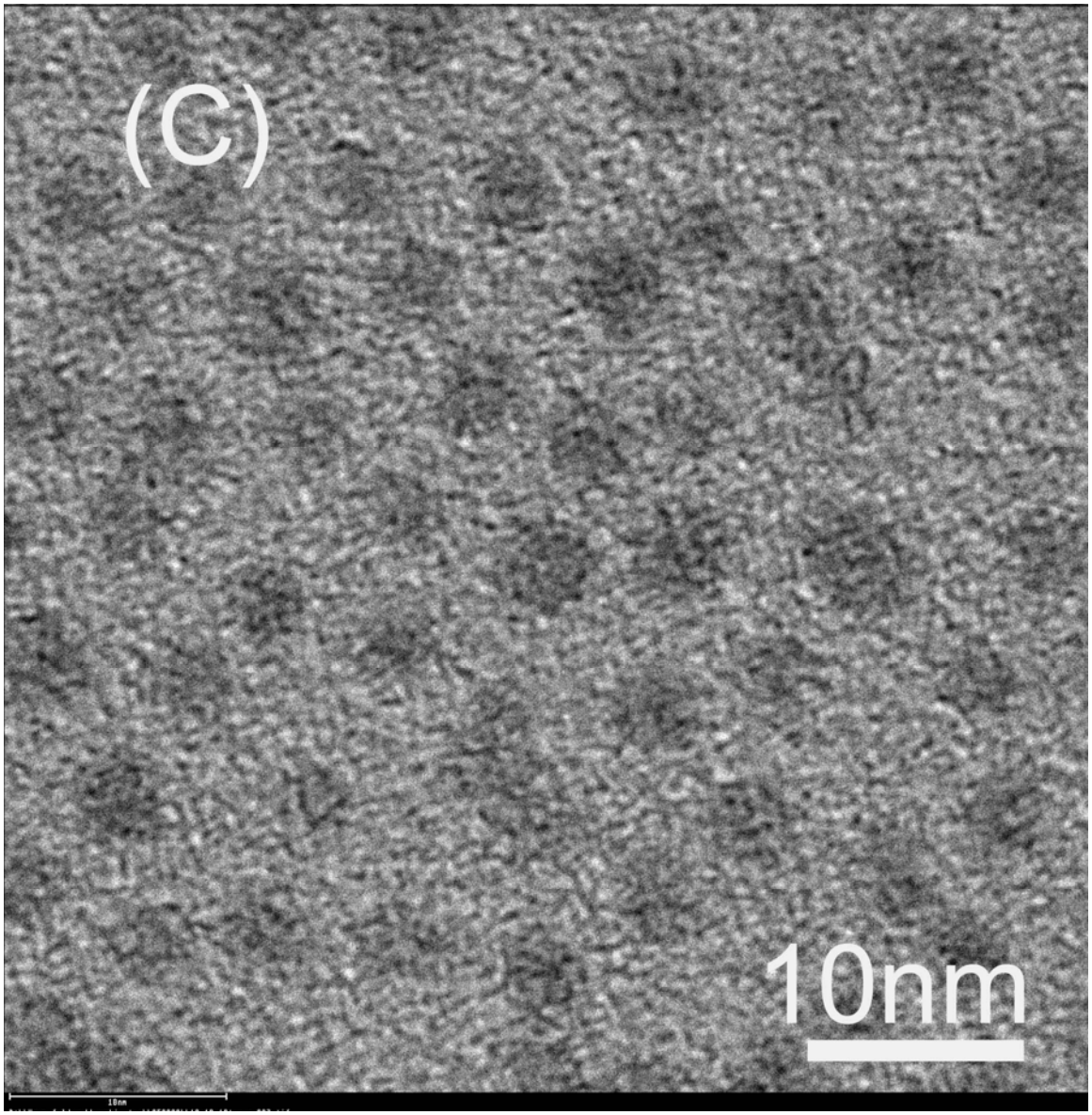

Figure 4.5C. TEM Decreasing Temperature Setpoint 3x CdSe

TEM of CdSe grown in a single MW reaction achieved by three subsequent MW cycling events in the presence of added precursor for the 3rd Precursor injection grown at 180 0C for 30s.

4.3.3 Influence of Selective Absorption by TOPSe.

While it is clear that the reaction temperature controls the observed QD size, it is unclear whether or not the growth behavior is traceable to selective activation into TOPSe in solution leading to the observation of an enhanced reaction rate. As suggested previously,[125,126] TOPSe has the largest MW cross-section, implying that TOPSe absorption accounts for the rate acceleration in the MW and subsequent growth behavior of the QDs. To confirm the MW growth behavior is attributable to selective absorption into TOPSe generating a highly activated Se monomer in the solute, a set of experimental controls were conducted to compare the results from a lyothermal method, a MW reaction carried out in the presence of a strong microwave absorber, and a MW reaction carried out without additional monomer. The reactions are conducted with identical reaction set-points (220^{o}C, 180^{o}C) via addition of monomer at RT and subsequent heating. The lyothermal reaction requires longer reaction times due to the slower heating rates.

Lyothermal Reaction. The absorption and PL spectra for the lyothermal reaction carried out with monomer addition and temperature ramping to 220°C followed by monomer addition at RT and reaction at 180°C are shown in Figure 4.6A. The initial absorption and PL for the 220°C growth can be assigned to the formation of a 4.42 nm CdSe QD (580 nm PL, 29 FWHM) (Figure 4.6A (i)). Following addition of fresh monomer and heating to 180°C (3h) yields an absorption and PL feature consistent with a 4.57nm QD (593 nm PL, 38 FWHM) (Figure 4.6A (ii)). Notably the absorption and PL data in Figure 4.6A for the lyothermal reaction do not exhibit two discrete PLs, exhibits PL broadening, and exhibits QD growth to a larger size following the second monomer addition, even though the reaction is carried out at a lower temperature set-point. Upon introduction of fresh monomer, the absorption FWHM broadens from 28 → 43 nm for absorption and the PL spectra broadens from 30 → 38 nm implying loss of size focus in the reaction. The temperature dependent growth behavior for a lyothermal growth reaction is consistent with repeated results. [130,148,149]

The time dependent changes in the absorption and PL features following the second monomer addition for the lyothermal reaction are telling (Figure 4.7). Inspection of the absorption and PL spectra following the second monomer addition at RT and subsequent heating to 180^{0}C indicates an appearance of a second nucleation/growth event at short experimental times, 30 -60 min. After 60 min, the second absorption feature is lost and the lowest energy

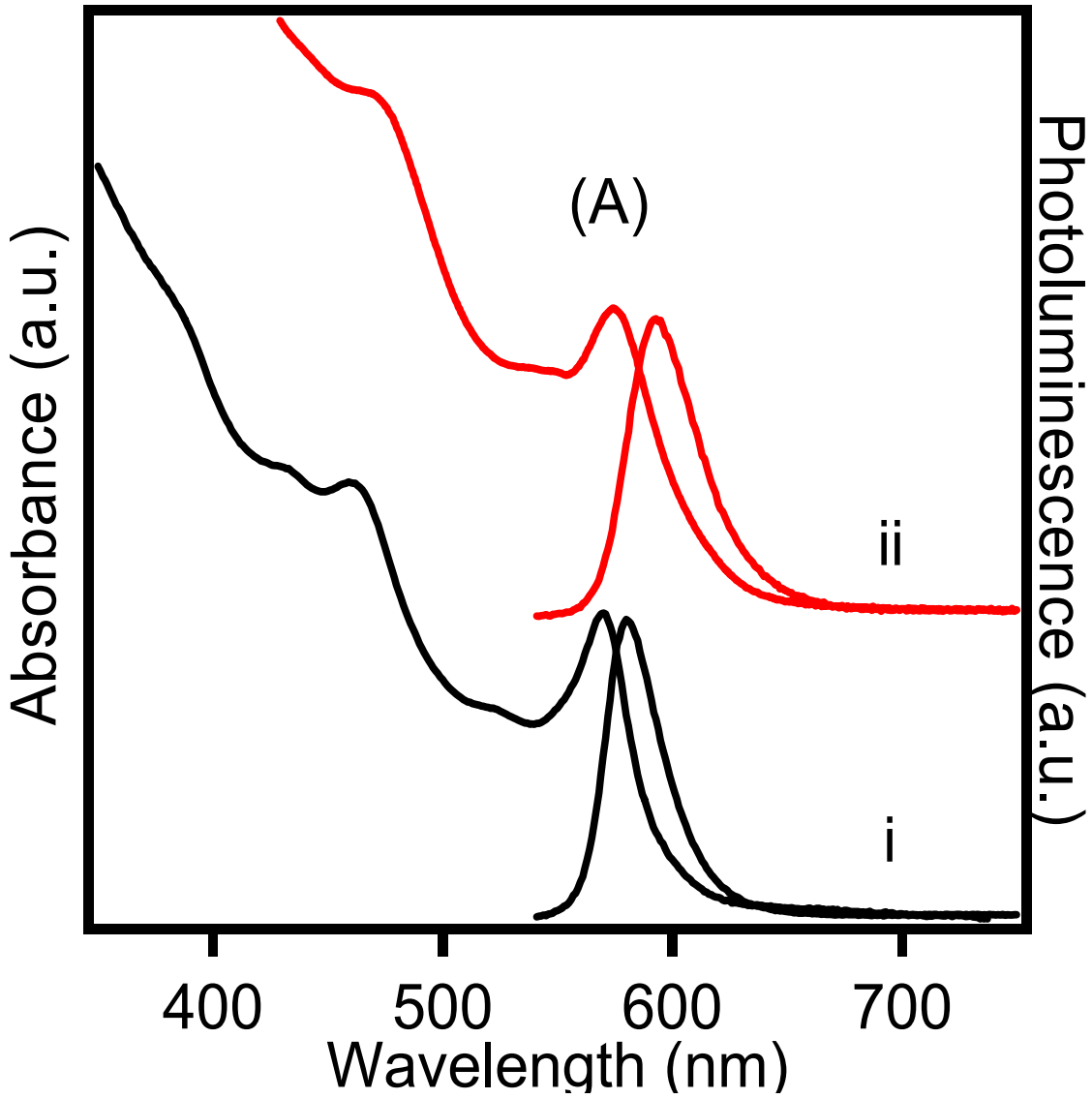

Figure 4.6A. Lyothermal Reaction 2x CdSe Injection

Absorption and PL spectra for lyothermal reaction with subsequent monomer addition carried out at i) 220°C and ii) 180°C.

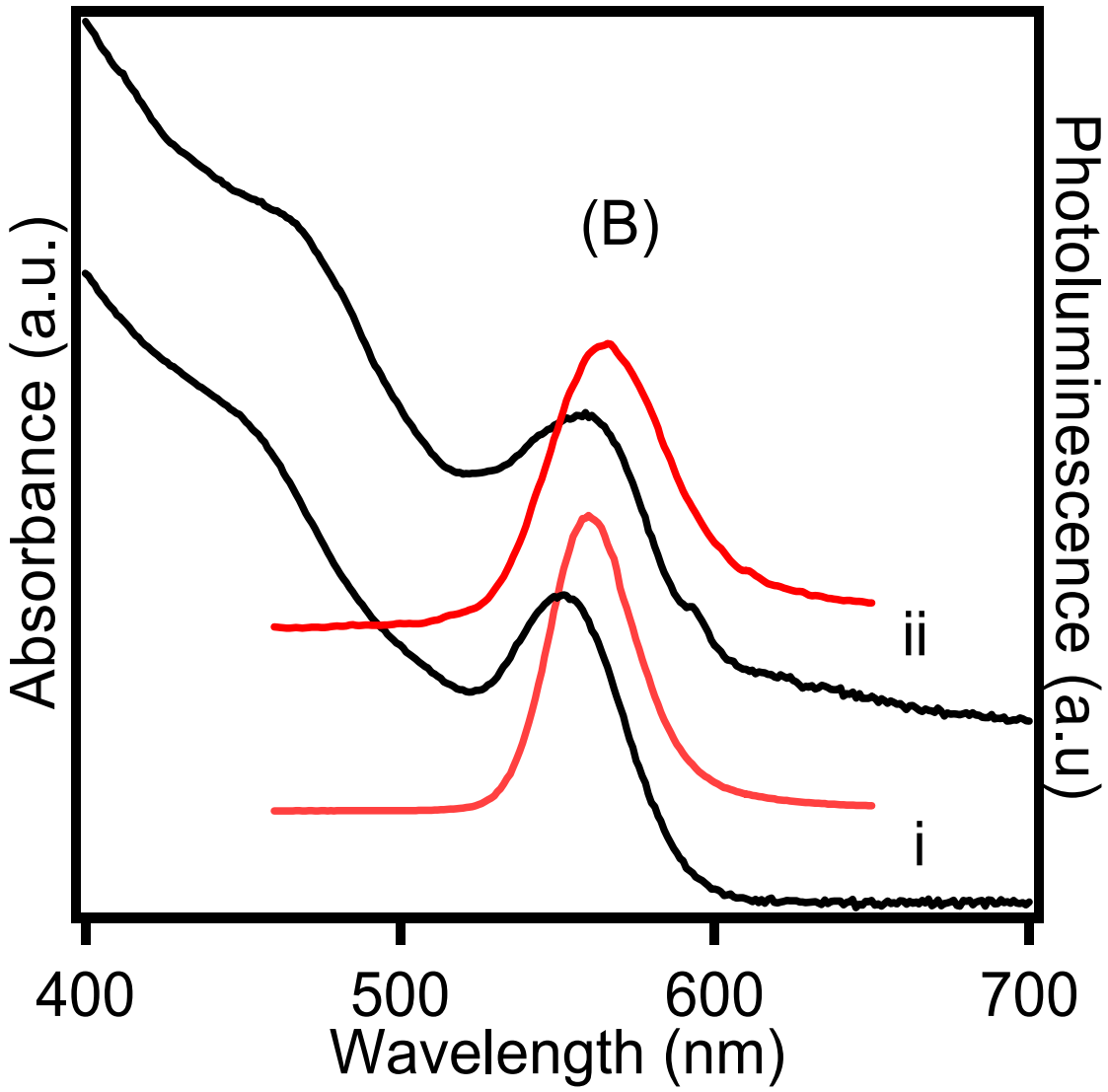

Figure 4.6B. Increasing Temperature Setpoint 2x CdSe w/ IL

The growth of CdSe QDs in the MW with two subsequent monomer injections in the presence of an IL, specifically 0.2mmol ImCl at i) 220°C and ii) 180°C.

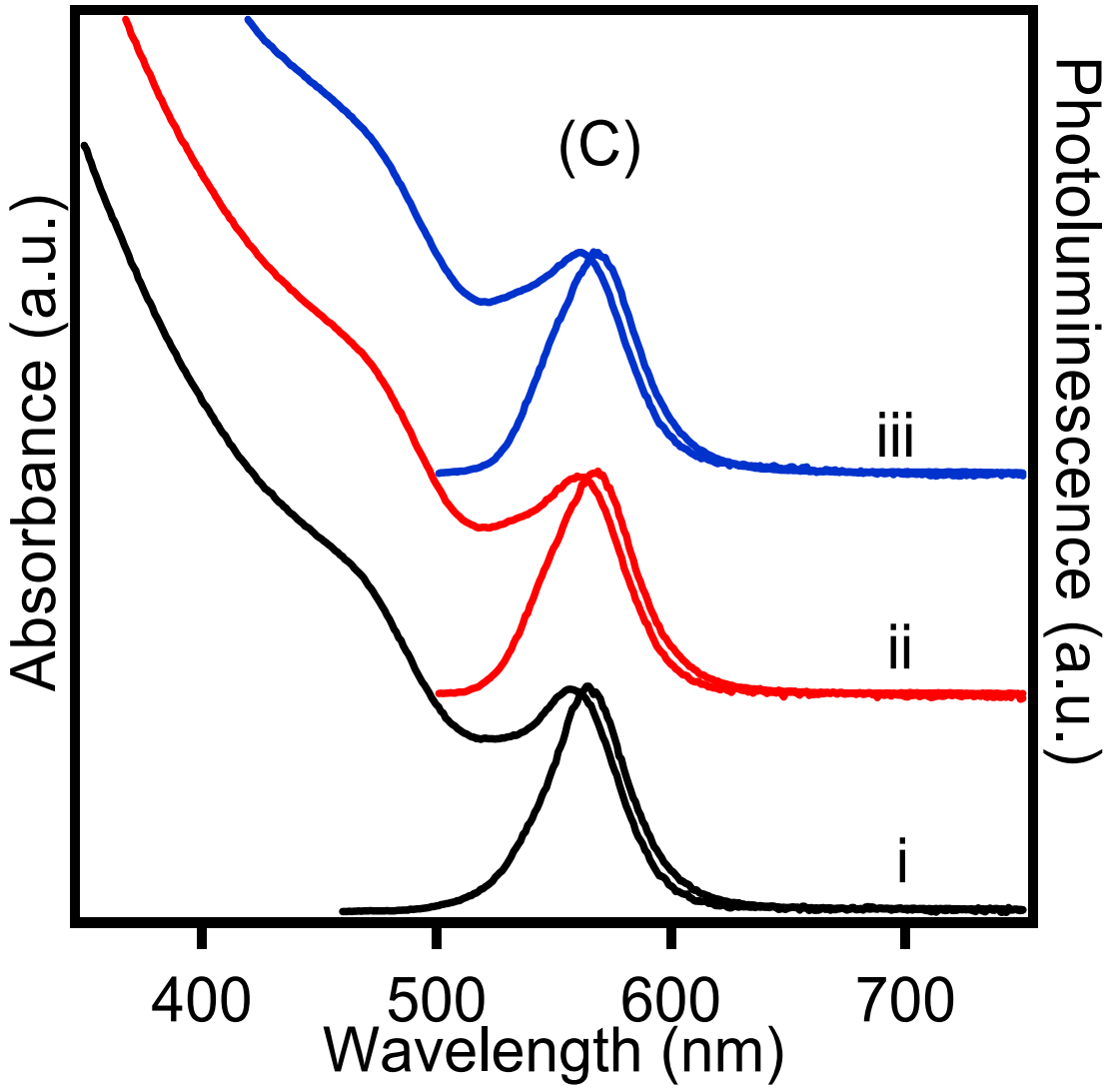

Figure 4.6C. 3x Microwave Cycling w/ Precursor Addition

MW cycling reaction in the absence of monomer addition at i) 220°C, ii) 200°C, and iii) 180°C.

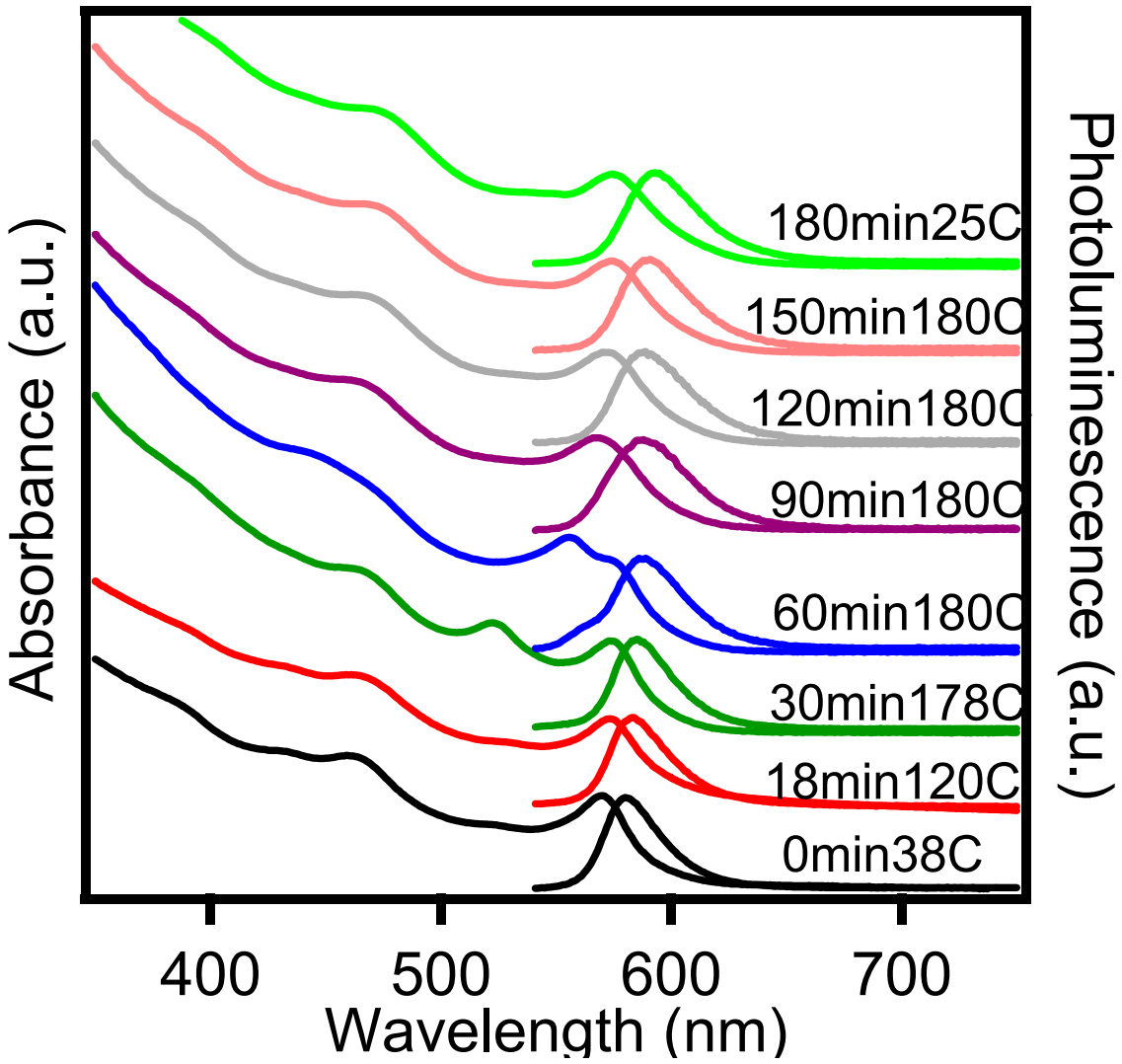

Figure 4.7. Thermal 2x Re-Injection at Increasing Temperature

Absorption and emission of the complete thermal re-nucleation with aliquots taken at 15-30min intervals.

exciton broadens. In conjunction with the absorption spectral changes, a small PL shoulder is observed, which is lost at longer reaction times. The observed time dependent growth and broadening observed in the spectral data can be attributed to classical Ostwald Ripening processes in a diffusion controlled reaction limit.[129,132] It is worth noting that lyothermal reactions do show size focusing (SILAR method), as well as separate nucleation events, if the monomer addition is added slowly at the same reaction temperature.[146]

Reaction in the Presence of a Strong MW Absorber. In the MW, it is well known that the strongest MW absorber will selectively absorb the MW energy.[150] Since the selectivity of MW absorption by molecules in solution should follow the magnitude of the molecular dipole and thus the dielectric constant of the material, carrying out the reaction in the presence of 1-hexyl-3-methyl imidazolium chloride (ImCl), an ionic liquid with a known large static dipole and large dielectric constant should increase the heating rate of the solution. [151,152] The experimental control was carried out by adding 0.2 mmol (0.0492g) ImCl to the reaction components, where ImCL is in a 1:5 mole ratio of TOPSe to ImCl. The assumption that the MW energy is more efficiently absorbed by ImCl rather than TOPSe is evidenced by the increased heating rate to reach reaction temperature which exhibits a 2.47 °C/s in the absence of ImCl and a value of 3.02 °C/s in the presence of 0.2 mmol ImCl in the reaction mixture.

MW absorption into TOPSe may either lead to activation of TOPSe (a_{solute}) consistent with a reaction controlled growth regime, or to rapid solvent heating by thermalization. If the observed reaction properties arise from TOPSe activation via selective absorption into TOPSe, than one would predict addition of a stronger MW absorbing molecule (larger dipole moment) to the reaction should have a large impact on the observed QD growth behavior by suppressing the fractional contribution of MW energy absorbed directly into TOPSe. On the other hand, if TOPSe only enhances reaching the reaction temperature and thus accelerates the reaction rate via thermally triggered nucleation, the addition of a strong MW absorber should further enhance the reaction rate.

The results for a two monomer addition protocol at 220°C and 180°C are shown in Figure 4.6B. For the same reaction temperature, the size of the QDs grown in the presence of ImCl is larger than the QDs isolated in the absence of ImCl. In the presence of ImCl, the QD grown at 220°C has a PL feature at 545 nm (FWHM 28 nm) corresponding to a 3.96 nm QD. For the reaction at 180°C, the PL shifts to 560 nm and broadens (PL FWHM 28 → 44 nm). The size of

the QD grows from 3.96 nm to 4.23 nm during the second reaction step. The broader PL feature for the samples grown in the presence of ImCl implies a loss of the QD size dispersity. Although it is difficult to distinguish between a reactant and a solvent heating effect, the competition for MW absorption when ImCl is added appears to eliminate the observed discrete QD formation and impacts the temperature dependent growth behavior. This suggests that a simple rate enhancement arising from accelerated solvent heating cannot be used to completely explain the observed reaction observations.

Reaction in the Absence of Monomer Addition. To further interrogate the impact of selective MW absorption by TOPSe, the affect of carrying out the identical reaction in the absence of fresh monomer are shown in Figure 4.6C. The reaction was carried out as shown in Figure 4.2; however, no fresh monomer is added prior to heating to the next temperature point. The absorption and PL spectra in Figure 6C show no observable shift in the spectral profile or spectral broadening for the reaction heated to 220°C, 200°C, and 180°C, sequentially. This indicates the growth behavior in the MW cannot be attributed to lowering the reaction temperature alone. The lack of a new PL feature, a PL spectral shift, or PL broadening for the exact same reaction without additional monomer being added implies the monomer is consumed during the initial MW ramping and thus does not contribute to changes in the QD size or dispersity unless fresh monomer is added. By comparison to the lyothermal reaction, one would have expected a loss of size focus due to Ostwald ripening, unless the QD distribution is tight and the surface of the QDs is smooth due to the lack of kinetic roughening.[129] Although the assumption of QD surface roughness being low contributing to the lack of apparent Ostwald ripening cannot be easily proven, it is reasonable to assume the MW energy is absorbed into the QD and may result in a continuous annealing effect of the QD surface within the MW cavity. The assumption is supported by the fact that a QD has a MW absorption cross section (approximately 1/3 of TOPSe) coupled to the fact that the monomer is depleted and the number of QDs (as well as size) increase as the reaction progresses, resulting in an increased fraction of the MW energy being absorbed by the QD.

4.3.4 Influence of Monomer Concentration on QD Growth.

The three results from the MW reaction controls, namely lyothermal growth, addition of fresh monomer in the presence of ImCl, and growth in the absence of fresh monomer implies the QD nucleation / growth is coupled to the absorption of MW energy by the TOPSe. While it is

clearly indicated that TOPSe absorption must be important, the temperature dependent growth is yet unexplained and the influence of monomer concentration on the number of nuclei generated in a solution following MW irradiation must be investigated. To investigate the number of nuclei formed at each step of the reaction and thus whether there is a change in the number of QDs in solution after the final heating cycle; the number of QDs generated at each reaction step was analyzed.

Number of QDs in Solution. Inspection of Figure 4.3A shows that for addition of equimolar concentrations of fresh monomer when corrected for the absorption cross-section, the CdSe PL intensity is not equivalent for each QD formation. While this might imply a lower number of QDs for each step, this is misleading as the extinction coefficient for a QD is size dependent. [153] Assuming the PL intensity will reflect the product of the probability for the absorption (ε) multiplied by the absorption cross section if the quantum yields are similar, then the observed PL can be correlated to the number of nuclei in solution.

In Figure 4.3A, the PL intensity ratio is 100 (537 nm, 3.11 nm): 41 (583 nm, 3.63 nm) : 15 (619 nm, 4.92 nm). The ratio of ε for the first two sizes (4.92 nm ε = 382,466.7 $ML^{-1}cm^{-1}$ and 3.63 nm ε = 167,466.7 $ML^{-1}cm^{-1}$) is 44% (a decrease of 2.28). Correction for the size dependent extinction coefficient accounts for the decrease in PL observed in Figure 4.3A for the first and second QD. Using the extinction coefficient ratio for the next two sizes (3.63 nm ε = 167,466.7 $ML^{-1}cm^{-1}$ and 3.11 nm ε = 80,800 $ML^{-1}cm^{-1}$), we expect a PL decrease of 48, which is slightly smaller than observed in the PL spectra (Figure 4.3A) but well within the experimental limit of this calculation. The observation of the equivalent number of nuclei formed at each step of the reaction suggests that in the MW the number of nuclei formed is concentration dependent. The observation of no change in the number of initially formed QDs or QD size evolution during the second heating cycle, is consistent with the suggestion that all of the initial monomer from a prior monomer addition is consumed and does not contribute to further QD size evolution. If the MW absorption into TOPSe was screened by the presence of the larger QD, one might expect that the number of nuclei would decrease for each subsequent reaction. Likewise, if the monomer was not consumed, then the number of nuclei would be expected to vary as the monomer concentration would effectively increase for each subsequent reaction event. The lack of changes in the number of QDs in solution and the size of the QD for the largest size after three reaction cycles indicates that the monomer does not react with a previously formed QD.

Monomer Concentration Dependence for Number of QDs. In an attempt to probe the relationship between the monomer concentration, number of nucleation events, and the formation of CdSe QDs in the MW for a two monomer addition protocol, a series of reactions were carried out at various concentrations for the second monomer addition (0.1 – 3.0 mmol) at fixed volume and monomer ion mole ratio (1:3 CdSA to TOPSe) . The absorption and the PL spectra (Figure 4.8A) exhibit an increase in the intensity of the higher energy feature with increasing monomer concentration. By spectral de-convolution, the red shift in the PL can be attributed to the overlapping PL features and not a shift in the size. Spectral de-convolution and fitting the width, frequency, and area using a Guassian profile for each concentration indicates no change in the exciton absorption wavelength, no change in FWHM, and only a change in the area for the smaller QD over the entire concentration range (0.1 – 3.0 mmol). A plot of the difference in absorption intensity (I_x (0.6 mmol TOPSe) – I^o (0 mmol TOPSe)) for the smaller QD at 520 nm as a function of the TOPSe concentration indicates the number of QDs generated is dependent on the concentration of monomer (Figure 4.8B). A linear increase in the absorption for the second QD with a slope of 4.23 is observed which indicates the reaction is Se limited. When the absorption and photoluminescence excitation (PLE) are plotted together, after the reinjection of new precursor and a microwave cycling event, there is a new peak the is evident in the PLE that is in the same position as the new peak seen in the absorption. With the addition of Imcl and new precursor, no new peak appears in either the absorption or PLE. (Figure 4.8C) After further investigation, the number of nuclei versus CdSe molar concentration shows a linear dependence indicating that nuclei formation follows directly with the amount of CdSe precursor added.

The observation that the number of QDs is linearly dependent on the TOPSe concentration is not surprising, as this is expected if the nucleation and growth occur instantaneously upon absorption of the MW energy into TOPSe. The constant number of the initial QD coupled to the concentration dependence for the smaller QD strongly implies the growth events are independent for each QD in solution and only relates to TOPSe absorption. (Figure 4.8D)

4.3.5 Influence of Addition of Only a Single Monomer.

To analyze the contribution ascribable to TOPSe, the reaction was carried out for a two-sep reaction (220^0C and 180^oC) where only one of the monomers is added (CdSA or TOPSe). The optical data is shown for addition of 0.3 mmol TOPSe in Figure 4.9A, while the change in

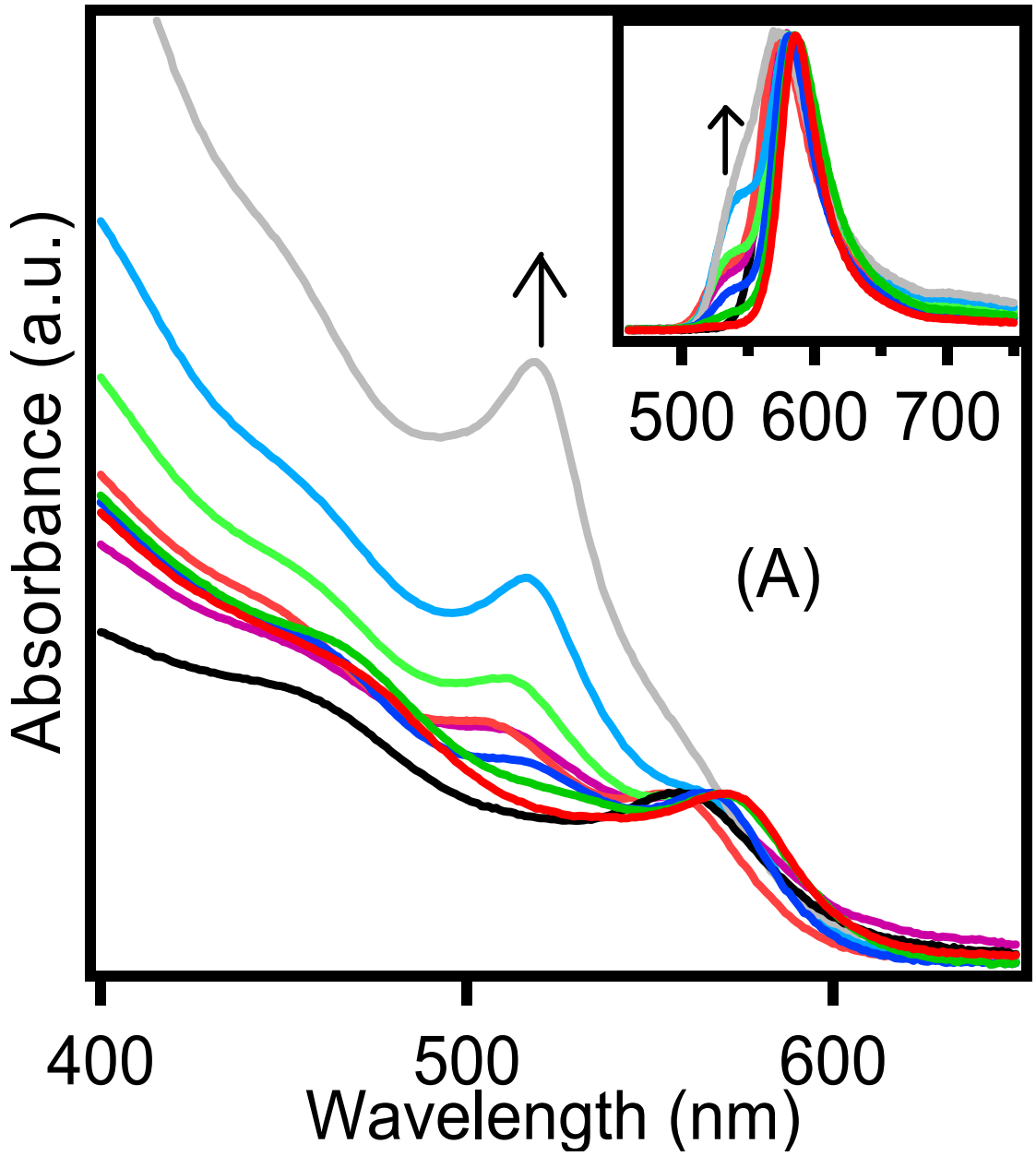

Figure 4.8A. Increasing Concentration for 2x CdSe Precursor Injection

Absorption and emission (inset) spectra for reaction with increasing concentration of fresh monomers effect during the second step.

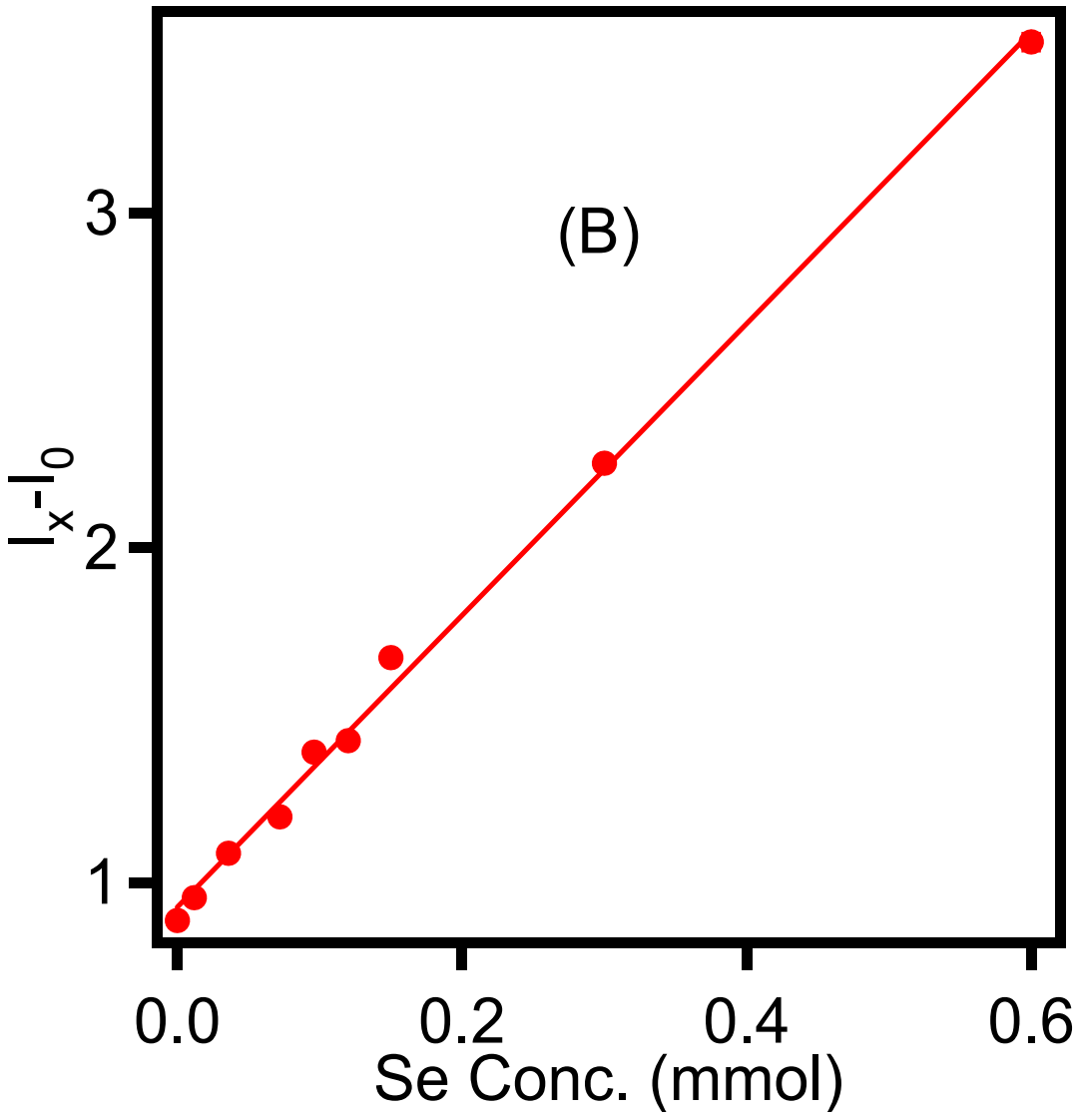

Figure 4.8B. Initial Se Concentration vs. Intensity Bandedge Abs Peak

Plot of the relative intensity of the absorption contributions for the two independent QDs generated in the two step reaction as a function of added TOPSe monomer in a 1:3 CdSA to TOPSe mole ratio.

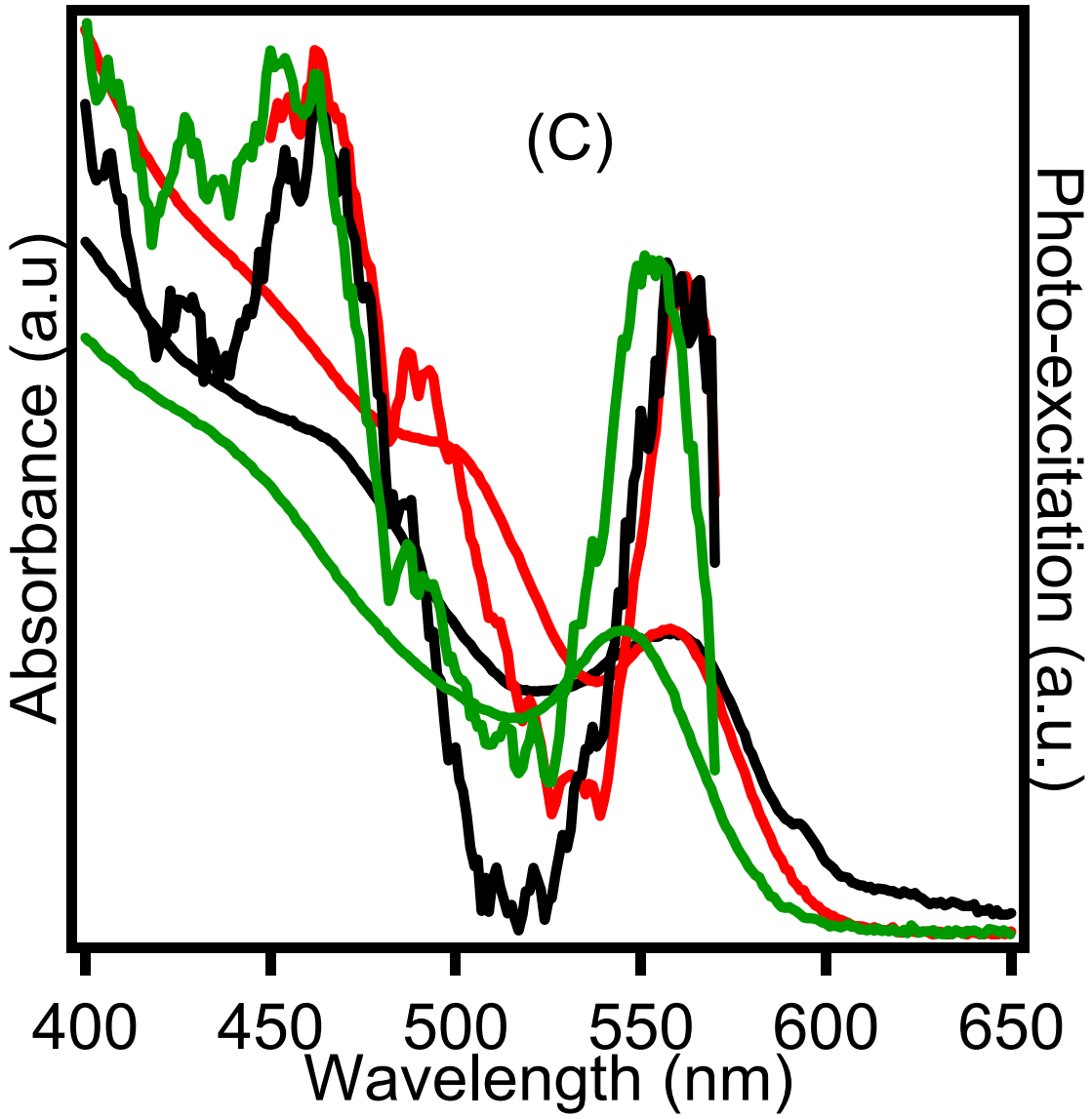

Figure 4.8C. Abs/PLE CdSe 2x Injection/MW Cycling

Absorption and PLE spectra for CdSe NC before (green), after re-nucleation (red) for the first and second precursor injection, and re-injection including the addition of ionic liquid (black) along with the precursor.

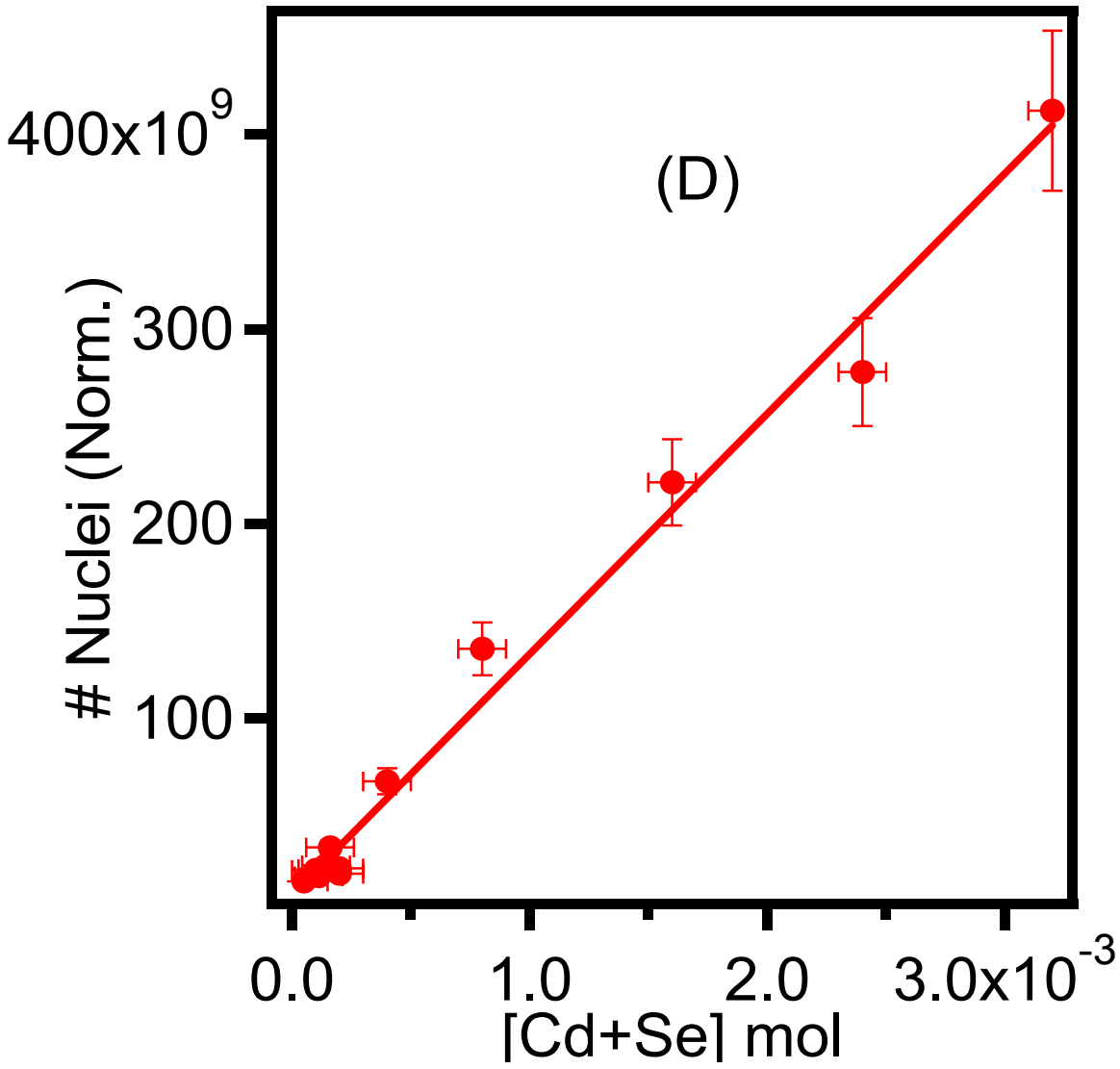

Figure 4.8D. # of Nuclei vs. Initial Monomer Concentration

Plot of the number of nuclei formed as a function of initial precursor concentration at a molar ratio of 1:3 Cd to Se using CdSA and TOPSe.

the optical data for addition of TOPSe between 0.072 mmol → 0.3 mmol, is shown in Figure 10. Upon addition of 0.3 mmol TOPSe in the absence of CdSA, a shift in the absorption exciton of 7 nm is observed, while a shift of 19 nm in the PL occurs. In addition a weak, new PL feature appears at higher energy. The spectral shift corresponds to a change in QD size from 4.18 to 4.42 nm. The observed spectral shift and weak PL feature that appears and the observed growth in the absence of CdSA supports the suggestion that the monomer is effectively and TOPSe is the limiting reagent.

Upon addition of 0.4 mmol CdSA in the absence of TOPSe, no new PL feature or significant growth is observed in the reaction although the reaction reaches the desired reaction temperature albeit at a slower rate (Figure 4.9B). The results support the analysis that the TOPSe is the critical reaction component in the MW reaction and independent of the solvent or other precurors, and suggests strongly that the QDs in solution absorb the MW energy as the TOPSe is depleted. (Figure 4.10)

4.3.6 Multiple QDs in One Reaction Mixture.

The ability to produce multiple materials in one solution as we have discussed here can be extended to the synthesis of multiple types of QDs in the same solution. The advantage of making materials in one batch stems from the idea of making a single reaction L.E.D. system where you have the RGB colors all in the same reaction mixture. Initial work began by attempting to synthesize a binary reaction including both CdS and CdSe nanoparticles. In Figure 4.11A, the absorption and emission spectra for CdS nanoparticles and CdS/CdSe nanoparticles indicates that the CdS is still present in the solution either as individual dots or fused together with the CdSe nanoparticles.[154, 155] The extreme decrease in the PL intensity for CdS by an order of magnitude provides some evidence that the particles are probably fused together although there is no conclusive evidence from TEM analysis at this time[156, 157,158] Taking this sample and adding an additional semiconductor (CdTe) gives an additional peak corresponding the CdTe absorption and PL feature. (Figure 4.11B) In addition, a very broad an intense PL feature is observed in the near infrared region of the spectra. The near IR fature is believed to arise from Type-II QD behavior by e^-/h^+ recombined with the CdS-CdTe or CdSe-CdTe interfaces.[159] This indicates that there is a direct transfer of energy from the CdS and CdSe excitons down to the CdTe. TEM analysis is currently unavailable to distinguish, although tetrapods can be observed. After careful analysis of the TEM in Figure 4.11C, the conclusion that the materials have fused

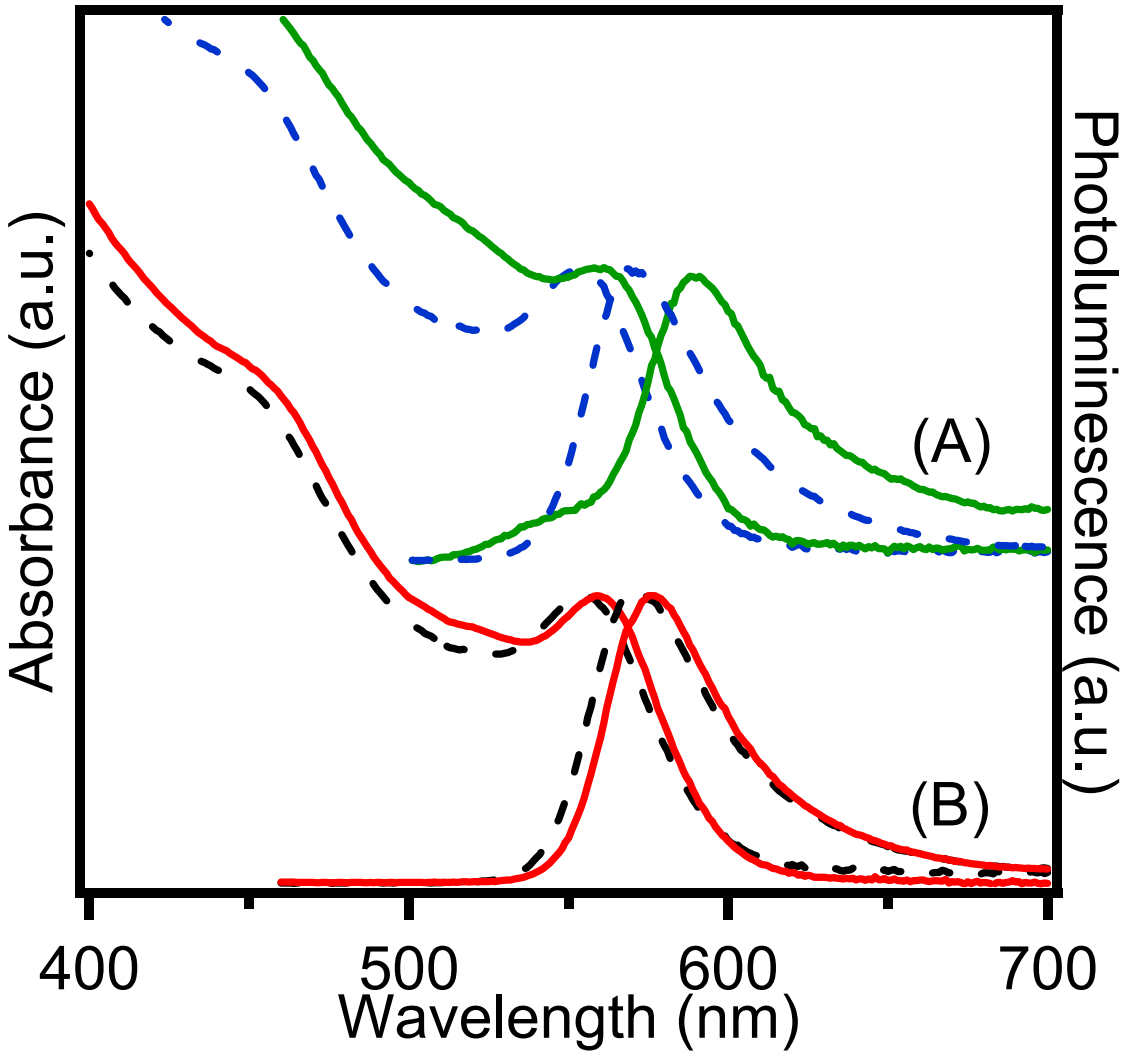

Figure 4.9. Addition of 0.3 mmol TOPSe or CdSA Monomers w/ MW Cycling

Absorption and PL spectra of CdSe reactions before (-----) and after (—) only a single monomer is added following an initial MW cycling event. A) 0.3 mmol TOPSe. B) 0.04 mmol CdSA/decane. All samples were heated at 220°C for 30s and 190°C for30s.

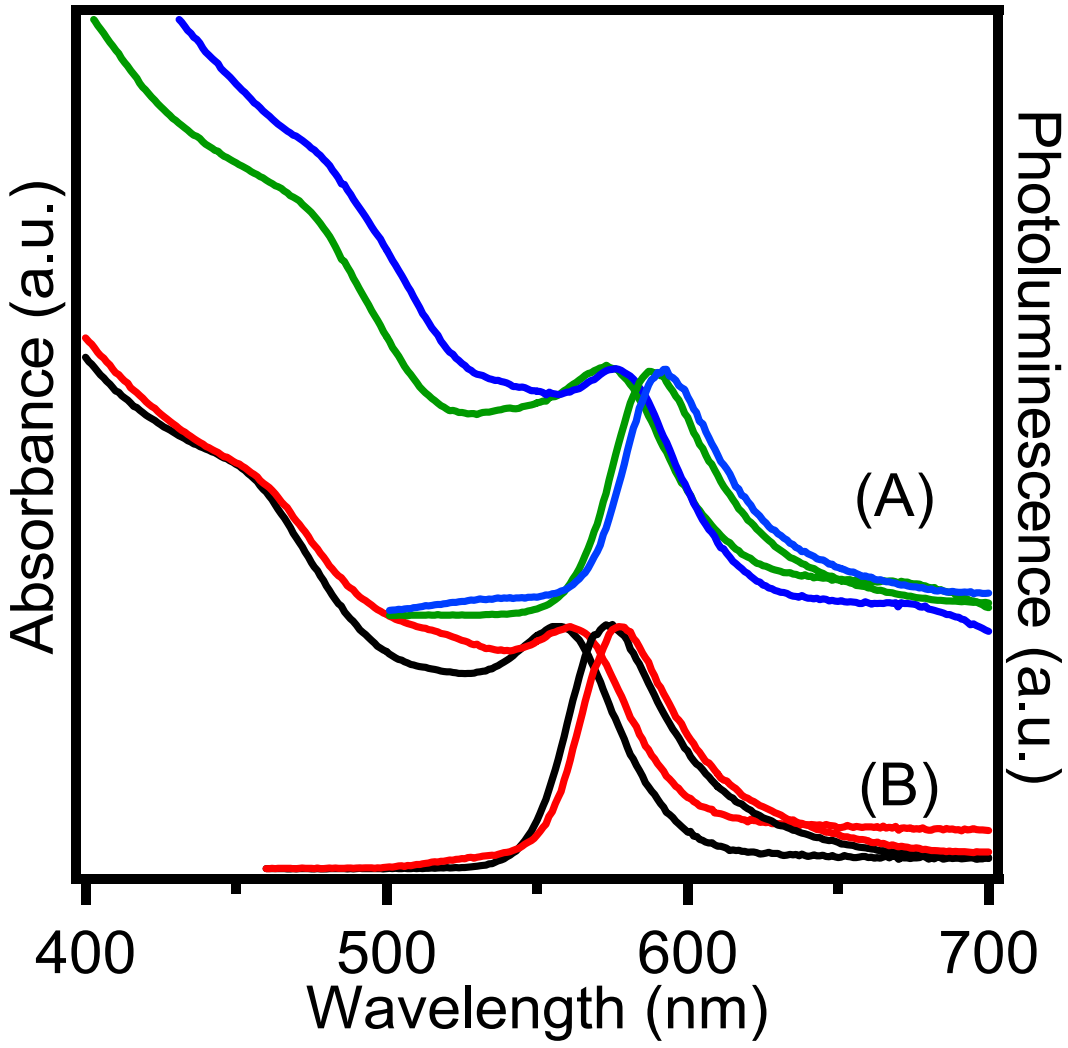

Figure 4.10A/B. Addition of 0.072 mmol TOPSe w/ MW Cycling

A) 0.072 mmol TOPSe/Decane B) 0.072 mmol TOPSe before (green/black)/after (blue/red) MW reheating. All samples were heated at 220°C for 30s and 190°C for30s.

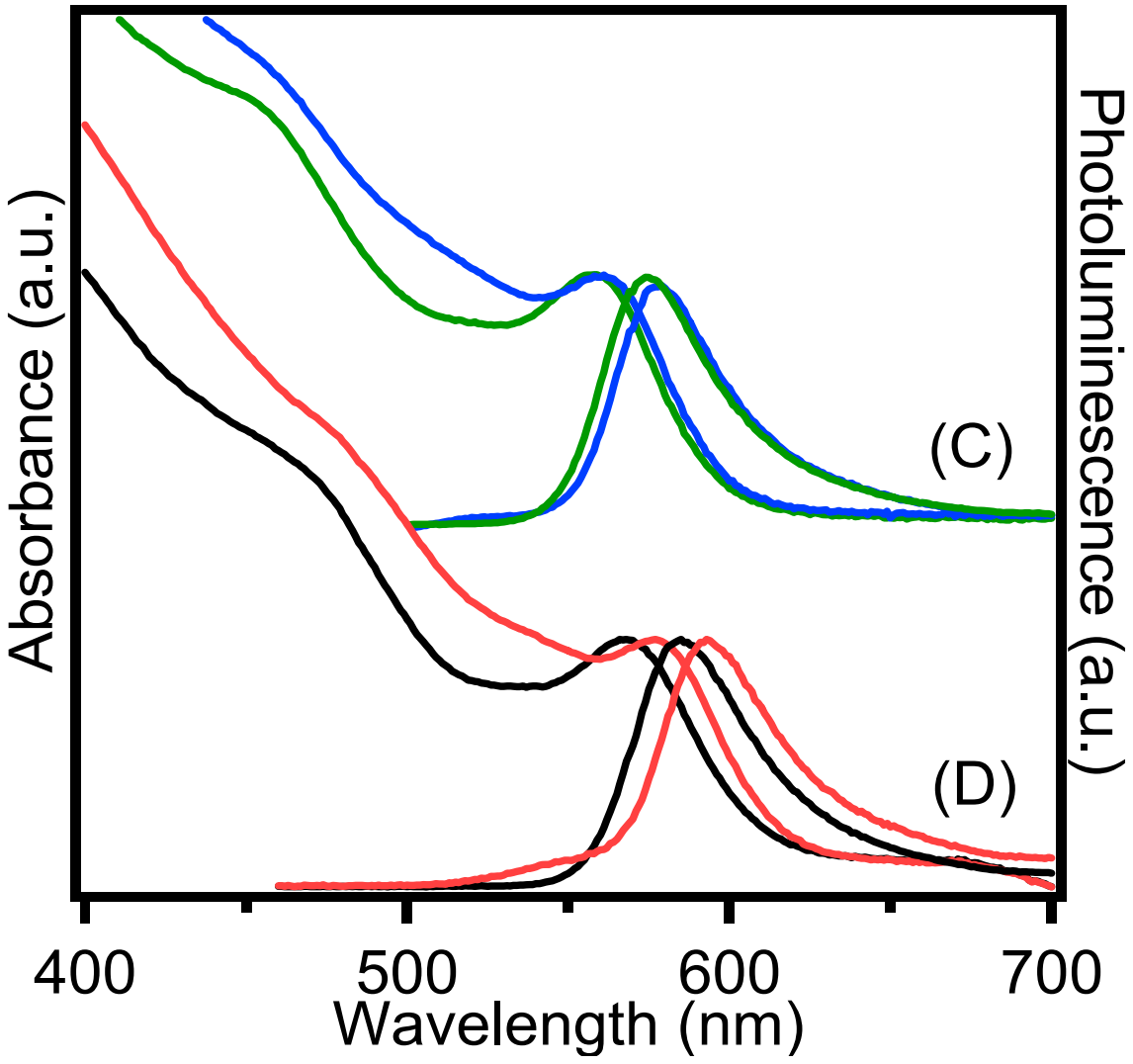

Figure 4.10C/D. Addtion of 0.12 mmol TOPSe w/ MW Cycling

C) 0.12 mmol TOPSe/Decane D) 0.12 mmol TOPSe before (green/black)/after (blue/red) MW reheating. All samples were heated at 220°C for 30s and 190°C for30s.

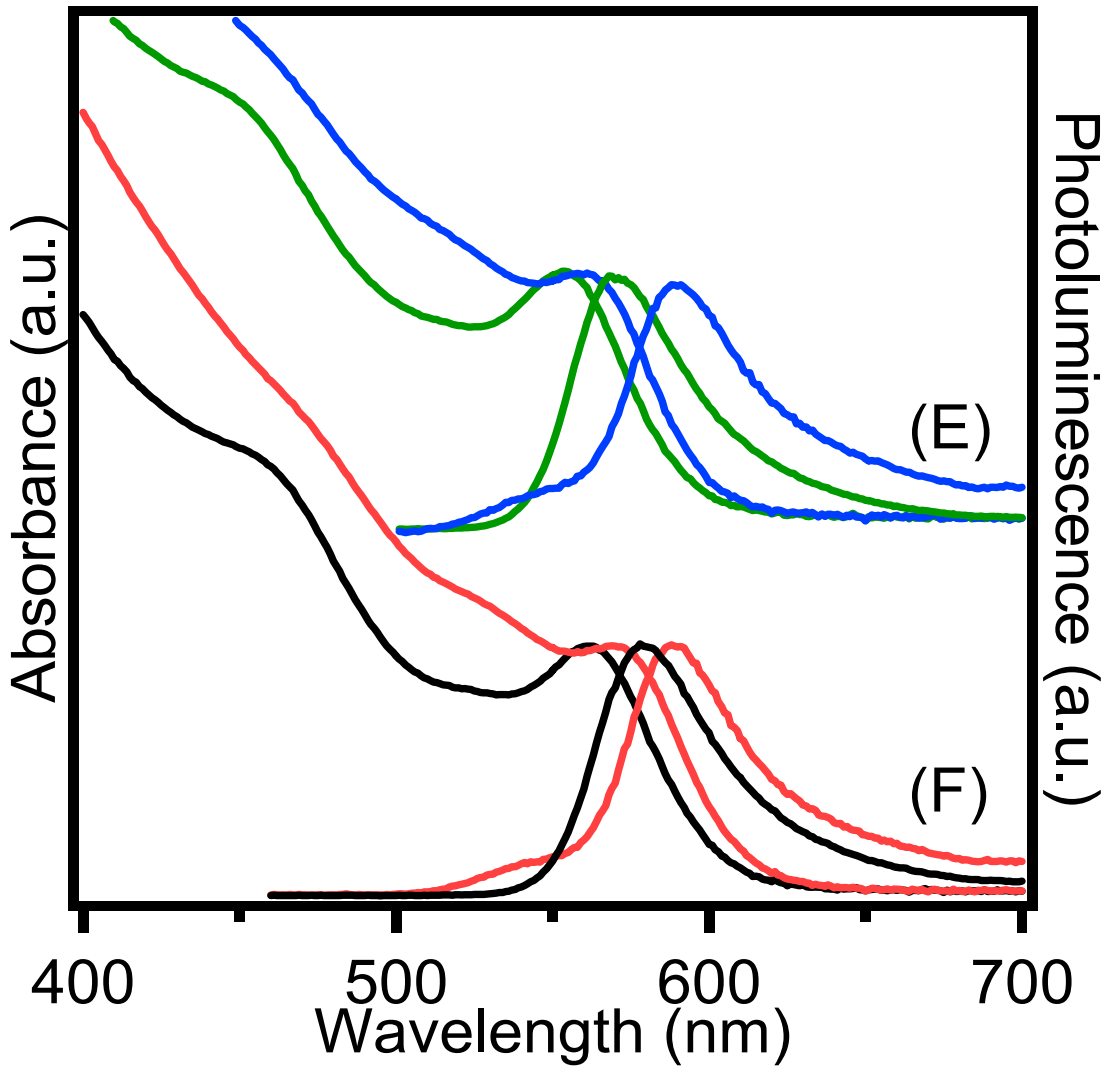

Figure 4.10E/F. Addition of 0.3 mmol TOPSe w/ MW Cycling

E) 0.3 mmol TOPSe/Decance F) 0.3 mmol TOPSe before (green/black)/after (blue/red) MW reheating. All samples were heated at 220°C for 30s and 190°C for30s.

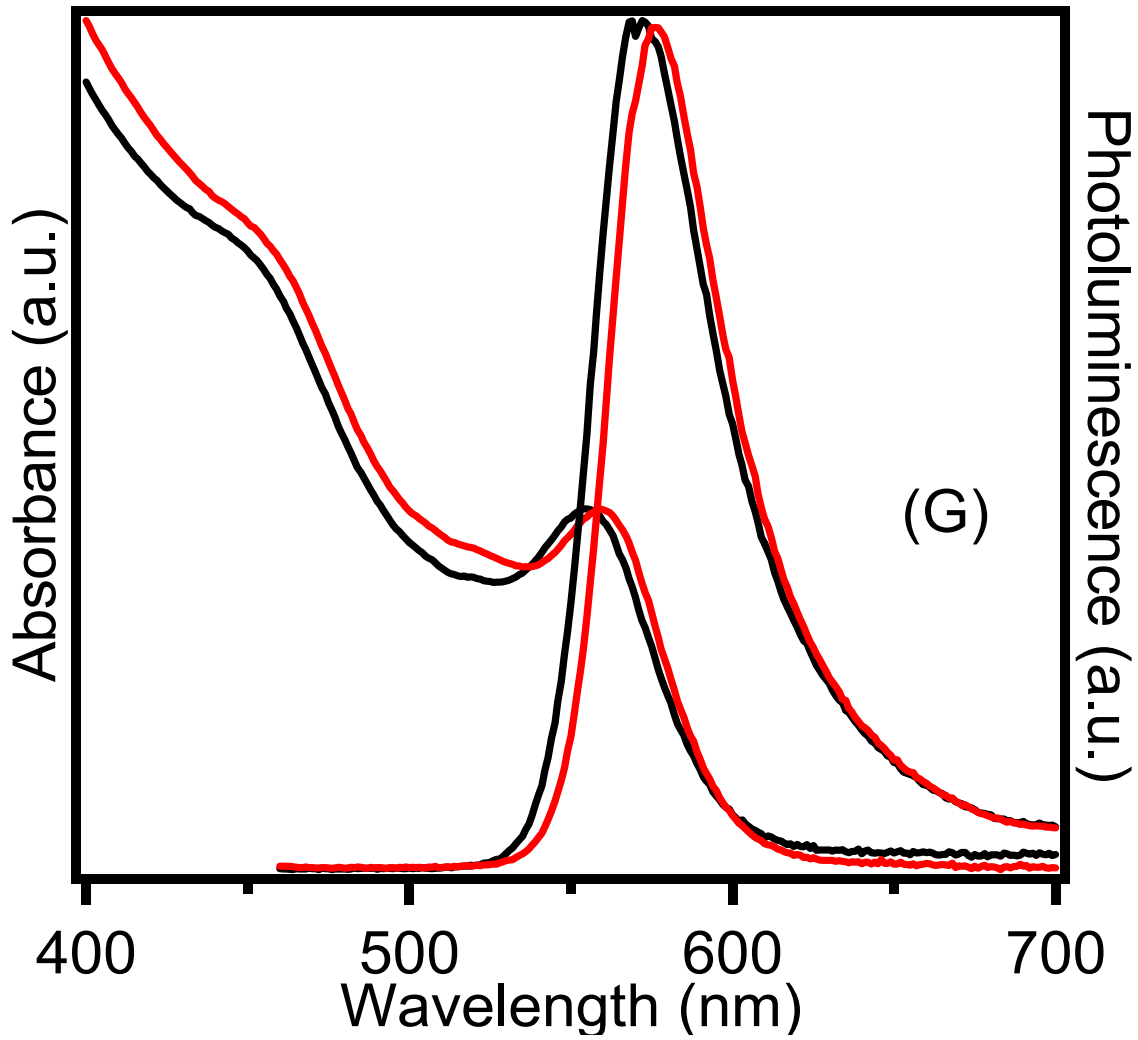

Figure 4.10G. Abs/Em Addition of CdSA w/ MW Cycling

0.04 mmol CdSA/decane before (green/black)/after (blue/red) MW reheating. All samples were heated at 220°C for 30s and 190°C for30s.

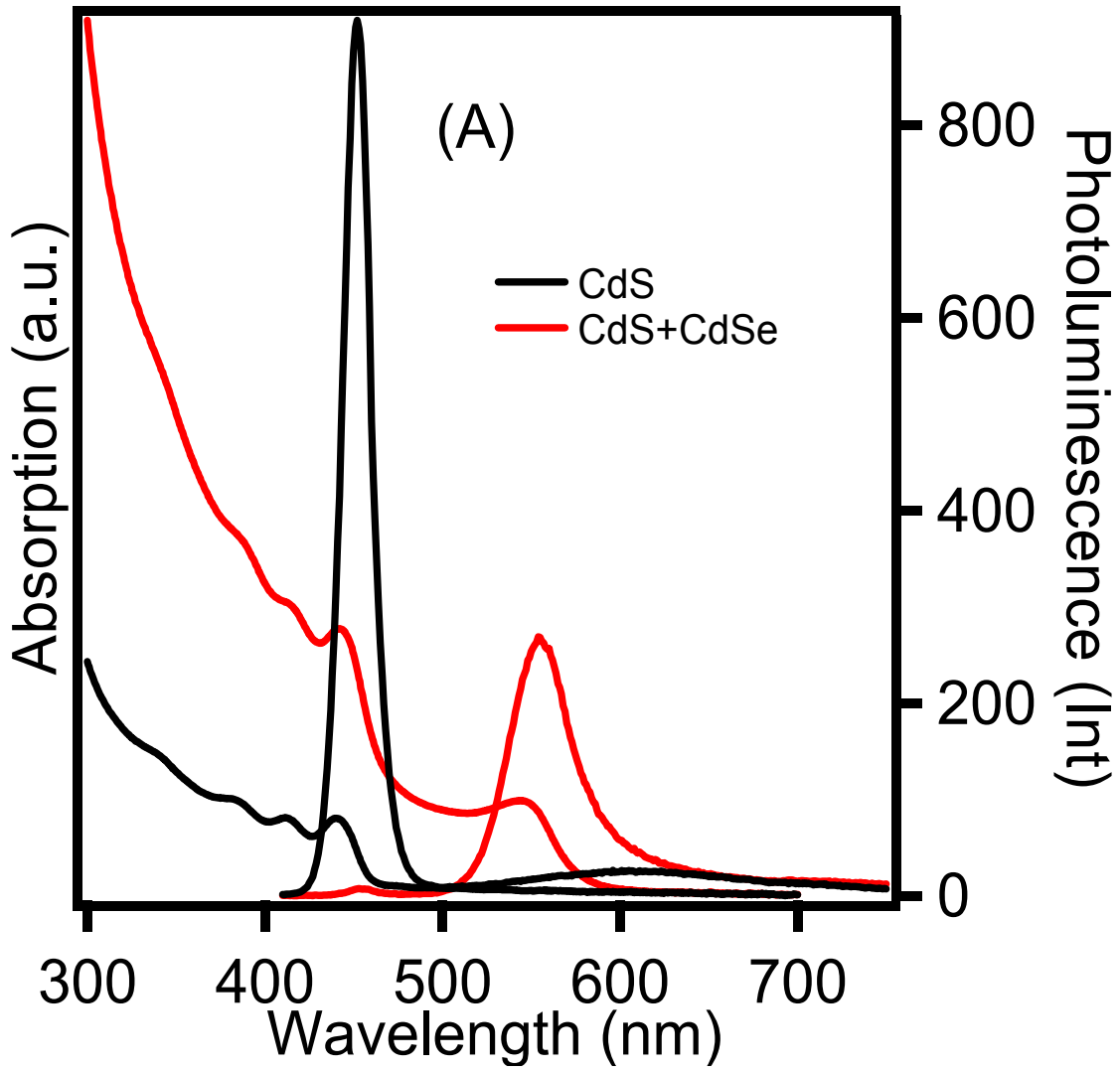

Figure 4.11A. Abs/Em CdS/CdSe

The absorption and emission spectra of CdS grown individually (black) and the CdSe/CdS grown consecutively (red) in the same reaction mixture.

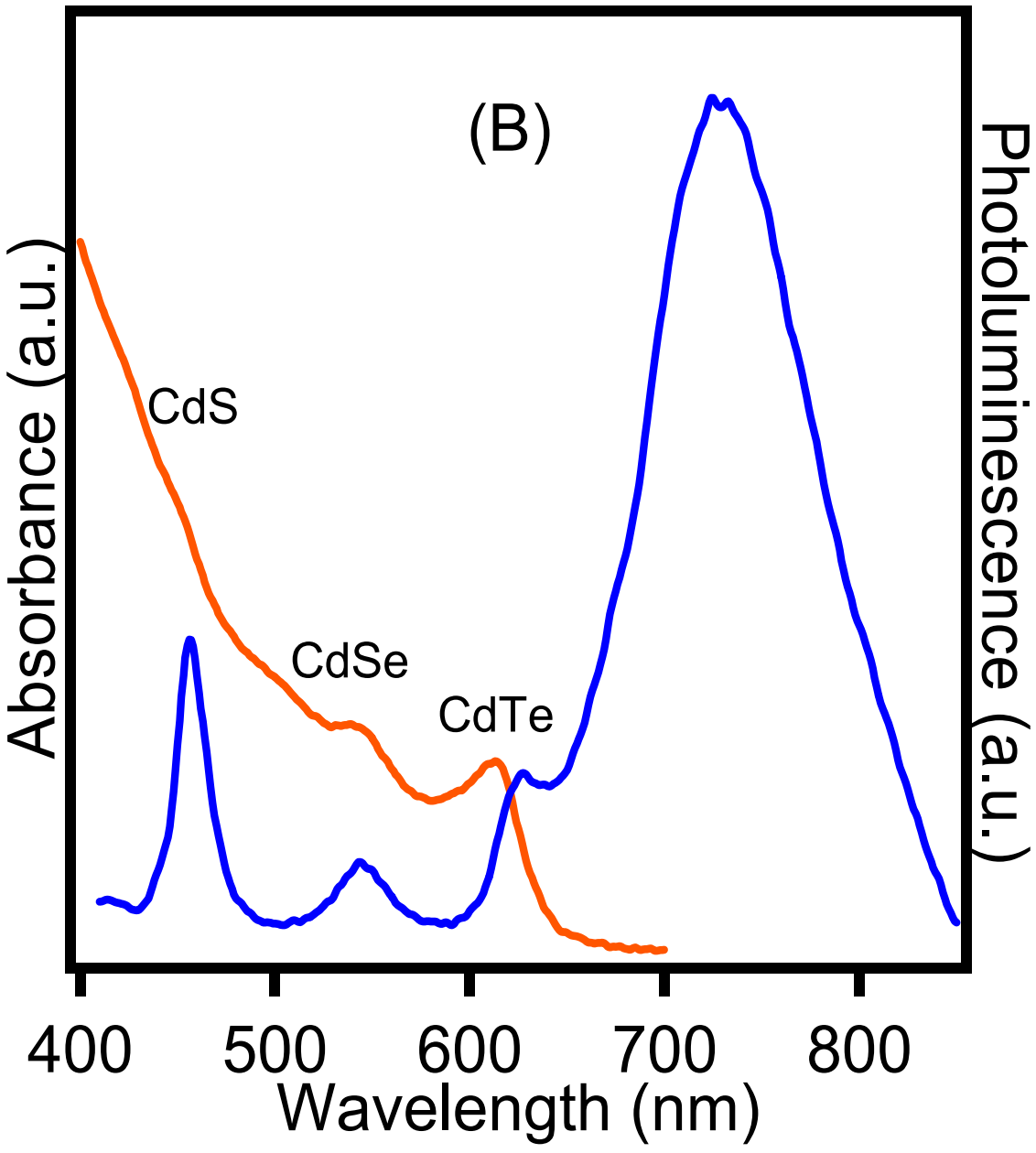

Figure 4.11B. Abs/Em CdS, CdSe, CdTe

Absorption and emission of multiple cadmium chalcogenide materials (CdS, CdSe, CdTe) with microwave cycling in one solution.

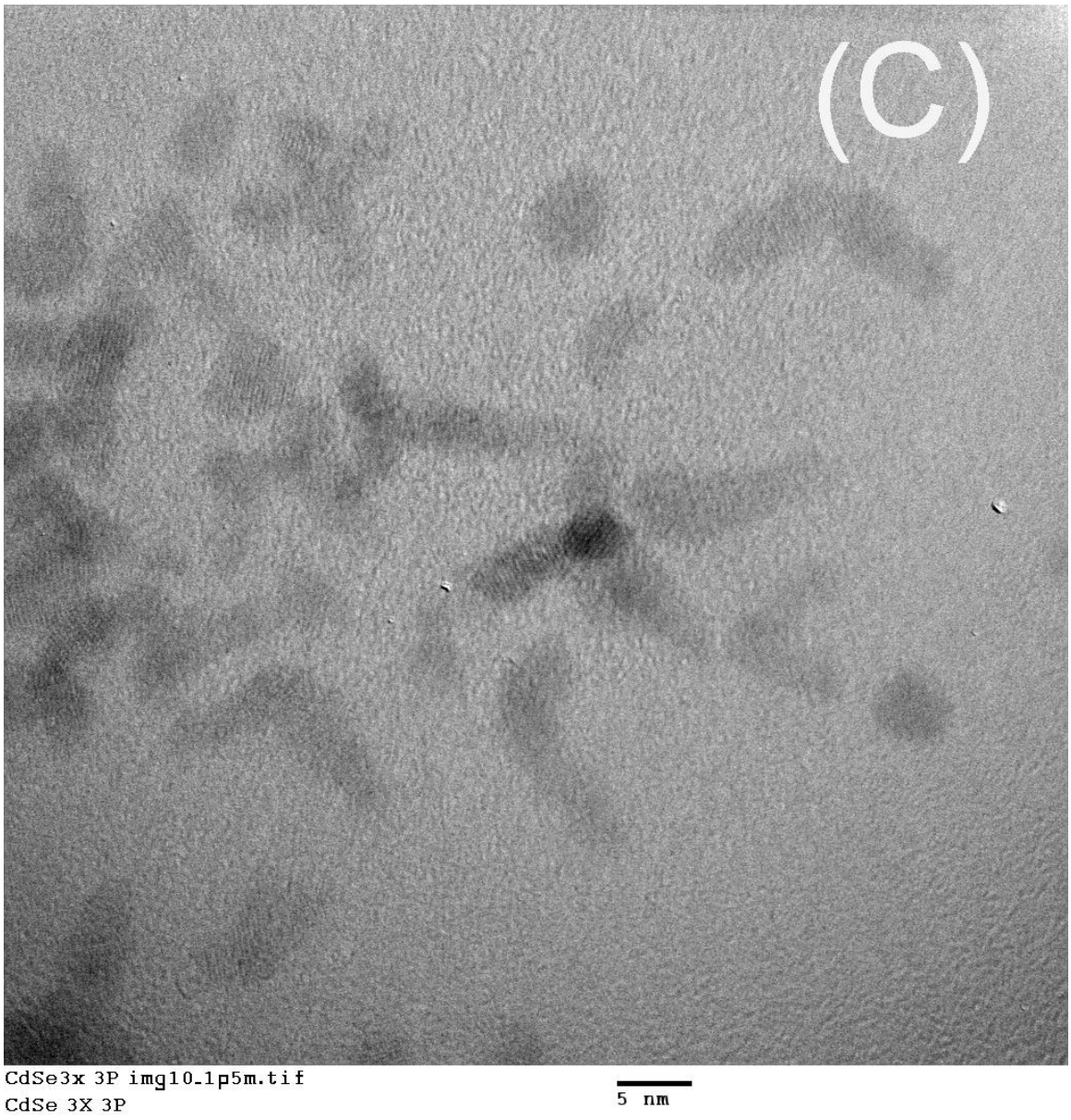

Figure 4.11C. TEM Heterostructures CdS, CdSe, CdTe

A TEM image showing the heterostructures formed as a result of adding CdS, CdSe, CdTe.

together to form heterostructures is confirmed. This direct linkage of the quantum dots explains the extreme decrease in the emission intensity of the parent dot as each successive material is added to the solution mixture. However, it is surprising that the aborption feature remains intact even though the materials are all sharing a face of their structure. Due to the complexity and small size, pXRD was determined to be in conclusive in determining the composition and structure of the heterostucture material. Further studies are underway.

4.4 Conclusion

The previously observed temperature dependent growth behavior of CdSe QDs in the MW suggested that the QD growth may be governed by a reaction controlled mechanism,[129,132] where the activity of the solute phase monomer relative to the monomer generated by QD dissolution must be large (K > 100 regime). We believe this is achieved by the selective activation of the Se monomer through MW absorption into TOPSe. The result of selective absorption into TOPSe leads to a large K value, zero growth conditions in solution, and the limit of the participation of Ostwald ripening during the timescale of the reaction. Under the limit of reaction controlled conditions, the size of the QD can be described as temperature controlled without the appearance of size defocusing arising from Ostwald ripening.

In the MW due to the rapid growth, monomer depletion, and QD surface energy the size of the QD is temperature dependent but will reflect a competition between growth and nuclei formation. Under these conditions the reaction is in the reaction-controlled limit described by Talapin,[130,133] which results in a narrow size dispersity for each growth event when the reaction temperature is lowered for the MW reaction. The lack of Ostwald ripening suggests a smooth (defect-free) surface most likely exists for these QDs, thus the QDs achieve zero growth rate. We believe the zero-growth rate arises from reconstruction of the QD during the reaction lowering the surface activity towards monomer addition via QD MW absorption following monomer depletion. The result can be understood by considering the fact that as the QDs grows, the MW absorption by the TOPSe decreases as the MW absorption form the growing CdSe QD increases providing the necessary energy for surface reconstruction to minimize kinetic roughness.[130]

CHAPTER 5 CONCENTRATION CONTROLLED CRYSTAL MOTIF IN NANOCRYSTAL GROWTH

The low energy difference in the sphalerite or wurtzite packing arrangement for CdSe can lead to polytypism at the nanoscale. According to Ostwald's rules the metastable phase stability is inverted at the initial nucleation point, leading to the initial formation of the sphalerite phase. By controlling reaction growth conditions such that the growth rate is slow, a binary phase diagram for isolation of CdSe as pure hexagonal (wurtzite) or pure cubic (sphalerite) crystal phases can be developed for CdSe between 3-15 nm. Isolation of the sphalerite phase is achieved at low monomer and low Se/Cd ratios, while the wurtzite phase is isolable at high monomer concentrations and large Se/Cd ratios. Based on TEM analysis, the pure phases exhibit no stacking faults while the mixed phase have stacking faults and readily interconvert from sphalerite to wurtzite at long thermal annealing times. Consistent with isolation of the pure phases, the exciton absorption tracks with the effective mass approximation predictions for the respective lattices.

5.1 Introduction

The size dependent physical properties observed in quantum dots (QDs), where the size of the crystal is smaller than the natural Bohr radius, have intrigued scientists for quite some time.[160] The fundamentals of the size dependent changes in the physical properties are well understood and are already finding applications for a wide range of fields.[161, 162, 163] The influence of nanocrystal habit (shape) [164,165,166,167] and crystal motif (structure) [168] have also attracted attention, since the confinement energy will depend not only on the different confinement length scales for non-spherical nanocrystals, but also the crystal motif of the nanocrystal.[169, 170, 171] The impact of crystal structure on confinement is important, as the confinement of the exciton wavepacket and the exciton splitting is dependent on crystal motif, since the bandgap energy and band structure change for different atom packing arrangements.

In a wide range of nanoscale materials, polytypism has been reported to be size dependent with the metastable (kinetic) crystal phase observed to be the energetically favorable phase below a critical diameter.[170, 172, 173, 174, 175, 176, 177, 178, 179, 180, 181, 182, 183, 184] The critical size

domain for phase stability in a binary semiconductor reflects the crossing point for the total free energy of the particular crystal phase, which is widely influenced by ligands, solvents, and the reactants.[175, 179]For nanocrystalline materials the critical size domain for phase stability will dominate the surface free energy and the core defect densities. In solvothermally grown materials, Ostwald's rules predict the metastable or kinetic structure will form rapidly and be the predominate species at nucleation.[176, 185] In the case of the metastable sphalerite and thermodynamic wurtzite phase, the sphalerite phase is preferred at the initial nucleation step since the structure approaches a spherical limit thus lowering the energy for nuclei formation.[176, 178, 186] As the nanocrystal grows a phase transition to the more thermodynamically favorable phase is expected to occur driven by stacking fault migration. The energy required to allow the stacking faults to collectively migrate and thus anneal in a growing nanocrystal is directly proportional to the number of stacking faults and vacancies in the material,[187, 188] becoming increasingly more energetically unfavorable as the crystallite grows in size and for nanocrystals exhibiting low defect densities.[189] The critical diameter for a phase transition from the kinetic to thermodynamic phase is therefore dependent on the presence of stacking faults, vacancies, the growth method, and the rate of growth of a particular nanocrystal system.

The observation of size dependent polytypism in binary nanocrystals can be attributed to an apparent reversal of structure stability for the different crystal motifs at small nanocrystal sizes.[175, 176] Polytypism in QDs does not lead to kinetically trapped phases but rather arises from thermodynamic influences.[172] CdSe grown by MOCVD or electrochemical methods exhibits both wurtzite and sphalerite phases over a wide size range, while lyothermal growth yield sphalerite below 3 nm and wurtzite for larger CdSe QDs. Observation of large CdSe QDs grown lyothermally in the sphalerite phase is rare,[170, 184] and is often attributed to the presence of stacking faults.[168] The observation of polytypism is not surprising in CdSe as energetically the ion packing for each lattice is very similar ~ 13-14 meV atom.[190] In addition, the similarity in packing motifs for the two phases leads to identical faces along the <111> face for sphalerite and the <0001> face for wurtzite lowering the barrier for stacking fault formation as the nanocrystal grows and thus acts as a low barrier for polytypism in these materials.

Since the energy difference between sphalerite and wurtzite for CdSe is small, either phase should be isolable over a wide size regime if the defect densities are controlled by the reaction conditions. For instance, if the growth rate is slow, the metastable product should be

able to be grown to larger sizes if stacking fault and vacancy formation are minimized, thus raising the energetic barrier for phase interconversion as the nanocrystal grows. The inability to isolate pure sphalerite CdSe over a large size regime reflects the increasing lattice disorder observed as the nanocrystal grows under the rapid growth conditions existing in the lyothermal process.[191] Studies on the size dependent disorder in CdSe have shown that nanocrystals formed under rapid growth rate conditions lead to a larger number of stacking faults. [192, 193] On the other hand, at slow growth rates the number of stacking faults is low as the nanocrystal growth is templated by the growing facet in analogy to epitaxial growth. While polytypism is known for II-VI nanocrystalline semiconductors, the ability to control the observed polymorph over a large size regime for CdSe nanocrystals has not been demonstrated.

In this manuscript, we explore the binary phase diagram for CdSe QDs crystal motifs demonstrating the ability to controllably isolate discrete sphalerite or wurtzite CdSe QDs over the entire confinement size range of 3 – 15 nm. In the reaction, three phase regions can be identified, namely the pure sphalerite, the pure wurtzite, and a mixed phase regime. The pure sphalerite and wurtzite samples exhibit no time dependent interconversion, although high temperature annealing of the powder yields a sphalerite to wurtzite transition at 380°C. The mixed phase exhibits a large degree of stacking faults and readily interconverts to the pure wurtzite lattice at long reaction times as previously observed in lyothermal reactions. In the binary phase diagram, it is observed that at high mole ratios (Se:Cd ratios > 3:1) and/or high precursor concentration the wurtzite lattice is observed. However, at low mole ratios < 0.4:1 for Se:Cd and low precursor concentration, the formation of the sphalerite phase is observed. The isolated QDs exhibit an aspect ratio of 1.2 and no stacking faults are observed for the pure phases in the TEM images. Consistent with the pure phases of the crystal motifs, the energy of the exciton absorption tracks a confinement model for their respective size in a given lattice motif. There is no change in crystallite phase over a wide size regime (growth domain in reaction) which implies the phase is controlled at the nucleation step and is not induced during QD growth. The isolation of the metastable phase is intriguing, although not unprecedented, and can be attributed to the lower energy for sphalerite nucleation resulting in a seed crystal. At low monomer flux, growth is achieved slowly allowing the low defect density materials to grow in the sphalerite phase. At high concentration, the monomer flux is higher leading to greater stacking fault errors, which in effect lowers the energetic barrier for interconversion to wurtzite.

5.2 Experimental

Synthesis of CdSe. CdSe QDs were grown by previously reported synthetic methods either via hot injection[194] or microwave[195] enhanced methods with the same results. In this manuscript only the hot injection (lyothermal) method is reported in order to generalize the results to a broader community. The binary phase diagram was generated by carrying out the reactions at various reactant concentration conditions (6mM, 10mM, 12.5 mM, 25Mm, 50mM, 200mM relative to Cd) in Octadecene with 1M TOPSe as the Se source. The mole ratio was fixed at a 5:1 molar ratio of Se to Cd for the wurtzite structure and a 1:1 Se to Cd ratio for the sphalerite structure. In order to produce mixed phase materials, a Se:Cd ratio of 3:1 was used. All samples were precipitated out of solution by addition of MeOH. The precipitate was centrifuged, redissolved in toluene, followed by a second precipitation step to remove excess ligand and monomer. The QD size was obtained by controlling the reaction temperature as previously described.[36]

5.3 Results

It is relatively easy to envision why polytypism occurs and is more favored for nanoscale materials. Inspection of the lattice projection reveals that the hexagonal lattice (*ab* packing) consists of a *zig-zag* stacking of atoms at a 60^{o} rotation and the sphalerite lattice (*abc* packing) consists of a helical 60^{o} twist of the planes of stacked atoms (Figure 5.1). If we consider the sphalerite and wurtzite lattices for CdSe, the structures are identical for the first two planes and develop a defined morphology at greater than three lattice planes, such that the <111> face of a sphalerite lattice is identical to the <0001> face of a wurtzite lattice. The ability to template one metastable phase during the growth of the QD therefore is energetically small for the first few planes and continued growth in the templated phase might be expected. In effect, if the reaction is controlled, the epitaxial templated structure will continue to grow preferentially without lattice reconstruction if the addition rate of ions is slow. Alternatively, rapid growth will minimize the impact of ion templating due to formation of stacking faults as the rate of addition of ions under a kinetic growth regime is random and faster than reconstruction. Precise control of the reaction conditions should allow isolation of the discrete phases over a wide size regime.

Evidence of Crystal Motif. The isolated crystal phase for CdSe is observed to be dependent on the concentration of monomers and the mole ratio of Cd to Se used during the lyothermal growth of CdSe. In Figure 5.2, the pXRD data on the isolated pure phases of CdSe passivated by TOP between 7 nm and 14 nm are shown. For concentrations $\leq$ 10mM, the powder XRD pattern can

A

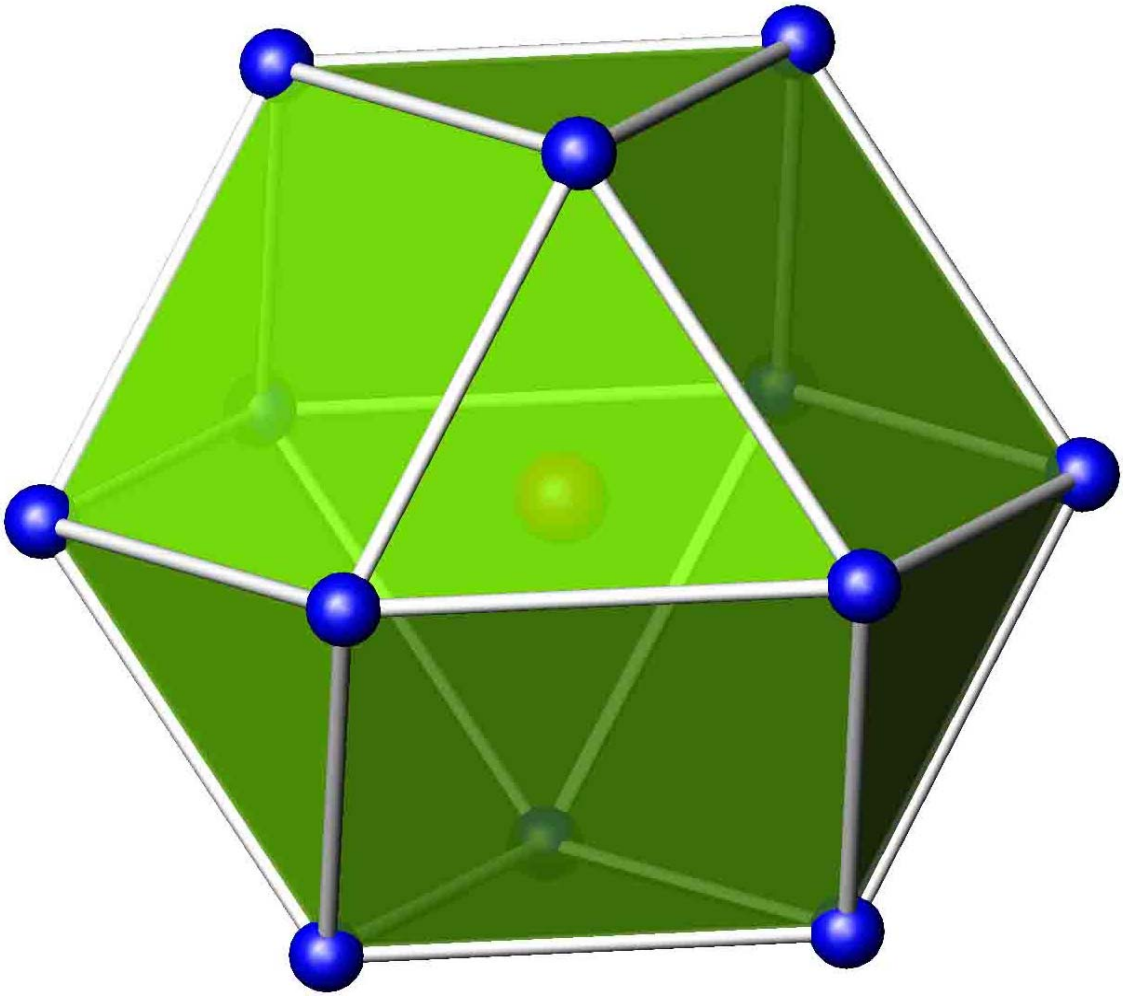

Figure 5.1A. 3-D Polyhedron of Sphalerite Particle

This figure shows how a full polyhedron of a sphalerite (A) would be projected.

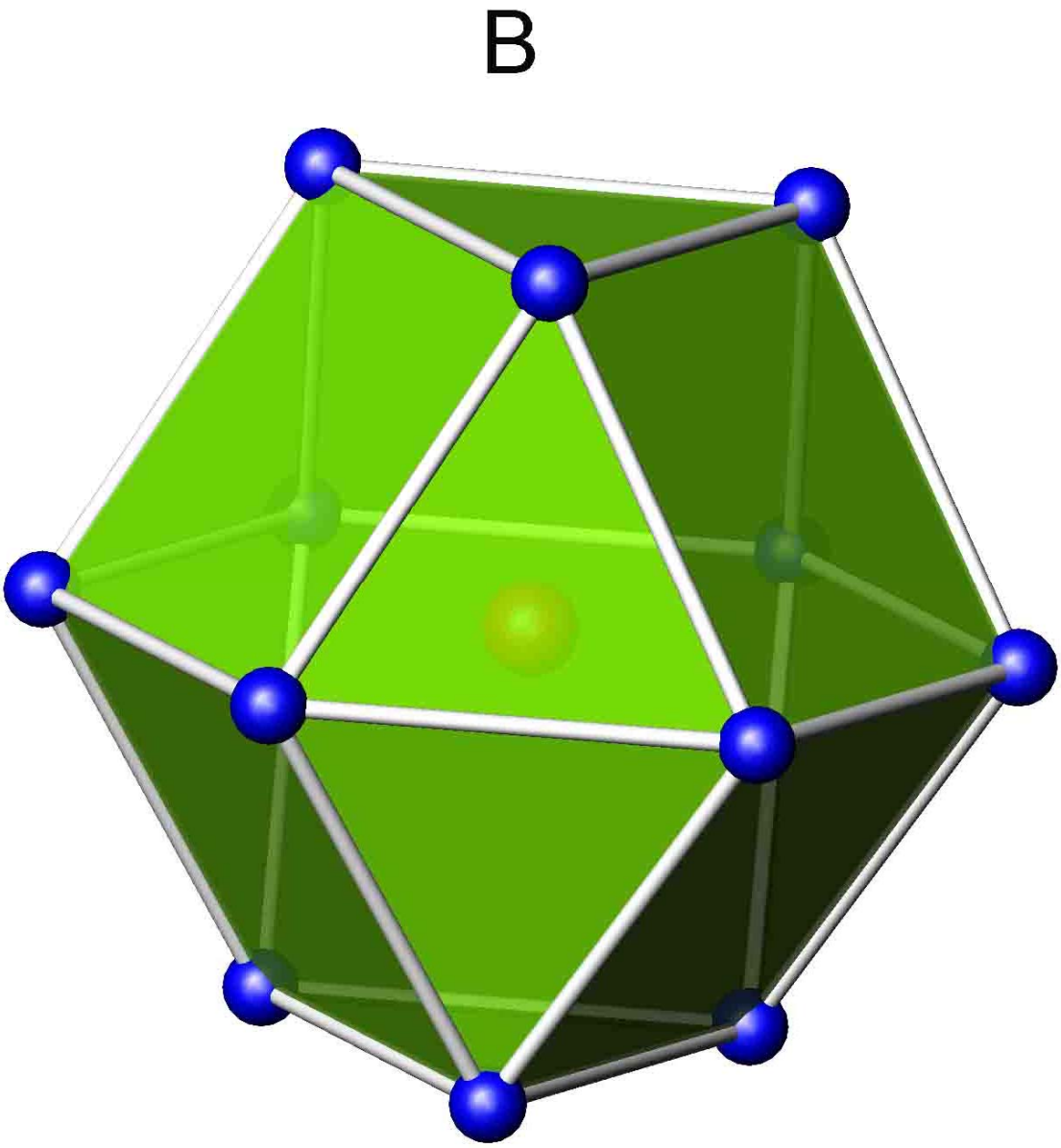

Figure 5.1B. 3-D Polyhedron of Wurtzite Particle

This figure shows how a full polyhedron of a wurtzite (B) would be projected.

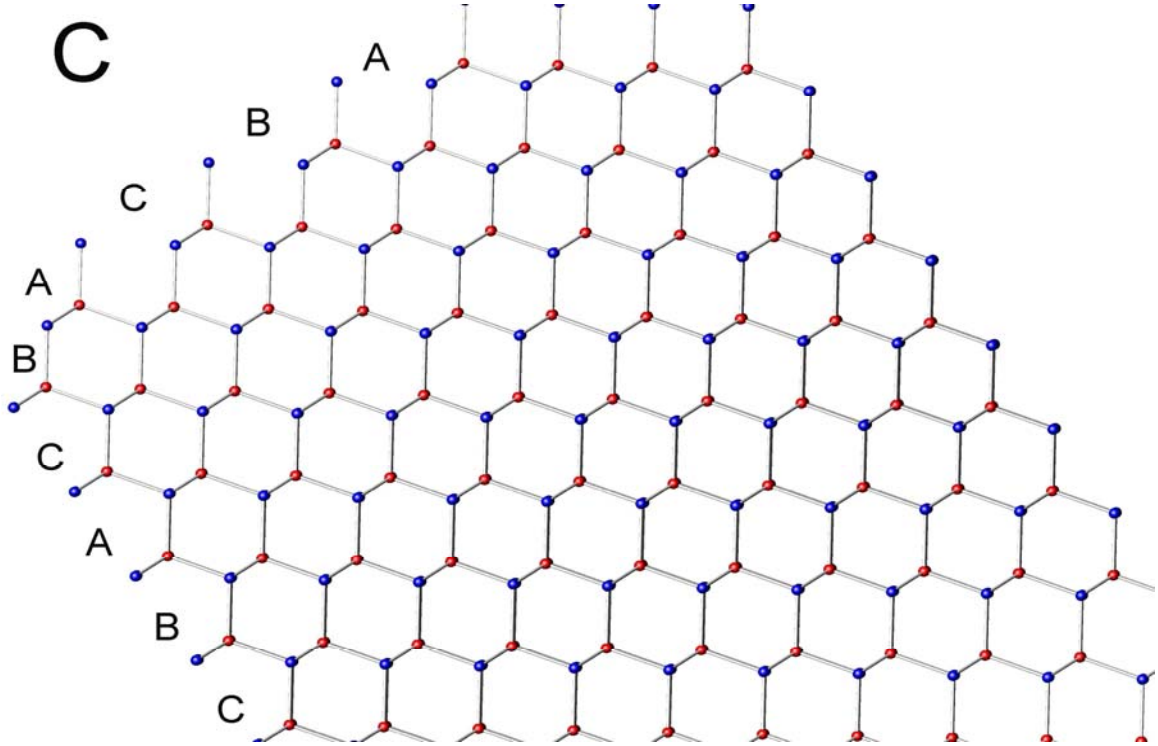

Figure 5.1C. Sphalerite Ball and Stick Model

The layers of the different stacking arrangement for sphalerite is shown in a ball and stick model.

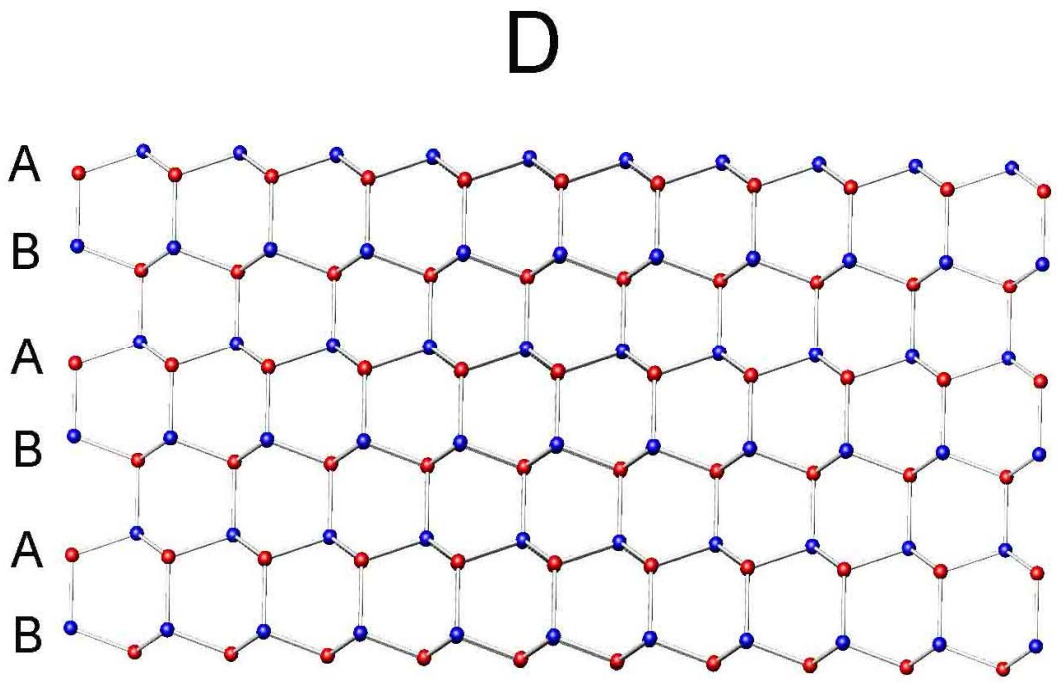

Figure 5.1D. Wurtzite Ball and Stick Model

The layers of the different stacking for wurtzite is shown in a ball and stick model.

be indexed to sphalerite (F43m, card # 216), while for reactions carried out above 10 mM, the wurtzite lattice is observed (P63mc, card #186). The most important reflection for wurtzite is <002> and <103>, while for sphalerite the observation of <111> and <200> confirms the assignment. For structures exhibiting multiple stacking faults the <103> wurtzite plane is broadened in the pXRD pattern suggesting the structure is sphalerite; however the <200> zinc blend plane is not observed. Only in the pure sphalerite phase is the <200> plane observed in the pXRD. The TEM image of the largest QD sizes are shown for the two distinct phases (Figure 5.2), confirming the pXRD assignments. Inspection of the TEM images is important, as no stacking faults are observable under high resolution TEM for either the sphalerite or wurtzite materials. Electron Diffraction imaging of the QDs confirms the pXRD assignments. (Figure 5.2 insert)

In Figure 5.3, at intermediate concentrations a mixed phase is observed, where loss of the <103> intensity for wurtzite is observed without the appearance of the <200> plane for sphalerite phase. Inspection of the TEM image confirms the appearance of stacking faults in the QDs (dark striations) (Figure 5.3B). The appearance of the striations in these materials suggests that loss of the <103> for wurtzite reflection without the appearance of the <200> sphalerite reflection is a good figure of merit for assigning a crystal phase with a large number of stacking faults.

Consistent with the assignment of an intermediate regime where stacking faults are observed, thermal annealing of the samples at 220^0C for > 29h results in a time dependent appearance of the <103> intensity expected for the pure wurtzite phase (Figure 5.3). Coupled to the increase in the (103) reflection intensity, the reflection is observed to shift ~3° in 2θ. The shift in the peak position is consistent with removal of sphalerite stacking faults via slow ion migration during annealing.[9 16]

The low energy barrier for sphalerite to wurtzite interconversion suggests that the QD lattice should be observed to transform from sphalerite to wurtzite at low temperatures for a mixed phase material containing stacking faults. Similar results have been demonstrated for materials grown by MOCVD and electrochemical deposition, where mixed phase materials are often observed. Using the intensity of the (103) reflection as a measure of the wurtzite character (Figure 5.4, Figure 5.5) a first order structural phase transition is observed in the powdered sample at ~380°C. The phase transition temperature is consistent with the reported value

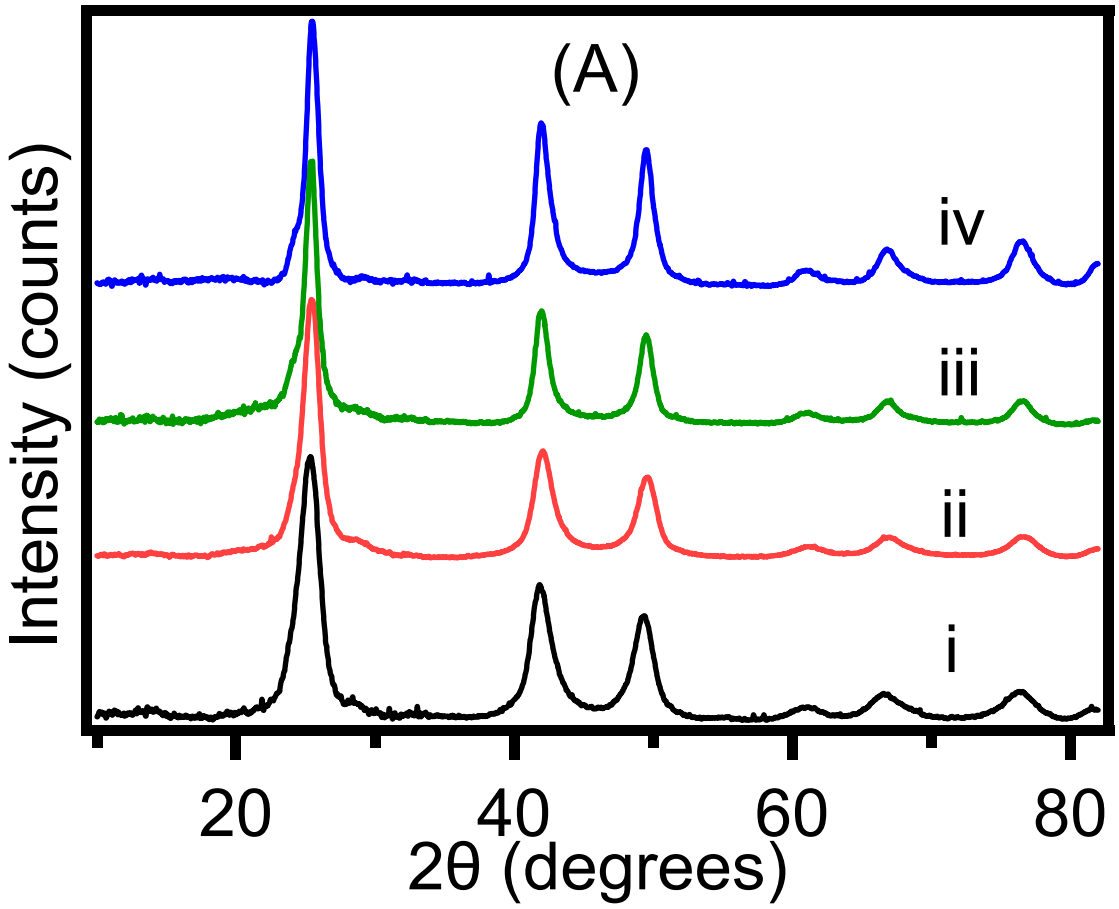

Figure 5.2A. pXRD of Sphalerite CdSe

Powder XRD spectra shows the ability to create stable A) sphalerite with sizes of i) 8.9nm ii) 9.6nm iii) 12.9nm iv) 14.3nm at 220°C in a conventional round bottom setup.

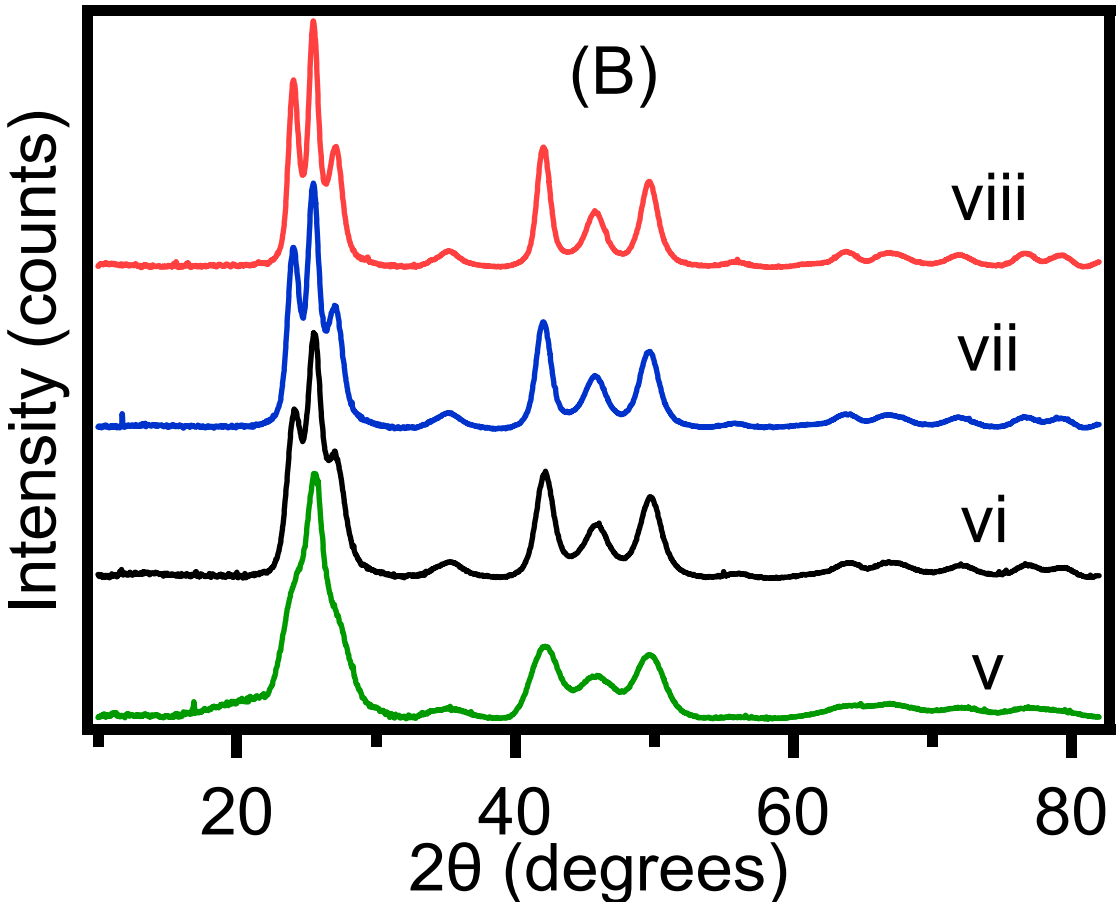

Figure 5.2B. pXRD of Wurtzite CdSe

Powder XRD spectra shows the ability to create stable wurtzite structures over various sizes including v) 7.2nm vi) 8.6nm vii) 9.6nm viii) 10.7nm at 220°C in a conventional round bottom setup.

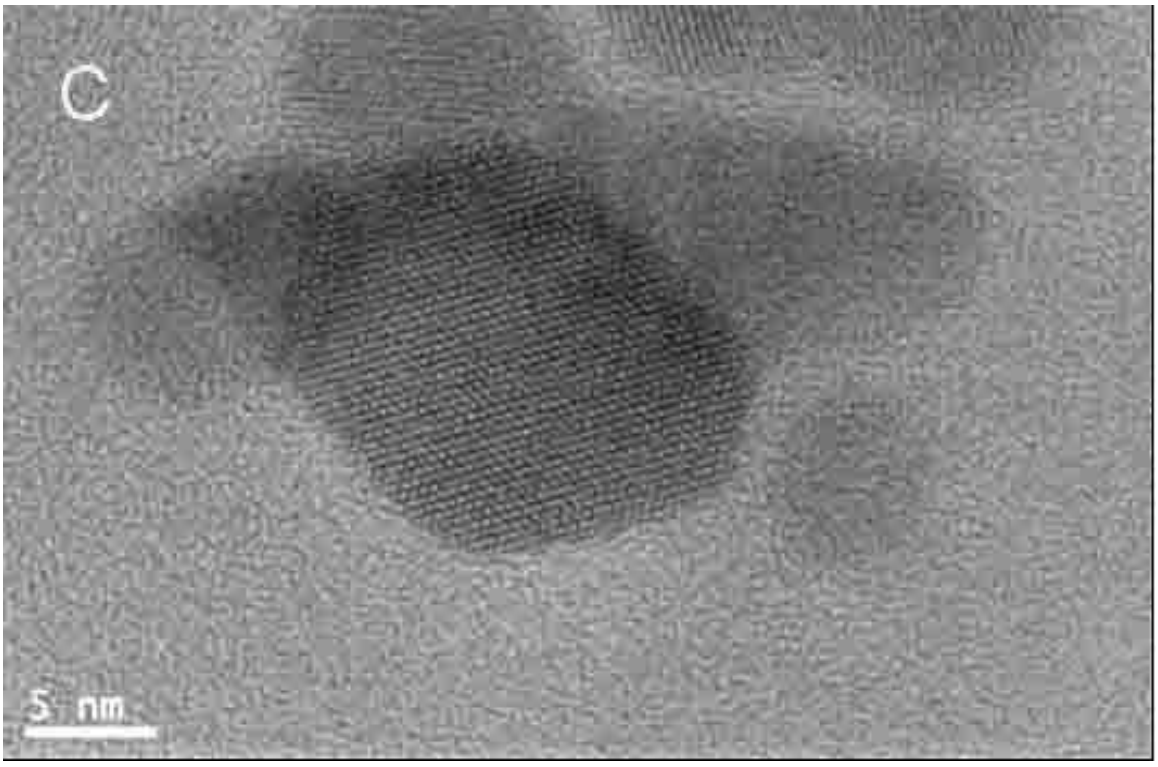

Figure 5.2C. TEM Sphalerite CdSe

HRTEM image of the sphalerite CdSe.

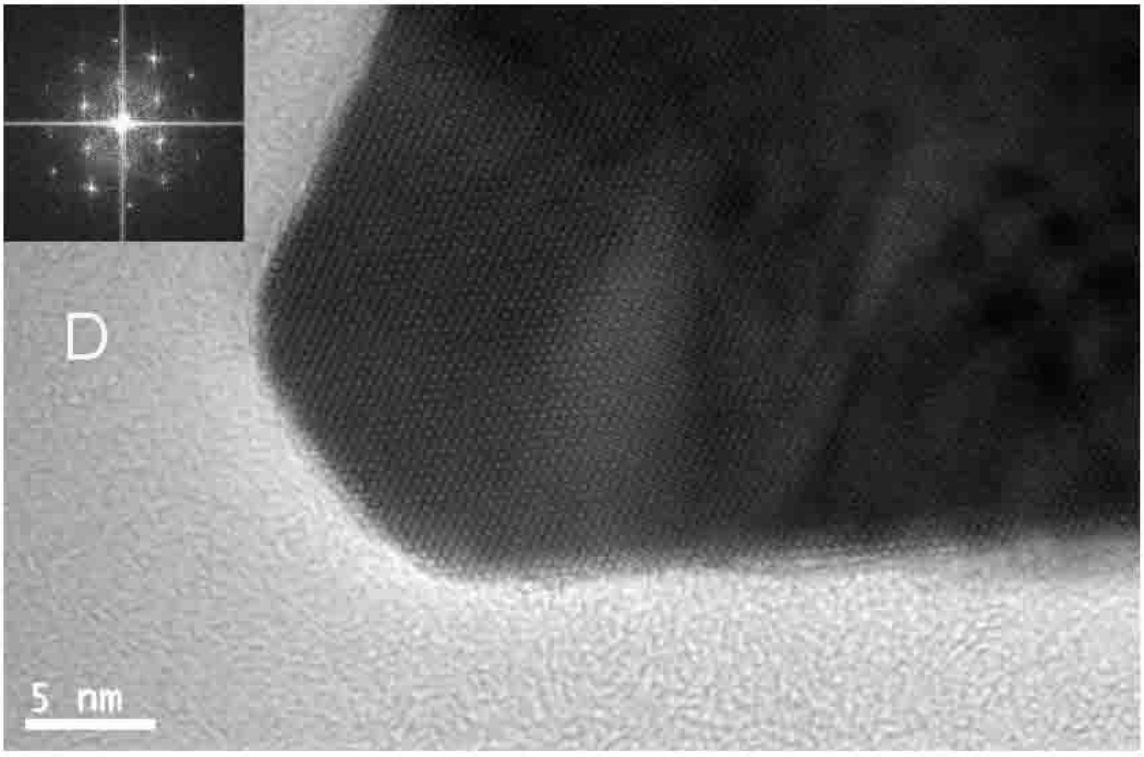

Figure 5.2D. HRTEM Wurtzite CdSe (w/SAED)

HRTEM image of wurtzite CdSe. Insert shows the selected area electron diffraction. (SAED)

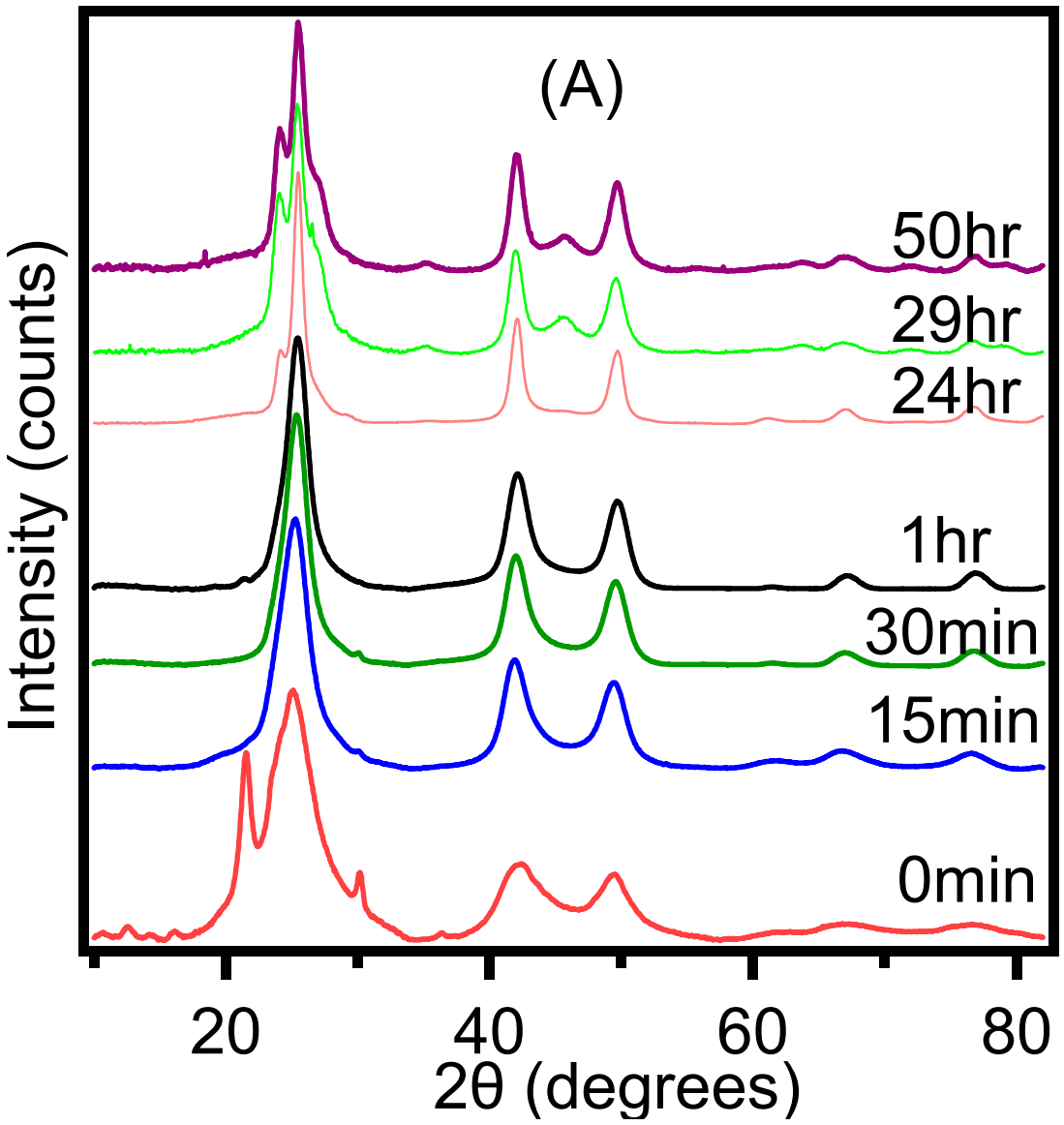

Figure 5.3A. pXRD Mixed Phase CdSe

pXRD data for mixed phase materials that undergo a phase transition in time. The sample was grown at a 10mM Cd stock precursor with Cd:Se ratio of 1:3 and heated to 220°C.

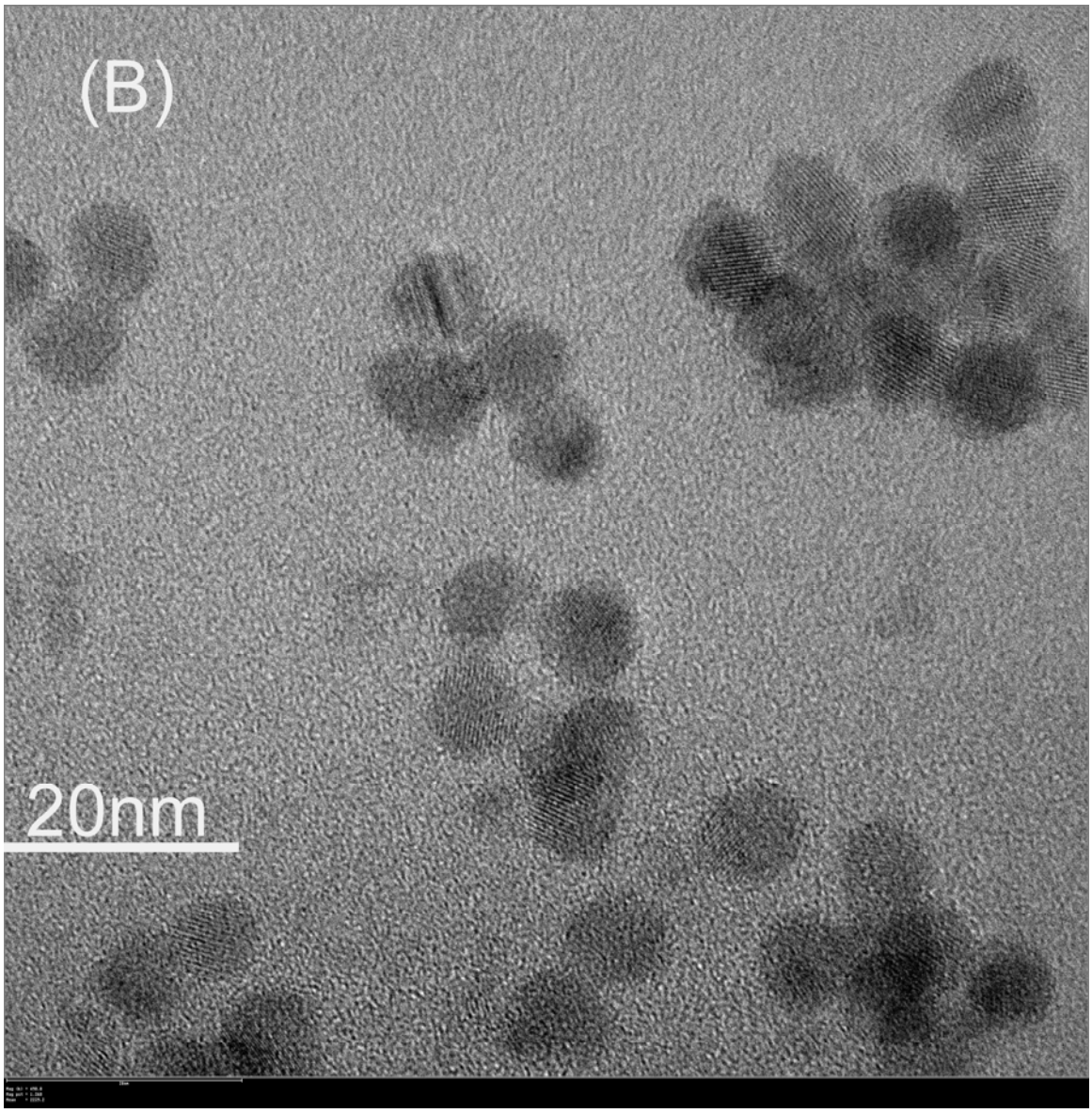

Figure 5.3B. TEM Mixed Phase CdSe

B) TEM image is shown for the interconverting sample after 1hr of growth. (size approx. 8.6 nm)

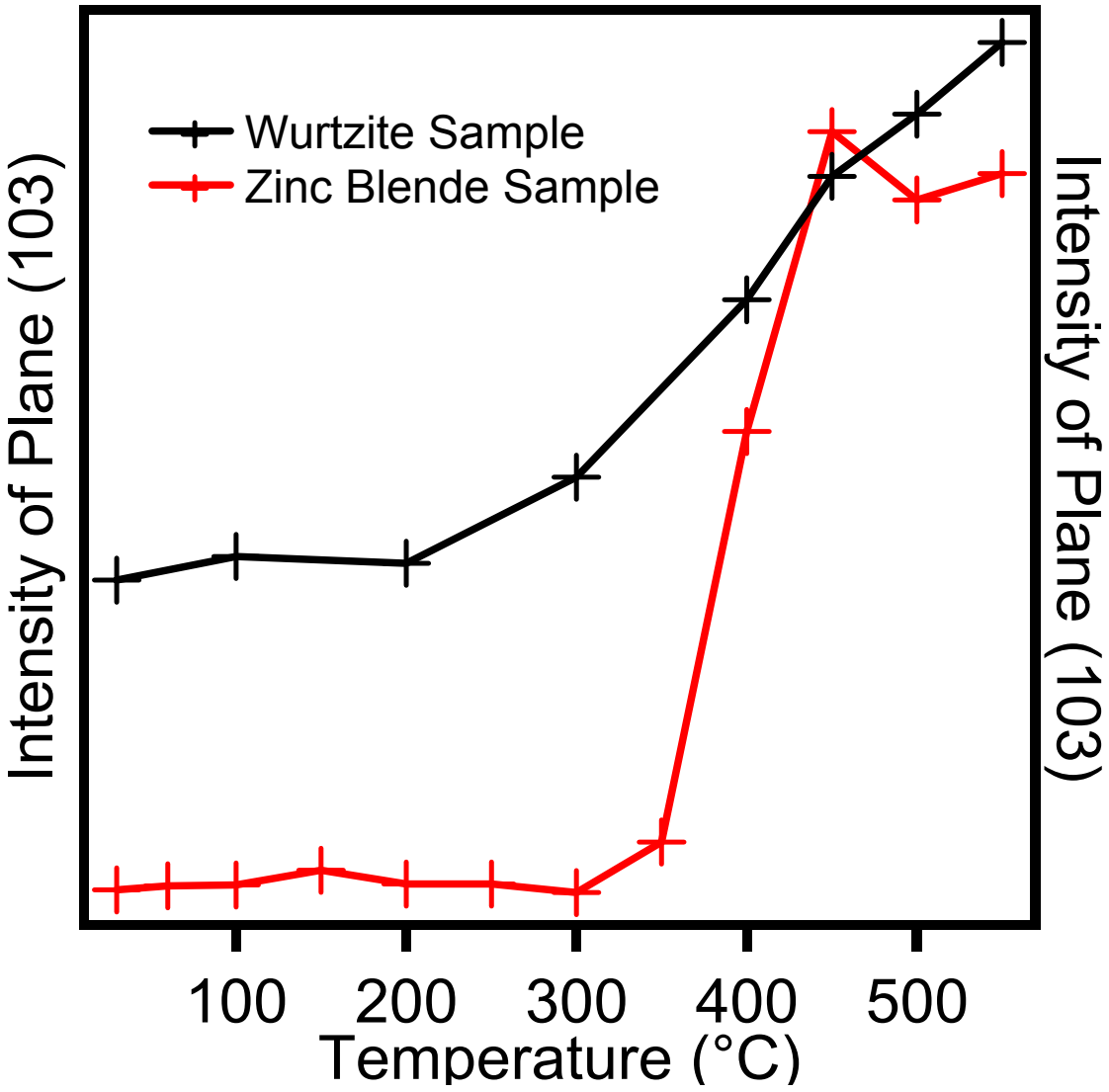

Figure 5.4. Intensity of (103) Plane vs. Temperature

A plot of the intensity of the wurtzite plane (103) as a function of increasing temperature according to pXRD data. The intensity of the plane for wurtzite and sphalerite (red) structures is shown.

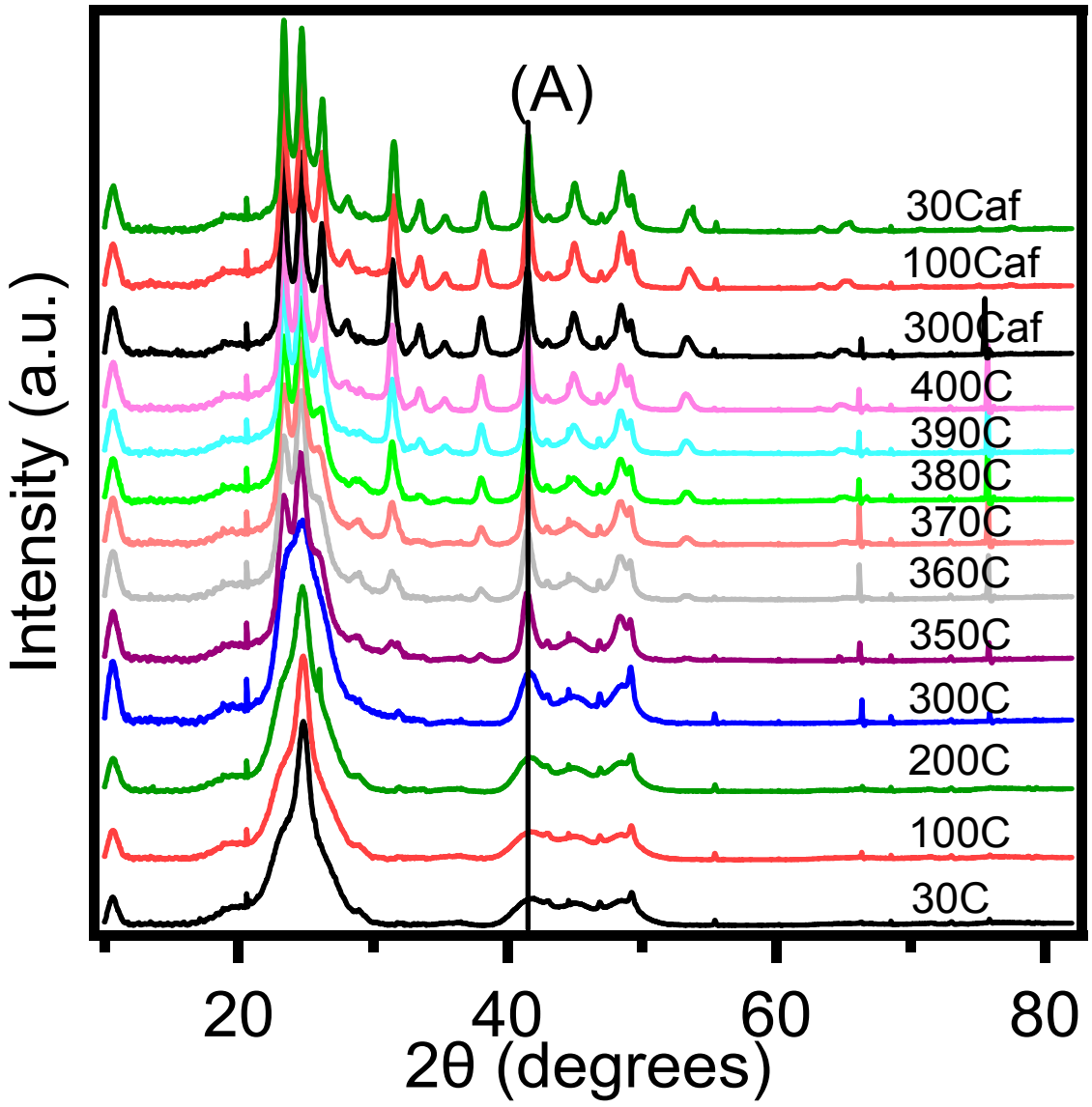

Figure 5.5A. Temperature Dependent pXRD Wurtzite CdSe

Temperature dependent pXRD spectra obtained by annealing a (A) hexagonal sample up to 400°C.

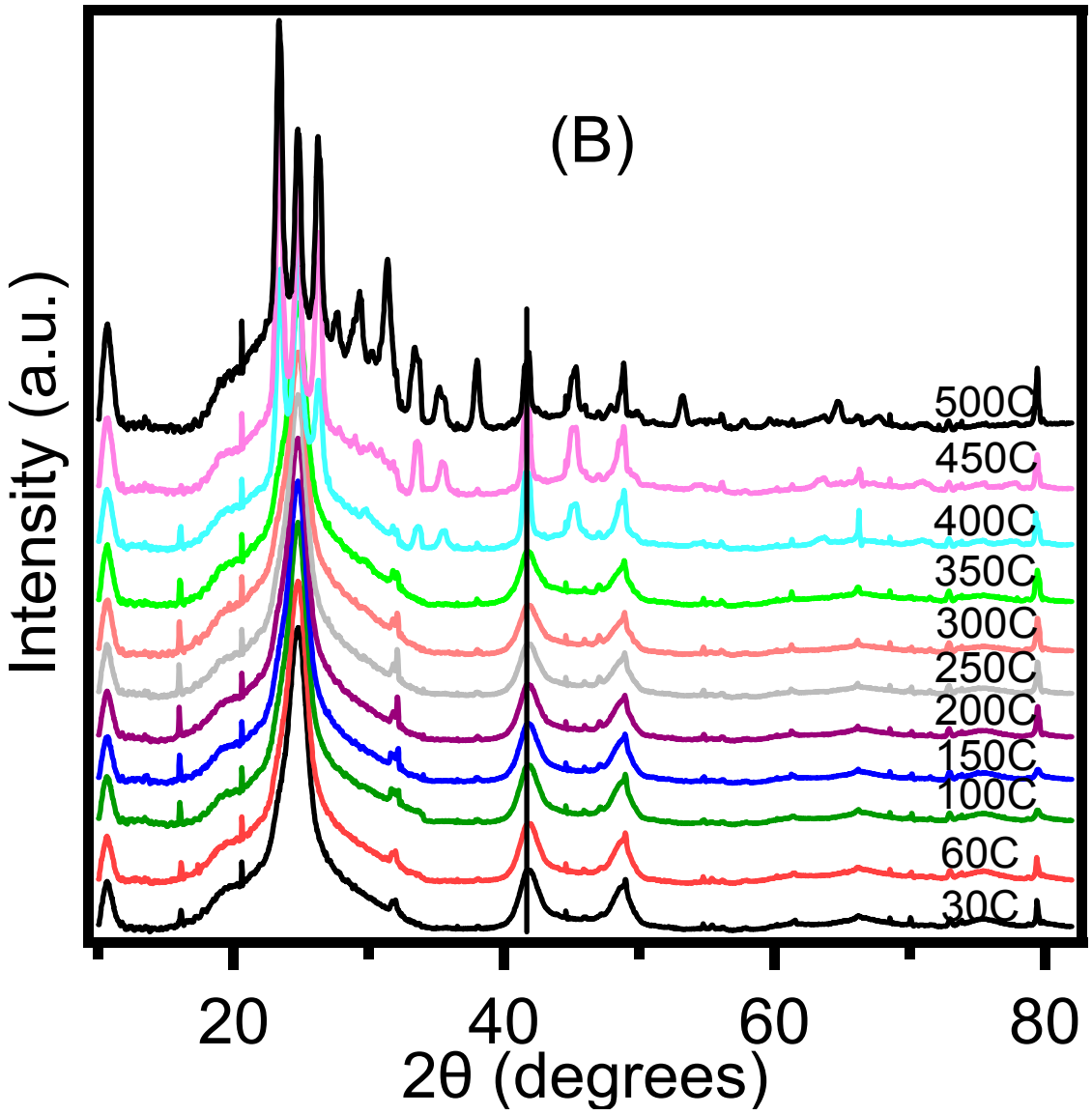

Figure 5.5B. Temperature Dependent pXRD Sphalerite CdSe

Temperature dependent pXRD spectra obtained by annealing a cubic sample from RT up to 500°C.

between 300-500^{o}C observed for CdSe phase instabilities in MOCVD, thin film, and electrochemically deposited mixed phase CdSe QDs.

Binary Phase Diagram. Inspection of the pXRD data for a wide range of concentrations and mole ratios allows a binary phase diagram to be drawn (Figure 5.6). Using the <111> plane of sphalerite and the <103> plane of wurtzite as a guide to whether the pure sphalerite or the pure wurtzite lattices are presents, the concentration dependent study yields three distinct identifiable regimes: a sphalerite domain, a wurtzite domain, and a mixed phase consisting of presumably a large number of lattice stacking faults in the CdSe QD. The results of the binary phase diagram shows the sphalerite structure is isolated only at low reactant and low Se mole ratios, while the wurtzite phase can be isolated at high monomer concentrations.

Phase Dependent QD Confinement. It is well known that the energy levels for the sphalerite and wurtzite phases of CdSe are unique.[196] Using an effective mass approximation for these materials,[9,11] the confinement function for the exciton transitions in QDs exhibiting a pure phase will depend strongly on the exhibited phase. A theoretical fit for the energy of the first exciton to the effective mass approximation (EMA) model yields a size to energy trajectory that is phase dependent (Figure 5.7). Plotting the absorption exciton of the isolated CdSe QDs in this study as a function of size reveals the exciton absorption energy for a specific size is consistent with the EMA predictions for the two phases. The remarkable agreement between the theoretical curve and the experimental data supports the suggestion that control of the concentration of reactants allows discrete crystal motifs to be isolated in the QD reaction.

5.4 Discussion

It is clear from the experimental data that the two crystal phases can be isolated by controlling the reaction concentration. At low monomer concentration the growth rate is slow and the obtained QD is templated by the nucleation event. At high monomer concentration, the growth rate is rapid leading to a large number of stacking faults and twinned crystals thus lowering the energy barrier for interconversion between phases. Due to the low energy difference between ions packing along the sphalerite phase or wurtzite phase arrangement at rapid growth rates, a high propensity for stacking faults and other defects is likely. Similar observations have been made in the preparation of CdSe using chemical bath deposition techniques, wherein the number of stacking faults scales with the reaction concentrations and monomer ratios in solution.[27] It was observed that at high monomer concentrations that the appearance of stacking

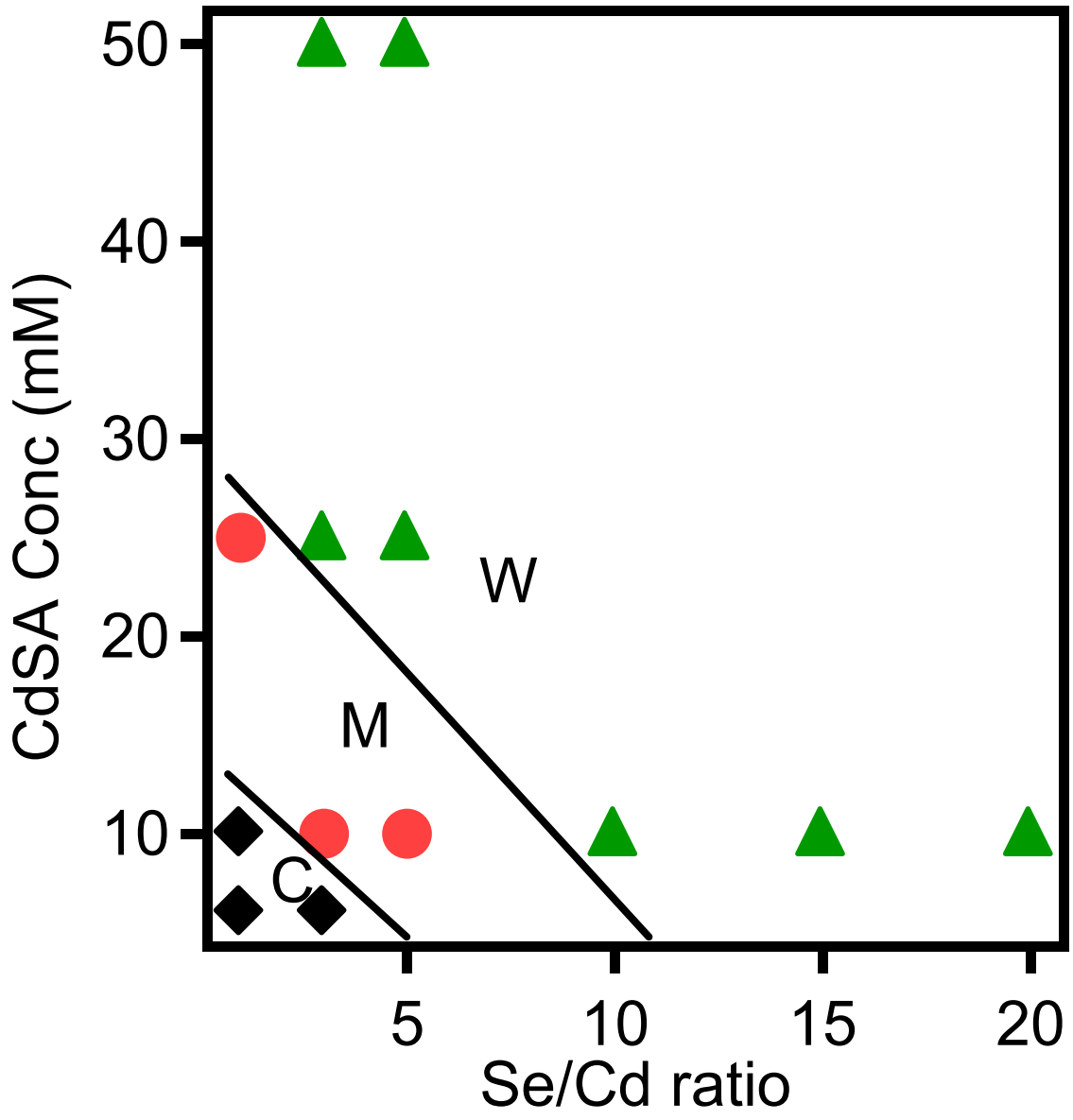

Figure 5.6. CdSe Phase Diagram

The different crystal motifs produced using multiple precursor concentrations and altering the ratio of Se to Cd. The Sphalerite (black diamond), mixed (red circle), and wurtzite (green triangle) are all stable in size up to 12-15nm.

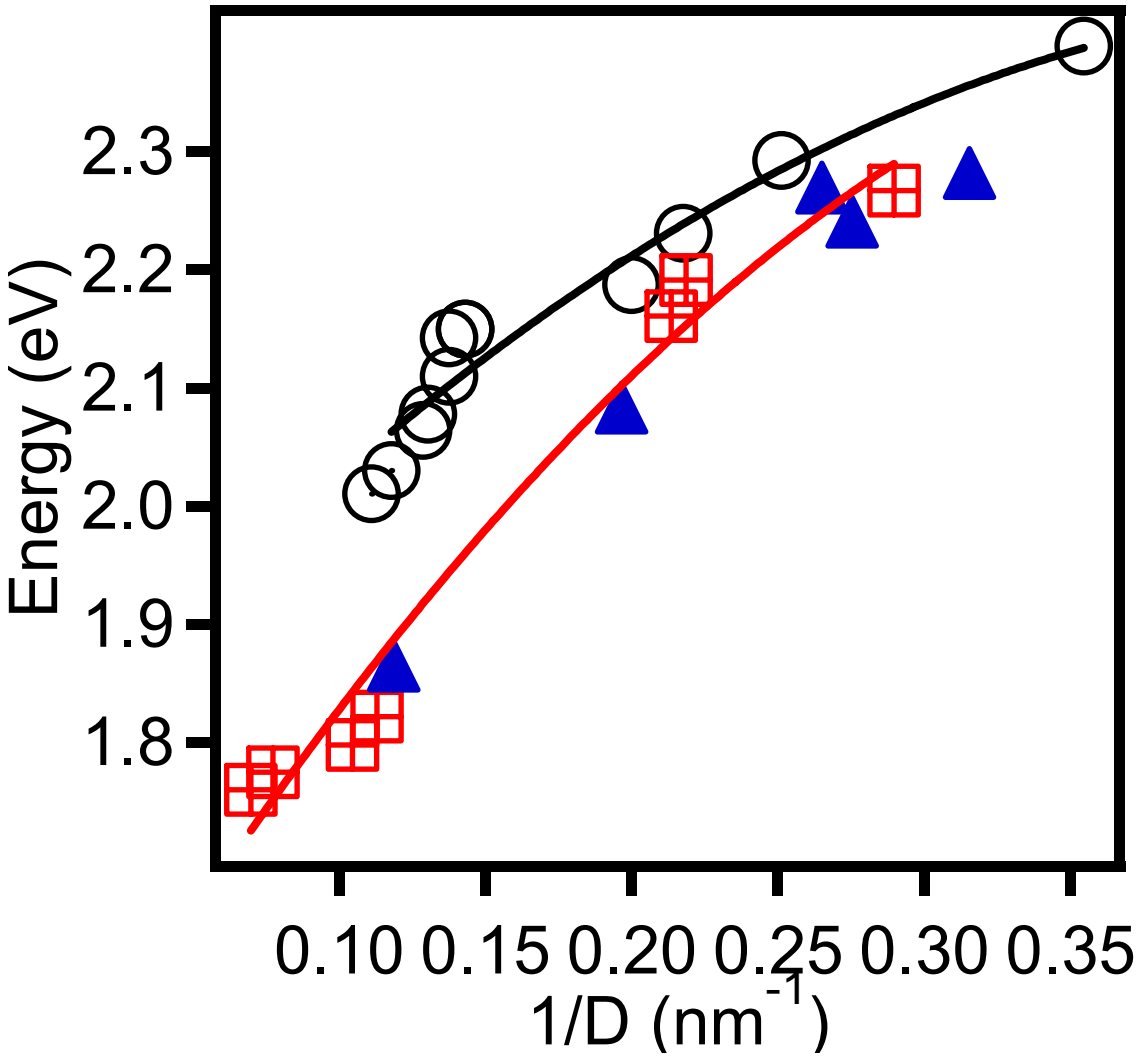

Figure 5.7. Bandedge Absorption vs. Inverse Size for Wurtzite and Sphalerite

A plot of the size versus bandedge absorption (eV) for Sphalerite (black circles), Wurtzite (red squares), and mixed structures (blue triangles). The fits are Sphalerite (black line) and Wurtzite (red line) that are correlated to the bandedge absorption for CdSe.

fault levels lead to isolation of the wurtzite phase, consistent with the current results. At low stacking fault levels obtained at lower concentrations, the sphalerite phase is observed with defect densities approaching the best levels obtained by MOCVD epitaxial growth methods. The results imply the growth of the binary materials is kinetically controlled and strongly influenced by the surface in these materials.

The results are readily understood using a simple growth mechanism dominated by a stepwise ion – by –ion addition mechanism where Ostwald's rules predict the lowest energy nucleation phase will be the metastable sphalerite phase. During nucleation, the surface free energy dominates the nucleation event and is minimized by a structure that can approximate a spherical shape due to the minimization of the surface to volume ratio. In CdSe this will give rise to a core nucleus with a large number of <111> facets expressed following the initial nucleation event. Growth is then dictated by the energy of the adding ions to the existing nanocrystal phase. CdSe polytypism will thus reflect the surface free energy ($\Delta G(p, T, \gamma)$) for the particular crystal motif, the nucleation critical size, and the shape of the initial nuclei formed for a given crystal motif.

The growth of a specific crystallite must reflect the structure of the preformed nuclei as long as the rate of growth is slow. Under this condition the growth can be described as a 3-D epitaxially templated growth problem. At slow growth rates the additional ions added to the face reconstruct to adopt the nuclei crystal morphology. At high reaction rates (kinetic growth), stacking faults appears as the additional ions added to the expressed face cannot reconstruct to match the expressed face under the fast growth conditions. While the growth of the pure phase can be rationalized the observation of a metastable phase for low concentrations conditions and the thermodynamically favored phase at high concentration suggest this is enthalpically controlled. Thus at high concentrations the thermodynamic phase is favored, while at low concentrations the metastable phase can be isolated. To understand the rationale, let's consider nucleation theory, which predicts that a stable nucleus exists when the free energy required to dissolve the nuclei is equal to the free energy in the nuclei, or in effect a stable nuclei exists when $\Delta G = G(\text{nuclei}) - G(\text{dissolution}) = 0$. Since $\Delta G = \Delta H - T\Delta S$, a stable nuclei exists at the point that $\Delta H = T\Delta S$. The critical nucleus in nucleation theory is defined as the $d\Delta G/d\text{size}$, or the first derivative of the free energy difference. When the nucleus is small, the surface area to

volume ratio of the nucleus is large, resulting in a larger Gibbs free energy. The Gibbs free energy will go as $1/R^2$.

5.5 Conclusion

Cadmium selenide quantum dots have been synthesized over a wide size range as pure wurzite (hexagonal) and sphalerite (sphalerite) crystal structures. The size of the particle plays no role in the structure as suggested previously. The only parameter that affects the structure of these materials is the concentration of the monomer precursor ions. Based on the data presented, the critical concentration for a phase change is between 11 and 12 mM concentration relative to CdSA and Se:Cd ratio of 3:1. The cadmium to selenium ratio is maintained at 1 to 3 because it is the optimal ratio for growing in this system. The observation of the concentration dependent binary phase diagram is believed to reflect thermodynamic equilibrium expression (Ksp) and the size of the critical nuclei as governed by nucleation theory. In the case of formation of CdSe QDs the amount of available free selenium in the system is believed to determine if the thermodynamic product (wurtzite) or the kinetic product (sphalerite) is formed.

REFERENCES

1 A presentation by Richard P. Feynman at an American Physical Society meeting at Caltech on December 29, 1959 where he outlined the first outlined the concept of nanotechnology as a top down technique for making materials and devices at the molecular scale.

2 Brus, L. E. J. Chem. Phys. (1984), 80(9), 4403-4409

3 Diguna, L. J.; Shen, Q.; Kobayashi, J.; Toyoda, T. App. Phys. Lett. (2007), 91(2) 023116/1-023116/3

4 Kronik, L.; Ashkenasy, N.; Leibovitch, M.; Fefer, E.; Shapira, Yoram; Gorer, S.; Hodes, G., J. Electrochem. Soc. (1998), 145(5), 1748-1755.

5 Kang, S.; Kumar, C. K.; Lee, Z.; Kim, K.; Huh, C.; Kim, E. Appl. Phys. Lett. 2008, 93(19), 191116/1-191116/3.

6 Brus, L. E. J. Chem. Phys. (1984), 80(9), 4403-4409.

7 Kippeny, Tadd; Swafford, Laura A.; Rosenthal, Sandra J. J. Chem. Ed. (2002), 79(9), 1094-1100.

8 Kippeny, Tadd; Swafford, Laura A.; Rosenthal, Sandra J. J. Chem. Ed. (2002), 79(9), 1094-1100.

9 Efros, A.L.; Rosen, M.; Kuno, M.; Nirmal, M.; Norris, D.J. Bawendi, M. 1996 Phys. Rev. B, 54, 4843-4856.

10 Micic, O. I.; Sprague, J. R.; Curtis, C. J.; Jones, K. M.; Machol, J. L.; Nozik, A. J.; Giessen, H.; Fluegel, B.; Mohs, G.; Peyghambarian, N. J. Phys. Chem. 1995, 99(19), 7754-9.

11 Vogel, R.; Pohl, K.; Weller, H. Chem. Phys. Lett. 1990, 174(3-4), 241-6.

12 Brus, L. E. J. Chem. Phys. (1984), 80(9), 4403-4409.

13 Bawendi, M.G.; Kortan, A.R.; Steigerwald, M. L.; Brus, L.E. J. Chem. Phys. 1989, 91, 7282.

14 Pileni, M. P.; Motte, L.; Petit, C. Chem. Mater. 1992, 4(2), 338-45.

15Murray, C.B.; Norris, D.J.; Bawendi, M.G. J. Am. Chem. Soc. 1993, 115, 8706.

16Steigerwald, M. L.; Sprinkle, C. R. J. Am. Chem. Soc. 1987, 7200.

17 Hines, M. A.; Guyot-Sionnest, P. J. Phys. Chem. 1996, 100(2), 468-71.

18 Peng, Z. A.; Peng, X. J. Am. Chem. Soc. 2001, 123(1), 183-184.

19 Cumberland, S.L.; Hanif, K.M.; Javier, A.; Khitrov, G.A.; Strouse, G.F.; Woessner, S.M.; Yun, C.S. Chem. Mater. 2002, 14, 1576-1584.

20 Gerbec J.A.; Magana, D.; Washington. A.; Strouse, G.F. J.Am.Chem.Soc. 2005, 127(45), 15791-15800.

21 DeGroot, M. W.; Rosner, H.; Corrigan, J. F. Chem.--A Euro. Journal 2006, 12(5), 1547-1554.

22 Archer, Paul I.; Santangelo, Steven A.; Gamelin, Daniel R. J. Am. Chem. Soc. 2007, 129(31), 9808-9818.

23 Wang, Ying; Herron, Norman. Phys. Rev. B: Cond. Matt. Mater. Phys. 1990, 42(11), 7253-5.

24 Cumberland, S.L.; Hanif, K.M.; Javier, A.; Khitrov, G.A.; Strouse, G.F.; Woessner, S.M.; Yun, C.S. Chem. Mater., 2002,14, 1576-1584.

25 Meulenberg, R.W.; Bryan, S.; Yun, C.S.; Strouse, G.F. J. Phys. Chem B, 2002, 106, 7774-7780.

26 Degroot, M. W.; Taylor, N.J.; Corrigan, J.F. J . Ma t e r . C h em., 2 0 0 4 , 1 4 , 6 5 4 – 6 6 0.

27 Archer, P. I.; Santangelo, S. A.; Gamelin, D. R. Nano Lett. 2007, 7(4), 1037-1043.

28 Magana, D.; Perera, S.; Harter, A.; Dalal, N.; Strouse, G.F. J. Am. Chem. Soc. 2006, 128(9), 2931-2939.

29 Gedye, R.; Smith, F.; Westaway, K.; Ali, H.; Baldisera, L.; Laberge, L.; Rousell, J. Tetrahedron Lett. 1986, 27(3), 279-82.

30 Washington, A.; Strouse, G.F. J. Am. Chem. Soc. 2008, 130(28), 8916-8922.

31 Abraham, F. F. *Homogeneous nucleation theory.* Academic Press, NY, 1974.

32 LaMer, V. K. Dinegar, R. H. J. Am. Chem. Soc. 1950, 72, 4847.

33 Karlin, K.; Bryan, J.D.; Gamelin, D.R. *Progress in Inorganic Chemistry.* 2005, 54, 55-70.

34 Microwave Processing of Materials. 1994. Committee on Microwave Processing of Materials: An Emerging Industrial Technology, Commission on Engineering and Technical System, National Research Council.

35 Washington, A.; Strouse, G.F. J. Am. Chem. Soc. 2008, 130(28), 8916-8922.

36 (a) De La Hoz, A.; Diaz-Ortiz, A.; Moreno, A. Current Organic Chemistry (2004), 8(10), 903-918.

37 Desai, Bimbisar; Danks, Timothy N.; Wagner, Gabriele. Dalton Transactions (2004), (1), 166-171.

38 Yadav, G.D.; Bisht, P.M. J. Molecular Catalysis A: Chemical (2005), 236(1-2), 54-64.

39 Peng, Z. Adam; Peng, Xiaogang. J. Am. Chem. Soc. (2002), 124(13), 3343-3353.

40 (a) de la Hoz, A.; Diaz-Ortiz, A.; Moreno, A. Chem. Soc. Rev. (2005), 34(2), 164-178. (b) Pchelka, B. K.; Loupy, A.; Petit, A. Tetrahedron (2006), 62(47), 10968-10979.

41 Pchelka, B. K.; Loupy, A.; Petit, A. Tetrahedron (2006), 62(47), 10968-10979.

42 Kingston, H.M.; Haswell, S. J. *Microwave-Enhanced Chemistry, Fundamentals, Sample Preparation and Applications.* American Chemical Society, 1997.

43 (a) Lazell, M.; O'Brien, P. J. Mater. Chem. (1999), 9, 1381-1382. (b) Cumberland, S.L.; Hanif, K.M.; Javier, A.; Khitrov, G.A.; Strouse, G.F.; Woessner, S.M.; Yun, C.S. Chem. Mater. (2002), 14, 1576-1584. (c) Yu, W. W.; Peng, X. Angew. Chem. Int. Ed. (2002), 41(13), 2368-2371.

44 (a) Peng, Z. A.; Peng, X. J. Am. Chem. Soc. (2002), 124(13), 3343-3353. (b) Qu, L.; Peng, X. J. Am. Chem. Soc. (2002), 124, 2094-2095. (c) Dabbousi, B.O.; Rodriguez-Viego, J.; Mikulee, F.V.; Heine, J.R.; Mattoussi, H.; Ober, R.; Jensen, K.F.; Bawendi, M. G. J. Phys. Chem. B (1997) 101, 9463-9475.

45 (a) Gao, M.; Kirstein, S.; Mohwald, H.; Rogach, A.L.; Kornowski, A.; Eychműller, A.; Weller, H. J. Phys. Chem. B (1998), 102, 8360-8363. (b) He, Y; Sai, L.; Lu, H.; Hu, M.; Lai, W.; Fan, Q.; Wang, L.; Huang, W. J. Phys Chem. B (2006) 110(27), 13352-13356. (c) He, Y; Sai, L.; Lu, H.; Hu, M.; Lai, W.; Fan, Q.; Wang, L.; Huang, W. J. Phys. Chem. B (2006), 110(27), 13370-13374. (d) Li, L.; Qian, H.; Ren, J. Chem. Comm. (Cambridge, UK) (2005), (4), 528-530.

46 (a) Diguna, L. J.; Shen, Q.; Kobayashi, J.; Toyoda, T. App. Phys. Lett. (2007), 91(2) 023116/1-023116/3. (b) Leschkies, K. S.; Divakar, R.; Basu, J.; Enache-Pommer, E.; Boercker, J.E.; Carter, C. B.; Kortshagen, U. R.; Norris, D. J.; Aydil, E. S. Nano. Lett. (2007), 7(6), 1793-1798.

47 (a) Kronik, L.; Ashkenasy, N.; Leibovitch, M.; Fefer, E.; Shapira, Yoram; Gorer, S.; Hodes, G., J. Electrochem. Soc. (1998), 145(5), 1748-1755. (b) Gao, X.; Chan, C.W.; Nie, S.J. Biomed. Opt. (2002), 7(4), 532-537.

48 (a) Liang, Hongjun; Angelini, Thomas E.; Ho, James; Braun, Paul V.; Wong, Gerard C. L. J. Am. Chem. Soc. (2003), 125(39), 11786-11787. (b) Sandros, M. G.; Gao, D.; Benson, D. E. J. Am. Chem. Soc. (2005), 127(35), 12198-12199.

49 (a) Yu, W. W.; Wang, Y. A.; Peng, X. Chem. Mater., (2003), 15(22), 4300-4308 (b) Pradhan, N.; Reifsnyder, D.; Xie, R.; Aldana, J.; Peng, X. J. Am. Chem. Soc. (2007), 129(30), 9500-9509.

50 (a) Munro, A. M.; Plante, I. J.; Ng, M. S.; Ginger, D. S. J. Phys. Chem. C (2007), 111(17), 6220-6227. (b) Kalyuzhny, G.; Murray, R. W. J. Phys. Chem. B (2005), 109(15), 7012-7021.

51 (a) Gao Xiaohu; Chan Warren C W; Nie Shuming J. Biomed. Opt. (2002), 7(4), 532-537. (b) Liang, Hongjun; Angelini, Thomas E.; Ho, James; Braun, Paul V.; Wong, Gerard C. L. J. Am. Chem. Soc. (2003), 125(39), 11786-11787. (c) Sandros, M. G.; Gao, D.; Benson, D. E. J. Am. Chem. Soc. (2005), 127(35), 12198-12199.

52 Murray, C. B.; Norris, D. J.; Bawendi, M. G. J. Am. Chem. Soc. (1993), 115(19), 8706-8715.

53 Peng, Z. Adam; Peng, Xiaogang. J. Am. Chem. Soc. (2001), 123(1), 183-184.

54 Peng, Xiaogang; Manna, Uberato; Yang, Weidong; Wickham, Juanita; Scher, Erik; Kadavanich, Andreas; Allvisatos, A. P. Nature (London) (2000), 404(6773), 59-61.

55 (a) Park, Jongnam; An, Kwangjin; Hwang, Yosun; Park, Je-Geun; Noh, Han-Jin; Kim, Jae-Young; Park, Jae-Hoon; Hwang, Nong-Moon; Hyeon, Taeghwan. Nature Mater. (2004), 3(12), 891-895. (b)Park, Jongnam; Joo, Jin; Kwon, Soon Gu; Jang, Youngjin; Hyeon, Taeghwan. Angew. Chem, Int. Ed. (2007), 46(25), 4630-4660.

56 Mohamed, Mona B.; Burda, Clemens; El-Sayed, Mostafa A. Nano Lett. (2001), 1(11), 589-593.

57 Peng, Z. Adam; Peng, Xiaogang. J. Am. Chem. Soc. (2001), 123(7), 1389-1395.

58 (a)Yang Y. A.; Wu H.; Williams K. R.; Cao Y.C. Angew. Chem. Int. Ed. (2005), 44(41), 6712-5. (b) Cao, Y. Charles; Wang, Jianhui. Journal of the American Chemical Society (2004), 126(44), 14336-14337.

59 Qu, L.; Yu, W.W.; Peng, X. Nano Lett. (2004), 4(3), 465-469.

60 Peng, Z. Adam; Peng, Xiaogang. J. Am. Chem. Soc. (2002), 124(13), 3343-3353.

61 (a) Gerbec, J. A.; Magana, D.; Washington, A.; Strouse, G. F. J. Am. Chem. Soc. 2005, 127(45), 15791-15800. (b) Ziegler, J.; Merkulov, A.; Grabolle, M.; Resch-Genger, U.; Nann, T. Lang. (2007), 23(14), 7751-7759. (c) Zhu, J.; Palchik, O.; Chen, S.; Gedanken, A. J. Phys. Chem. B (2000), 104(31), 7344-7347.

62 (a) Jiang, Y.; Zhu, Y. Chem. Lett. (2004), 33(10), 1390-1391. (b) Chu, M.; Shen, X.; Liu, G. Nanotech (2006), 17(2), 444-449. (c) Wang, Q.; Seo, D. Chem Mater. (2006), 18(24), 5764-5767. (d) Rogach, A.L.; Nagesha, D.; Ostrander, J.W.; Giersig, M.; Kotov, N.A. Chem. Mater. (2000), 12, 2676-2685.

63 (a) De La Hoz, A.; Diaz-Ortiz, A.; Moreno, A. Current Organic Chemistry (2004), 8(10), 903-918. (b) Desai, Bimbisar; Danks, Timothy N.; Wagner, Gabriele. Dalton Transactions (2004), (1), 166-171. (c) Yadav, G.D.; Bisht, P.M. J. Molecular Catalysis A: Chemical (2005), 236(1-2), 54-64.

64 (a) de la Hoz, A.; Diaz-Ortiz, A.; Moreno, A. Chem. Soc. Rev. (2005), 34(2), 164-178. (b) Pchelka, B. K.; Loupy, A.; Petit, A. Tetrahedron (2006), 62(47), 10968-10979.

65 (a) Talapin, D.V.; Shevchenko, E.V.; Murray, C.B.; Kornowski, A.; Foerster, S.; Weller, H. J. Am. Chem. Soc. (2004), 126(40), 12984-12988. (b) Peng, X.; Wickham, J.; Alivisatos, A.P. J. Am. Chem. Soc. (1998), 120(21), 5343-5344.

66 (a) Bryan, J.D.; Gamelin, D.R. Progress. Inorg. Chem. D.K.K. Ed.; John Wiley: New Jersey, (2005), 54, 47-126.

67 (a) Chen, Y.; Johnson, E.; Peng, X. J. Am. Chem. Soc. (2007), 129(35), 10937-10947. (b) Joshi, S.; Sen, S.; Ocampo, P.C. J. Phys. Chem. C (2007), 111(11), 4105-4110.

68 Liu, H.; Owen, J.S.; Alivisatos, A. P. J. Am. Chem. Soc. (2007), 129(2), 305-312.

69 Ferreira, W. S.; de Sousa, J. S.; Freire, J. A. K.; Farias, G. A.; Freire, V. N. Brazilian J. Phys. (2006), 36(2A), 438-439.

70 (a) Al-Salim, N.; Young, A. G.; Tilley, R. D.; McQuillan, A. J.; Xia, J. Chem. Mater. (2007), 19(21), 5185-5193. (b) Nag, A.; Sapra, S.; Chakraborty, S.; Basu, S.; Sarma, D. D J. Nanosci. and Nanotech. (2007), 7(6), 1965-1968. (c) Dai, Q.; Li, D.; Chen, H.; Kan, S.; Li, H.; Gao, S.; Hou, Y.; Liu, B.; Zou, G. J. Phys. Chem. B (2006), 110(33), 16508-16513. (d) Foos, E. E.; Wilkinson, J.; Maekinen, A. J.; Watkins, N. J.; Kafafi, Z. H.; Long, J. P. Chem. Mater. (2006), 18(12), 2886-2894.

71 Deng, Zhengtao; Cao, Li; Tang, Fangqiong; Zou, Bingsuo. J. Phys. Chem. B (2005), 109(35), 16671-16675.

72 (a) Granasy, L.; James, P.F. J. Chem. Phys. (2000), 113(21), 9810-9821. Kim (b) Yong-Sung; Randolph T.W.; Stevens F.J.; Carpenter J.F. J. Bio. Chem. (2002), 277(30), 27240-27246.

73 (a) Shevchenko E.V.; Talapin D.V.; Schnablegger H.; Kornowski A.; Festin O.; Svedlindh P.; Haase M.; Weller H. J. Am. Chem. Soc. (2003), 125(30), 9090-101. (b) Yu K.; Singh S.i;

Patrito N.; Chu V. Langmuir (2004), 20(25), 11161-11168. (c) He, Y.; Sai, L.; Lu, H.; Hu, M.; Lai, W.; Fan, Q.; Wang, L.; Huang, W. Chem. Mater. (2007), 19(3), 359-365.

74 Qu., L; Peng, A.Z.; Peng, X. Nano Lett. (2001) 1(6), 333-337.

75 Liu, H., Owen, J.S., Alivisatos, A.P. J. Am. Chem. Soc. (2007), 129, 305-312.

76 Bunten, K.A.; Chen, L.; Fernandez, A.L.; Poe, A.J. Coordination Chem. Rev. (2002), 233-234, 41-51.

77 (a) Yen, B.K.H.; Stott, N.E.; Jensen, K.F.; Bawendi, M.G. Adv. Mater. (2003), 15(21), 1858-1862. (b) Kawa, M.; Morii, H.; Ioku, A.; Saita, S.; Okuyama, K. J. Nanoparticle Research (2003), 5(1-2), 81-85. (c) Krishnadasan, S.; Tovilla, J.; Vilar, R.; deMello, A. J.; deMello, J. C. J. Mater. Chem. (2004), 14(17), 2655-2660. (d) Yen, B.K.H.; Gunther, A.; Schmidt, M.A.; Jensen, K.F.; Bawendi, M.G. Angew. Chem., Int. Ed. (2005), 44(34), 5447-5451.

78 Rossetti, R.; Ellison, J.L.; Gibson, J.M.; Brus, L.E. J. Chem. Phys. 1984, 80 (90), 4464.

79 Empedocles, S. A.; Norris, D. J.; Bawendi, M. G. Phys. Rev. Lett. (1996), 77(18), 3873-3876.

80 Mews, A.; Eychmueller, A.; Giersig, M.; Schooss, D.; Weller, H. J. Phys. Chem. 1994, 98(3), 934-41.

81 Rajh, T.; Micic, O. I.; Nozik, A. J. J. Phys. Chem. 1993, 97(46), 11999-2003.

82 Micic, O. I.; Curtis, C. J.; Jones, K. M.; Sprague, J. R.; Nozik, A. J. J. Phys. Chem. 1994, 98(19), 4966-9.

83 Peng, Z. A.; Peng, X. J. Am. Chem. Soc. 2001, 123(1), 183-184.

84 Dabbousi, B. O.; Rodriguez-Viejo, J.; Mikulec, F. V.; Heine, J. R.; Mattoussi, H.; Ober, R.; Jensen, K. F.; Bawendi, M. G. J. Phys. Chem. B 1997, 101(46), 9463-9475.

85 Xi, L.; Tan, W. X. W.; Boothroyd, C.; Lam, Y. M. Chem. Mater. 2008, 20(16), 5444-5452.

86 Talapin, D. V.; Rogach, A. L.; Shevchenko, E. V.; Kornowski, A.; Hasse, M.; Weller, H. J. Am. Chem. Soc. 2002, 124 (20), 5782-5790.

87 Peng, A. Z.; Peng, X. G. J. Am. Chem. Soc. 2002, 124, 3343

88 Lui, H.; Owen, J. S.; Alivisatos, A.P. J. Am. Chem. Soc. 2007, 129 (2), 305-312.

89 Cao, Y. C.; Wang, J. J. Am. Chem. Soc. 2004, 126, 14336-14337

90 Mohamed, M. B.; Tonti, D.; Al-Salman, A.; Chemseddine, A.; Chergui, M. J. Phys. Chem. B 2005, 109(21), 10533-10537.

91 Murray, C. B.; Norris, D. J.; Bawendi, M. G. J. Am. Chem. Soc. 1993, 115, 8706.

92 Manna, L.; Scher, E. C.; Alivisatos, A. P. J. Am. Chem. Soc. 2000, 122, 12700.

93 Rogach, A. L.; Kornowski, A.; Gao, M. Y.; Eychmuller, A.; Weller, H. J. Phys. Chem. B 1999, 103, 3065.

94 Vossmeyer, T.; Katsikas, L.; Giersig, M.; Popovic, I. G.; Diesner, K.; Chemseddine, A.; Eychmuller, A.; Weller, H. J. Phys. Chem. 1994, 98, 7665

95 Qu, L. H.; Peng, X. G. J. Am. Chem. Soc. 2002, 124, 2049.

96 Yu, W. W.; Wang, Y. A.; Peng, X. G. *Chem. Mater.* **2003**, *15*, 4300.

97 Talapin, D. V.; Rogach, A. L.; Haase, M.; Weller, H. J. Phys. Chem. B. 2001, 105(49), 12278-12285.

98 Washington, II, A.L.; Strouse, G.F. J. Am. Chem. Soc. 2008, 130(28), 8916-8922.

99 Talapin, D. V.; Nelson, J. H.; Shevchenko, E. V.; Aloni, S.; Sadtler, B.; Alivisatos, A. P. Nano Lett. 2007, 7(10), 2951-2959

100 Shieh, F.; Saunders, A. E.; Korgel, B. A. J. Phys. Chem. B. 2005, 109 (18), 8538-8542

101 Drowart, J.; Myers, C. E.; Szwarc, R; Vander Auwera-Mahieu, A.; Uy, O. M.; High Temp. Sci., 1973, 5, 482.

102 Yu, W. W.; Peng, X. Angew. Chem. Int. Ed. 2002, 41(13), 2368-2371.

103 Karan, S.; Malik, B. J. Phys.Chem. C. 2007, 111 (45), 16734-16741.

104 De La Hoz, A.; Diaz-Ortiz, A.; Moreno, A. Current Organic Chemistry (2004), 8(10), 903-918.

105 de la Hoz, A.; Diaz-Ortiz, A.; Moreno, A. Chem. Soc. Rev. (2005), 34(2), 164-178.

106 Steckel, J.S.; Zimmer, J.P.; Coe-Sullivan, S.; Stott, N.E.; Bulovic, V.; Bawendi, M.G. Angew. Chem. Int. Ed. 2004, 43, 2154.

107 Swafford, L. A.; Weigand, L. A.; Bowers, M. J., II; McBride, J. R.; Rapaport, J. L.; Watt, T. L.; Dixit, S. K.; Feldman, L. C.; Rosenthal, S. J. J. Am. Chem. Soc. 2006, 128(37), 12299-12306.

108 Washington, II, A.L.; Strouse, G.F. J. Am. Chem. Soc. 2008, 130(28), 8916-8922.

109 Joo, J.; Bin Na, H.; Yu, T.; Ho Yu, J.; Woon Kim, Y.; Wu, F.; Zhang, J. Z.; Hyeon, T. J. Am. Chem. Soc. 2003, 125, 11100-11105

110 Meulenberg, R.W.; Strouse, G.F. J. Phys. Chem. B 2001, 105, 7438-7445

111 Talapin, D. V.; Rogach, A. L.; Kornowski, A.; Haase, M.; Weller, H. Nano Lett. 2001, 1, 207.

112 Talapin, D. V.; Rogach, A. L.; Mekis, I.; Haubold, S.; Kornowski, A.; Haase, M.; Weller, H. Colloids Surf., A 2002, 202, 145.

113 Jasieniak, J.; Mulvaney, P. J. Am. Chem. Soc. 2007, 129(10), 2841-2848.

114 Landes, C. F.; Braun, M.; El-Sayed, M. A. J. Phys. Chem. B 2001, 105(43), 10554-10558.

115 Pai, C. K.; Smith, M. B. J. Org. Chem. 1995, 60(12), 3731-3735.

116 Kiddle, J. J. Tetrahedron Lett. 2000, 41(9), 1339-1341.

117 Hajek, M. Microwaves in Organic Synthesis (2nd Edition). 2006, 2, 615-652.

118 Ziegler, J.; Merkulov, A.; Grabolle, M.; Resch-Genger, U.; Nann, T. Lang. 2007, 23(14), 7751-7759.

119 Huang, W.; Richert, R. J. Phys. Chem. B. **2008**, 112(32), 9909-9913.

120 Karan, S.; Mallik, B. J. Phys. Chem. C. 2007, 111(45), 16734-16741.

121 Roy, M. D.; Herzing, A. A.; De Paoli L., Silvia H.; Becker, M. L. Chem. Comm. (Cambridge, U.K.) 2008, 18, 2106-2108.

122 Microwave Processing of Materials. 1994. Committee on Microwave Processing of Materials: An Emerging Industrial Technology, Commission on Engineering and Technical System, National Research Council.

123 Kappe, C.O. Chem. Soc. Rev. 2008, 37(6), 1127-1139.

124 Varma, R.S.; Ju, Y. Microwaves in Organic Synthesis (2nd Edition). 2006, 1, 362-415.

125 Washington, II, A.L.; Strouse, G.F. J. Am. Chem. Soc. 2008, 130(28), 8916-8922.

126 Gerbec, J.A.; Magana, D.; Washington, A. J. Am. Chem. Soc. 2005, 127(45), 15791-15800.

127 Lovingood, D.; Strouse, G. F. Nano Lett. 2008, 8(10), 3394-3397.

128 Peng, X.; Wickham, J.; Alivisatos, A. P. J. Am. Chem. Soc. 1998, 120(21), 5343-5344.

129 Talapin, D. V.; Rogach, A. L.; Shevchenko, E. V.; Kornowski, A.; Hasse, M.; Weller, H. J. Am. Chem. Soc. 2002, 124 (20), 5782-5790.

130 Lifshitz, I.M.; Slyozov, V.V. J. Phys. Chem. Solids. 1961. 19. 35.

131 Sugimoto, T. Adv. Colloid Interface Sci. 1987, 28, 65.

132 Talapin, D. V.; Rogach, A. L.; Haase, M.; Weller, H. J. Phys. Chem. B. 2001, 105(49), 12278-12285.

133 Tuinenga, C.; Jasinski, J.; Iwamoto, T.; Chikan, V. ACS Nano 2008, 2(7), 1411-1421.

134 Yang, Y. A.; Wu, H.; Williams, K. R.; Cao, Y. C. Angew. Chem. Int. Ed. 2005, 44 (41), 6712–6715.

135 Park, J.; An, K.; Hwang, Y.; Park, J.; Noh, H.; Kim, J.; Park, J.; Hwang, N; Hyeon, T. Nature Mater. 2004, 3(12), 891-895.

136 Fournier-Bidoz, S.; Jennings, T. L.; Klostranec, J. M.; Fung, W.; Rhee, A.; Li, D.; Chan, W. C. Angew. Chem., Int. Ed. 2008, 47(30), 5577-5581.

137 Nam, J.; Thaxton, C. S.; Mirkin, C. A. Science. 2003, 301(5641), 1884-1886.

138 Wang, L.; Tan, W. Nano Lett. 2006, 6(1), 84-88.

139 Yang, Y.; Li, Y.; Fu, S.; Xiao, H. J. Phys. Chem. C 2008, 112(28), 10553-10558.

140 Milliron D. J.; Hughes S. M.; Cui Y.; Manna L.; Li J.; Wang L.; Alivisatos, A. P. Nature 2004, 430(6996), 190-195.

141 Lee, Y.; Huang, B.; Chien, H. Chem. Mater. 2008, 20(22), 6903-6905

142 Nozik, A. J. Chem. Phys. Lett. 2008, 457(1-3), 3-11.

143 Nozik, A. J. Next Generation Photovoltaics. 2004, 196-222.

144 Weiss, E. A.; Chiechi, R. C.; Geyer, S. M.; Porter, V. J.; Bell, D. C.; Bawendi, M. G.; Whitesides, G. M. J. Am. Chem. Soc. 2008, 130(1), 74-82.

145 Qu, L.; Peng, X. J. Am. Chem. Soc. 2002, 124(9), 2049-2055

146 Li, J. J.; Wang, Y. A.; Guo, W.; Keay, J. C.; Mishima, T. D.; Johnson, M. B.; Peng, X. J. Am. Chem. Soc. (2003), 125(41), 12567-12575.

147 Reiss, P.; Bleuse, J.; Pron, A. Nano Lett. 2002, 2(7), 781-784.

148 Peng, X.; Manna, U.; Yang, W.; Wickham, J.; Scher, E.; Kadavanich, A.; Allvisatos, A. P. Nature (London). 2000, 404(6773), 59-61.

149 Peng, Z. A.; Peng, X. J. Am. Chem. Soc. 2001, 123(1), 183-184.

150 Gabriel, C.; Gabriel, S.; Grant, E. H.; Halstead, B. S. J.; Mingos, D. M. P. Chem. Soc. Rev. (1998), 27(3), 213-224.

151 Shiflett, M. B.; Yokozeki, A. J. Chem. & Eng. Data. 2008, 53(11), 2683-2691.

152 Jin, H.; Baker, G. A.; Arzhantsev, S.; Dong, J.; Maroncelli, M. J. Phys. Chem. B. 2007, 111(25), 7291-7302.

153 Protasenko, V.; Bacinello, D.; Kuno, M. J. Phys. Chem. B. 2006, 110(50), 25322-25331.

154 Mauser, C.; Limmer, T.; Como, E. D.; Becker, K.; Rogach, A. L.; Feldmann, J.; Talapin, D.V. Phys. Rev. B. 2008, 77, 153303.

155 Koo, B.; Korgel, B.A. Nano Lett 2008, 8 (8), 2490-2496.

156 Talapin, D.V; Nelson, J.H.; Shevchenko, E.V.; Aloni, S.; Sadtler, B.; Aliisatos, A.P. Nano Lett. 2007, 7(!0), 2951-2959.

157 Shieh, F.; Saunders, A. E.; Korgel, B. A. J. Phys. Chem. B 2005, 109(18), 8538-8542.

158 Pons, T.; Medintz, I. L.; Sapsford, K. E.; Higashiya, S.; Grimes, A. F.; English, D. S.; Mattoussi, H. Nano Lett. 2007, 7(10), 3157-3164.

159 Kim, S.; Fisher, B.; Eisler, H. ; Bawendi, M. G. J. Am. Chem. Soc. 2003, 125(38), 11466-11467.

[160] Brus, L. E. J. Chem. Phys. 1984, 80(9), 4403-4409.

161 Leschkies, K. S.; Divakar, R.; Basu, J.; Enache-Pommer, E.; Boercker, J.E.; Carter, C. B.; Kortshagen, U. R.; Norris, D. J.; Aydil, E. S. Nano. Lett. (2007), 7(6), 1793-1798.

162 Gao, X.; Chan, C. W.; Nie S. J. Biomed. Opt. (2002), 7(4), 532-537.

163 Sandros, M. G.; Gao, D.; Benson, D. E. J. Am. Chem. Soc. (2005), 127(35), 12198-12199.

164 Talapin D. V.; Nelson J. H.; Shevchenko E. V.; Aloni S.; Sadtler B.; Alivisatos A P. Nano Lett. 2007, 7(10), 2951-2959.

165 Talapin, Dmitri V.; Shevchenko, Elena V.; Murray, Christopher B.; Kornowski, Andreas; Foerster, Stephan; Weller, Horst. J. Am. Chem. Soc. 2004, 126(40), 12984-12988.

166 Kuno, M. Phys. Chem. Chem. Phys. 2008, 10, 620-639.

167 Kumar, S.; Ade, M.; Nann, T. Chem. Eur. J. 2005, 11, 2220-2224.

168 Bawendi, M. G.; Kortan, A.R.; Steigerwald, M. L.; Brus, L. E. J. Chem. Phys. 1989, 91, 7282.

169 Murray C.B.; Norris D.J.; Bawendi, M.G. J. Am. Chem. Soc. 1993, 115(19), 8706-8715.

170 Swafford, L.A., Welgand, L.A., Bowers, II, M.J., McBride, J.R., Rapaport, J.L., Watt, T.L., Dixit, S.K., Feldman, L.C., Rosenthal, S.J. J. Am. Chem. Soc. 2006, 128, 12299-12306.

171 Tilley, R.D., Jefferson, D.A. J. Phys. Chem. B. 2002, 106, 10895-10901

172 B. Gilbert, H. Zhang, F. Huang, J. F. Banfield, Y. Ren, D. Haskel, J.C. Lang, G. Srajer, A Jugensen, G. A. Waychunas, J. Chem. Phys. 2004, 120, 11785-11795.

173 McHale, J.M.; Aurouz, A.; Perotta, A.J.; Navarotsky, A. Science. 1997, 277, 788-791.

174 Zhang, H. Banfield, J.F. J. Mater. Chem. 1998, 8, 2073-2076.

175 Gilbert, B.; Zhang, H.; Huang, F.; Finnegan, M.P.; Waychunas, G.A.; Banfield, J.F. Geochem. Trans. 2003, 4, 20-27.

176 Erk, C.; Rohner, C.; Schlect, S. Z. Anorg. Allg. Chem. 2008, 634, 3001-3004.

177 Wang, Z.; Finkelstein, K.; Ma, C.; Wang, Z.L. Appl. Phys. Lett. 2007, 90, 113115.

178 Bandaranayake, R.J.; Wen, G.W.; Lin, J.Y.; Jiang, H.X.; Sorensen, C.M. Appl. Phys. Lett. 1995, 67, 831- 833.

179 Epifani, M.; Pelliccer, E.; Arbiol, J.; Sergent, N.; Pagnier, T.; Morante, J.R. Lang. 2008, 24, 11182-11188.

180 Vogel, W.; Borse, P.H.; N. Deshmuukh, S.K. Kulkarni, Langmuir. 2000, 16, 2032-2037.

181 Decremps, F.; Pellcer-Porres, J.; Datchi, F.; Itie, J.P.; Polian, A.; Baudelet, F.; Zhang, J.Z. Appl. Phys. Lett. 2002, 81, 4820-4822.

182 Jacobs, K.; Wickham, J.; Alivisatos, A.P. J. Phys. Chem. B. 2002, 106, 3759-2762.

183 Higginson, K.A.; Kuno, M.; Bonevich, J.; Qadri, S.B.; Yousef, M.; Mattoussi, H. J. Phys. Chem. B. 2002, 106, 9982-9985.

184 Yang, Y. A.; Wu, H.; Williams, K. R.; Cao, Y. C. Angew. Chem. Int. Ed. 2005, 44 (41), 6712–6715.

185 Llinas, A.; Goodman, J.M. Drug Discovery Today. 2008, 13, 198-210.

186 Kale, R.B.; Lokhande, C.D. J. Phys. Chem. B, 109, 20288-20294, 2005.

187 Rogach, A.L.; Kornowshki, A.; Gao, M.Y.; Eychmuller, A.; Weller, H. J. Phys. Chem. B 1999, 103, 3065.

188 Huang, F.; Banfield, J. J. Am. Chem. Soc. 2005, 127, 4523-4529.

189 Forment, M.; Lincot, D. Electrochimica Acta.1995, 10, 1293-1303.

190 Takeuchi, S.; Suzuki, K.; Maeda, K. Philos. Mag. A. 1984, 50, 171.

191 Zhang, X.; Sun, Z.; Yen, W.; Wei, F.; Wei, S.Q. Mater. Chem. and Phys. 2008, 111, 513-516.

192 Deng, Z.; Li, C.; Tang, F.; Zou, B. J. Phys. Chem. B 2005, 109, 16671-16675.

193 Ricolleau, C.; Audinet, L.; Gandais, M.; Gacoin, T. Eur. Phys. J. D. 1999, 9, 565-570.

194 Peng, Z. A.; Peng, X. J. Am. Chem. Soc. 2001, 123 (1), 183-184.

195 Washington, II, A.L.; Strouse, G. F. J. Am. Chem. Soc. 2008, 130 (28), 8916-8922.

196 von Grunberg, H.H. Phys Rev. B. 1997, 55(4), 2293-2302.

BIOGRAPHICAL SKETCH

Education

- Florida State University, Tallahassee, Florida, Ph.D in Inorganic Chemistry, February 2009. Thesis: *Control over Kinetics and Thermodynamics in Microwave-Assisted Synthesis of Nanocrystals*
- University of Florida, Gainesville, Florida, B.S. in Chemistry, August, 2004.

Appointments

- Graduate Researcher – Florida State University……..200
- Graduate Teaching Assistant – Florida State University…….

Skills

- **Microwave Chemistry**
  - Developed new synthetic route to CdSe quantum dots
  - Stop-Flow/Continuous Flow configurations
- **Optical Spectroscopy**
  - Absorption Spectroscopy, Fluorescence Spectroscopy (multiple temperatures),
  - Attenuated Infrared Spectroscopy
- **Powder X-ray Diffractometer**
  - Analysis using various settings including: high temperature attachment, CCD detector, scintillation detector, micro-area stage
- **TEM**
  - Experience with imaging samples
  - Low resolution and high resolution
- **Raman Spectroscopy**
  - Using an Argon Ion laser source at multiple wavelengths (457.8, 488.0, 514.0)
  - Data collected from a CCD detector
  - Cryogenic Temperatures (RT down to 10K)
- **X-ray Fluorescence Spectroscopy**
  - Elemental Analysis of Cadmium and Zinc Chalcogenides
  - Observation of Doped Materials (In, Mn, Cr)
- **Superconducting Quantum Interference Device (SQUID)**
  - Magnetization Analysis (DC/AC)
  - Field Sweep/Temperature Sweep
- **Nuclear Magnetic Resonance (NMR)**
  - Proton and Carbon-13
  - 7.05 Telsa Varian Spectrometer

Publications

1) ***Microwave-Enhanced Reaction Rates for Nanoparticle Synthesis***. Gerbec, J. A., Magana, D., Washington, A. J. Am. Chem.Soc., 127(45), 15791-15800, (2005).
2) ***Microwave Synthesis of CdSe and CdTe Nanocrystals in Non-Absorbing Alkanes***. Washington, A., Strouse, G.F. J. Am. Chem. Soc., 130(28), 8916-8922, (2008).
3) **Selective Microwave Absorption by TOPSe: Does it play a role in producing multiple sized quantum dots in a single reaction?** Washington, II, A. L., Strouse, G.F., Accepted to Chemistry of Materials (2009)
4) **Microwave Synthetic Route for Highly Emissive TOP/TOP-S Passivated CdS Quantum Dots.** Washignton, II, A.L., Strouse, G.F., Submitted to Chemistry of Materials (2009)
5) ***Concentration Controlled Crystal Motif for Growth in Nanocrystals.*** Washington, A. Strouse, G. F. *In Preparation.*

Meeting Presentations

1) Interviewee and Participant. **Best Conference At Dow Chemical.** Midland, Mi. September 2008.
2) Oral Presentation: ***The Observation of Re-Nucleation in Microwave Reactions of Nanomaterials.*** ACS Meeting, Philadelphia, Pa. August. 2008.
3) Oral Presentation: ***Utilizing and Controlling the Ostwald Ripening Phenomenon in Microwave Synthesis of Nanocrystals.*** ACS Fall Meeting, Philadelphia, Pa. August 2008.
4) Interviewee and Participant. ***Research and Technical Careers in Industry Conference at Proctor and Gamble.*** Cincinnati, OH., May 2008.
5) Poster Presentation: ***Microwave Methodology for Control of Crystal Motif and Growth in Nanocrystals***. MRS Fall Meeting, Boston, Ma. Nov. 2007
6) Oral Presentation: ***Transition from Thermal to Microwave Synthesis of Quantum Dots***. 83rd Annual Florida Meeting and Exposition, Orlando, FL. May 2007
7) Poster Presentation: ***Microwave Synthesis of CdSe and CdTe Nanoparticles***. 4th Annual Florida Inorganic Mini-Symposium, Gainesville, FL. Oct. 2006
8) Oral Presentation: ***Diffusion of Zinc into Wide-Bandgap CdSe Semiconductor Quantum Dots Monitored by Optical and Structural Analysis***. 82rd Annual Florida Meeting and Exposition, Orlando, FL. May 2006

Affiliations

- ACS - The American Chemical Society
- MRS – Materials Research Society